

Copyright is owned by the Author of the thesis. Permission is given for a copy to be downloaded by an individual for the purpose of research and private study only. The thesis may not be reproduced elsewhere without the permission of the Author.

# Towards DNA-Chromophore Supramolecular Assemblies for Photon Upconversion

A thesis submitted in the partial fulfilment  
of the requirements for the degree of

Doctor of Philosophy in Chemistry

Massey University,

Palmerston North, New Zealand



**MASSEY UNIVERSITY**  
**TE KUNENGA KI PŪREHUROA**  

---

**UNIVERSITY OF NEW ZEALAND**

Saymore Mutsamwira

2015





## Abstract

The interactions of long DNAs of biological origin with small molecules have intrigued scientists for a while now, with particular emphasis on medical applications like cancer therapy. Recently, DNA's unique highly ordered structures, self-assembly capabilities and ease of chemical modification have led to a more broad based approach for potential applications in photonic and electronic devices. In this thesis, we show that DNA can be used as a scaffold for supramolecular assembly of selected organic chromophores for tuning photon upconversion based on a triplet-triplet annihilation (TTA) mechanism.

Green-to-blue photon upconversion was observed using tris(bipyridine)ruthenium(II),  $[\text{Ru}(\text{bpy})_3]^{2+}$  as a long wavelength absorber and an *in-situ* energy donor to an acceptor (*R*)-1-*O*-[4-(1-pyrenylethynyl)phenylmethyl]glycerol), abbreviated PEPy and also known as a twisted intercalating nucleic acid (TINA) monomer which acts as an annihilator and short wavelength photoemitter. This result prompted us to investigate interactions of the ligands ( $[\text{Ru}(\text{bpy})_3]^{2+}$  and ZnTMPyP4, the  $\text{Zn}^{2+}$  derivative of 5,10,15,20-tetrakis-(1-methyl-4-pyridyl)-21*H*,23*H*-porphine) with TINA moieties attached to a DNA scaffold. Zinc metallated porphyrins and ruthenium polypyridyl complexes are well known to act as donors in TTA-based energy upconversion. TINA-modified DNA duplexes and G-quadruplexes significantly improved the interaction between TINA and ZnTMPyP4/  $[\text{Ru}(\text{bpy})_3]^{2+}$  as shown by fluorescence, circular dichroism (CD), and UV-Vis spectroscopy studies. In contrast to dynamic quenching of the TINA monomer fluorescence by  $[\text{Ru}(\text{bpy})_3]^{2+}$  and ZnTMPyP4 for free monomers in solution, ground state complex formation was the predominant mechanism of interaction between TINA-modified DNAs and  $[\text{Ru}(\text{bpy})_3]^{2+}$ / ZnTMPyP4.

Energy upconversion was observed with a  $[\text{Ru}(\text{bpy})_3]^{2+}$  donor and TINA-modified DNAs. The results presented in this thesis lay a foundation for further energy upconversion studies utilizing appropriate organic chromophores using DNA as a scaffold.



## Acknowledgements

*To my parents, Cephas Taringwandisho and Kenesia Mutsamwira, for being the best parents and instilling in me the importance of education.*

My journey towards achieving my lifelong dream to obtain a Doctoral Degree took a somewhat unusual path, with some twists and turns along the way. I would not have been able to navigate the journey without some unconditional, sometimes undeserved support from a lot of people who I owe for the rest of my life, some of whom I may not be able to name here. For that reason, this PhD does not belong to me; it is a triumph of dedication, love, trust, perseverance, overcoming obstacles and is dedicated to the lovely people who have been there for me I don't even know who to start with.

Firstly, I would like to thank the Lord that you made me, you gave me direction through the good and the bad times, you never left me alone. There are no words that can express the gratitude that I give to my parents who have been there throughout spending sleepless nights talking to me, praying for me, inspiring me to never give up. My children, little Tinotenda Kelendria and Tatenda have been an ever present psychological boost when the chips were down, and Tatenda's words as a little boy "Dad never give up" always echo in my ears. I am truly thankful to my wife Kudzai for the love and being an ever present inspiration throughout my studies. Kudzai, thank you for being my rock, keeping up with the moods, sometimes pushing me out of bed to go to school, as well as helping me to write. I could not have achieved this without you and I am grateful that you are a part of my life. My siblings, thank you so much for your genuine love always.

I will forever be indebted to my supervisors Eric Ainscough, Vyacheslav Filichev, Peter Derrick and Ashton Partridge for their patience, support and guidance throughout the project. I take Eric to be my second father for his emotional and life skills advice outside of the project, Vyacheslav for being a big brother in all personal matters. Finally, I thank all colleagues in IFS for their assistance throughout the years.



## Table of Contents

Abbreviations .....	xi
1 Introduction .....	1
1.1 Energy Upconversion (EU) .....	1
1.1.1 Two-photon absorption (TPA) followed by fluorescence .....	1
1.1.2 Energy transfer upconversion (ETU) .....	2
1.1.3 Triplet-triplet annihilation (TTA) based EU .....	3
1.1.4 Mechanisms of Energy Transfer between light sensitive molecules .....	4
1.1.5 TTA-based EU in detail .....	9
1.1.6 Advantages of TTA in EU .....	13
1.2 Supramolecular Assembly-based Energy Upconversion.....	13
1.2.1 Supramolecular Chemistry Principles .....	13
1.3 Aspects of Supramolecular assembly-based energy upconversion (EU).....	16
1.4 Research Aim .....	17
1.4.1 Covalent Assembly .....	19
1.4.2 Non covalent Assembly .....	19
1.5 Thesis Outline.....	20
1.6 References .....	22
2 Spectroscopic properties of Organic Chromophores applied in EU .....	25
2.1 Porphine and Porphyrins .....	25
2.1.1 Zinc tetramethylpyridinium porphyrin (ZnTMpyP4).....	27
2.2 Ru <sup>2+</sup> Polypyridyl Complexes .....	29
2.2.1 Polycyclic aromatic hydrocarbons (PAHs).....	31
2.3 References .....	35
3 DNA in Creation of Functional $\pi$ -systems .....	37
3.1 DNA Structure .....	37
3.2 G-Quadruplexes .....	40
3.3 DNA Functional $\pi$ -systems .....	41
3.4 DNA –Chromophore Arrangements.....	42
3.5 DNA Automated Synthesis.....	46
3.6 DNA Analysis Methods.....	50
3.6.1 Gel Electrophoresis .....	50

3.6.2	Melting temperature ( $T_m$ ) .....	51
3.6.3	Mass Spectrometry .....	52
3.6.4	UV-Vis Thermal Difference Spectra (TDS) .....	52
3.6.5	Circular Dichroism (CD) Spectroscopy .....	53
3.6.6	Fluorescence properties of unmodified DNA .....	55
3.7	References .....	56
4	Interactions of Free Chromophores in Organic Solvents and their use in EU .....	59
4.1	Introduction .....	59
4.2	Chapter Summary .....	59
4.3	Stern-Volmer Analysis .....	60
4.3.1	Combined dynamic and static quenching .....	63
4.3.2	Deviations from the Stern-Volmer equation .....	64
4.4	Fluorescence Quenching Characteristics .....	65
4.4.1	Interaction between $[Ru(bpy)_3]^{2+}$ and TINA monomer (PEPy) in solution .....	65
4.4.2	Interaction between ZnTMPyP4 and TINA monomer (PEPy) in solution .....	67
4.5	Analysis of Photon Upconversion .....	69
4.5.1	A typical energy upconversion analysis .....	69
4.5.2	Experimental Requirements for Energy Upconversion .....	71
4.5.3	$[Ru(bpy)_3]^{2+}$ and TINA monomer (PEPy) in EU .....	72
4.5.4	$[Ru(bpy)_3]^{2+}$ and DPA in EU .....	76
4.5.5	ZnTMPyP4 and TINA monomer (PEPy) in EU .....	76
4.6	References .....	78
5	Arrangement of Chromophores on DNA using “Click Chemistry” for EU .....	79
5.1	DNA Chemical Modification .....	79
5.1.1	Covalent modification .....	79
5.1.2	Click Chemistry on DNA .....	80
5.2	Chapter Summary .....	82
5.3	Synthesis of Organic Chromophores for DNA modification .....	85
5.3.1	Synthesis of 1C and 1D .....	85
5.3.2	Synthesis of 1F .....	86
5.3.3	Synthesis of 2D .....	86
5.3.4	Synthesis of 3B .....	87
5.3.5	Synthesis of 4C .....	87
5.3.6	Synthesis of 5B and 5C .....	88

5.3.7	Synthesis of 6C and 6D.....	88
5.3.8	Synthesis of 7C.....	89
5.3.9	Synthesis of 8B and 8C.....	89
5.4	Post-synthetic DNA functionalization.....	89
5.4.1	DNA synthesis.....	89
5.4.2	DNA modification.....	90
5.5	Conclusions.....	97
5.6	References.....	99
6	Interactions of TINA-modified DNA Duplexes with a Zinc Cationic Porphyrin.....	101
6.1	Introduction.....	101
6.2	Chapter Summary.....	103
6.3	DNA Duplex Design.....	104
6.4	UV-Vis Spectroscopy of porphyrin/TINA-DNA complexes.....	105
6.5	DNA Melting Studies.....	107
6.6	Thermal Difference Spectra (TDS) of porphyrin/TINA-DNA complexes.....	109
6.7	Fluorescence Spectroscopy of porphyrin/TINA-DNA complexes.....	110
6.7.1	Stern-Volmer Analysis.....	112
6.7.2	K <sub>4</sub> Fe(CN) <sub>6</sub> – ZnTMPyP4 Quenching Studies.....	116
6.8	Circular Dichroism of porphyrin/TINA-DNA complexes.....	118
6.9	Conclusions and Future Directions.....	120
6.10	References.....	122
7	Interactions of TINA-modified DNA Duplexes with [Ru(bpy) <sub>3</sub> ] <sup>2+</sup> .....	125
7.1	Introduction.....	125
7.2	stDNA - [Ru(bpy) <sub>3</sub> ] <sup>2+</sup> studies.....	125
7.3	UV-Vis Spectroscopy of [Ru(bpy) <sub>3</sub> ] <sup>2+</sup> /TINA-DNA complexes.....	128
7.4	DNA Melting Studies.....	130
7.5	UV-Vis thermal difference spectra (TDS) of [Ru(bpy) <sub>3</sub> ] <sup>2+</sup> /TINA-DNA complexes.....	131
7.6	Fluorescence Spectroscopy of [Ru(bpy) <sub>3</sub> ] <sup>2+</sup> /TINA-DNA complexes.....	133
7.6.1	Stern-Volmer Analyses.....	137
7.6.2	K <sub>4</sub> Fe(CN) <sub>6</sub> – [Ru(bpy) <sub>3</sub> ] <sup>2+</sup> Fluorescence Quenching Studies.....	139
7.7	Circular Dichroism of [Ru(bpy) <sub>3</sub> ] <sup>2+</sup> /TINA-DNA complexes.....	141
7.8	Conclusions.....	142
7.9	References.....	143
8	Interactions of TINA-modified G-quadruplexes with [Ru(bpy) <sub>3</sub> ] <sup>2+</sup> and ZnTMPyP4.....	145



8.1	Introduction .....	145
8.2	G-Quadruplex Design .....	146
8.3	UV-Vis Spectroscopy of $[\text{Ru}(\text{bpy})_3]^{2+}$ / G-Quadruplex complexes.....	147
8.4	Fluorescence Spectroscopy of $[\text{Ru}(\text{bpy})_3]^{2+}$ /G-Quadruplex complexes .....	148
8.4.1	$\text{K}_4\text{Fe}(\text{CN})_6 - [\text{Ru}(\text{bpy})_3]^{2+}$ Quenching Studies .....	150
8.5	Fluorescence Spectroscopy of Porphyrin/ G-Quadruplex complexes .....	151
8.6	Energy Transfer .....	156
8.7	Circular Dichroism of $[\text{Ru}(\text{bpy})_3]^{2+}$ /G-Quadruplex and ZnTMPyP4/G-Quadruplex Complexes .....	156
8.8	UV-Vis Thermal Difference Spectra (TDS) of $[\text{Ru}(\text{bpy})_3]^{2+}$ /G-Quadruplex and ZnTMPyP4/G-Quadruplex Complexes.....	158
8.9	G-Quadruplex Melting Studies.....	160
8.10	Conclusions .....	161
8.11	References .....	163
9	DNA-based Energy Upconversion (EU) .....	165
9.1	Introduction .....	165
9.2	TINA-modified G-quadruplex DNA in EU .....	165
9.3	TINA-modified DNA, extended study.....	167
9.4	References .....	173
10	Final Conclusions and Future Directions.....	175
10.1	Final Conclusions.....	175
10.2	Future Directions .....	177
11	Experimental Methods.....	179
11.1	Experimental Procedures for Chapter 5 .....	179
11.1.1	General Experimental .....	179
11.1.2	Synthesis of Organic Chromophores.....	179
11.1.3	Synthesis of Oligonucleotides .....	190
11.1.4	General Procedure for CuAAC Reaction on DNA .....	190
11.1.5	Procedure for Nitrobenzaldehyde Oxime NO/AC Reaction on DNA .....	190
11.1.6	General procedure for nitrobenzaldehyde hydroximinoyl chloride NO/AC reaction on DNA .....	191
11.1.7	General cleavage/deprotection and precipitation procedure.....	191
11.2	Experimental Procedures for Chapters 4, 5 - 8.....	191
11.2.1	Materials .....	191

11.2.2	Synthesis and Purification of TINA Modified Oligonucleotides .....	192
11.2.3	Stock Solutions.....	193
11.2.4	DNA annealing procedures .....	193
11.2.5	Instrumentation.....	193
11.3	Experimental Procedures for Chapters 4 and 9.....	195
11.3.1	Materials and instrumentation .....	195
11.3.2	Upconverted fluorescence measurements.....	196
11.4	References .....	197
12	Appendix .....	199
12.1	General.....	199
12.1.1	NMR and UV-Vis Spectra of $[\text{Ru}(\text{bpy})_3]^{2+}$ .....	199
12.1.2	NMR and UV-Vis spectra of ZnTMPyP4 .....	200
12.2	Appendix for Chapter 6.....	203
12.2.1	Determination of Binding Constants of ZnTMPyP4 to Duplexes .....	205
12.2.2	Example of binding constant calculation for the complex of salmon testes DNA- ZnTMPyP4 by fluorescence spectroscopy .....	207
12.2.3	Example of Stoichiometry calculation.....	208
12.3	Appendix for Chapter 7 .....	210
12.4	Appendix for Chapter 8.....	212
12.5	References .....	214



## Abbreviations

A	adenosine
<sup>0</sup> A	ground state acceptor molecule
<sup>1</sup> A*	excited singlet state acceptor molecule
<sup>3</sup> A*	excited triplet state acceptor molecule
ACN	acetonitrile
aq	aqueous
ATR	attenuated total reflection
bp	base pair
C	cytosine
Calcd	calculated
CD	circular dichroism spectroscopy
conc	concentrated
COSY	correlation spectroscopy
CPG	controlled porous glass
CT	cytosine thymine sequence
ctDNA	calf thymus DNA
CuAAC	Cu <sup>I</sup> catalysed Huisgen 1,3-dipolar azide alkyne cycloaddition
d	doublet
<sup>0</sup> D	ground state donor molecule
<sup>1</sup> D*	singlet excited state donor molecule
<sup>3</sup> D*	triplet excited state donor molecule
dA	2'-deoxyadenosine
dC	2'-deoxycytosine
DCA	dichloroacetic acid
DCM	dichloromethane
dG	2'-deoxyguanosine
dsDNA	double stranded deoxyribonucleic acid
dT	thymidine
DMA	9,10-dimethylanthracene
DMF	<i>N,N</i> -dimethylformamide
DMT	4,4'-dimethoxytrityl
DMSO	dimethyl sulfoxide

DNA	deoxyribonucleic acid
DPA	9,10-diphenylanthracene
DSSC	dye sensitised solar cell
EDTA	ethylenediaminetetraacetic acid
ESI	electrospray ionization
ETU	sequential energy transfer upconversion
EU	energy upconversion
eq	equivalent
eqn	equation
EtOH	ethanol
FRET	Förster resonance energy transfer
G	guanosine
h	hour
HPLC	high performance liquid chromatography
ICD	induced circular dichroism
IR	infra-red spectroscopy
ISC	intersystem crossing
ITC	isothermal titration calorimetry
$K_a$	association constant
$K_{app}$	apparent quenching constant
$K_d$	dissociation constant
$K_D$	Stern-Volmer dynamic quenching constant
$K_S$	Stern-Volmer static quenching constant
$K_{SV}$	Stern-Volmer quenching constant
m	multiplet
MALDI	matrix assisted laser desorption ionisation
MeOH	methanol
ml	millilitres
MLCT	metal to ligand charge transfer
MsCl	methanesulfonyl chloride
MS	mass spectrometry
NCS	<i>N</i> -chlorosuccinimide
NMR	nuclear magnetic resonance
NO/AC	nitrile oxide/azide cycloaddition

ON	oligodeoxynucleotide
OLED	organic light emitting diode
PAGE	polyacrylamide gel electrophoresis
PAH	polycyclic aromatic hydrocarbon
PDT	photodynamic therapy
PEPy	( <i>R</i> )-1- <i>O</i> -[4-(1-pyrenylethynyl)phenylmethyl]glycerol
Ph	phenyl
ppm	parts per million
Q	quencher
RNA	ribonucleic acid
ROS	reactive oxygen species
RT	room temperature
[Ru(bpy) <sub>3</sub> ] <sup>2+</sup>	2,2'-tris(bipyridine)ruthenium(II)
s	singlet
S <sub>0</sub>	singlet ground state
S <sub>1</sub>	first singlet excited state
S <sub>2</sub>	second singlet excited state
stDNA	salmon testes DNA
t	triplet
T	thymidine
T <sub>1</sub>	triplet excited state
TBE	tris-borate-EDTA buffer
TCA	trichloroacetic acid
TDS	thermal difference spectra
TEMED	<i>N,N,N',N'</i> -Tetramethylethylenediamine
TFA	trifluoroacetic acid
THF	tetrahydrofuran
TINA	twisted intercalating nucleic acid
TLC	thin layer chromatography
<i>T</i> <sub>1/2</sub>	mid-transition temperature
<i>T</i> <sub>m</sub>	melting temperature
TMS	tetramethylsilane
TOF	time of flight

TPA	two photon absorption
TPP	5,10,15,20-tetraphenylporphyrin
TPPps	5,10,15,20-tetraphenylporphyrin phosphonium salt
TTA	triplet-triplet annihilation
TTeT	triplet-triplet energy transfer
U	uridine
UV-Vis	ultraviolet-visible spectroscopy
$\mu\text{l}$	microlitres
$\mu\text{mol}$	micromole
ZnTMpyP4	<i>meso</i> -tetrakis(4- <i>N</i> -methylpyridyl) zinc (II) porphyrin
$\Phi_{\text{F}}$	fluorescence quantum yield

## 1 Introduction

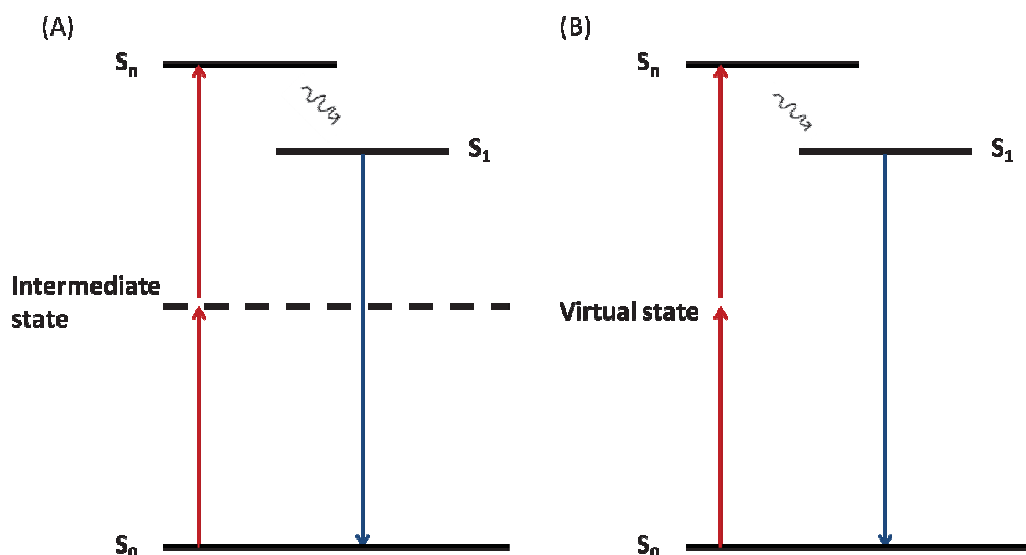
### 1.1 Energy Upconversion (EU)

Energy upconversion (EU) or anti-Stokes emission is the emission of higher energy photons with respect to excitation energy. The most important approaches for energy upconversion to date include two photon absorption followed by fluorescence emission (TPA)<sup>[1]</sup> with organic materials, sequential energy transfer upconversion (ETU)<sup>[2]</sup> in rare-earth ion-doped glasses, and triplet-triplet annihilation (TTA).<sup>[3]</sup> TPA is process by which two photons combine in a nonlinear medium to produce a higher-energy photon with a frequency that is the sum of those two photons. ETU occurs if a laser-active ion in an excited state transfers energy to another excited laser-active ion. If this occurs, the ion receiving the energy will be excited to a higher energy state than that of the initial photon absorbed. TPA, ETU and TTA are discussed in detail below.

#### 1.1.1 Two-photon absorption (TPA) followed by fluorescence

Two-photon absorption (TPA) occurs when there is absorption of two photons by a molecule. The molecule is excited from one state (usually the ground state) to a higher energy electronic state. If the excited molecule radiatively goes to the ground state it gives anti-Stokes fluorescence. Hence, this process can also be called two photon excitation fluorescence.<sup>[4]</sup> One process occurs when the photons are absorbed by a stepwise process, in which the first photon is absorbed, exciting the molecule through an intermediate state. The second photon brings the intermediate state to the final state, followed by higher energy emission (Figure 1.1A).<sup>[5]</sup> Alternatively, the photons simultaneously excite a species through a virtual state created by the interaction of the photons with the molecule (Figure 1.1B).<sup>[4]</sup> The absorbed photons could be of identical or different frequencies. The excited upper state of the molecule is at an energy that is equal to the sum of the energies of the two photons.<sup>[6]</sup>



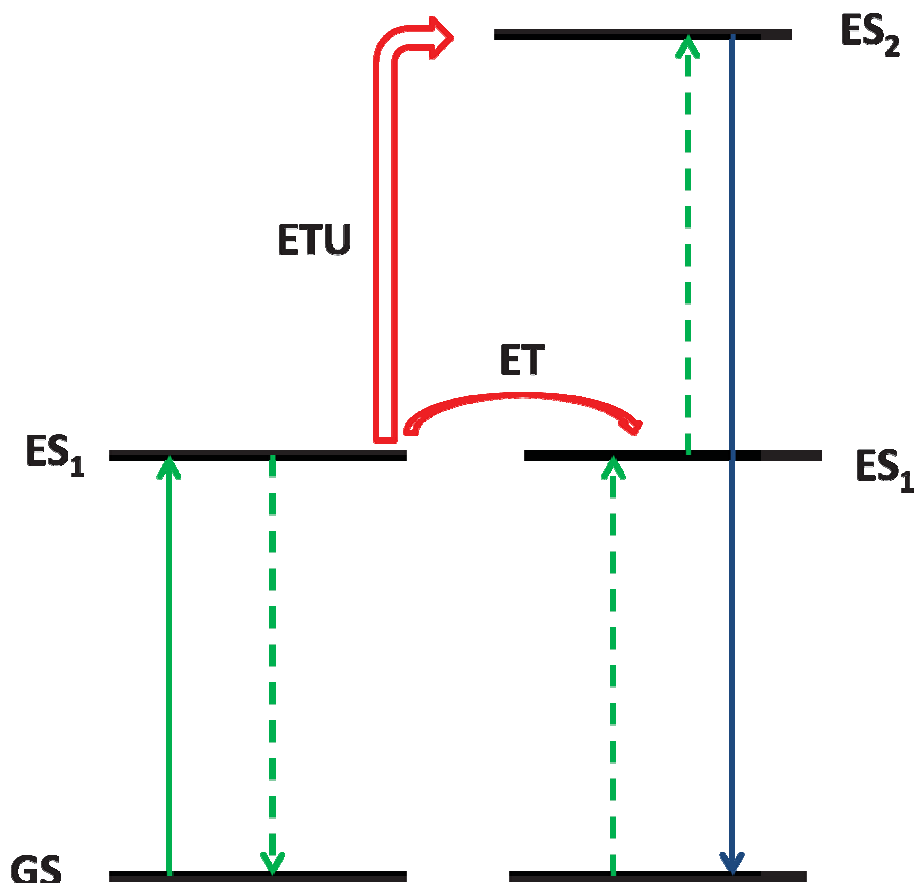


**Figure 1.1** Schematic diagrams for two photon absorption by (A) a sequential process involving an intermediate state and (B) a simultaneous process, followed by anti-Stokes fluorescence.  $S_0$  is the singlet ground state,  $S_n$  and  $S_1$  are different vibrational states of the singlet excited state.

TPA is a nonlinear optical process that has a quadratic dependence of the light intensity, and it can dominate over linear absorption at high intensities. TPA is most efficient at very high intensities. The requirement for high light intensity means that lasers are required to observe TPA, and monochromatic light is also desired to measure the TPA cross section at different wavelengths. As a result, tunable pulsed lasers are the favoured excitation source.<sup>[6]</sup>

### 1.1.2 Energy transfer upconversion (ETU)

Energy transfers between excited ions could take place between two ions, both of them being in an excited state at the energy transfer initial step. Energy Transfer Upconversion (ETU) takes place between two neighbouring ions.<sup>[7]</sup> ETU involves the transfer of energy from an excited ion (donor ion) undergoing non-radiative decay to another excited ion (receiving ion). The receiving ion is excited to a level above that which would be achieved by simple absorption of a pump photon (Figure 1.2).<sup>[8]</sup>



**Figure 1.2** A schematic diagram for energy transfer upconversion (ETU) following energy transfer (ET). GS is the ground state, ES<sub>1</sub> and ES<sub>2</sub> are the excited states.

ETU is a step-wise process that occurs through real electronic states. Rare-earth ions are convenient hosts for ETU because their f-valence electrons have energy level spacings that correspond to near-infrared and visible photon energies. Excited ions can be excited from their intermediate state by accepting energy from another species *via* energy transfer (ET), followed by relaxation to the ground state. An example of ETU is the luminescence observed in Yb<sup>3+</sup>, Er<sup>3+</sup> co-doped Y<sub>2</sub>O<sub>3</sub> films excited by a pulsed laser.<sup>[9]</sup> Another, possibility occurs when the excited ion gains another photon in what is known as excited state absorption (ESA).<sup>[4]</sup>

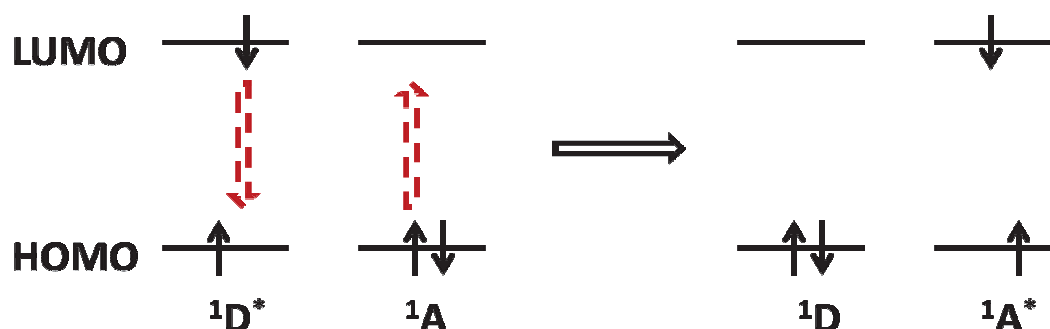
### 1.1.3 Triplet-triplet annihilation (TTA) based EU

Before discussing TTA-based EU, the concepts of Dexter and Förster energy transfer mechanisms need to be addressed.

### 1.1.4 Mechanisms of Energy Transfer between light sensitive molecules

#### 1.1.4.1 Förster resonance energy transfer (FRET)

Förster resonance energy transfer (FRET) is a non-radiative process that occurs when an excited donor chromophore transfers energy to an acceptor chromophore through nonradiative dipole–dipole coupling, without transfer or exchange of electrons (Figure 1.3)



**Figure 1.3** A schematic diagram for singlet-singlet Förster energy transfer.

Generally, the emission spectrum of the donor overlaps with the absorption spectrum of the acceptor.<sup>[10]</sup> The efficiency of FRET is inversely proportional to the 6<sup>th</sup> power of the distance between donor and acceptor, making FRET extremely sensitive to small changes in distance.<sup>[11]</sup>

The rate of energy transfer  $k_{ET}$  is given by:

$$k_{ET} = (1/\tau_D)(R_0/r)^6 \quad \text{eqn 1.1}$$

where  $r$  is the distance between the donor ( $D$ ) and acceptor ( $A$ ),  $\tau_D$  is the lifetime of the donor in the absence of energy transfer, and  $R_0$  is the Förster distance of this pair of donor and acceptor, i.e. the distance at which the energy transfer efficiency is 50%.<sup>[12]</sup>

The efficiency of energy transfer by a Förster mechanism ( $E$ ) is the quantum yield of the energy transfer transition. This is defined as the fraction of energy transfer that occurs per donor excitation event.<sup>[13]</sup>

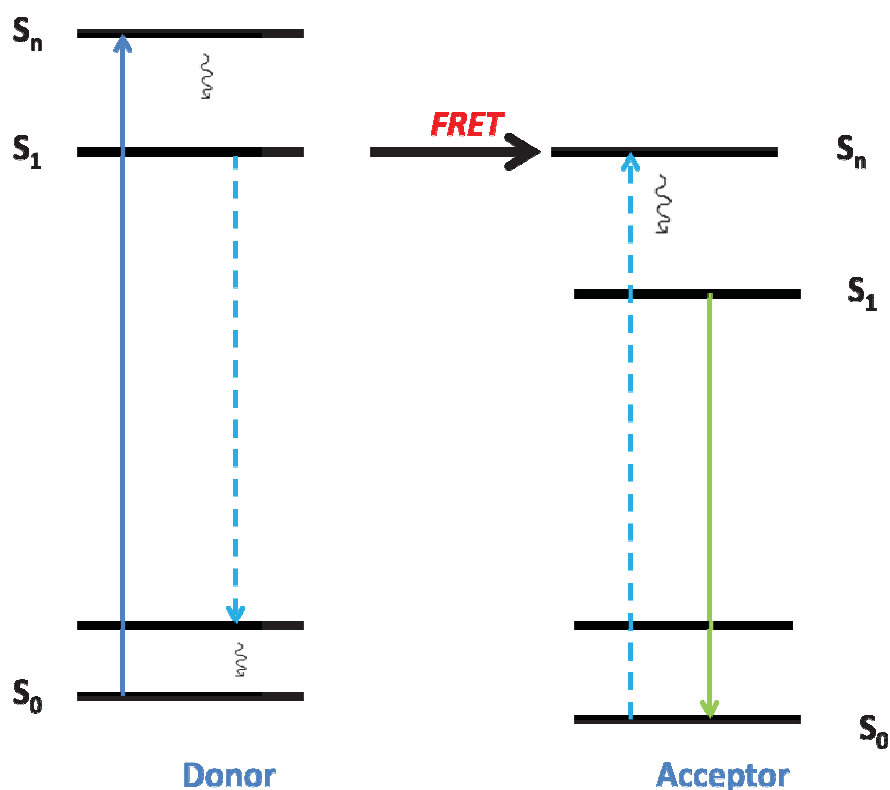
$$E = k_{ET}/(k_f + k_{ET} + \sum k_i) \quad \text{eqn 1.2}$$

where  $k_{ET}$  is the rate of energy transfer,  $k_f$  is the radiative decay rate, and the  $k_i$  are the rate constants of any other de-excitation pathways.<sup>[12]</sup>

The efficiency of energy transfer for a single donor–acceptor pair at a fixed distance ( $E$ ) depends on the donor-to-acceptor separation distance with an inverse 6th power law due to the dipole-dipole coupling mechanism:

$$E = R_0^6/(R_0^6 + r^6) \quad \text{eqn 1.3}$$

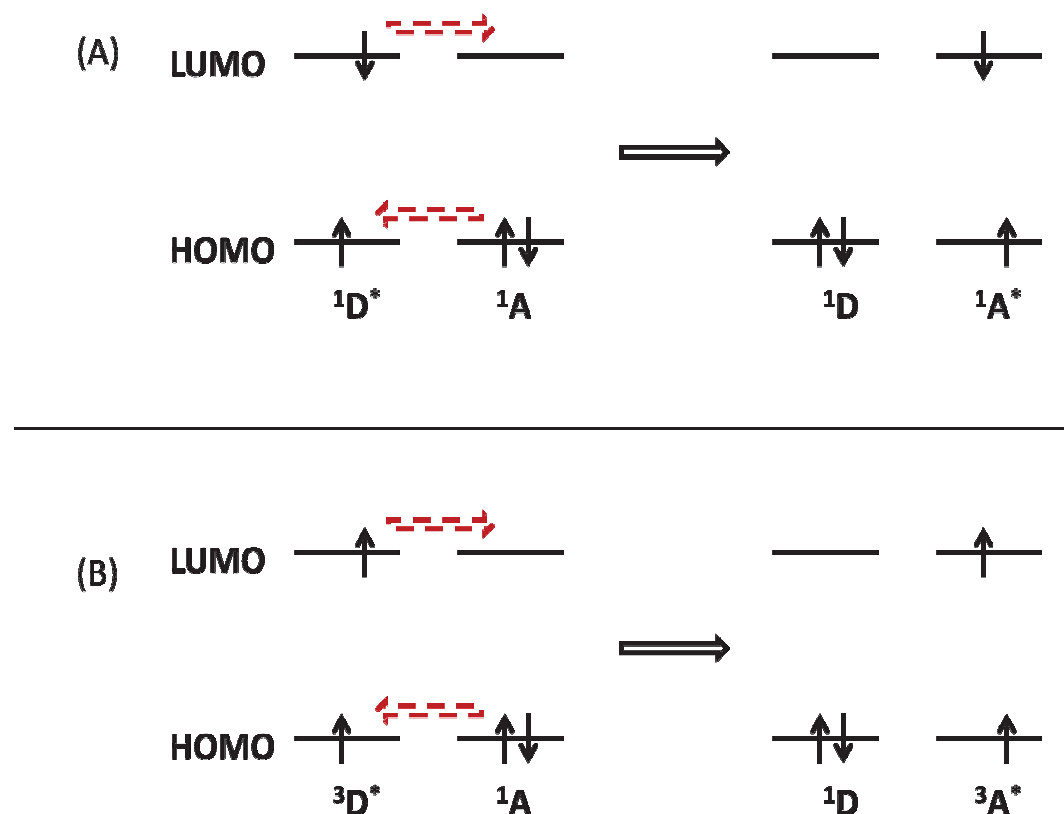
FRET efficiency depends on factors such as: (i) distance between the donor and the acceptor (typically in the range of 10 - 100 Å), (ii) the spectral overlap of the donor emission spectrum and the acceptor absorption spectrum, and (iii) the relative orientation of the donor and acceptor transition dipoles caused by the Coulombic term of interaction.<sup>[10]</sup> A Jablonski diagram of Förster resonance energy transfer (FRET) is illustrated in Figure 1.4:



**Figure 1.4** A Jablonski diagram energy transfer by a Förster mechanism. Dashed arrows are non-radiative processes. Wavy arrows represent internal conversion.

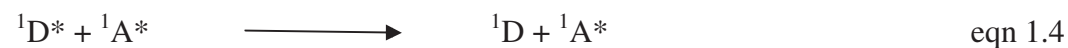
### 1.1.4.2 Dexter Energy transfer

Dexter energy transfer is a short range non-radiative process generally attributed to direct exchange of electrons.<sup>[14]</sup> The excited electron from the highest occupied molecular orbital (HOMO) of the donor moves over to the HOMO of the acceptor, followed by the migration of the lowest occupied molecular orbital (LUMO) electron to the LUMO of the donor. A schematic diagram for both a singlet-singlet and a triplet-triplet energy transfer is shown on Figure 1.5.<sup>[14]</sup>



**Figure 1.5** A schematic diagram for singlet-singlet Dexter energy transfer (A) and for triplet-triplet Dexter energy transfer (B).

The exchange mechanism could be singlet-singlet energy transfer (eqn 1.4) or triplet-triplet energy transfer (eqn 1.5) *via* a Wigner's spin conservation rule. Wigner's spin conservation rule states that; in any allowed electronic transfer process, the overall spin angular momentum of the system should not change.<sup>[15]</sup>



Since Dexter energy transfer involves electron transfer, it requires an overlap of the wavefunctions of the donor and acceptor electrons, in addition to the overlap of the emission spectrum of the donor to the absorption spectrum of the acceptor. As a result, it can only occur at short distances; typically the exchange mechanism occurs within 10 Å.<sup>[14]</sup> The Dexter energy transfer rate ( $k_{ET}$ ) is given by the following equation:

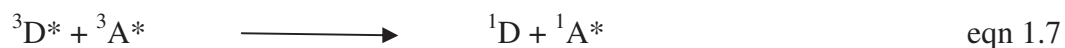
$$k_{ET} = KJ\exp(-2R_{DA}/L) \quad \text{eqn 1.6}$$

where  $R_{DA}$  is the distance between the donor and the acceptor,  $K$  is an experimental factor,  $L$  is the sum of the *van der Waals radii* of the donor and the acceptor, and  $J$  is the normalized spectral overlap integral.

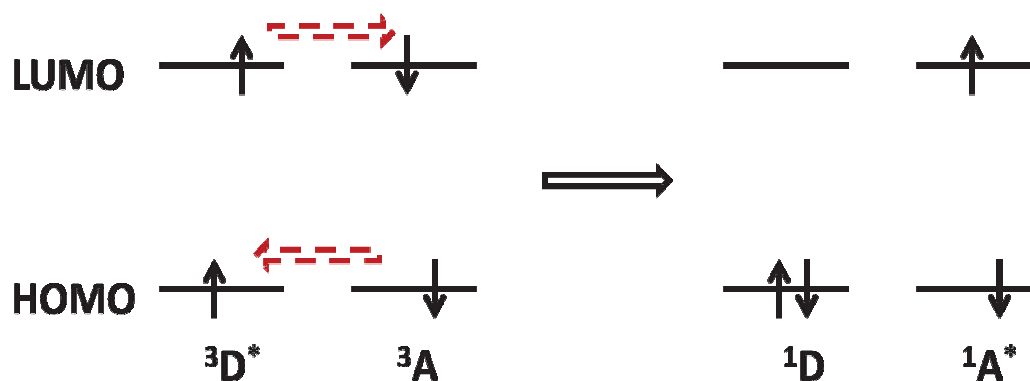
The rate constant of Dexter energy transfer decays exponentially as the distance between the acceptor and the donor increases. Dexter energy transfer is a short-range energy transfer process as opposed to the Förster mechanism that is a long-range energy transfer.<sup>[16]</sup>

#### 1.1.4.3 Triplet-triplet annihilation (TTA)

TTA is a special case of Dexter energy transfer involving exchange of electrons between a donor and an acceptor.<sup>[17]</sup> Two triplet states of the donor and the acceptor react to produce a higher energy acceptor singlet state and a singlet ground state donor (eqn 1.7), followed by fluorescence from the acceptor. Even though TTA is a Dexter process, it does not follow Wigner's Conservation rule, which makes it an exceptional case of Dexter energy transfer.

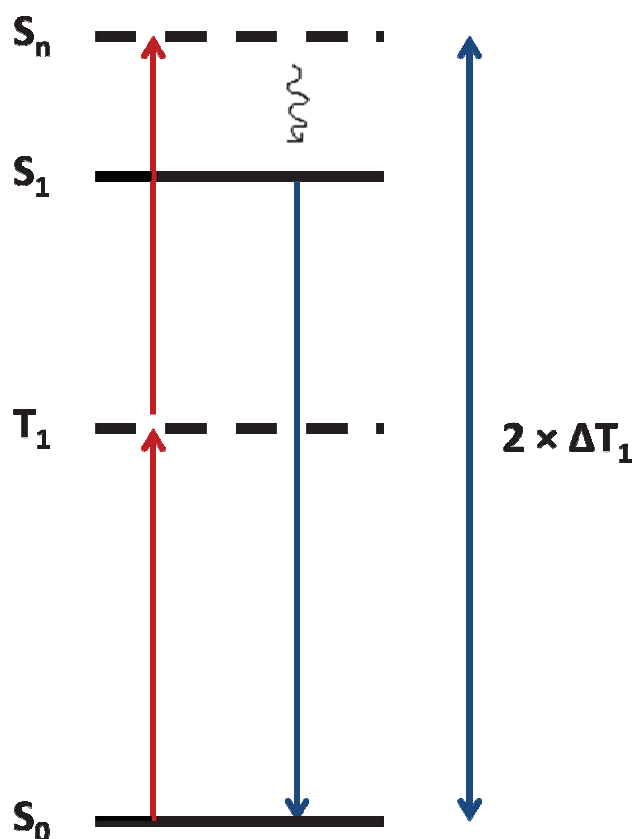


A schematic of TTA is shown below in Figure 1.6:



**Figure 1.6** A schematic diagram for triplet-triplet annihilation by a Dexter energy transfer mechanism.

In the case of TTA-EU both the donor and the acceptor are the same type of molecules (the same dye), resulting in an excited singlet and ground state species of the same molecule.<sup>[17]</sup> The energy of the singlet excited state ( $S_1$ ) is less than twice the energy of the excited triplet ( $S_n = 2 \times T_1$ ), due to internal conversion (Figure 1.7):



**Figure 1.7** A Jablonski diagram for triplet-triplet annihilation by a Dexter energy transfer mechanism. Wavy arrow is internal conversion.

TTA-based EU involves steps that require the components (chromophores) to be in close contact. As a result, the donor and acceptor are typically within Dexter distances ( $\leq 10\text{\AA}$ ) of each other in order for efficient TTA-EU to occur. Therefore, TTA-EU involves Dexter energy exchange processes which do not require dipole moment interaction between components as expected for Förster mechanisms. However, since in TTA-EU electron exchange occurs there has to be an overlap of the donor and acceptor wavefunctions.

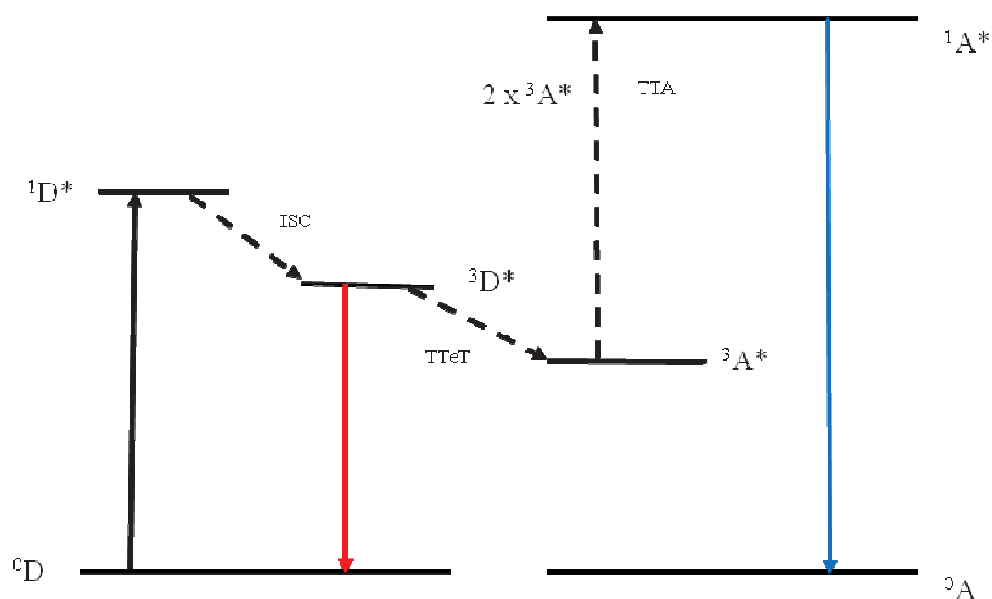
### 1.1.5 TTA-based EU in detail

TTA-based EU involves the transfer of energy between a photosensitizer, which acts as an energy donor, and a photoemitter, which acts both as an energy acceptor and annihilator, see eqns 1.8–1.12 below. Long wavelength excitation of the ground state donor ( $^0D$ ) produces the singlet excited state ( $^1D^*$ ), eqn 1.8, followed by intersystem crossing (ISC) to give the triplet excited state of the donor ( $^3D^*$ ), eqn 1.9. The triplet donor then transfers its energy to the ground state acceptor ( $^0A$ ) in a bimolecular triplet quenching process called triplet-triplet energy transfer (TTeT), eqn 1.10. The crucial step in this process is triplet-triplet annihilation (TTA) where the energy stored in two separate excited triplet state molecules is combined to generate a higher energy excited singlet state ( $^1A^*$ ) and a corresponding ground state species ( $^0A$ ),<sup>[18]</sup> eqn 1.11. It is important to note that acceptor excited singlet state ( $^1A^*$ ) energy lies lower than twice the energy of the acceptor triplet state ( $^3A^*$ ).<sup>[19]</sup> Radiative decay of  $^1A^*$  generates shorter wavelength energy than the excitation wavelength i.e.  $h\nu_2 > h\nu_1$ .



A generalized Jablonski diagram summarizing the processes involved in energy upconversion via TTA is presented below (Figure 1.8):



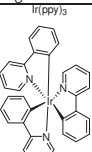
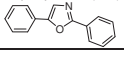
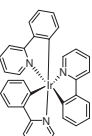

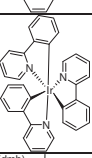
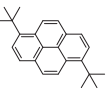
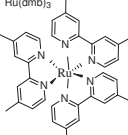
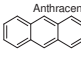
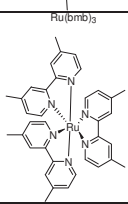
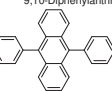
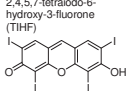
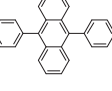
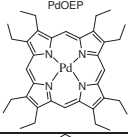
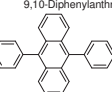
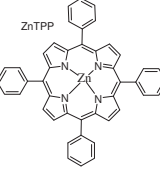
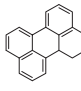
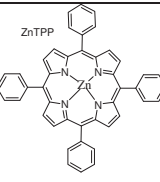
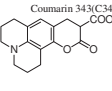


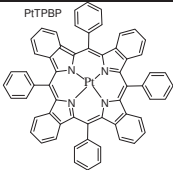
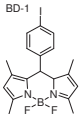
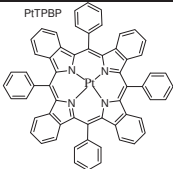
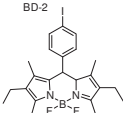
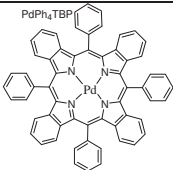
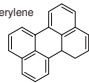
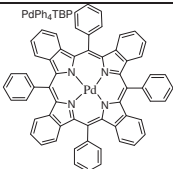
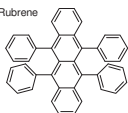
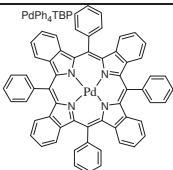

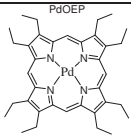
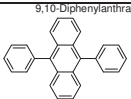
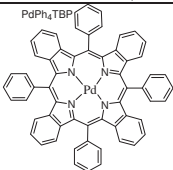

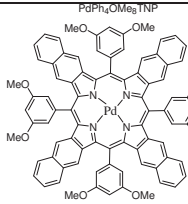
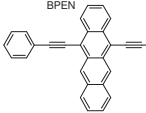
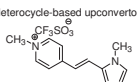
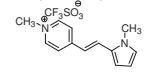
**Figure 1.8** Qualitative Jablonski Diagram of TTA supported energy upconversion.  $^0$ ISC is intersystem crossing, TTeT is triplet-triplet energy transfer and TTA is triplet-triplet annihilation. The solid coloured lines represent radiative processes.

A lot of factors have to be considered when selecting a viable pair of chromophores to use in a TTA-EU system. The photosensitizer must be able to absorb long wavelength radiation in the visible to near-IR region, sensitizer's triplet energy must be rapidly transferred to the emitter molecules and the emitter triplet states must be long lived with respect to the TTA rate<sup>[3]</sup> The commonly used photosensitizers are organometallic complexes containing metals such as  $\text{Ir}^{3+}$  and  $\text{Ru}^{2+}$  that exhibit metal-to-ligand charge transfer transitions,<sup>[18, 20]</sup> simple organics,<sup>[17, 21]</sup> and metallated porphyrins/phthalocyanines that contain metals such as  $\text{Pt}^{2+}$ ,  $\text{Pd}^{2+}$ ,<sup>[22]</sup> or  $\text{Zn}^{2+}$  (Table 1.1). The presence of a heavy metal in porphyrins and phthalocyanines strongly enhances spin-orbit coupling which yields intersystem crossing (ISC) near unity.<sup>[3]</sup> If the triplet excitation energy of the acceptor is lower than that of the donor then bimolecular quenching of the triplet donor may occur by triplet-triplet energy transfer.<sup>[19]</sup> The energetics of upconversion require that the singlet and triplet excited states of the donor be enveloped between those of the acceptor. As a result, acceptor/annihilator molecules have been largely limited to polycyclic aromatic hydrocarbons as they conveniently possess large splitting in their singlet-triplet energy gaps.<sup>[22d]</sup> This permits the relevant photosensitizer levels to be sandwiched between singlet-triplet energy gaps of the acceptor. To date, several reports have been published on EU systems in solution. However, only a few reports have

appeared on EU systems where chromophores are immobilized on a support. It is on this background that this current research finds relevance. A table illustrating some donors and acceptors used previously in EU along with their solvent systems is presented below (Table 1.1).

**Table 1.1** Some energy upconversion systems reported in the literature.

*S	Donor	$\lambda$ excitation /nm	Acceptor	$\lambda$ emission /nm	Solvent	Mechanism
[21b]1	2,3-Butadione 	442	2,5-Diphenyloxazole (PPO) 	360	benzene	TTA
[18]2		450	Pyrene 	360-420	DCM	TTA
[18]3		450	1,6-di-tert-butylpyrene 	390+/-8	DCM	TTA
[20]4	Ru(dmb) <sub>3</sub> 	514.5, 488	Anthracene 	430	CH <sub>3</sub> CN	TTA
[20b]5	Ru(bmb) <sub>3</sub> 	514.5, 488	9,10-Diphenylanthracene 	430	CH <sub>3</sub> CN	TTA
[20b]6	2,4,5,7-tetraiodo-6-hydroxy-3-fluorone (THF) 	540, 532	9,10-Diphenylanthracene 	434	THF-MeOH	TTA
[22a]7	PdOEP 	532	9,10-Diphenylanthracene 	440	benzene	TTA
[23]8	ZnTPP 	532	Perylene 	450-495 nm	benzene	TTA
[23]9	ZnTPP 	532	Coumarin 343(C343) 	450-495 nm	benzene	TTA

[22d]10		635+/-5		527	benzene	TTA
[22d]11		635+/-5		548	benzene	TTA
[22e]12		635		475	styrene oligomer matrix	TTA
[22e]13		635		560	styrene oligomer matrix	TTA
[22e]14		635		513	styrene oligomer matrix	TTA
[22b]15		532		440	toluene	TTA
[22b]16		635		approx 495	toluene	TTA
[22b]17		695		570	toluene	TTA
[24]18		800		543	polymeric matrix	TPA

\*S is the EU system and the reference

### 1.1.6 Advantages of TTA in EU

The main drawbacks of TPA and ETU are the high power density and coherent light requirements.<sup>[17]</sup> Recently, photon upconversion has been achieved by TTA using low excitation intensities<sup>[20b, 21b, 22b, 22e]</sup> and non coherent light sources.<sup>[22a]</sup>

It is crucial to realize, for the purposes of this thesis, that TTA is the preferred mechanism as continuous wave light sources (most importantly solar irradiation) are useable as opposed to TPA and ETU where pulsed lasers are most commonly used. This enables practical applications to be possible using sunlight as well as ordinary light sources. Furthermore, TPA and ETU can be eliminated as possible mechanisms for EU systems investigated in this thesis. TPA occurs in a single system, where a single species is sequentially or simultaneously excited by two photons, before fluorescence emission. In TPA the excited state is at an energy level that is the sum of the absorbed photons. ETU occurs in rare-earth ion systems, and high light intensities are required. The chromophores used in this thesis, polycyclic aromatic hydrocarbons and organometallics, have been extensively used in TTA-based EU.<sup>[18, 20]</sup> In addition, the absorption and emission characteristics of a TTA-based system are a spectroscopic signature of the donor and acceptor molecules.

## 1.2 Supramolecular Assembly-based Energy Upconversion

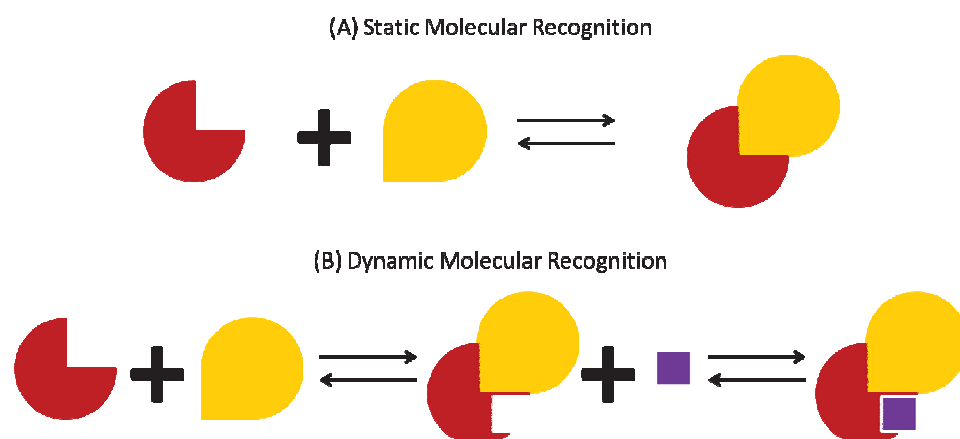
### 1.2.1 Supramolecular Chemistry Principles

Supramolecular chemistry deals with the interactions between molecules, their recognition and how they assemble and function on a molecular scale.<sup>[25]</sup> This provides a bottom up approach to nanoscale systems applicable to biology and materials science.<sup>[26]</sup> A supramolecular device is an assembly of molecular components designed to achieve specific functions.<sup>[27]</sup> We propose a careful choice of the components to design a supramolecular species specifically designed to carry out photon upconversion. The components can be either organic or inorganic and the components are complexed to each other so there is no dependence on a bimolecular reaction for energy or electron transfer to occur. It is in this phenomenon that we anticipate creating more efficient photon upconversion systems which are not diffusion controlled.

Supramolecular chemistry is an area that involves developing highly complex chemical systems from components interacting by noncovalent intermolecular forces such as electrostatic, hydrophobic, hydrogen bonding, van der Waals,  $\pi$ - $\pi$  stacking as well as metal co-ordination.<sup>[28]</sup> These interactions can generate highly stable assemblies whose balance govern the shape and function of the final assembly.<sup>[29]</sup> The main themes of supramolecular chemistry relevant to our studies; molecular recognition and self-assembly are described below.<sup>[28]</sup>

### 1.2.1.1 Molecular recognition

Molecular recognition refers to the directed assembly of two or more components through non-specific, non-covalent forces such as hydrogen bonding, dipole-dipole interactions,  $\pi$ - $\pi$  interactions and co-ordinate bonding. The interactions of the individual subunits involved in molecular recognition require that they are able to discriminate the identity and orientation of other components.<sup>[30]</sup> Molecular recognition relies on preorganization, based on the making and breaking of non-covalent bonds following a strategy incorporated into the design of the molecular components.<sup>[31]</sup> Molecular recognition can be static or dynamic (Figure 1.9). Static molecular recognition resembles the lock and key model; takes only enthalpy into account, whereas in dynamic molecular recognition, both enthalpy and entropy contributions have to be considered.<sup>[32]</sup>



**Figure 1.9** Static molecular recognition occurs between a guest and a host binding site (A). An example of dynamic recognition where binding the first guest induces a conformational change that promotes association of the second guest at the second binding site (B).

In dynamic recognition, when the first guest molecule binds at the first binding site a conformational change occurs that affects the association constant of the second

guest at the second binding site.<sup>[33]</sup> Allosteric systems exhibit dynamic molecular recognition properties which are important to regulate binding in biological systems. Positive allosterism occurs when the binding of the first guest increases the association constant of the second guest to the host (Figure 1.9B). In negative allosteric systems the binding of the first guest decreases the association constant of the second one.<sup>[33]</sup>

#### **1.2.1.2 Self-assembly**

Molecular self-assembly is the spontaneous organization of molecules under equilibrium conditions into stable, structurally well-defined aggregates joined usually by non-covalent bonds without control from an external source.<sup>[34]</sup> Covalent self-assembly is also observed with alkoxysilanes in silanization in which a surface of mineral components like mica, glass and metal oxide is functionalized with organofunctional alkoxysilane molecules. These surfaces can all be silanized, because they contain hydroxyl groups which attack and displace the alkoxy groups on the silane thus forming a covalent -Si-O-Si- bond.<sup>[35]</sup> Self-assembly can be classified into intra and inter-molecular self-assembly

A particularly important example of self assembly provided by duplex DNA has inspired the greatest efforts to design non-biological self-assembling structures.<sup>[29]</sup> DNA provides a predictable and programmable self-assembly system material according to simple Watson-Crick and other higher order base-pairing rules.<sup>[36]</sup> A single strand of DNA can find its complement in solution with extraordinary selectivity through hydrogen-bonding,  $\pi$ - $\pi$  stacking and other non-covalent forces. The unique predictable control with DNA gives researchers a precise assembly code to define which strands will pair, and result in double helices and other uniform structures that can be easily well-characterized. These desirable properties of DNA coupled with the development of automated DNA synthesis are crucial in DNA nanotechnology, in which strands of nucleic acids spontaneously organize into stable 2D and 3D structures. DNA nanotechnology encompasses synthesizing and characterizing nucleic acid complexes and materials that assemble into a static equilibrium end state or complexes with useful non-equilibrium behavior such as the ability to reconfigure based on a chemical or physical stimulus.

### 1.3 Aspects of Supramolecular assembly-based energy upconversion (EU)

Recent reviews by Singh-Rachford and Castellano<sup>[3]</sup> and Ceroni<sup>[37]</sup> provide in-depth analyses of the practical considerations that need to be taken into account to make EU viable. Here, we summarize some of the important points raised. Firstly, to make progress towards practical applications development of solid state devices is more preferable to solution based ones. Solid state EU materials would enable development of wavelength-shifting films, tuneable solid state lasers, can be used for harnessing of red and near IR parts of the solar spectrum in photovoltaics.<sup>[3]</sup> However, the two crucial steps in the EU process; namely triplet-triplet energy transfer and triplet-triplet annihilation are dynamic processes which require collision of chromophores. This means this mechanism takes place only if there is a certain degree of translational mobility.<sup>[37]</sup> In addition, it is essential that such chromophores are brought in close proximity (within Dexter distances) so that the bimolecular energy transfer processes can occur. This is supported by experiments in which EU from chromophores incorporated in a rubbery polymeric matrix was suppressed at 77 K below the glass transition temperature of the polymer.<sup>[3]</sup> Increase in temperature up to 400 K was followed by increasing upconverted fluorescence emission intensity, as a result of faster diffusion rates until polymer could no longer serve as a host.<sup>[3]</sup>

Secondly, in some cases selective excitation of the donor results in simultaneous sensitization of both singlet excited state and excimer of the acceptor, with the latter inevitably degrading the energy stored in the all-important acceptor singlet excited state.<sup>[18]</sup> As a result, some chromophore mixtures such as  $[\text{Ru}(\text{dmb})_3]^{2+}$  (dmb = 4,4'-dimethyl-2,2'-bipyridine) and 9,10-dimethylantracene (DMA) are capable of producing either predominantly upconversion from singlet excited state emission (~425 nm), or predominantly excimer downconversion (~700 nm). In some cases both upconversion and excimer emission are produced in almost equal portions, thereby resulting in an overall broad-band emission profile (400 – 700 nm) appearing white in color, depending on concentrations and/or excitation power.<sup>[38]</sup>

Thirdly, in order to have any viable EU system in the solid state the distance between the donor and the acceptor must be optimized to have (i) a fast rate of TTeT, (ii) a

slow rate of reverse energy transfer from the excited singlet acceptor back to the donor, and (iii) sufficient exclusion of oxygen, normally achieved in solution systems by standard deaeration techniques.<sup>[37]</sup>

## 1.4 Research Aim

The aim of this research project is to create a novel energy upconversion (EU) system using a DNA scaffold and organic chromophores. This system is meant to achieve energy upconversion through triplet-triplet annihilation (TTA). Energy upconversion using organic chromophores captured into a water-soluble dendrimer,<sup>[39]</sup> and organic chromophores incorporated into solid polymer films<sup>[40]</sup> have been reported. The use of a scaffold in an energy upconversion system enables careful control of the distances between system components as well as the number of interacting chromophores. This makes it possible to optimize conditions for upconversion and to create a switchable EU system which can be switched on and off depending on the environment. Energy upconversion in solution has been reported previously in the literature.<sup>[17-18, 20b, 21b, 22a, 22d, 23]</sup> However, it is difficult to carefully control the number of interacting chromophores as well as distances between chromophores in solution.

We hypothesize that the requirement of TTA-based EU for chromophores to be within Dexter distances can be achieved using DNA as a scaffold. DNA can be used to control the number and distance between chromophores due to its helical structure with an inter-base pair distance of 3.4 Å between adjacent bases. This means that if chromophores are assembled on to DNA, and if chromophores are within 3 base pairs (10.2 Å) then TTA-based EU may occur. This thesis aims to evaluate various assemblies of chromophores on DNA and find conditions which lead to TTA-based EU using DNA.

Based on literature reports summarized in Table 1.1, we decided to use metallated porphyrins and ruthenium polypyridyl complexes as donors for EU, and polycyclic aromatic hydrocarbons, such as anthracene and pyrene derivatives as acceptors for EU. The need for chromophores to be attached to DNA narrows the range of



modified molecules, depending on the chemical functionalization that can be performed on these chromophores.

The proposed system assembly includes the following components:

- (i) DNA which serves the purpose of a scaffold on which organic chromophores are attached/ arranged.
- (ii) A triplet photosensitizer, a metallated porphyrin or a ruthenium polypyridyl complex in our case, which acts as a long wavelength light absorber.
- (iii) A singlet photoemitter, a pyrenyl or anthracenyl derivative in our case, which acts as a short wavelength light emitter.

Energy upconversion systems are very desirable as they have the potential for a wide range of applications. As mentioned in the previous section, a scaffold allows for careful control of the distances between system components as well as the number of interacting chromophores. In addition, scaffolded EU systems could be easily incorporated into thin films compared to systems in solution. EU systems that are incorporated into thin films could be easily fabricated for practical uses.<sup>[40]</sup>

These systems may find the following applications, among others:

- (i) To harness longer wavelength radiation from the sun in dye sensitized solar cells (DSSCs). This in turn helps to improve the efficiency of DSSCs.
- (ii) To help sensitize photodynamic therapy (PDT) agents which require shorter wavelength radiation to function. Red light has good tissue penetration. A red-blue EU system then produces blue light from the red light *in vivo*.
- (iii) A green-blue EU system could be used to upconvert a green organic light emitting diode (OLED) input to produce a blue OLED output. This could be applied to other colours.
- (iv) To produce UV light from visible light, or alternatively visible light from infra-red light.

We propose two different approaches to achieve DNA templated energy upconversion; covalent attachment of the chromophores of interest to a DNA backbone and non-covalent assembly of chromophores on DNA.

### 1.4.1 Covalent Assembly

The following steps are proposed for the DNA-based system.

- (i) Synthesis of various porphyrins as photosensitizers for EU with different absorption and emission properties as well as different functional groups for DNA attachment. Azide and oxime functionalities were proposed for attaching porphyrins to DNA through the formation of 1,2,3-triazoles and isoxazoles, respectively.
- (ii) Synthesis of various anthracenyl and pyrenyl derivatives with azide and oxime functionalities as possible photoemitters.
- (iii) Synthesis of oligonucleotides (ONs) with terminal triple bond modifications at different positions on the sequence using an automated DNA synthesizer.
- (iv) Covalent attachment of photosensitizers and photoemitters to different positions on DNA which will allow for precise control of number of chromophores and controlling the distance between them.

### 1.4.2 Non covalent Assembly

This approach entails pre-synthetic modification of DNA using (*R*)-1-*O*-[4-(1-pyrenylethynyl)phenylmethyl]glycerol, commonly known as a twisted intercalating nucleic acid (TINA monomer, referred to as PEPy in the free state in this thesis), which acts as a photoemitter in EU. The TINA monomer has been extensively studied in our lab and its phosphoramidite is available for insertion into DNA in place of a nucleobase. We plan to determine the interactions of TINA-modified DNAs with free photosensitizers in solution. By studying several assemblies we aim to find the most suitable systems for EU. In this thesis, TINA monomer will be referred to as PEPy when free in solution, as done in Chapter 4.

We assume that TINA moieties attached on the DNA sequence form a hydrophobic cluster. We hypothesize that free chromophores (photosensitizers) in solution will be more attracted to the TINA clusters than the polyphosphate DNA backbone, thereby bringing chromophores in close enough proximity (Dexter distances) to allow TTA-based EU to take place.

## 1.5 Thesis Outline

This thesis discusses the use of DNA as a scaffold for the organized assembly and communication of different chromophores for application in energy upconversion systems. Chapters 1-3 are devoted to the presentation of concepts important for the thesis and Chapters 4-8 describe results obtained, followed by a Final conclusion and Future Directions. Chapters 11 and 12 describe experimental details.

Chapter 2 describes the desirable properties of polycyclic aromatic hydrocarbons, porphyrins and ruthenium polypyridyl complexes for EU.

In Chapter 3, we discuss the use of DNA as a nano-tool for constructing functional photonic systems.

Chapter 4 gives an in-depth insight into the potential feasibility of our targeted DNA-based energy upconversion systems. Herein, we describe a comprehensive study of the interactions of our chosen chromophores when they are free in solution. The interactions of ZnTMPyP4, the  $\text{Zn}^{2+}$  derivative of 5,10,15,20-tetrakis-(1-methyl-4-pyridyl)-21*H*,23*H*-porphine with free TINA monomer and  $[\text{Ru}(\text{bpy})_3]^{2+}$ , tris(2,2'-bipyridine)ruthenium(II) with TINA in organic solvents were carried out. Furthermore, ZnTMPyP4-TINA and  $[\text{Ru}(\text{bpy})_3]^{2+}$ -TINA energy upconversion systems free in solution were analyzed in detail as proof of concept for our motivation to attempt studies using DNA as a scaffold.

Chapter 5 is dedicated to the synthesis of appropriately functionalized organic chromophores together with numerous attempts to covalently attach these chromophores to DNA bearing terminal alkynes. This chapter highlights the successes and failures involved in covalent modification of DNA with chromophores.

Chapter 6 gives a detailed description of the interactions of ZnTMPyP4 with TINA-modified DNA duplexes. This work was published in the *Journal of Photochemistry and Photobiology A: Chemistry*, **2014**, 288, 76-81. This supramolecular assembly strategy was preferred in our case for building DNA-scaffolded energy upconversion

systems, described later in this thesis. Our results obtained showed enhanced interaction between ZnTMpyP4 and TINA on a DNA duplex template, which provided motivation for expanding the study to the interaction of  $[\text{Ru}(\text{bpy})_3]^{2+}$  with DNA duplexes (Chapter 7), and  $[\text{Ru}(\text{bpy})_3]^{2+}/\text{ZnTMpyP4}$  with G-quadruplexes (Chapter 8).

In Chapter 7 we replace ZnTMpyP4 with  $[\text{Ru}(\text{bpy})_3]^{2+}$  as our chromophore in solution interacting with TINA-modified DNA duplexes.

Chapter 8 is an extension of the work described in Chapters 6 and 7. This section describes the improved interaction of the chosen chromophores, ZnTMpyP4 and  $[\text{Ru}(\text{bpy})_3]^{2+}$  with TINA-modified G-quadruplex structures compared to duplexes.

Chapter 9 goes into details on energy upconversion of systems involving DNA and selected chromophores. Analysis of systems of interest and the first proof of principle of DNA-based EU by TTA are described.

Chapter 10 provides final conclusions and describes future directions.

Experimental procedures and Appendix are in Chapters 11 and 12 respectively.

## 1.6 References

- [1] W. Denk, J. Strickler, W. Webb, *Science* **1990**, 248, 73.
- [2] a)F. Auzel, *Chemical Reviews* **2003**, 104, 139; b)T. Soukka, T. Rantanen, K. Kuningas, *Annals of the New York Academy of Sciences* **2008**, 1130, 188.
- [3] T. N. Singh-Rachford, F. N. Castellano, *Coordination Chemistry Reviews* **2010**, 254, 2560.
- [4] E. M. Chan, *Chemical Society Reviews* **2015**, 44, 1653.
- [5] J. Collins, in *Biophotonics: Spectroscopy, Imaging, Sensing, and Manipulation*, Springer, **2011**, pp. 261.
- [6] N. V. Tkachenko, *Optical spectroscopy: methods and instrumentations*, Elsevier, **2006**.
- [7] F. Auzel, *Chemical Reviews* **2004**, 104, 139.
- [8] W. Clarkson, *Journal of Physics D: Applied Physics* **2001**, 34, 2381.
- [9] G. Wang, Q. Peng, Y. Li, *Accounts of Chemical Research* **2011**, 44, 322.
- [10] J. R. Lakowicz, *Principles of fluorescence spectroscopy*, Springer Science & Business Media, **2007**.
- [11] D. C. Harris, *Quantitative chemical analysis*, Macmillan, **2010**.
- [12] A. Periasamy, R. Day, *Molecular imaging: FRET microscopy and spectroscopy*, Elsevier, **2011**.
- [13] D. L. Andrews, A. A. Demidov, *Resonance energy transfer*, Wiley New York, **1999**.
- [14] D. L. Dexter, *The Journal of Chemical Physics* **1953**, 21, 836.
- [15] K. Rohatgi-Mukherjee, *Fundamentals of photochemistry*, New Age International, **1978**.
- [16] B. Valeur, M. N. Berberan-Santos, *Molecular fluorescence: principles and applications*, John Wiley & Sons, **2012**.
- [17] H.-C. Chen, C.-Y. Hung, K.-H. Wang, H.-L. Chen, W. S. Fann, F.-C. Chien, P. Chen, T. J. Chow, C.-P. Hsu, S.-S. Sun, *Chemical Communications* **2009**, 4064.
- [18] W. Zhao, F. N. Castellano, *The Journal of Physical Chemistry A* **2006**, 110, 11440.
- [19] H. Sternlicht, G. C. Nieman, G. W. Robinson, *The Journal of Chemical Physics* **1963**, 38, 1326.
- [20] a)R. R. Islangulov, F. N. Castellano, *Angewandte Chemie* **2006**, 118, 6103; b)R. R. Islangulov, D. V. Kozlov, F. N. Castellano, *Chemical Communications* **2005**, 3776.
- [21] a)T. R. Monguzzi A, F. Meinardi, *J. Phys. Chem.* **2009**, 113, 1171; b)T. N. Singh-Rachford, F. N. Castellano, *The Journal of Physical Chemistry A* **2009**, 113, 5912.

- [22] a)S. Balushev, T. Miteva, V. Yakutkin, G. Nelles, A. Yasuda, G. Wegner, *Physical Review Letters* **2006**, 97, 143903; b)S. Balushev, V. Yakutkin, T. Miteva, G. Wegner, T. Roberts, G. Nelles, A. Yasuda, S. Chernov, S. Aleshchenkov, A. Cheprakov, *New Journal of Physics* **2008**, 10, 013007; c)T. N. Singh-Rachford, F. N. Castellano, *The Journal of Physical Chemistry Letters* **2009**, 1, 195; d)T. N. Singh-Rachford, A. Haefele, R. Ziessel, F. N. Castellano, *Journal of the American Chemical Society* **2008**, 130, 16164; e)M. Tzenka, Y. Vladimir, N. Gabriele, B. Stanislav, *New Journal of Physics* **2008**, 103002.
- [23] S. K. Sugunan, U. Tripathy, S. M. K. Brunet, M. F. Paige, R. P. Steer, *The Journal of Physical Chemistry A* **2009**, 113, 8548.
- [24] A. Abbotto, L. Beverina, R. Bozio, S. Bradamante, G. A. Pagani, R. Signorini, *Synthetic Metals* **2001**, 121, 1755.
- [25] J.-M. Lehn, *Science* **1993**, 260, 1762.
- [26] a)J.-M. Lehn, *Proceedings of the National Academy of Sciences* **2002**, 99, 4763; b)J.-M. Lehn, *Science* **2002**, 295, 2400.
- [27] J.-M. Lehn, *Angewandte Chemie International Edition in English* **1988**, 27, 89.
- [28] G. V. Oshovsky, D. N. Reinhoudt, W. Verboom, *Angewandte Chemie International Edition* **2007**, 46, 2366.
- [29] A. C. Mendes, E. T. Baran, R. L. Reis, H. S. Azevedo, *Wiley Interdisciplinary Reviews: Nanomedicine and Nanobiotechnology* **2013**, 5, 582.
- [30] J. Rebek, *Angewandte Chemie International Edition in English* **1990**, 29, 245.
- [31] a)G. M. Whitesides, E. E. Simanek, J. P. Mathias, C. T. Seto, D. Chin, M. Mammen, D. M. Gordon, *Accounts of Chemical Research* **1995**, 28, 37; b)M. C. T. Fyfe, J. F. Stoddart, *Accounts of Chemical Research* **1997**, 30, 393; c)P. Timmerman, Leonard J. Prins, *European Journal of Organic Chemistry* **2001**, 2001, 3191; d)L. J. Prins, D. N. Reinhoudt, P. Timmerman, *Angewandte Chemie International Edition* **2001**, 40, 2382.
- [32] M. Albrecht, *Naturwissenschaften* **2007**, 94, 951.
- [33] S. Shinkai, M. Ikeda, A. Sugasaki, M. Takeuchi, *Accounts of Chemical Research* **2001**, 34, 494.
- [34] G. Whitesides, J. Mathias, C. Seto, *Science* **1991**, 254, 1312.
- [35] B. Seed, in *Current Protocols in Cell Biology*, John Wiley & Sons, Inc., **2001**.
- [36] C. K. McLaughlin, G. D. Hamblin, H. F. Sleiman, *Chemical Society Reviews* **2011**, 40, 5647.

- [37] P. Ceroni, *Chemistry – A European Journal* **2011**, 17, 9560.
- [38] T. N. Singh-Rachford, R. R. Islangulov, F. N. Castellano, *The Journal of Physical Chemistry A* **2008**, 112, 3906.
- [39] K. Tanaka, K. Inafuku, Y. Chujo, *Chemical Communications* **2010**, 46, 4378.
- [40] R. R. Islangulov, J. Lott, C. Weder, F. N. Castellano, *Journal of the American Chemical Society* **2007**, 129, 12652.

## 2 Spectroscopic properties of Organic Chromophores applied in EU

### 2.1 Porphine and Porphyrins

Porphyrins are organic compounds which occur in nature, where they perform biological roles involving photophysical and redox processes. Porphyrins are heterocyclic macrocycles composed of four modified pyrrole subunits interconnected at their  $\alpha$  carbon atoms via methine bridges to give highly-conjugated aromatic systems with 18  $\pi$  electrons delocalized. The parent porphyrin is porphine (Figure 2.1).

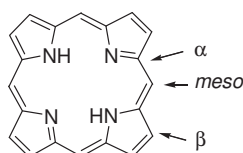


Figure 2.1 Structure of porphine, the parent porphyrin.

5,10,15,20-Tetraphenylporphyrin ( $H_2TPP$ ) consists of four phenyl rings in the *meso* positions, which are orthogonal to the plane of the porphyrin core (Figure 2.2).

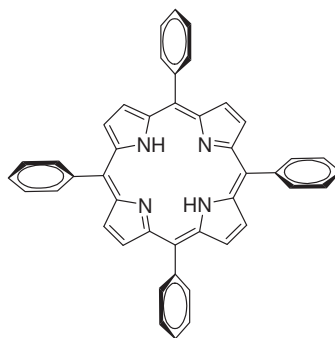


Figure 2.2 Structure of 5,10,15,20-tetraphenylporphyrin ( $H_2TPP$ ).

The free base porphyrin has two protons bound to the nitrogens as in the tautomers A and B (Figure 2.3).

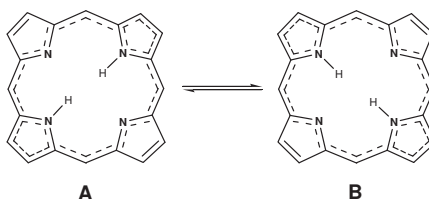
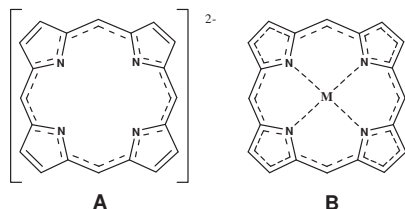


Figure 2.3 Tautomeric forms of free base porphine.

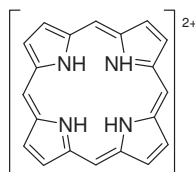


Deprotonation gives the dianion, which with few exceptions acts as a tetraligand with most metal ions to give metalloporphyrins (Figure 2.4). The resulting internal and external aromatic ring system gives the porphyrin considerable chemical and thermal stability.



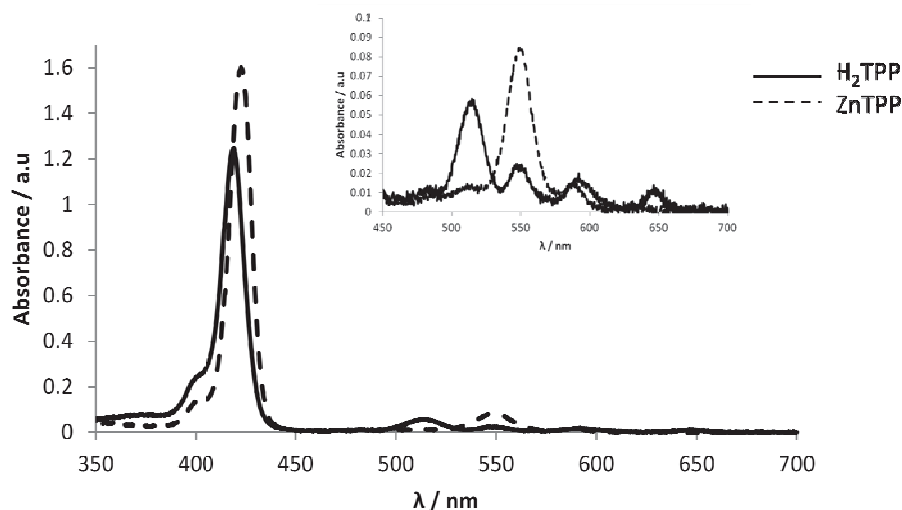
**Figure 2.4** Deprotonated porphyrins. Unmetallated (A), metallated (B).

Alternatively, protonation of the free porphyrin nitrogens could occur, giving rise to the positively charged acidified form (Figure 2.5).



**Figure 2.5** Protonated porphine.

Porphyrins typically have very intense absorption bands in the visible region and may be deeply coloured due to  $\pi$ - $\pi^*$  transitions. The  $\pi$ - $\pi^*$  transitions dominate the spectra due to their high molar absorptivities. The spectra have a very intense Soret or B band (380-500 nm) and weaker Q bands in the visible region 500-750 nm, Figure 2.6. The Soret band involves the transition from the ground state to the second excited state ( $S_0$  to  $S_2$ ), whilst the Q band region consists of weak transitions to the first excited state ( $S_0$  to  $S_1$ ).<sup>[1]</sup> The B band transition is strongly allowed, whereas the Q band transitions are only weakly allowed.<sup>[2]</sup> It was the intention of this project to use porphyrins as photosensitizers due to their high molar absorptivities in the visible region.<sup>[1]</sup>



**Figure 2.6** Typical UV-Vis absorption spectra of a free base porphyrin ( $H_2TPP$ ) and Zn (II) metalloporphyrin ( $ZnTPP$ ) in toluene showing the Soret and Q bands. Insert: expanded Q band region.

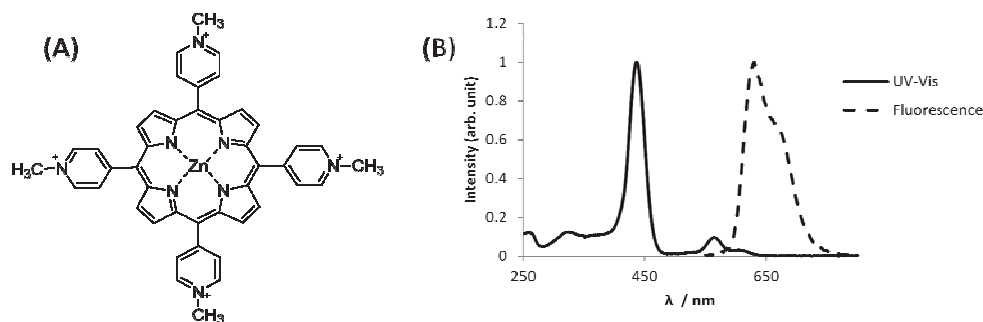
The structure of the porphyrin allows for two main positions for the chemical extension of the molecule, the  $\beta$ -pyrrolic position and the *meso* position (Figure 2.1). In both free base and metallated porphyrins, the photophysical and photochemical properties of the macrocycle are influenced by the various substituents attached to the perimeter ( $\beta$ -pyrrolic and *meso* positions) of the porphyrin ring. We initially attempted  $\beta$ -pyrrolic functionalized porphyrins for covalent attachment to DNA as they have advantages over *meso* functionalization (Chapter 5).<sup>[3]</sup> Groups attached to the *meso* phenyl ring result in the disruption of the conjugation between the porphyrin core and the attached group due to the phenyl *meso* ring sitting orthogonal to the plane of the porphyrin core. In contrast, modifications at the  $\beta$ -pyrrolic position result in a system that is in the same plane as the porphyrin core. On the other hand, *meso*-functionalized porphyrins are easily accessible, can be made water soluble by using quaternary pyridinium moieties, and they are known to interact with DNA.<sup>[4]</sup> Hence, Chapters 4, and 6 - 9 made use of a zinc cationic porphyrin, tetrakis(4-*N*-methylpyridyl) zinc (II) porphyrin, abbreviated as ZnTMpyP4.

### 2.1.1 Zinc tetramethylpyridinium porphyrin (ZnTMpyP4)

Porphyrins have many key roles essential for life processes. A wide variety of porphyrins have been synthesized over the years as they have proven to be useful in anti-cancer therapy, catalysis, electronics, photonics and many other research

fields.<sup>[5]</sup> The porphyrin ring provides a vacant site at its center that binds metals to form complexes. Metallation typically changes the absorption spectrum from four Q – bands (~ 500 – 750 nm) to two Q – bands in addition to the Soret band (~ 400 – 450 nm) attributed to enhancing of the  $D_{2h}$  symmetry of the free-base porphyrin to  $D_{4h}$  (Figure 2.6).<sup>[6]</sup> The most intense, higher energy Soret or B – band of free-base porphyrins result from strongly allowed  $\pi$ -  $\pi^*$  transitions whereas the less intense Q – bands are quasi-allowed. The first set of Q – bands is the x-component of Q, while the second set is its y-component. The  $Q_x$  and  $Q_y$  components are composed of two types of vibrational excitations too, resulting in the four lines  $Q_{x,(0,0)}$ ,  $Q_{x(1,0)}$ ,  $Q_{y(0,0)}$  and  $Q_{y(1,0)}$  in increasing order of energy. In metallated porphyrins the two Q bands are vibronic components of the same transition. Metallation of porphyrins is generally desirable for our studies since heavy atoms can promote intersystem crossing producing triplet excited states essential for triplet-triplet energy transfer to a suitable acceptor leading to photon upconversion.<sup>[6]</sup>

Cationic porphyrins particularly have several interesting properties which make them attractive photosensitizers, for use in possible photon upconversion systems. ZnTMPyP4 (Figure 2.7A) is a water soluble porphyrin and it has a high quantum yield for triplet state formation (0.90).<sup>[7]</sup>



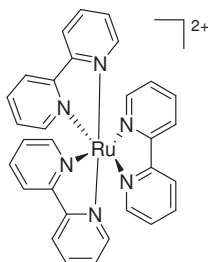
**Figure 2.7** Structure of ZnTMPyP4 (A). Normalized UV-Vis absorption and fluorescence emission spectra of 10.0  $\mu$ M ZnTMPyP4 in MilliQ  $H_2O$  at  $C$ ,  $\lambda_{ex} = 430$  nm (B).

ZnTMPyP4 possesses several desirable properties required for a donor in a photon upconversion system such as strong visible light absorption, efficient intersystem crossing, a long lived triplet state and a large singlet-triplet energy gap to prevent back intersystem crossing to the singlet state.<sup>[8]</sup> ZnPMpyP4 is a water soluble analogue of ZnTPP which was used in TTA-based EU (Table 1.1).

The UV-Vis absorption spectrum of ZnTMpyP4 typically has an intense absorption peak at around 438 nm assigned to the Soret or B(0,0) band and weaker peaks at around 564 nm and 605 nm assigned to Q(1,0) and Q(0,0) bands respectively (Figure 2.7B). The steady state fluorescence spectra typically have a peak at 630 nm with a shoulder at 660 nm.<sup>[9]</sup>

## 2.2 Ru<sup>2+</sup> Polypyridyl Complexes

Ruthenium polypyridyl complexes are among the most studied family of compounds in inorganic photochemistry. They are very interesting since they have a comparatively long excited state lifetime and have a variety of applications ranging from light harvesting, photovoltaics and organic light emitting diodes, information storage, and oxygen sensors.<sup>[10]</sup> Such complexes are widely considered for applications in biodiagnostics, photovoltaics and organic light-emitting diode. In addition, they are well known DNA binders.<sup>[11]</sup>



**Figure 2.8** Structure of tris(bipyridine)ruthenium(II), [Ru(bpy)<sub>3</sub>]<sup>2+</sup>.

[Ru(bpy)<sub>3</sub>]<sup>2+</sup>, in particular, has been chosen for our studies because of its unique properties such as strong fluorescence, long emission lifetime, energy and electron transfer reactions, strong long wavelength absorption (~450 nm with an extinction coefficient of ~11,500 M<sup>-1</sup>cm<sup>-1</sup>), chemical stability and photostability.<sup>[12]</sup> The triplet excited state of [Ru(bpy)<sub>3</sub>]<sup>2+</sup> has both oxidizing and reducing properties because it can be described as a Ru<sup>3+</sup> complex containing a bpy<sup>-</sup> (anionic bi-pyridine ligand). After absorbing a photon, excited [Ru(bpy)<sub>3</sub>]<sup>2+\*</sup> transfers an electron, located on one bpy ligand, to a sacrificial oxidant such as persulfate. The resulting [Ru(bpy)<sub>3</sub>]<sup>3+</sup> is a powerful oxidant and oxidizes water into O<sub>2</sub> and protons via a metal oxide catalyst.<sup>[13]</sup> Alternatively, the reducing power of [Ru(bpy)<sub>3</sub>]<sup>2+\*</sup> can be harnessed to reduce methylviologen, a recyclable carrier of electrons, which in turn reduces protons at a platinum catalyst. For this process to be catalytic, a sacrificial reductant,

such as triethanolamine is provided to return the  $\text{Ru}^{3+}$  back to  $\text{Ru}^{2+}$ . Photoredox catalysis using a combination of  $[\text{Ru}(\text{bpy})_3]^{2+}$  catalyst and visible light has been considered as a bond-forming strategy for organic synthesis<sup>[14]</sup>. Depending on the choice of suitable reductive or oxidative quencher, the  $[\text{Ru}(\text{bpy})_3]^{2+}$  catalyst can be used to trigger photoreduction or photooxidation, respectively.<sup>[14-15]</sup>  $[\text{Ru}(\text{bpy})_3]^{2+}$  has been recently used as a photosensitizer, which acts as a long wavelength absorber and an energy donor to an acceptor in photon upconversion.<sup>[16]</sup>

$[\text{Ru}(\text{bpy})_3]^{2+}$  is an octahedral coordination complex, which can be resolved into its enantiomers, which are kinetically stable (Figure 2.8). We used a racemic mixture as our studies do not necessarily require enantiomerically pure isomers.

$\text{Ru}^{2+}$  is a  $d^6$  electronic configuration, and so as an octahedral complex its electrons are in the low-spin  $t_{2g}^6$  configuration. Incident light at about 450 nm ( $\sim 2.0$  eV) promotes one of these electrons to a ligand anti-bonding orbital, so a metal to ligand charge transfer occurs ( $^1\text{MLCT}$ ), (Figure 2.9). Transfer to  $^3\text{MLCT}$  by intersystem crossing is efficient (heavy atom effect) and emission by the radiative  $^3\text{MLCT}$  state to the ground state occurs at  $\sim 600$  nm ( $\sim 2.0$  eV) in water. The typical absorption and emission data are shown in Figure 2.10.

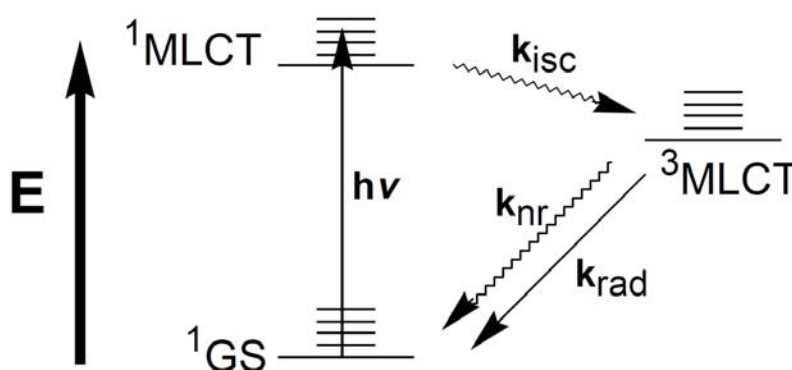
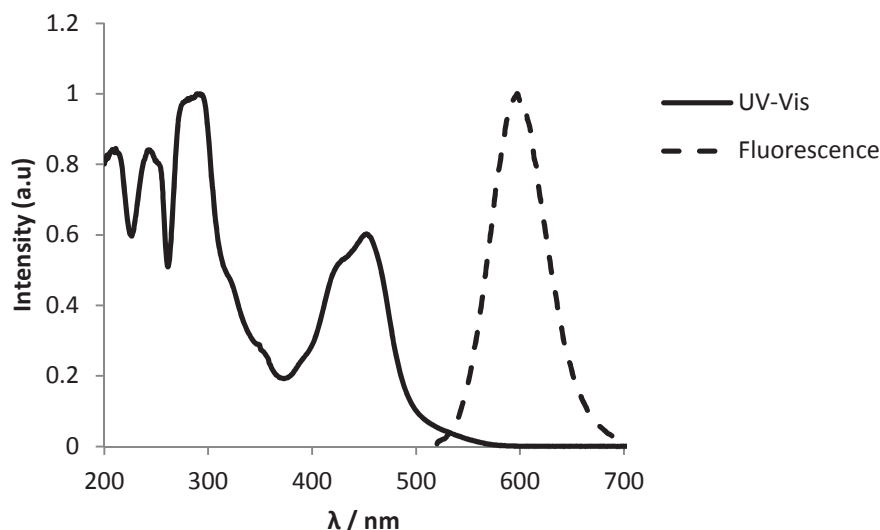


Figure 2.9 Jablonski diagram of  $[\text{Ru}(\text{bpy})_3]^{2+}$  luminescence.

The absorption peaks in the UV range between 200 – 300 nm are assigned to ligand-ligand transitions (L-L) while the long wavelength absorption around 450 nm is assigned to a metal to ligand charge transfer ( $^1\text{MLCT}$ ).



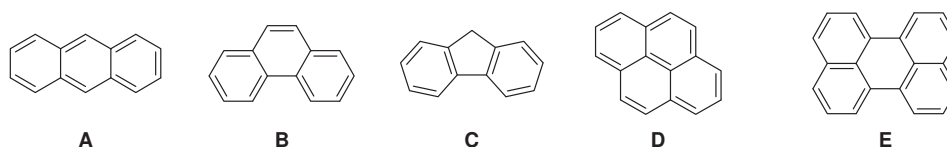
**Figure 2.10** Normalized UV-Vis absorption and fluorescence emission spectra of 100  $\mu\text{M}$   $[\text{Ru}(\text{bpy})_3]^{2+}$  recorded in  $\text{H}_2\text{O}$  at 25  $^\circ\text{C}$ ,  $\lambda_{\text{ex}} = 500$  nm.

The luminescence properties of the excited state of this complex are very sensitive to solvent polarity and viscosity. The excited state is stabilized in polar solvents which means that there is better overlap of the vibrational levels of the ground and excited state, so the non radiative deactivation process is more efficient. Therefore on changing to a less polar solvent the emission lifetime and the quantum yield of emission increases.

### 2.2.1 Polycyclic aromatic hydrocarbons (PAHs)

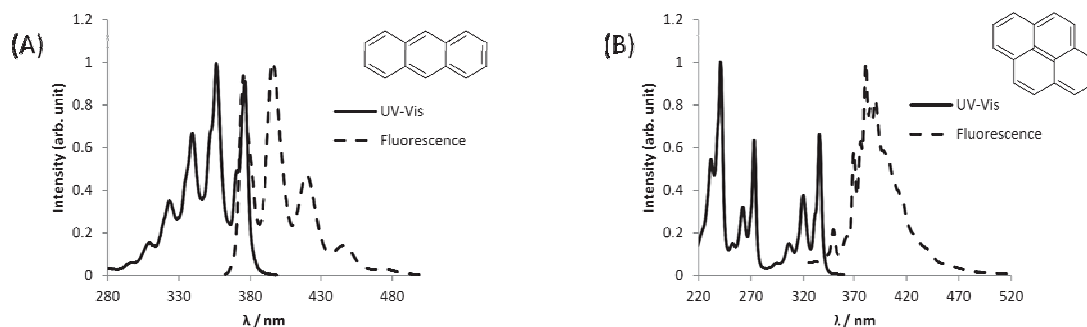
Anthracene and pyrene fall in a class of organic compounds called polycyclic aromatic hydrocarbons (PAHs), also known as polyaromatic hydrocarbons or polynuclear aromatic hydrocarbons. PAHs consist of fused aromatic rings. Phenanthrene and anthracene, which both contain three fused aromatic rings, are the simplest examples of PAHs. PAHs occur in oil, coal, and tar deposits, and are produced as by-products of fuel burning. As a pollutant, they are of concern because some compounds have been identified as carcinogenic, mutagenic, and teratogenic. PAHs are also found in cooked foods, for example, in meat cooked at high

temperatures such as grilling or barbecuing, and in smoked fish. PAHs may contain four-, five-, six- or seven-member rings, but those with five or six are most common. Anthracene and pyrene contain only six-membered rings (Figure 2.11). Anthracene consists of three rings whilst pyrene consists of four rings.



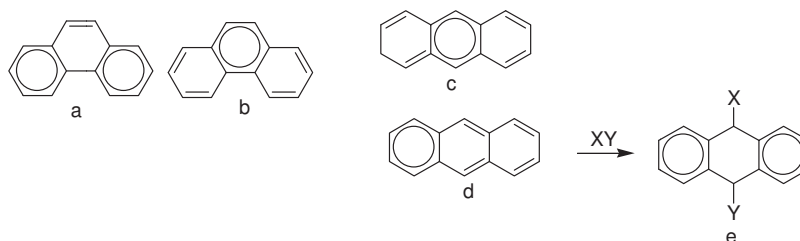
**Figure 2.11** Examples of PAHs. (A) anthracene, (B) phenanthrene, (C) fluorene, (D) pyrene, (E) perylene.

PAHs possess very characteristic UV absorbance spectra. These often possess many absorbance bands and are unique for each ring structure. In general, the frequency of  $S_1 \rightarrow S_0$  transition decreases as the number of aromatic rings increases. This increase in  $\pi$  conjugation causes the energy spacing between the highest occupied molecular orbital and lowest unoccupied molecular orbital to decrease resulting in a red shifting of the absorption spectrum (e.g. tetracene is yellow while anthracene is white).<sup>[17]</sup> The introduction of groups such as methyl, vinyl, phenyl groups, or heteroatoms results in a shift in absorption spectra, whereas no effect is observed when the heteroatom is separated from the aromatic ring system. Most PAHs are also fluorescent, emitting characteristic wavelengths of light when they are excited. The PAHs normally fluoresce efficiently in homogeneous media.<sup>[17]</sup> Planar rigid PAHs such as anthracene and pyrene fluoresce more efficiently than their non planar counterparts at the expense of their less efficient radiationless deactivation of the excited singlet state ( $^1S^*$ ). Fluorescence spectra and lifetimes of PAHs are sensitive to solvent polarity.<sup>[17]</sup> The potential application of anthracenyl and pyrenyl derivatives depend on their high fluorescence quantum yields as well as their fluorescence emission on the blue end of the spectrum (Figure 2.12). The quantum yields of anthracene and pyrene in cyclohexane are 0.36 and 0.32, respectively.<sup>[18]</sup>



**Figure 2.12** Normalized UV-Vis and fluorescence emission spectra of anthracene (0.5 mM, A) and pyrene (25 μM, B) dissolved in cyclohexane at 25°C.  $\lambda_{\text{ex}}$  (anthracene) = 350 nm,  $\lambda_{\text{ex}}$  (pyrene) = 317 nm.

Although PAHs clearly are aromatic compounds, the degree of aromaticity can be different for each ring segment according to Clar's model.<sup>[19]</sup> In this model for PAHs the resonance structure with the most disjoint aromatic  $\pi$ -sextets (benzene-like moieties) is the most important for the characterization of the properties. For example, in phenanthrene the Clar structure (a) has two sextets at the extremities, while resonance structure (b) has just one central sextet (Figure 2.13). Therefore in this molecule the outer rings are firmly aromatic while its central ring is less aromatic and therefore more reactive.



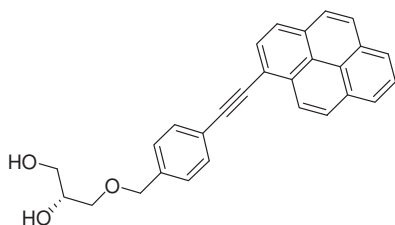
**Figure 2.13** Clar structures of phenanthrene (a and b), anthracene (c and d). Addition reaction on anthracene (d-e).

In contrast, in anthracene (Figure 2.13) the number of sextets is just one and aromaticity spreads out. However, reaction at the central ring by addition leads to a product that has two aromatic sextets (outer rings), a gain of one extra aromatic sextet compared to anthracene itself. Clar's model can also be used to explain the decrease in stability and aromaticity of larger acenes. The accuracy of Clar's model in predicting PAH reactivity has been confirmed experimentally in a number of cases.<sup>[17]</sup>



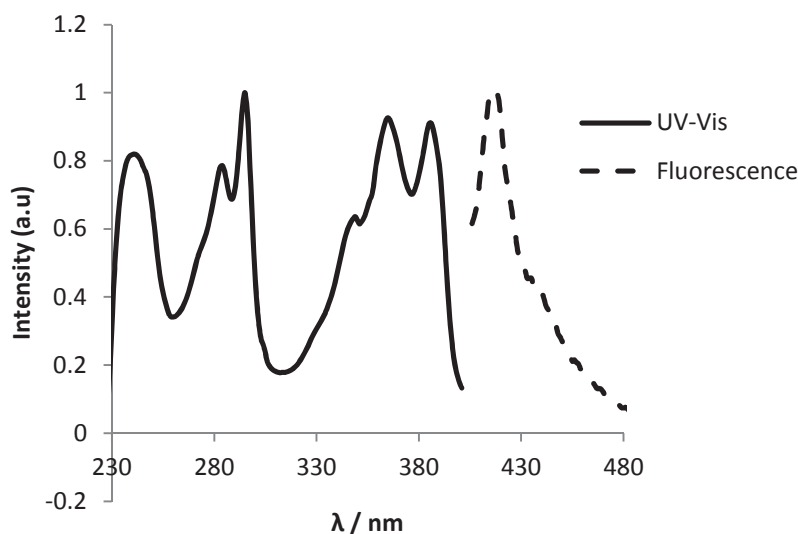
### 2.2.1.1 (*R*)-1-*O*-[4-(1-Pyrenylethynyl)phenylmethyl]glycerol

The absorption maxima of arylalkynyl-substituted pyrenes are red-shifted compared to pyrene due to  $\pi$ -conjugation extension.<sup>[20]</sup> Pyrene exhibits monomer fluorescence emission peaks (375 – 405 nm) and an additional excited dimer band around 460 nm when an excited pyrene fluorophore encounters another ground state pyrene.<sup>[21]</sup> The absorption coefficients of alkynylpyrenes are increased relative to pyrene.<sup>[20a]</sup> This is accompanied by increased fluorescence emission quantum yields, from ~0.32 for pyrene to ~0.99 for alkynylpyrenes.<sup>[20a]</sup> In addition, fluorescent alkynylpyrenes are less sensitive to quenching by oxygen dissolved in solvents.<sup>[20a]</sup> The pyrene derivative (*R*)-1-*O*-[4-(1-pyrenylethynyl)phenylmethyl]glycerol (TINA monomer), was used in this thesis.



**Figure 2.14** (*R*)-1-*O*-[4-(1-Pyrenylethynyl)phenylmethyl]glycerol, PEPy or free TINA monomer. The TINA monomer in the free state is abbreviated as PEPy in Chapter 4.

The UV-Vis and emission spectra for PEPy are illustrated, with the fluorescence maximum at 417 nm (Figure 2.15).



**Figure 2.15** Normalized UV-Vis absorption and fluorescence emission spectra of 25.0  $\mu$ M TINA monomer (PEPy) in DCM at 25  $^{\circ}$ C,  $\lambda_{\text{ex}}$  = 375 nm.

## 2.3 References

- [1] R. Giovannetti, *The Use of Spectrophotometry UV-Vis for the Study of Porphyrins*, InTech Publisher, Rijeka, **2012**.
- [2] L. R. Milgrom, *The Colours of Life: An Introduction to the Chemistry of Porphyrins and related Compounds*, Vol. 232, Oxford University Press, Oxford, **1997**.
- [3] A. W. I. Stephenson, N. Bomholt, A. C. Partridge, V. V. Filichev, *ChemBioChem* **2010**, *11*, 1833.
- [4] a)J. M. Kelly, M. J. Murphy, D. J. McConnell, C. OhUigin, *Nucleic Acids Research* **1985**, *13*, 167; b)F. Qu, N.-Q. Li, *Electroanalysis* **1997**, *9*, 1348.
- [5] A. E. H. Machado, W. R. Gomes, D. M. S. Araújo, H. S. Miglio, L. T. Ueno, R. D. Paula, J. A. S. Cavaleiro, N. M. B. Neto, *Molecules* **2011**, *16*, 5807.
- [6] K. Kahn, T. C. Bruice, *The Journal of Physical Chemistry B* **2003**, *107*, 6876.
- [7] A. Harriman, G. Porter, M.-C. Richoux, *Journal of the Chemical Society, Faraday Transactions 2: Molecular and Chemical Physics* **1981**, *77*, 833.
- [8] C. P. Ponce, R. P. Steer, M. F. Paige, *Photochemical & Photobiological Sciences* **2013**, *12*, 1079.
- [9] M. John Plater, S. Aiken, G. Bourhill, *Tetrahedron* **2002**, *58*, 2415.
- [10] S. Glazier, J. A. Barron, N. Morales, A. M. Ruschak, P. L. Houston, H. D. Abruña, *Macromolecules* **2003**, *36*, 1272.
- [11] a)Y. Xiong, X.-F. He, X.-H. Zou, J.-Z. Wu, X.-M. Chen, L.-N. Ji, R.-H. Li, J.-Y. Zhou, K.-B. Yu, *Journal of the Chemical Society, Dalton Transactions* **1999**, *19*; b)L.-N. Ji, X.-H. Zou, J.-G. Liu, *Coordination Chemistry Reviews* **2001**, *216*, 513; c)H. Chao, L.-N. Ji, *Bioinorganic Chemistry and Applications* **2005**, *3*, 15; d)S. Satyanarayana, J. C. Dabrowiak, J. B. Chaires, *Biochemistry* **1993**, *32*, 2573; e)J. K. Barton, J. M. Goldberg, C. V. Kumar, N. J. Turro, *Journal of the American Chemical Society* **1986**, *108*, 2081; f)J. K. Barton, A. Danishefsky, J. Goldberg, *Journal of the American Chemical Society* **1984**, *106*, 2172.
- [12] M. Asha Jhonsi, A. Kathiravan, G. Paramaguru, C. Manivannan, R. Renganathan, *Journal of Solution Chemistry* **2010**, *39*, 1520.
- [13] M. Hara, C. C. Waraksa, J. T. Lean, B. A. Lewis, T. E. Mallouk, *The Journal of Physical Chemistry A* **2000**, *104*, 5275.
- [14] J. M. R. Narayanam, C. R. J. Stephenson, *Chemical Society Reviews* **2011**, *40*, 102.
- [15] K. Zeitler, *Angewandte Chemie International Edition* **2009**, *48*, 9785.
- [16] B. M. Wilke, F. N. Castellano, *Journal of Chemical Education* **2013**, *90*, 786.

- [17] R. Dabestani, I. N. Ivanov, *Photochemistry and Photobiology* **1999**, 70, 10.
- [18] I. Berlman, *Handbook of fluorescence spectra of Aromatic Molecules*, Academic Press, San Diego, **1971**.
- [19] Z. Chen, H. Jiao, D. Moran, A. Hirsch, W. Thiel, P. v. Ragué Schleyer, *Journal of Physical Organic Chemistry* **2003**, 16, 726.
- [20] a)H. Maeda, T. Maeda, K. Mizuno, K. Fujimoto, H. Shimizu, M. Inouye, *Chemistry-a European Journal* **2006**, 12, 824; b)S.-W. Yang, A. Elangovan, K.-C. Hwang, T.-I. Ho, *The Journal of Physical Chemistry B* **2005**, 109, 16628.
- [21] G. K. Bains, S. H. Kim, E. J. Sorin, V. Narayanaswami, *Biochemistry* **2012**, 51, 6207.

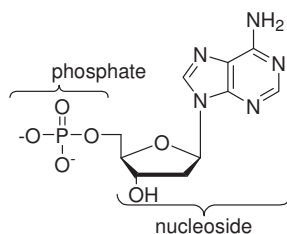
### 3 DNA in Creation of Functional $\pi$ -systems

#### 3.1 DNA Structure

Deoxyribonucleic acid (DNA) is a nucleic acid which carries genetic instructions for the biological development of all cellular forms of life and many viruses. The main function of DNA molecules is the long-term storage of information. In bacteria and other simple cell organisms, DNA is distributed more or less throughout the cell. In plants, animals and in other multi-celled organisms, most of the DNA is located in the cell nucleus. The energy-generating organelles known as chloroplasts and mitochondria also carry DNA.

The information in DNA is stored as a code made up of four chemical bases: adenine (A), guanine (G), cytosine (C), and thymine (T), (Figure 3.3). A fifth base, uracil (U), replaces thymine in RNA. These bases are classified into two types; adenine and guanine are fused five- and six-membered heterocyclic compounds called purines, while cytosine, thymine and uracil are six-membered rings called pyrimidines (Figure 3.3).

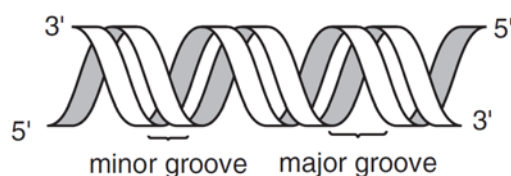
The four bases are attached to the sugar/phosphate to form the complete nucleotide, as shown for 2'-deoxyadenosine monophosphate (Figure 3.1). A base linked to a sugar is called a nucleoside. The pentafuranose sugar 2'-deoxyribose found in DNA is replaced by ribose in RNA. A nucleotide is a nucleoside monophosphate. DNA and RNA are polynucleotides.



**Figure 3.1** A nucleotide, 2'-deoxyadenosine monophosphate

In a polynucleotide, nucleosides are joined together by phosphate groups that form phosphodiester bonds between the third (3') and fifth (5') carbon atoms of adjacent sugar rings. These asymmetric bonds mean a strand of DNA has a direction. In living

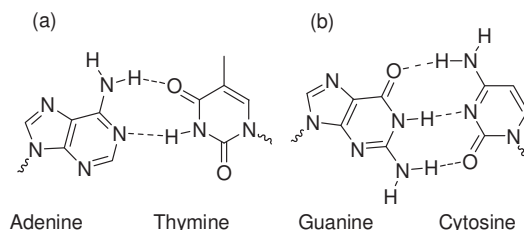
organisms, DNA exists as a pair of molecules that are held tightly together in the form of a right-handed spiral called a double helix or double stranded DNA (dsDNA) (Figure 3.2).<sup>[1]</sup> In a double helix the direction of the nucleotides in one strand is opposite to their direction in the other strand. The strands are said to be antiparallel (Figure 3.2 below).



**Figure 3.2** A representation of the DNA antiparallel duplex.

The nucleotide repeats contain both the segment of the backbone of the molecule, which holds the chain together, and a base, which interacts with the other DNA strand in the double helix. The shape of the double helix depends on a set of forces involved in the formation of DNA complexes and also the hydration level of the DNA complex. The forces are hydrogen bonding between matching bases (Watson-Crick base pairing),  $\pi$ - $\pi$  stacking interactions of neighbouring bases, and electrostatic repulsions between the negatively charged phosphate groups on the backbones.<sup>[2]</sup>

In Watson-Crick base pairing, each type of base on one strand forms a bond with just one type of base on the other strand. This is called complementary base pairing and it determines the specificity of which strands stay associated. Purines form hydrogen bonds to pyrimidines, A to T, and C to G (Figure 3.3). These are called base pairs.<sup>[3]</sup>

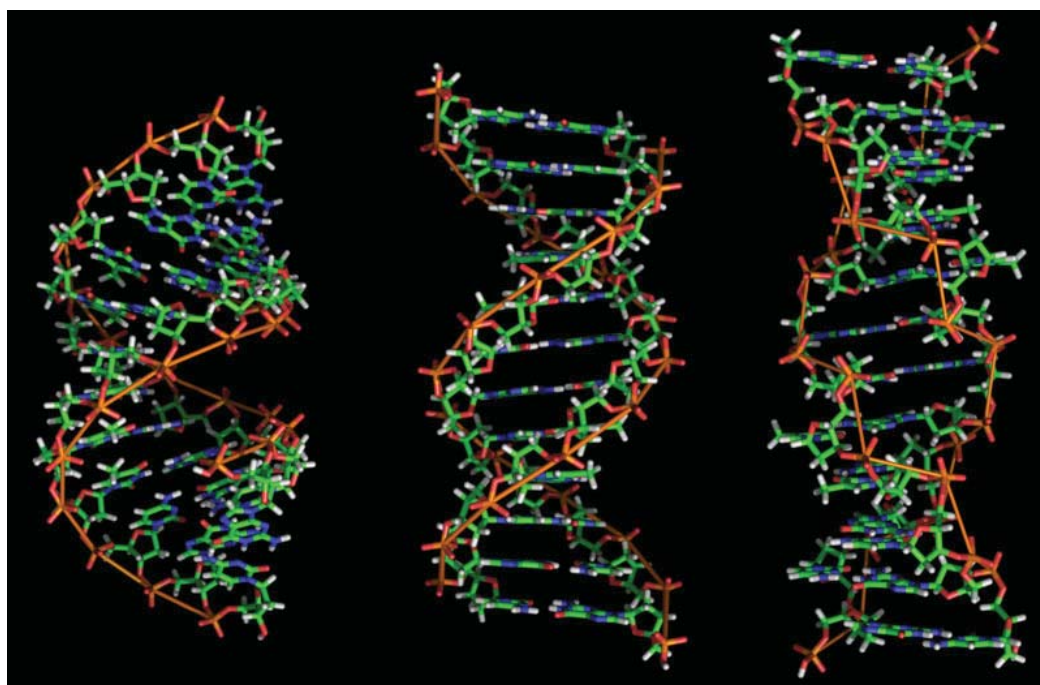


**Figure 3.3** Watson-Crick base pairing. (a) A-T base pair with two hydrogen bonds. (b) G-C base pair with three hydrogen bonds. Hydrogen bonds between the pairs are shown as dashed lines.

A G-C base pair has three hydrogen bonds whilst an A-T base pair has two hydrogen bonds (Figure 3.3). DNA with high GC content is more stable than DNA with low

GC content, but contrary to popular belief, this is not due to the extra hydrogen bond of a GC base pair but rather the contribution of stacking interactions.<sup>[4]</sup>

Depending on the sequence and environment, DNA duplexes can exist in various secondary structures that include A-DNA, B-DNA, and Z-DNA forms (Figure 3.4). Factors such as hydration level, DNA sequence, the amount and direction of supercoiling, chemical modifications of the bases, the type and concentration of metal ions, as well as the presence of polyamines in solution determine the conformation that is adopted by double helical DNA.<sup>[5]</sup> B-DNA is a family of related DNA conformations that is most common at the high hydration levels present in living cells. The B-form of DNA helix twists  $360^\circ$  per 10.6 base pairs in the absence of strain, with 3.4 Å distance between base pairs. But many molecular biological processes can induce strain. A DNA segment with excess or insufficient helical twisting is referred to, respectively, as positively or negatively "supercoiled". The A form is likely to occur only in dehydrated samples of DNA, and possibly in hybrid pairings of DNA and RNA strands. Segments of DNA that cells have methylated for regulatory purposes may adopt the Z geometry, in which the strands turn about the helical axis in a left-handed spiral, the opposite of the more common B form.<sup>[6]</sup>



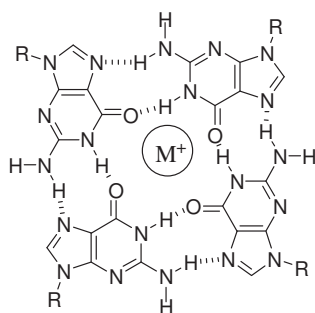
**Figure 3.4** Structures of A, B, and Z-DNA from left to right, respectively. Figure was reproduced from [http://www.die-formatierte-dna.de/html/General%20Theory%20of%20Genexpression/2-die\\_formatierte\\_dna.html](http://www.die-formatierte-dna.de/html/General%20Theory%20of%20Genexpression/2-die_formatierte_dna.html)

In the more common B-form, two grooves twist around the surface of the double stranded DNA duplex, dsDNA (Figure 3.2).<sup>[2]</sup> One groove, the major groove, is 22 Å wide and the other, the minor groove, is 12 Å wide.<sup>[2, 7]</sup> The narrowness of the minor groove means that the edges of the bases are more accessible in the major groove. These grooves are adjacent to the base pairs and may provide a binding site.

Alternative base pairs to Watson-Crick base pairing, called Hoogsteen and reverse-Hoogsteen, result in high order DNA and RNA structures that include DNA triplexes and G-quadruplexes.

### 3.2 G-Quadruplexes

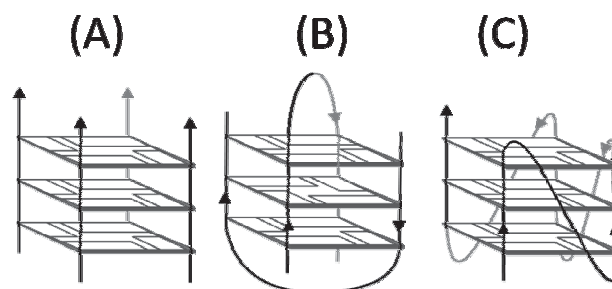
Nucleic acid sequences rich in guanine are capable of forming G-quadruplexes. G-quadruplexes are four-stranded structures built of stacked guanine tetrads (G-tetrads),<sup>[8]</sup> (Figure 3.5). A G-tetrad has each guanine base engaged in four hydrogen bonds via Hoogsteen bonding and such that guanines are related by a four-fold rotation axis and are almost coplanar. Each guanine directs its O6' carboxyl oxygen into the central core of the tetrad and repulsions between these carboxyl oxygens cause destabilization of the complex. Monovalent ions, such as  $K^+$  or  $Na^+$  in the core stabilize the complex by compensating for the repulsion between the carboxyl oxygens.



**Figure 3.5** Hydrogen bond formation in a G-tetrad,  $M^+$  is a monovalent metal cation, such as  $K^+$  or  $Na^+$ . R is ribose or 2'-deoxyribose.

G-Quadruplexes can be formed of DNA, and RNA and may be intra, or intermolecular (Figure 3.6). G-quadruplexes can display a wide variety of topologies based on variations in strand polarity, loop geometry and length, presence of metal ions, concentration in solutions, and so forth.<sup>[2]</sup> A G-quadruplex can adopt a parallel

or an anti-parallel topology depending on how the individual runs of guanine bases are arranged.



**Figure 3.6** Examples of inter (A, B) and intramolecular G-quadruplexes (C). Each square is a G-tetrad. Arrows indicate the 5' to 3' direction.

### 3.3 DNA Functional $\pi$ -systems

DNA has recently been the subject of intense research towards nanotechnological applications. DNA has been reported as a scaffold for carbon nanotube-based electronic devices,<sup>[9]</sup> organic synthesis,<sup>[10]</sup> nanoparticle arrays,<sup>[11]</sup> protein arrays and nanowires,<sup>[12]</sup> and polymers.<sup>[13]</sup> Complementary strand recognition through Watson–Crick or Hoogsteen base-pairing together with fast, standardized and automated solid phase synthesis using phosphoramidite building blocks, as well as the development of numerous methods to introduce molecules in any desired position of the sequence, can be used to specifically design new functional molecules.<sup>[2, 14]</sup> The modifications can be incorporated into the DNA strands at precise sites, and the formation of the duplex will place the substituents in a predetermined and well-defined three-dimensional arrangement.<sup>[15]</sup>

In particular, DNA provides a good structural scaffold for molecular functional  $\pi$ -systems suitable for energy upconversion system since the properties depend on the relative orientation and the resulting photophysical interactions of each of the molecular components to the others.<sup>[14]</sup> The following properties of DNA make it an ideal choice:<sup>[2, 14-16]</sup>

- (i) The ability of two or more oligonucleotide chains with complementary sequences to self-assemble into a defined secondary structure.
- (ii) A regular helical structure with a base pair distance of 3.4 Å which provides a basis for photophysical interactions.

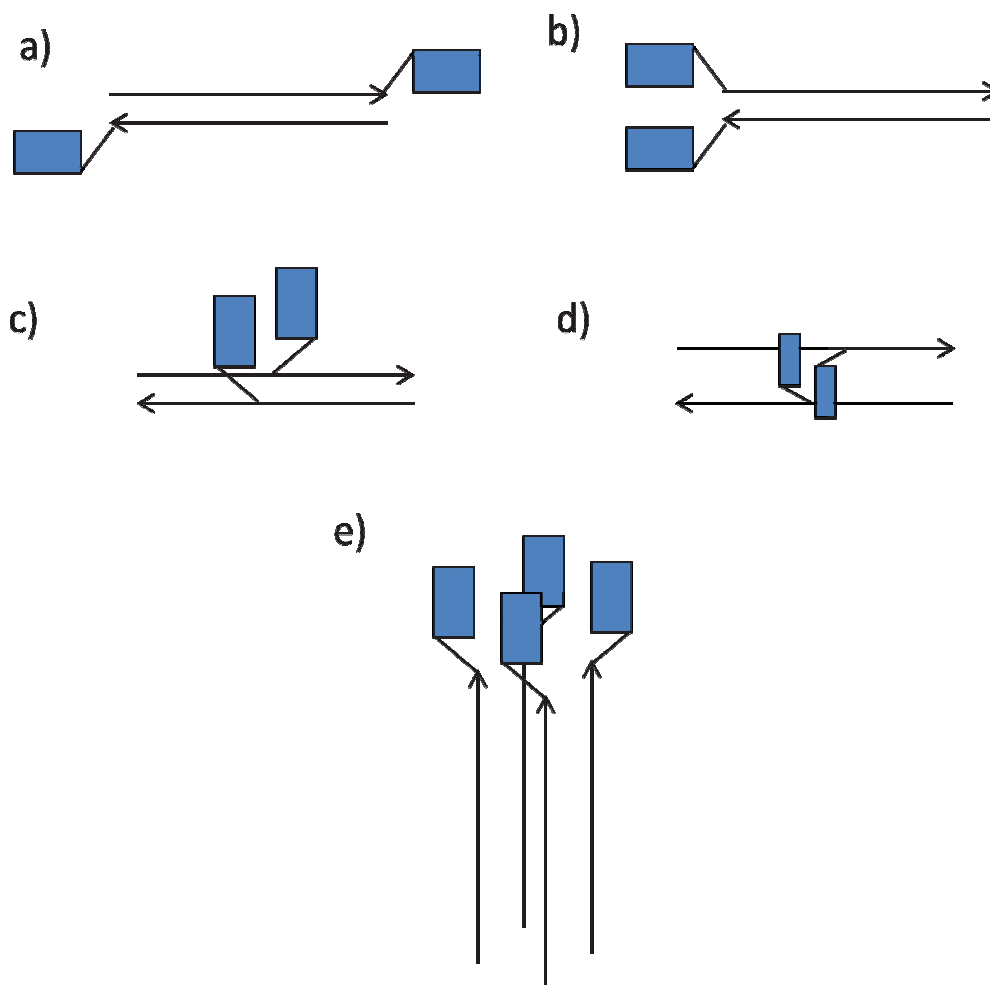


- (iii) DNA is easy to synthesize by standard automated solid phase synthesis.
- (iv) DNA is easy to modify covalently or non-covalently by well established methods.
- (v) Sequence-specific recognition by DNA-binding proteins or other molecules is possible.

In addition, modified DNA can be used to craft functional bioorganic  $\pi$ -system, complex 2D and 3D nanostructures can be formed, and model photonic devices can be created.

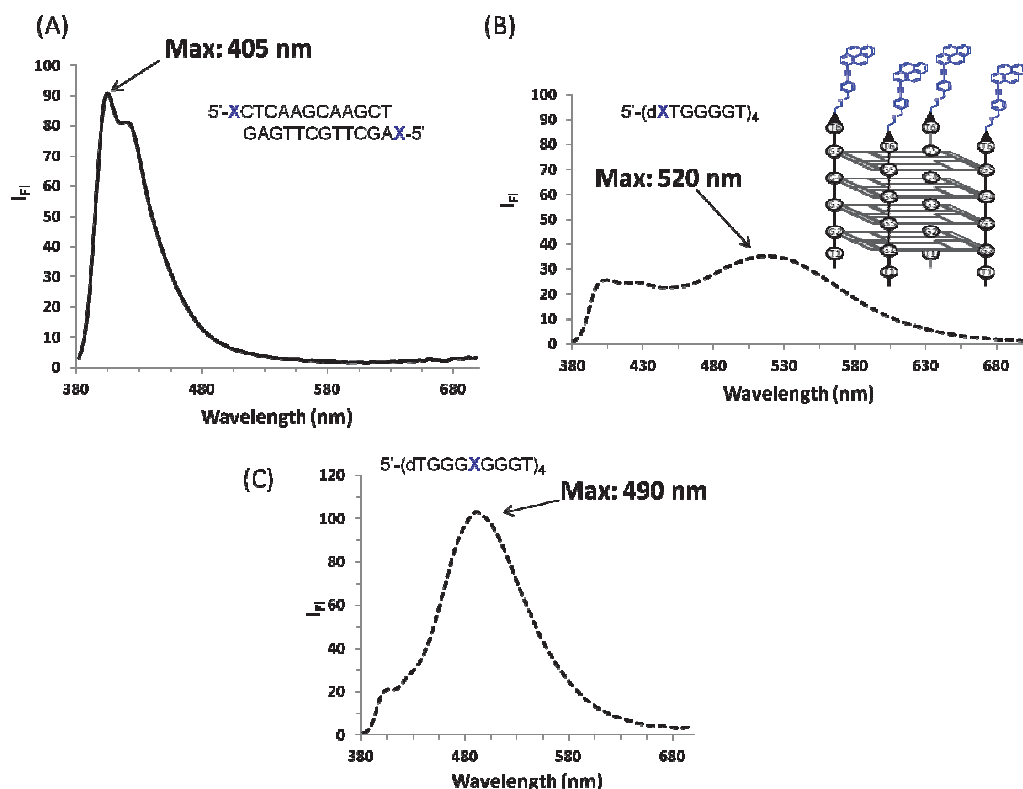
### 3.4 DNA –Chromophore Arrangements

Figure 3.7 shows examples of how chromophores can be arranged on a DNA template. When chromophores are attached to the DNA structure, their UV-Vis and fluorescence spectroscopic properties can be altered.<sup>[17]</sup> There are several known methods of attaching molecules covalently to DNA offering a wide range of options.<sup>[2, 18]</sup> This allows the attachment of chromophores on different positions of DNA; which could be at the end of DNA strands (Figure 3.7a and b) in one of the DNA grooves (Figure 3.7c) or in the middle of the DNA as a base substituent (Figure 3.7d) with duplex DNAs. Furthermore, it is also possible to attach chromophores on G-quadruplexes; which could be at the end of the DNA strands (Figure 3.7e), or in the middle of the DNA strands.



**Figure 3.7** Schematic representation of the arrangement of chromophores on the DNA backbone, an individual chromophore is represented as a blue rectangle, an arrow represents a 5'-end of a DNA strand: a) attachment of a chromophore at the 5'-end of each strand in the duplex; b) arrangement of chromophores on one end of the duplex; c) arrangement of chromophores in minor or in the major groove of the duplex; d) arrangement of chromophores as nucleobase substituents in the duplex; e) arrangement of chromophores at the 5'-end of a parallel intermolecular G-quadruplex.

The difference in fluorescence properties as a result of different arrangements of a chromophore on the DNA can be illustrated using the TINA monomer. It is in this context that we have to introduce the structural perturbations of TINA fluorescence when attached to DNAs.

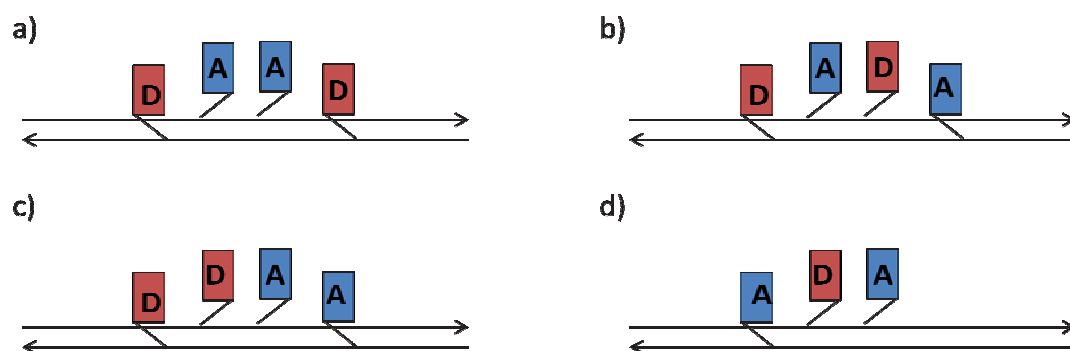


**Figure 3.8** Fluorescence emission spectra of the TINA monomer (X) when positioned at various positions of the DNA template. The TINA monomer was positioned at the 5'-ends of a synthetic DNA duplex (A) and a G-quadruplex (B), as well as in the middle of a G-quadruplex (C). C, pH = 7, 10 mM sodium phosphate buffer, 0.1 mM EDTA, 50 mM NaCl,  $\lambda_{\text{ex}} = 375$  nm.

The TINA exhibits two monomeric bands in the fluorescence emission spectra around 405 and 425 nm in a DNA duplex upon excitation at 375 nm (Figure 3.8A). A similar profile is observed when two TINA monomers are placed opposite each other in the duplex (Figure 3.7d), which is a result of a poor overlap of pyrenes.<sup>[19]</sup> In contrast, when the TINA monomer was placed at the end of a G-quadruplex forming sequence, **5'-dXTG4T**, a strong excited dimer (excimer) band with maximum at 520 nm was observed in the fluorescence emission spectra as a result of pyrene-pyrene interactions realized after G-quadruplex formation (Figure 3.8B). When the TINA monomer was placed in the middle of a G-quadruplex sequence **5'-dTG3XG3T**, the maximum of an excimer band was shifted to 490 nm, which was attributed to the change in the orientation of pyrene units within the complex. (Figure 3.8C).<sup>[20]</sup>

Following a discussion of properties of DNA, described earlier in Chapter 1, Section 1.4 and (ii) above, DNA provides a structural scaffold on which donors and acceptors for EU can be arranged on pre-determined positions (examples in Figure

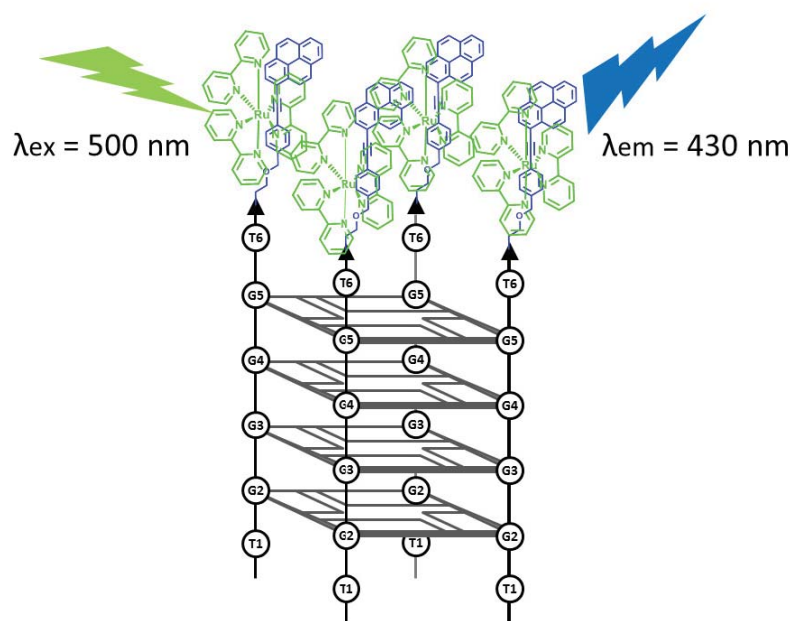
3.9 below). In Figure 3.10  $[\text{Ru}(\text{bpy})_3]^{2+}$  is the donor and TINA monomer the acceptor. Since the TTA-based mechanism involves a bimolecular TTA step involving two acceptors, we hypothesize that it is essential to have at least two acceptors within the DNA structure in close proximity. However, the presence of one or more acceptor/s in close proximity to a donor is required in order for the bimolecular TTeT step to occur between an excited donor and a ground state acceptor. It is quite feasible that one donor could be used to sensitize two acceptors. This could only happen if the rates of acceptor's decay to the ground state, ISC of the donor to the triplet state and TTeT processes combined are far slower than the donor excitation process. This is because the donor has to be excited for the second time, followed by a cross-over to the triplet state, and a transfer of its energy to the second acceptor before the first acceptor decays to the ground state.



**Figure 3.9** Schematic representation of examples of possible arrangements of a donor (D), such as  $[\text{Ru}(\text{bpy})_3]^{2+}$  and an acceptor (A), such as the TINA monomer, in one of the grooves of the DNA duplex. The distance between individual chromophores can be changed depending on the site of their attachment.

It is quite likely that the resulting constructs shown above can lead to effective quenching of fluorescence of both D and A, which is detrimental to EU. As it has been suggested earlier,<sup>[21]</sup> by changing the distance between chromophores on the scaffold the efficiency of EU in multichromophoric systems can be optimized. This can be realized using DNA in which the relative position of chromophores can be determined by the DNA sequence and the site of the chromophores' attachment to the DNA. In light of the above information, we propose that it is worthwhile covalently attaching donor and acceptor molecules on different positions of DNA templates using well known chemical modification methods, thereby altering the

distance between the chromophores (examples in Figure 3.9) This would enable us to identify optimum distances and conditions for EU to occur. It is important to mention that the examples shown in Figure 3.9 are in no way exhaustive. This forms a foundation for a covalent strategy being attempted in this thesis.



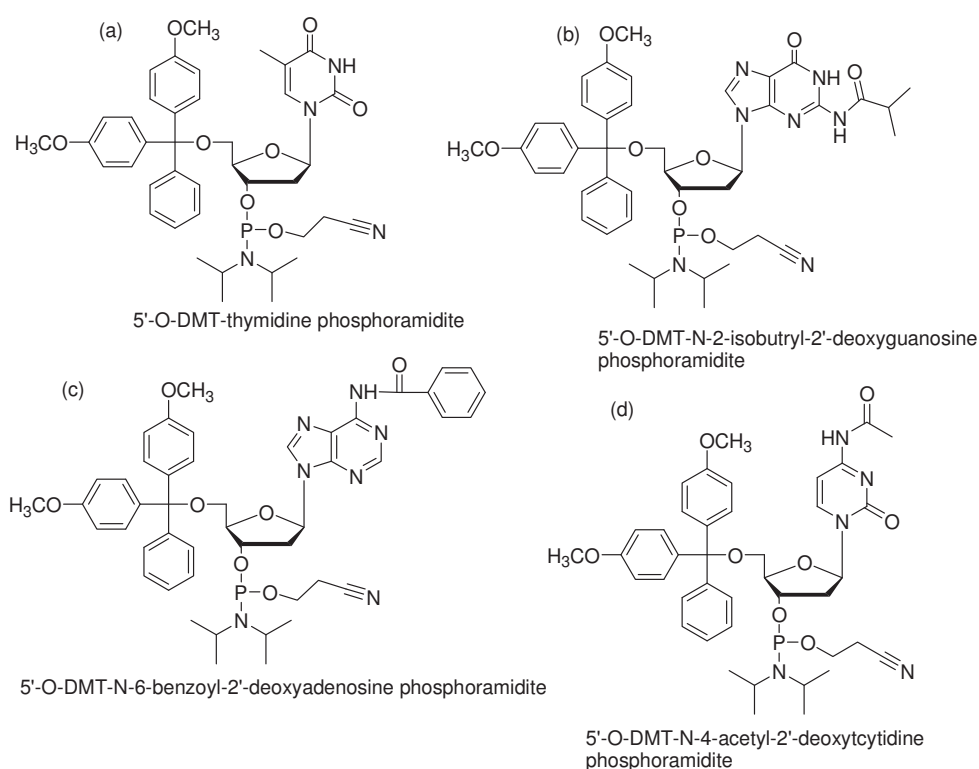
**Figure 3.10** Schematic representation of the arrangement of a G-quadruplex modified with a TINA monomer (acceptor) at the end of the strands in the presence of a donor ( $[\text{Ru}(\text{bpy})_3]^{2+}$ ).

We also hypothesize that the DNA-based EU assembly can be created when either the donor or the acceptor is covalently tethered to DNA, and then the other chromophore is allowed to interact with modified DNA in solution without being covalently attached to DNA (Figure 3.10). Figure 3.10 exemplifies how a G-quadruplex formed by **TG4TX**, onto which a TINA monomer (**X**, acceptor) is covalently attached to the DNA strands, can be allowed to interact with a donor free in solution ( $[\text{Ru}(\text{bpy})_3]^{2+}$ ). The same concept can be applied to other G-quadruplex and DNA structures. This forms a foundation for a 2<sup>nd</sup> strategy (the Supramolecular approach, Section 1.4.2).

### 3.5 DNA Automated Synthesis

The chemical synthesis of DNA has gone through rapid changes that have seen the development of four major methods. The methods are H-phosphonate synthesis, phosphodiester synthesis, phosphotriester synthesis and the phosphoramidite method. The phosphoramidite method is favoured as it uses mild and more selective

reaction conditions. The phosphoramidite technique has been standardized and automated since the late 1970s. As a result, it provides a rapid and inexpensive route to short oligonucleotides up to 200 nucleotide residues in length. The synthesis is based on the use of phosphoramidite monomers as building blocks, the first oligonucleotide is linked to a 5  $\mu\text{m}$  controlled pore glass bead (CPG) solid support, and the synthesis proceeds in the 3' to 5' direction rather than the 5' to 3' synthesis used in nature. 3'-*O*-(*N,N*-Diisopropyl phosphoramidite) derivatives of nucleosides (nucleoside phosphoramidites) are more reactive than the naturally occurring nucleotides (nucleoside 3'- or 5'-phosphates). Exocyclic amine and hydroxy groups have to be rendered unreactive by attaching protective groups, such as acid-labile DMT (4,4'-dimethoxytrityl) or base-labile 2-cyanoethyl groups (Figure 3.11), so as to prevent undesired side reactions.

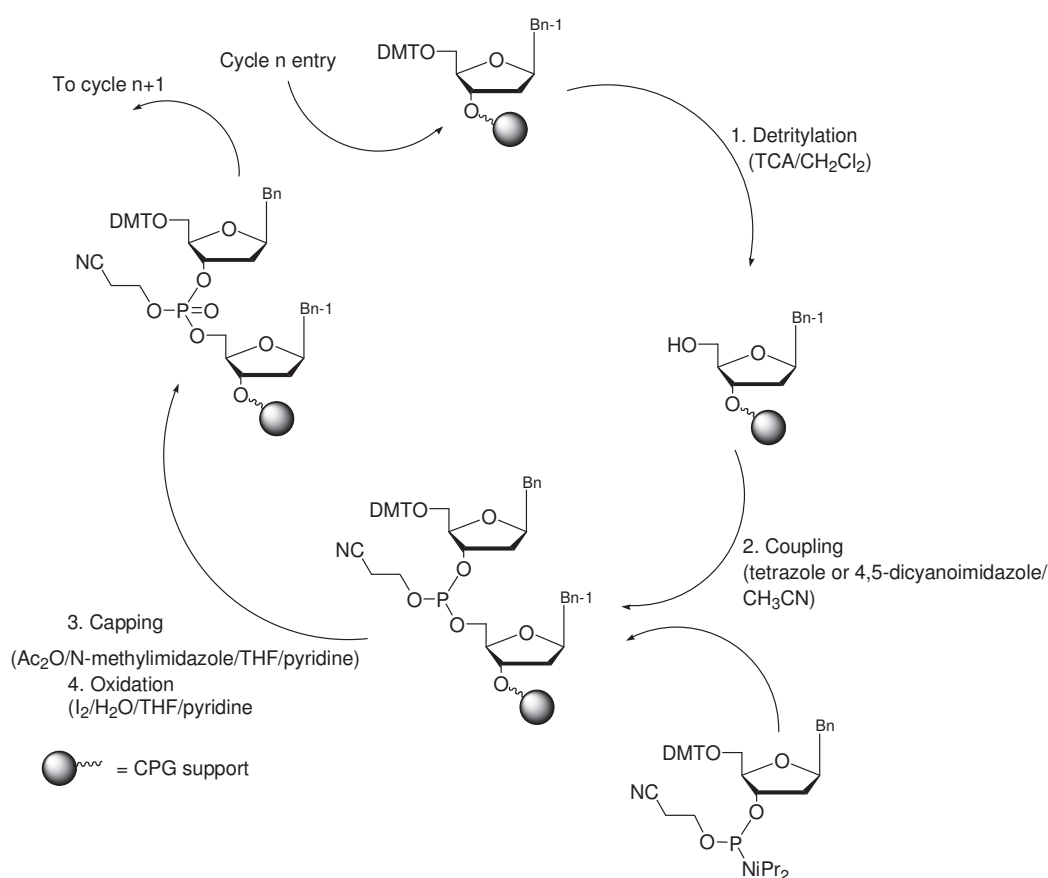


**Figure 3.11** Protected 2'-deoxynucleoside phosphoramidites. The acetyl and isobutryl protecting groups on the A, C, and G monomers are shown, DMT is the 4,4'-dimethoxytrityl group.

The 5'-hydroxyl group is protected by an acid-labile DMT group. The exocyclic amino group of nucleic bases adenine, cytosine, and guanine are protected with base-labile groups. Nucleic bases of thymidine and uridine do not have exocyclic amino groups and hence do not require any protection. The phosphite group is protected by

a base-labile 2-cyanoethyl group. Upon the completion of the oligonucleotide (ON) chain assembly, all the protecting groups are removed and the oligonucleotide is released from the solid support to yield the desired oligonucleotides.

Phosphoramidite synthesis begins with the 3'-nucleotide and proceeds through a series of synthetic cycles composed of four steps that are repeated on each addition of a nucleotide to the 5'-terminus until the desired sequence is assembled. These steps are deprotection, coupling, capping, and oxidation (Figure 3.12).



**Figure 3.12** Synthetic cycle for the preparation of DNA oligonucleotides by the phosphoramidite method.

**Step 1. De-blocking (detritylation):** The DMT group, which is attached to the 5' carbon of the deoxyribose sugar of the recipient nucleotide, is removed by trichloroacetic acid (TCA) or dichloroacetic acid (DCA) leaving a reactive hydroxyl group to which the next base is added.

**Step 2. Coupling:** The next nucleoside phosphoramidite monomer is activated by adding an acidic azole catalyst, 1*H*-tetrazole, 2-ethylthiotetrazole, 2-benzylthiotetrazole or 4,5-dicyanoimidazole. The catalyst protonates the 3'-O-phosphoramidite. The 5'-hydroxy group of the oligonucleotide precursor reacts with the activated phosphoramidite moiety of the incoming nucleoside phosphoramidite to form a phosphite triester linkage. This reaction is very rapid. The phosphoramidite coupling is also highly sensitive to the presence of water and is commonly carried out in anhydrous acetonitrile. The use of 4,5-dicyanoimidazole increases coupling efficiency to greater than 99% which allows longer oligonucleotides to be synthesized.

**Step 3. Capping:** A coupling failure results when an oligonucleotide retains a reactive hydroxyl group on its 5' end. If this were to remain freely reactive, it would be able to couple in the next round and would result in a missing base in the synthesis. Thus, coupling failures must be removed from further participation in the synthesis. This is accomplished by acetylation of the unreacted 5'-hydroxy groups using a mixture of acetic anhydride and *N*-methyl imidazole as a catalyst. This reagent mixture reacts only with free hydroxyl groups to irreversibly cap the oligonucleotides in which coupling failed.

**Step 4. Oxidation:** The last step in the cycle is oxidation which stabilizes the phosphate linkage between the growing oligonucleotide chain and the most recently added base. The phosphate linkage between the first and second base must be stabilized by making the phosphate group pentavalent. This is achieved by adding iodine and water in the presence of a weak base (pyridine, lutidine, or collidine) which leads to the oxidation of the phosphite into phosphate leaving the phosphotriester bond stabilized.

At the end of the synthesis the oligonucleotide protecting groups remain on three of the four bases. The completed synthesis is detritylated and then cleaved off the CPG leaving a hydroxyl on both the 3' and 5' ends. At this point the oligo (base and phosphate) is deprotected by base hydrolysis using ammonium hydroxide at 55 °C. The final product is a functional single-stranded DNA molecule.



### 3.6 DNA Analysis Methods

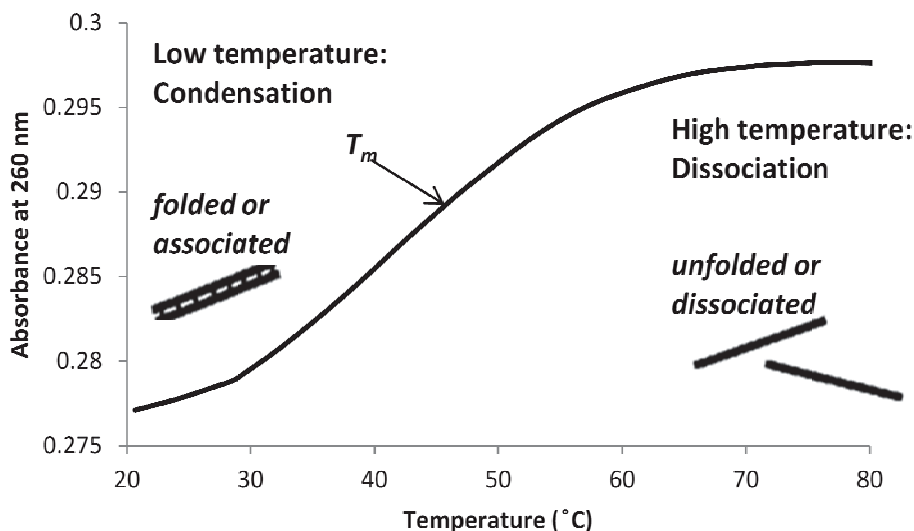
A number of methods exist that are used to study and characterize DNA and its complexes with organic chromophores. The most important ones for this thesis are discussed below:

#### 3.6.1 Gel Electrophoresis

Gel electrophoresis is a method that separates (based on size, electrical charge and other physical properties) macromolecules such as nucleic acids or proteins. Gel electrophoresis is an easy way to separate DNA fragments by their sizes and visualize them. The technique of electrophoresis is based on the fact that DNA is negatively charged at neutral pH due to its phosphate backbone. For this reason, when an electrical potential is placed on the DNA it will move toward the positive pole. The rate at which the DNA will move toward the positive pole is slowed by making the DNA move through a gel. Larger molecules will move slower than smaller molecules. As a result, a mixture of large and small fragments of DNA that has been run through a gel will be separated by size. This enables us to determine the purity of synthesized DNAs as well as establish if chemical modification of DNA has occurred. Polyacrylamide gel is a synthetic gel, thermo-stable, transparent, strong, relatively chemically inert, can be prepared with a wide range of average pore sizes. The gels generally consist of acrylamide, bisacrylamide, urea, and a tris-borate-EDTA (TBE) buffer with adjusted pH. The solution is degassed *in vacuo* to prevent air bubbles during polymerization. Ammonium persulfate and *N,N,N',N'*-tetramethylethylenediamine (TEMED) are added when the gel is ready to be polymerized. The pore size of a gel is determined by two factors, the total amount of acrylamide present and the amount of cross-linker. Polyacrylamide gel electrophoresis (PAGE) can be performed under denaturing or non-denaturing (native PAGE) conditions. DNA samples for denaturing PAGE must be denatured prior to loading, to avoid time dependent denaturation artifacts on the gel. This is usually carried out by the addition of urea or formamide, and heating the samples at 95 – 100 °C for 5 – 10 minutes.

### 3.6.2 Melting temperature ( $T_m$ )

The melting temperature,  $T_m$ , sometimes called midtransition temperature, of an oligonucleotide is its most critically important value.  $T_m$  is the temperature at which 50% of the oligonucleotides exist as single strands and the other 50% as the secondary structure (Figure 3.13).<sup>[22]</sup>



**Figure 3.13** Typical thermal melting of duplex DNA recorded as a function of changes in absorptivity at 260 nm versus temperature.

The factors affecting  $T_m$  are salt concentration, strand concentration, the presence of denaturants, sequence, length, and hybridization conditions. Melting of DNA complexes can be performed by fitting UV-vis, fluorescence, or CD spectrometers with a Peltier temperature programmer. The most common method for determining  $T_m$  is using the maximum of the first derivative plots of the melting curves obtained by measuring absorbance at 260 nm against increasing temperature.  $T_m$  is used as a measure of the relative stability of a particular assembly.

Sometimes DNA does not have the same midtransition temperature during the melting and annealing processes, giving rise to hysteresis, which is more common for DNA in triplexes and G-quadruplexes. In order for the  $T_m$  value to be considered a true representation of thermodynamic stability, the dissociation and association constant of the structure must be reversible. That is, both the heating and cooling properties must match. In most cases, hysteresis can be overcome by heating and cooling the complex at a slower rate.<sup>[22]</sup> Hysteresis is usually not a problem for DNA duplexes. However, hysteresis is usually unavoidable in the case of tetramolecular

G-quadruplexes since they form so slowly that a sufficiently slow temperature ramp becomes impractical. In such cases, the observed inflection point for the heating curve is referred to as a  $T_{1/2}$  value and the heating rate is specified.

### 3.6.3 Mass Spectrometry

Matrix assisted laser desorption ionization time of flight spectrometry (MALDI TOF-MS) is a very valuable tool for obtaining accurate mass determinations of oligonucleotides, and therefore confirm the oligonucleotide composition. The matrix is normally an organic aromatic weak acid, which should strongly absorb energy at the wavelength of the laser. The matrix should not modify or react with the analyte before laser irradiation. Further, it must be possible to dissolve the matrix in the same solvent as the analyte in order to obtain proper mixing. The mixture is then allowed to dry as a crystalline coating on a metal probe. The matrix molecules absorb laser energy, causing translational motion and ionization of molecules which then are accelerated towards the detector.

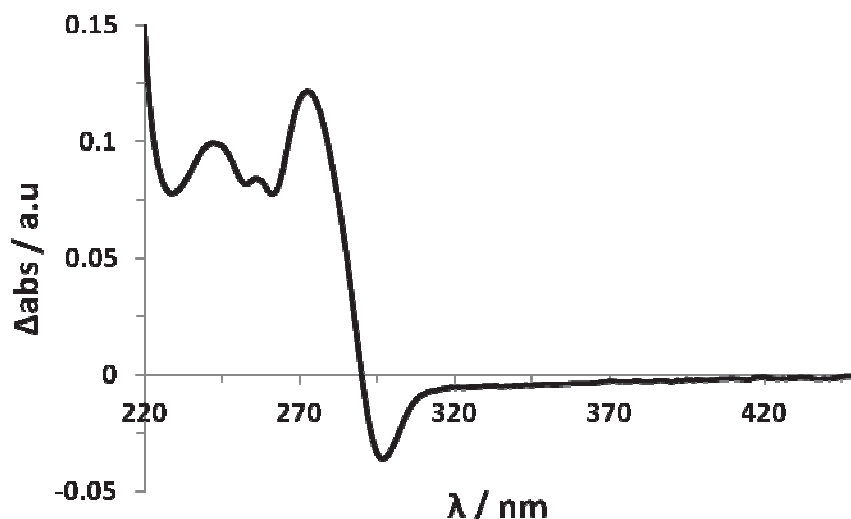
Electrospray ionization mass spectrometry (ESI-MS) can be used to determine complex formation with additives.

### 3.6.4 UV-Vis Thermal Difference Spectra (TDS)

The thermal difference spectrum (TDS) of a nucleic acid is typically obtained by subtracting the absorbance spectrum of the folded state at low temperature from that of the unfolded state at a higher temperature. In our case the TDS was obtained by subtraction of the UV-vis absorption spectrum of DNA at 20 °C from UV-vis absorption spectrum at 90 °C. The TDS data provide a distinctive spectroscopic signature for different secondary nucleic acid structures. More significantly, analysis of TDS data in the  $\lambda_{\text{max}}$  absorbance region for a ligand gives valuable information about the binding events involved between relevant ligand/s and DNA.<sup>[23]</sup>

The TDS spectra of B-DNA is affected by base composition, where 100 % AT composition is accompanied by a major positive peak around 259 nm and sometimes a negative peak around 284 nm, 100 % GC content leads to a positive peak around 277 nm and a smaller positive peak around 237 nm, and 50 % GC contents results in a positive peak around 237 nm.<sup>[24]</sup> Parallel DNA triplexes show a TDS positive peak between 245 and 270 nm and may also show a negative peak around 295 nm,

whereas antiparallel triplexes have a peak around 270 nm.<sup>[24]</sup> The TDS of parallel G-quadruplexes is characterized by two major positive peaks around 240 and 270 nm and a negative peak around 295 nm (Figure 3.14).<sup>[25]</sup>



**Figure 3.14** TDS spectrum of a parallel G-quadruplex formed by 5'-d(TG<sub>4</sub>T) at 10  $\mu$ M strand concentration in the presence of 10 mM sodium phosphate buffer, 0.1 mM EDTA, pH = 7.0 in the presence of NaCl (50 mM).

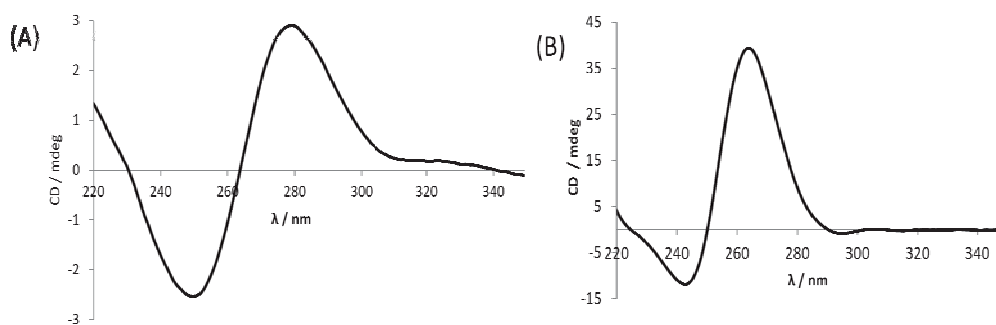
### 3.6.5 Circular Dichroism (CD) Spectroscopy

CD spectroscopy is very useful to study secondary structures of DNA. Circular dichroism arises from the different absorbances of left and right circularly polarized light in optically active chiral molecules. Circular dichroism can only be exhibited in the spectral region where absorbance occurs. Linearly polarized light occurs when the electric field vector oscillates only in one plane, whilst circularly polarized light occurs when the direction of the electric field vector rotates about its propagation direction while the vector retains constant magnitude.

When circularly polarized light passes through an absorbing optically active medium, the speeds between right and left polarizations differ ( $c_L \neq c_R$ ) as well as their wavelength ( $\lambda_L \neq \lambda_R$ ), and the extent to which they are absorbed ( $\epsilon_L \neq \epsilon_R$ ). Circular dichroism is expressed as a difference  $\Delta\epsilon = \epsilon_L - \epsilon_R$ .

CD of DNA arises from the asymmetric backbone sugars and the helical arrangement of nucleobases. CD spectroscopy is ideal for tracing conformational

transitions between discrete nucleic acids arrangements. The method is handy, fast, highly sensitive, and relatively inexpensive.<sup>[26]</sup> B-DNA, the most common form of DNA in aqueous solution and in nature exhibits a positive band around 260-280 nm and a negative one around 245 nm (Figure 3.15A).



**Figure 3.15** CD spectra of the duplex B-DNA **D1** (1.0  $\mu$ M, A) and a parallel G-quadruplex formed by 5'-d(TG<sub>4</sub>T) 10.0  $\mu$ M, B) in the presence of 10 mM sodium phosphate buffer, 0.1 mM EDTA, pH = 7.0 in the presence of NaCl (50 mM). See Figure 4.2 for the structure of **D1**.

CD spectra of parallel G-quadruplexes are characterized by a dominant positive band at 260 nm (Figure 3.15B), whereas the spectra of antiparallel G-quadruplexes display a negative band at 260 nm and a positive band at 295 nm.<sup>[26]</sup> In addition, all G-quadruplexes display another positive band around 215 nm.

### 3.6.5.1 Induced CD Spectroscopy (ICD)

Induced circular dichroism (ICD) occurs due to molecular interactions between chiral and achiral molecules giving rise to a CD signal from the achiral component, if it absorbs in the UV or visible region. The CD induced in an achiral molecule upon interaction with a chiral substrate occurs as a result of the achiral molecule being perturbed to adopt a chiral conformation or it may gain optical activity through electric and/or magnetic interaction.<sup>[27]</sup> ICD can thus be used to study the interaction and relative orientation of achiral molecules to chiral ones, which can provide vital information about supramolecular events both in solution and in the solid state.<sup>[28]</sup> Also possible, is the fact that the CD of the chiral inducer may also change as a result of the different environment in which the molecules are located.<sup>[29]</sup>

DNA can bind small molecules by electrostatic interactions, intercalation or groove binding to the either the minor or major groove. Optically inactive chromophores

usually show induced CD upon binding to DNA because the binding causes the electronic energy states of the chromophore to be coupled with the electronic energy states of chiral DNA.<sup>[30]</sup> Generally, groove binding and electrostatic interaction produces negative induced CD whilst intercalation produces a positive CD signal.<sup>[30]</sup>

### 3.6.6 Fluorescence properties of unmodified DNA

Natural nucleobases have weak fluorescence or phosphorescence quantum yields in the ranges of  $0.86 \times 10^{-4}$  for dA to  $1.32 \times 10^{-4}$  for dT with lifetimes in the order of picoseconds.<sup>[31]</sup> This is due to decay to the ground state by internal conversion. This is arguably believed to be a result of life evolving with this set of genetic machinery. The short lifetime of the excited nucleobases protects them from photochemistry, and thus degradation especially important in the wavelength range of 280 to 300 nm, as solar irradiance is present on earth in this high energy, ultra violet range. This means internal conversion may be vital to the preservation of life on earth.<sup>[32]</sup> The absence of fluorescence from natural DNA nucleobases offers the advantage that fluorescent signals from unnatural fluorophores can be observed without any competing background signals. Changes in absorption intensity, emission intensity, excited state lifetime, anisotropy, or a shift in  $\lambda_{\text{max}}$  of absorbance, emission, or excitation upon changes in its physical environment can all provide useful structural information.

Fluorescence spectroscopy is an important technique for studying the structure and dynamics of DNA that allows for real-time observations of changes in its microenvironment. However, the fluorescence of unmodified DNA at room temperature is very weak and typically occurs in the UV region which makes it difficult for practical applications. DNA can be made fluorescent by using dyes that spontaneously non-covalently bind to DNA such as ethidium bromide, substituting natural nucleobases with fluorescent DNA base analogues such as 2-aminopurine (2-AP), or covalently attaching fluorescent chromophores to DNA (pyrene).

### 3.7 References

- [1] J. D. Watson, F. H. Crick, *Nature* **1953**, 171, 737.
- [2] V. V. Filichev, E. B. Pedersen, T. P. Begley, *DNA-Conjugated Organic Chromophores in DNA Stacking Interactions*, John Wiley & Sons, Inc., **2007**.
- [3] K. Zong, S. I. Shin, D. J. Jeon, J. N. Lee, E. K. Ryu, *Journal of Heterocyclic Chemistry* **2000**, 37, 75.
- [4] P. Yakovchuk, E. Protozanova, M. D. Frank-Kamenetskii, *Nucleic Acids Research*, **34**, 564.
- [5] H. S. Basu, B. G. Feuerstein, D. A. Zarling, R. H. Shafer, L. J. Marton, *J Biomol Struct Dyn* **1988**, 6, 299.
- [6] S. Rothenburg, F. Koch-Nolte, F. Haag, *Immunological Reviews* **2001**, 184, 286.
- [7] R. Wing, H. Drew, T. Takano, C. Broka, S. Tanaka, K. Itakura, R. E. Dickerson, *nature* **1980**, 287, 755.
- [8] E. B. Pedersen, J. T. Nielsen, C. Nielsen, V. V. Filichev, *Nucleic Acids Research*.
- [9] a)K. Keren, R. S. Berman, E. Buchstab, U. Sivan, E. Braun, *Science* **2003**, 302, 1380; b)M. Hazani, F. Hennrich, M. Kappes, R. Naaman, D. Peled, V. Sidorov, D. Shvarts, *Chemical Physics Letters* **2004**, 391, 389; c)C. Dwyer, et al., *Nanotechnology* **2004**, 15, 1240.
- [10] Z. J. Gartner, B. N. Tse, R. Grubina, J. B. Doyon, T. M. Snyder, D. R. Liu, *Science* **2004**, 305, 1601.
- [11] a)Y. Y. Pinto, J. D. Le, N. C. Seeman, K. Musier-Forsyth, T. A. Taton, R. A. Kiehl, *Nano Letters* **2005**, 5, 2399; b)S. Xiao, F. Liu, A. E. Rosen, J. F. Hainfeld, N. C. Seeman, K. Musier-Forsyth, R. A. Kiehl, *Journal of Nanoparticle Research* **2002**, 4, 313; c)M. G. Warner, J. E. Hutchison, *Nat Mater* **2003**, 2, 272; d)H. Björn, O. Håkan, *Journal of Physics: Conference Series* **2007**, 61, 458.
- [12] a)H. Yan, S. H. Park, G. Finkelstein, J. H. Reif, T. H. LaBean, *Science* **2003**, 301, 1882; b)S. H. Park, P. Yin, Y. Liu, J. H. Reif, T. H. LaBean, H. Yan, *Nano Letters* **2005**, 5, 729.
- [13] Y. K. Luu, K. Kim, B. S. Hsiao, B. Chu, M. Hadjiargyrou, *Journal of Controlled Release* **2003**, 89, 341.
- [14] R. Varghese, H.-A. Wagenknecht, *Chemical Communications* **2009**, 2615.
- [15] T. J. Bandy, A. Brewer, J. R. Burns, G. Marth, T. Nguyen, E. Stulz, *Chemical Society Reviews* **2011**, 40, 138.
- [16] H.-A. Wagenknecht, *Angewandte Chemie International Edition* **2009**, 48, 2838.

- [17] a)S. Mutsamwira, E. W. Ainscough, A. C. Partridge, P. J. Derrick, V. V. Filichev, *Journal of Photochemistry and Photobiology A: Chemistry* **2014**, 288, 76; b)P. Conlon, C. J. Yang, Y. Wu, Y. Chen, K. Martinez, Y. Kim, N. Stevens, A. A. Marti, S. Jockusch, N. J. Turro, *Journal of the American Chemical Society* **2008**, 130, 336; c)V. L. Malinovskii, A. L. Nussbaumer, R. Häner, *Angewandte Chemie International Edition* **2012**, 51, 4905; d)N. Bouquin, V. L. Malinovskii, R. Häner, *Chemical Communications* **2008**, 1974; e)O. Khorev, C. D. Bösch, M. Probst, R. Häner, *Chemical Science* **2014**, 5, 1506.
- [18] C. Holzhauser, M. M. Rubner, H.-A. Wagenknecht, *Photochemical & Photobiological Sciences* **2013**, 12, 722.
- [19] V. V. Filichev, I. V. Astakhova, A. D. Malakhov, V. A. Korshun, E. B. Pedersen, *Chemistry-a European Journal* **2008**, 14, 9968.
- [20] O. Doluca, J. Withers, T. S. Loo, P. Edwards, C. Gonzalez, V. Filichev, *Org. Biomol. Chem.* **2015**, 13, 3742.
- [21] P. Ceroni, *Chemistry-a European Journal* **2011**, 17, 9560.
- [22] J. Mergny, L. Lacroix, *Oligonucleotides* **2004**, 13 515.
- [23] a)S. Satyanarayana, J. C. Dabrowiak, J. B. Chaires, *Biochemistry* **1993**, 32, 2573; b)I. Haq, P. Lincoln, D. Suh, B. Norden, B. Z. Chowdhry, J. B. Chaires, *Journal of the American Chemical Society* **1995**, 117, 4788.
- [24] J.-L. Mergny, J. Li, L. Lacroix, S. Amrane, J. B. Chaires, *Nucleic Acids Research* **2005**, 33, e138.
- [25] P. L. T. Tran, J.-L. Mergny, P. Alberti, *Nucleic Acids Research* **2011**, 39, 3282.
- [26] M. Vorlíčková, I. Kejnovská, K. Bednářová, D. Renčiuk, J. Kypr, *Chirality* **2012**, 24, 691.
- [27] M. Kubista, B. Aakerman, B. Norden, *The Journal of Physical Chemistry* **1988**, 92, 2352.
- [28] S. Allenmark, *Chirality* **2003**, 15, 409.
- [29] J. Gawronski, J. Grajewski, *Organic Letters* **2003**, 5, 3301.
- [30] G. G. Hammes, *Physical chemistry for the biological sciences*, Wiley. com, **2007**.
- [31] M. Hawkins, *Cell Biochemistry and Biophysics* **2001**, 34, 257.
- [32] E. Nir, K. Kleinermmanns, L. Grace, M. S. de Vries, *The Journal of Physical Chemistry A* **2001**, 105, 5106.

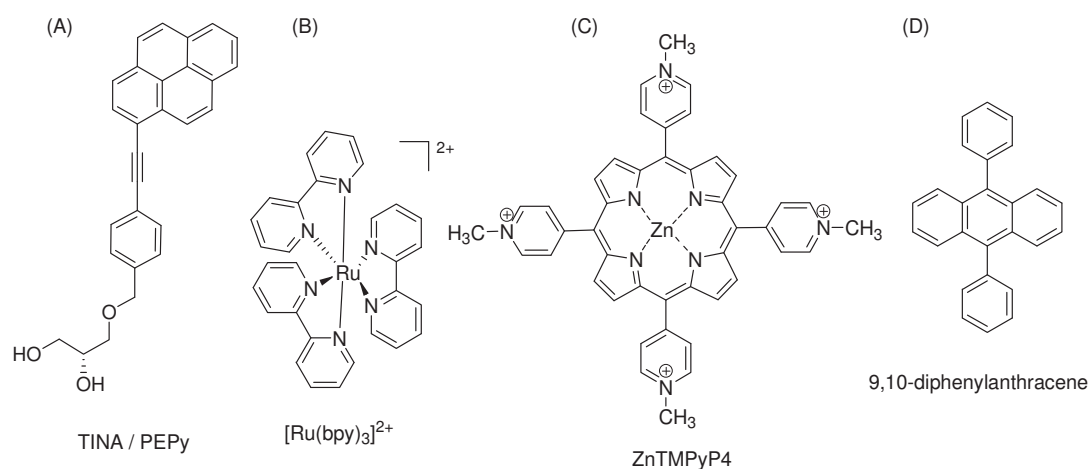




## 4 Interactions of Free Chromophores in Organic Solvents and their use in EU

### 4.1 Introduction

Porphyrins, phthalocyanines, polycyclic aromatics and organometallic complexes have a wide range of applications, and have been used in low-to-high photon upconversion systems (Table 1.1, Chapter 1). In the present chapter, we investigated the interactions of PEPy with  $[\text{Ru}(\text{bpy})_3]^{2+}$  and ZnTMPyP4 in organic solvents by using Stern-Volmer fluorescence quenching analysis (Figure 4.1).



**Figure 4.1** Structures of twisted intercalating nucleic acid monomer (TINA monomer, PEPy), (A),  $[\text{Ru}(\text{bpy})_3]^{2+}$  (B), ZnTMPyP4 (C) and 9,10-diphenylanthracene, DPA (D). TINA and 9,10-diphenylanthracene are potential acceptors,  $[\text{Ru}(\text{bpy})_3]^{2+}$  and ZnTMPyP4 are potential energy donors in EU.

The aim of this chapter was to establish the feasibility of EU using the free chromophores later used in the thesis in the presence of a DNA scaffold.

### 4.2 Chapter Summary

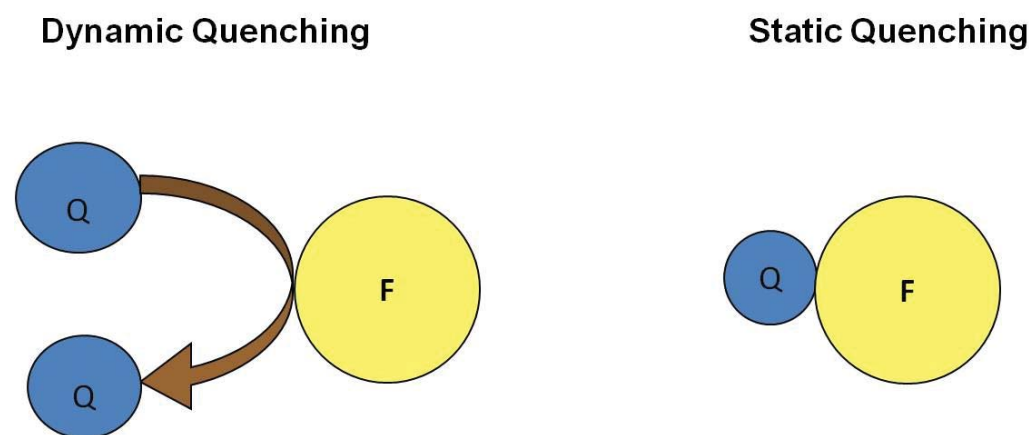
Herein we show perturbation of fluorescence characteristics of the potential donor and acceptors of EU in solution. A system comprehensively studied by Zhao and Castellano using  $[\text{Ru}(\text{bpy})_3]^{2+}$  and 9,10-diphenylanthracene (DPA) in DCM was used as a model for the work in this chapter.<sup>[1]</sup> The following systems were evaluated, in which  $[\text{Ru}(\text{bpy})_3]^{2+}$  and ZnTMPyP4 act as long wavelength absorbers, and donors (D), whereas PEPy acts as the acceptor (A) and triplet-annihilator to produce the excited singlet state which then emits at a shorter wavelength. Green-to-blue emission was observed from PEPy with free  $[\text{Ru}(\text{bpy})_3]^{2+}$  in dichloromethane

(DCM) upon excitation using a laser (see details on Section 11.3.2, Experimental methods, Chapter 11), as well as a conventional fluorimeter. These results lay the foundation for a possible photon upconversion using DNA as a scaffold.

### 4.3 Stern-Volmer Analysis

Fluorescence quenching refers to any process which decreases the fluorescence intensity of a given substance. A number of processes can lead to a reduction in fluorescence intensity. These processes include collisional encounters, energy transfer, charge transfer reactions or ground state complex formation.<sup>[2]</sup> Thus, quenching can be used to study interactions between molecules, where at least one of them is fluorescent. Stern-Volmer quenching data of the donor (D) by the acceptor (A) at a selected donor concentration  $[D]$  can be used to establish the acceptor concentrations  $[A]$  required to achieve EU from the maximum quenching concentrations.<sup>[1, 3]</sup> Stern-Volmer quenching studies of ZnTMpyP4 and  $[\text{Ru}(\text{bpy})_3]^{2+}$  by free TINA in solution and TINA-modified DNAs were performed in this thesis.

There are two main mechanisms of fluorescence quenching – dynamic (collisional) quenching or static quenching (Figure 4.2). Dynamic quenching results from collisional encounters between fluorophore and quencher. Upon contact the fluorophore returns to the ground state, without the emission of a photon. Static quenching occurs due to the formation of a non-fluorescent complex between the fluorophore and a quencher. When this complex absorbs light, it immediately returns to the ground state without the emission of a photon.



**Figure 4.2** Dynamic and static quenching between a fluorophore (F) and a quencher (Q).

Fluorescence quenching data are usually analysed by the Stern–Volmer equation:

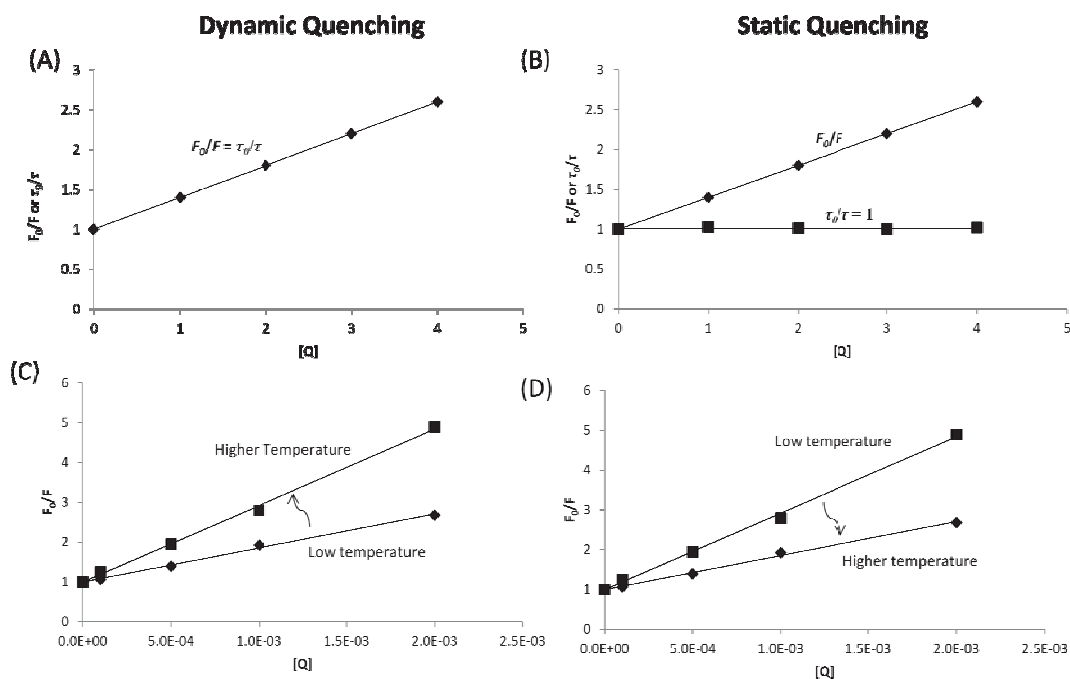
$$F_0/F = 1 + K_{SV}[Q] \quad \text{eqn 4.1}$$

where  $F_0$  and  $F$  are the fluorescence intensities observed in the absence and presence of quencher, respectively.  $[Q]$  is the quencher concentration and  $K_{SV}$  is the Stern–Volmer quenching constant. In the simplest cases, then, a plot of  $F_0/F$  versus  $[Q]$  should yield a straight line with a slope equal to  $K_{SV}$  (Figure 4.3A and B). This could be due to a case of a collision between the fluorophore and the quencher (dynamic quenching), where  $K_{SV} = K_D$  (dynamic quenching constant), or alternatively static quenching occurring as a result of the formation of a non-fluorescent ground state complex between the fluorophore and the quencher and  $K_{SV} = K_S$  (static quenching constant). In the case of purely dynamic quenching:

$$F_0/F = \tau_0/\tau \quad \text{eqn 4.2}$$

$$\text{Hence in this case: } \tau_0/\tau = 1 + K_{SV}[Q] \quad \text{eqn 4.3}$$

where  $\tau_0$  and  $\tau$  are the excited state lifetimes in the absence and presence of a quencher, respectively. In this case, then, a plot of  $F_0/F$  versus  $[Q]$  should yield a straight line with a slope equal to  $K_D$ , Figure 4.3A.



**Figure 4.3** Examples of dynamic and static quenching trends as represented in Stern–Volmer graphs.

In the case of static quenching, the fluorophore forms a ground-state non-fluorescent stable complex with another molecule:



In such a case, the association constant is given by:

$$K_a = ([FQ])/([F][Q]) \quad \text{eqn 4.5}$$

and the dependence of the fluorescence as a function of the quencher concentration follows the relation:

$$F_0/F = 1 + K_a[Q] \quad \text{eqn 4.6}$$

where  $K_a$  is the association constant of the complex and:

$$K_a = K_s \quad \text{eqn 4.7}$$

In the case of static quenching the lifetime of the sample is not reduced, since those fluorophores which are not complexed are able to emit after excitation and will have the normal excited state lifetime. Hence, for static quenching (Figure 4.3B):

$$\tau_0/\tau = 1 \quad \text{eqn 4.8}$$

The fluorescence of the sample is reduced since the quencher is essentially reducing the number of fluorophores which can emit.

Dynamic and static quenching also have different temperature dependencies (Figure 4.3C and D, respectively). Higher temperatures result in faster diffusion leading to more collisions and hence larger dynamic quenching. In contrast, higher temperatures typically cause the dissociation of the weakly bound complexes, and hence less static quenching. However, in both static and dynamic quenching:

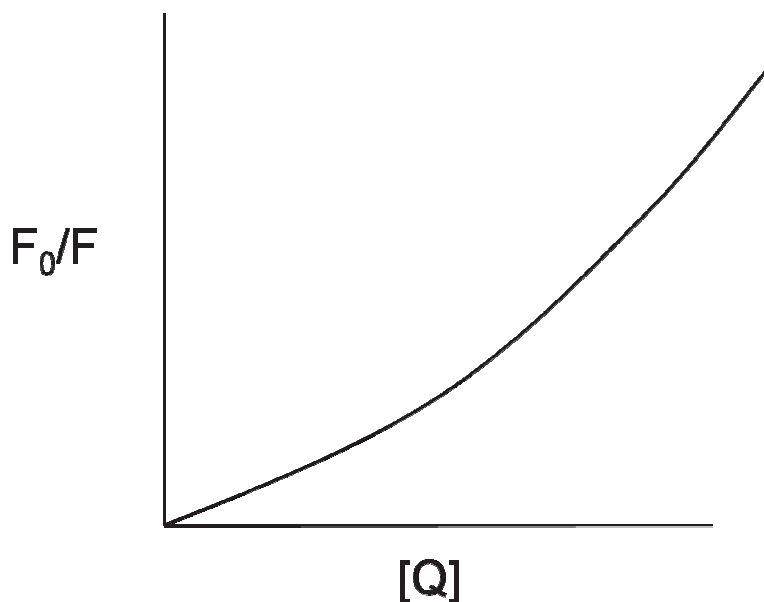
$$K_{sv} = \tau_0 k_q \quad \text{eqn 4.9}$$

where  $k_q$  is the bimolecular quenching rate constant and  $K_{sv}$  could be either  $K_s$  or  $K_D$ . Thus, the bimolecular quenching constant ( $k_q$ ) can be obtained by analyzing the luminescence data. It can either be done in a time resolved mode, i.e. by measuring  $\tau$  at different quencher concentrations; or by monitoring the luminescence intensity as a function of the quencher concentration. The bimolecular quenching constant reflects the efficiency of quenching or the accessibility of the fluorophores to the quencher.

### 4.3.1 Combined dynamic and static quenching

In some instances, the fluorophore is quenched by both static and dynamic mechanisms by the same quencher. This results in an upward curvature (Figure 4.4), concave towards the y-axis in a plot of  $F_0/F$  versus  $[Q]$  due to the  $[Q]^2$  term:<sup>[2]</sup>

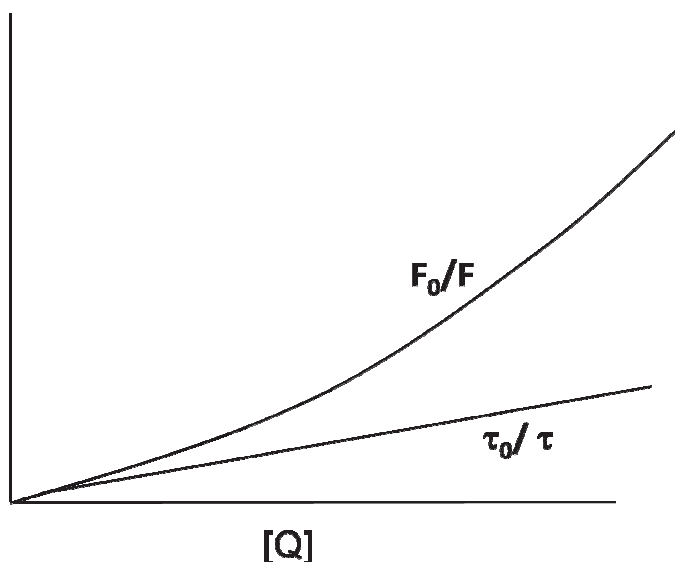
$$F_0/F = (1 + K_D[Q])(1 + K_S[Q]) \quad \text{eqn 4.10}$$



**Figure 4.4** Example of a Stern-Volmer graph which indicates combined dynamic and static quenching of the same population of fluorophores.

The dynamic portion of the observed quenching can be determined by lifetime measurements, since the lifetime is unaffected by the presence of quencher in cases of pure static quenching (Figure 4.5). That gives the dynamic component lifetime as a straight line as opposed to the static quenching lifetime:<sup>[2]</sup>

$$\tau_0/\tau = 1 + K_D[Q] \quad \text{eqn 4.11}$$

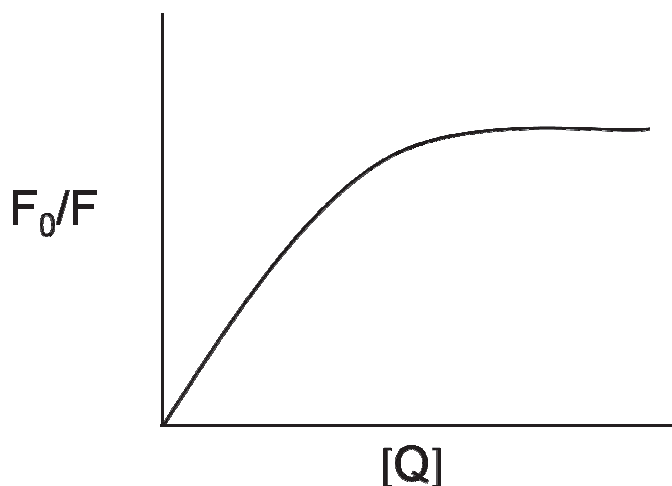


**Figure 4.5** Example of a Stern-Volmer graph which shows trends observed in combined dynamic and static quenching of the same population of fluorophores. A plot of the fluorescence intensity versus quencher concentration indicates the combined static and dynamic quenching. The plot of lifetime versus quencher concentration gives the dynamic portion of the quenching process.

Hence, a Stern-Volmer steady state fluorescence analysis of the combined quenching (described later in the thesis) can provide the static and dynamic components of the quenching mechanisms.<sup>[2]</sup>

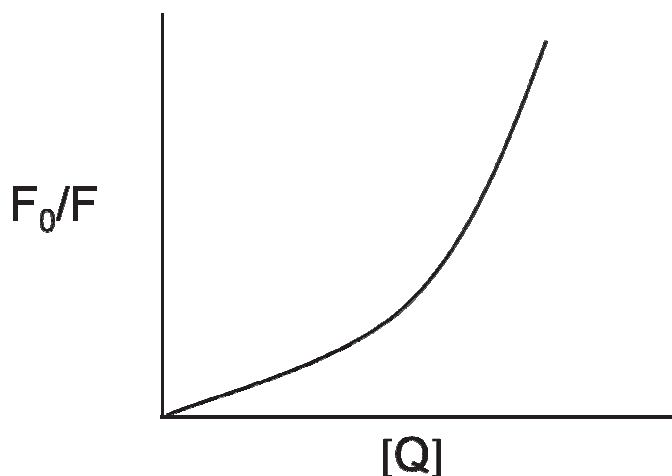
#### 4.3.2 Deviations from the Stern-Volmer equation

There are some cases where the Stern-Volmer relationship does not hold, leading to non-linear Stern-Volmer plots occurring. This could be due to purely collisional quenching if some of the fluorophores are less accessible than others. As reported previously, multiple tryptophan residues in a protein would result in some of them more accessible to quenchers in the solvent than others.<sup>[4]</sup> In the extreme case, a Stern-Volmer plot for a system having accessible and inaccessible fluorophores could result in downward curvature (Figure 4.6).



**Figure 4.6** A case of non Stern-Volmer quenching resulting in a negative curve deviation.

If the extent of quenching is large then positive deviations from the Stern-Volmer equation are sometimes observed. This could result in upward-curving Stern-Volmer plots, which are analyzed in terms of the quencher being adjacent to the fluorophore at the moment of excitation (Figure 4.7). In this close proximity, the fluorophore and the quencher have a high probability of interacting before these molecules diffuse apart in a "sphere of action".<sup>[2]</sup>



**Figure 4.7** A case of non Stern-Volmer quenching resulting in a positive curve deviation.

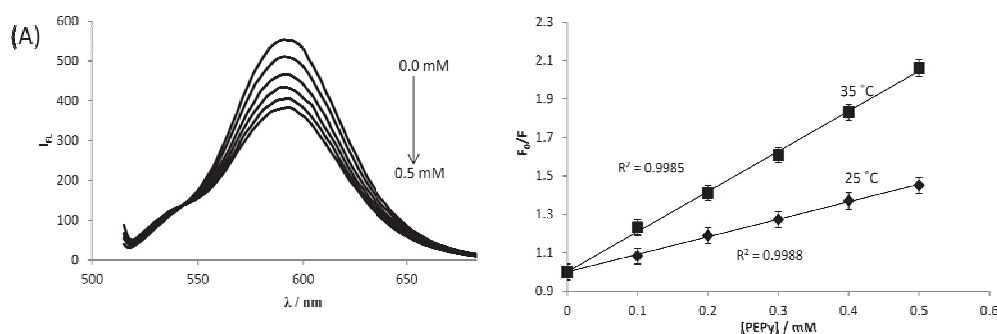
## 4.4 Fluorescence Quenching Characteristics

### 4.4.1 Interaction between $[\text{Ru}(\text{bpy})_3]^{2+}$ and TINA monomer (PEPy) in solution

In this section, we investigated the interaction of PEPy with  $[\text{Ru}(\text{bpy})_3]^{2+}$  and ZnTMPyP4 using a steady state fluorescence quenching mechanism. Figure 4.8A shows the emission spectra of  $[\text{Ru}(\text{bpy})_3]^{2+}$  in the absence and presence of PEPy in DCM. This figure shows that the emission intensity of  $[\text{Ru}(\text{bpy})_3]^{2+}$  decreases



gradually with increasing concentration of PEPy, showing that quenching has occurred.



**Figure 4.8.** Steady state fluorescence quenching of  $[\text{Ru}(\text{bpy})_3]^{2+}$  (100  $\mu\text{M}$ ) by PEPy in the concentration range 0 – 0.5 mM in DCM at 25  $^{\circ}\text{C}$ ,  $\lambda_{\text{ex}} = 500$  nm (A). Stern-Volmer plots for the fluorescence quenching of  $[\text{Ru}(\text{bpy})_3]^{2+}$  by PEPy in DCM at 25 and at 35  $^{\circ}\text{C}$  (B).

The Stern-Volmer plots of  $F_0/F$  versus  $[\text{Q}]$  were linear at 25 and 35  $^{\circ}\text{C}$ . Higher temperature results in faster diffusion and hence larger amounts of collisional encounters, indicating the dynamic nature of the quenching process (Figure 4.8B). The addition of PEPy causes neither a peak shift nor formation of a new peak and there is no change in the absorption spectrum of  $[\text{Ru}(\text{bpy})_3]^{2+}$  (data not shown), which suggests there is no ground state complex formation between  $[\text{Ru}(\text{bpy})_3]^{2+}$  and PEPy.

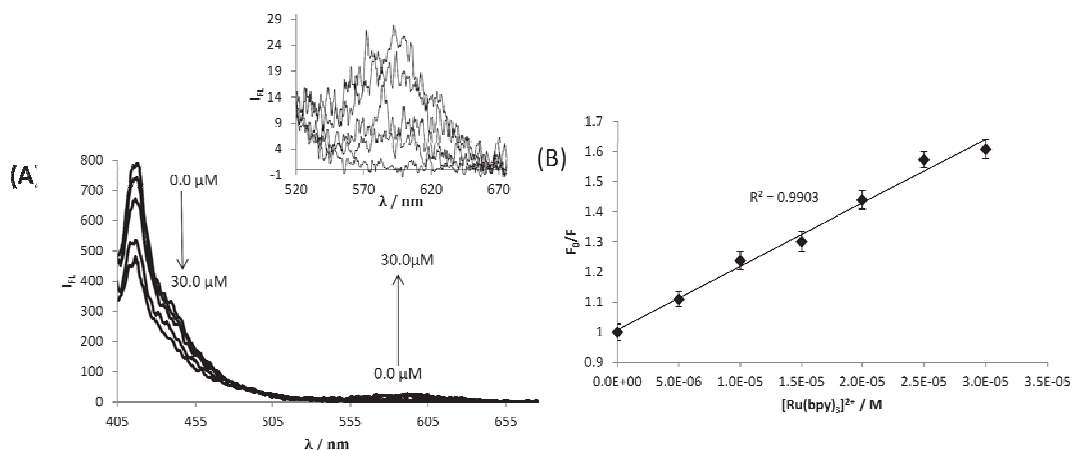
The Stern-Volmer constant for dynamic quenching ( $K_D$ ) was found to be  $91.5 \text{ M}^{-1}$ . The bimolecular quenching rate constant ( $k_q$ ) was calculated using eqn 4.9 and  $\tau_0$  (700 ns) obtained from the literature (Table 4.1).<sup>[3]</sup> The quenching efficiency of  $[\text{Ru}(\text{bpy})_3]^{2+}$  by PEPy ( $1.31 \times 10^8 \text{ M}^{-1} \text{ s}^{-1}$ ) compares favourably with a good quencher of  $[\text{Ru}(\text{bpy})_3]^{2+}$ , 9,10-diphenylanthracene ( $2.5 \times 10^9 \text{ M}^{-1} \text{ s}^{-1}$ ),<sup>[3]</sup> which also acts as an acceptor in TTA-assisted energy upconversion. Furthermore, other quenchers such as anthraquinone and azo dyes have quenching efficiencies ranging from  $0.8$  to  $7.0 \times 10^8 \text{ M}^{-1} \text{ s}^{-1}$ .<sup>[5]</sup> The quenching of  $[\text{Ru}(\text{bpy})_3]^{2+}$  by the anthraquinone and azo dyes is dynamic and involves an electron transfer mechanism, where  $[\text{Ru}(\text{bpy})_3]^{2+}$  acts as an electron donor and dyes as electron acceptors in what is termed oxidative quenching.

**Table 4.1** Stern–Volmer dynamic quenching constants ( $K_D$ ) and bimolecular quenching constants of  $[\text{Ru}(\text{bpy})_3]^{2+}$  (in DCM) and ZnTMpyP4 (9:1 DMSO/ $\text{H}_2\text{O}$ ) by PEPy at 25 °C.

Fluorophore	$K_D / \text{M}^{-1}$	$k_q / \text{M}^{-1}\text{s}^{-1}$
$[\text{Ru}(\text{bpy})_3]^{2+}$	91.5	<sup>a</sup> $1.31 \times 10^8$
ZnTMpyP4	857.0	<sup>b</sup> $6.6 \times 10^{11}$

<sup>a</sup>Determined using  $\tau = 700 \text{ ns}$ .<sup>[3]</sup> <sup>b</sup>Determined using  $\tau = 1.3 \text{ ns}$ .<sup>[6]</sup>

We also observed that not only does PEPy quench  $[\text{Ru}(\text{bpy})_3]^{2+}$  fluorescence, but the reverse quenching of PEPy fluorescence by  $[\text{Ru}(\text{bpy})_3]^{2+}$  also occurs (Figure 4.9). More interestingly, we observed energy transfer from the excited state of PEPy to  $[\text{Ru}(\text{bpy})_3]^{2+}$ . This is shown in Figure 4.9A, as quenching of the PEPy fluorescence peak at about 417 nm with increasing  $[\text{Ru}(\text{bpy})_3]^{2+}$  concentration is accompanied by the appearance of a 600 nm  $[\text{Ru}(\text{bpy})_3]^{2+}$  emission peak. The mechanism of energy transfer was not explored. Analysis of the Stern-Volmer plot of PEPy fluorescence quenching by  $[\text{Ru}(\text{bpy})_3]^{2+}$  (Figure 4.9B, straight line) confirmed that there is only one mechanism of quenching.

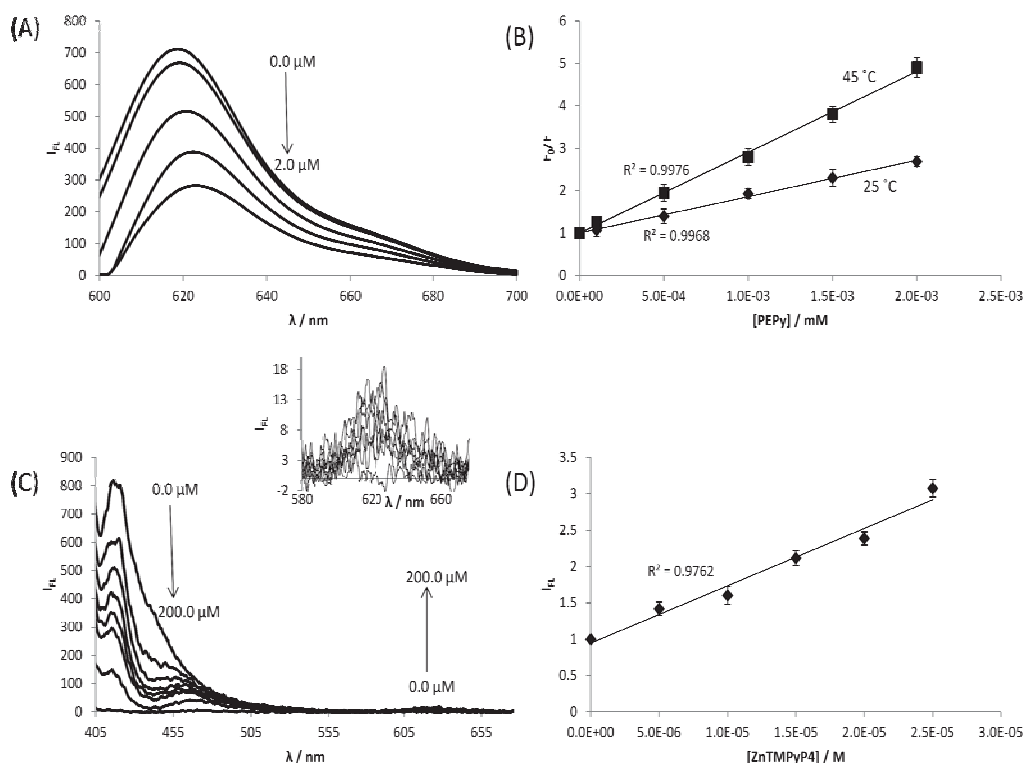


**Figure 4.9.** Steady state fluorescence quenching of PEPy (0.25  $\mu\text{M}$ ) by  $[\text{Ru}(\text{bpy})_3]^{2+}$  in the quencher concentration range of 0.0 – 30.0  $\mu\text{M}$  in DCM at 25 °C,  $\lambda_{\text{ex}} = 375 \text{ nm}$  (A), insert picture shows energy transfer from PEPy to  $[\text{Ru}(\text{bpy})_3]^{2+}$ . A Stern-Volmer plot for the quenching of the fluorescence of PEPy (0.25  $\mu\text{M}$ ) by  $[\text{Ru}(\text{bpy})_3]^{2+}$  (B).

#### 4.4.2 Interaction between ZnTMpyP4 and TINA monomer (PEPy) in solution

The fluorescence of ZnTMpyP4 at 630 nm in 9:1 (DMSO/ $\text{H}_2\text{O}$ ) was quenched by PEPy through a dynamic mechanism just like for  $[\text{Ru}(\text{bpy})_3]^{2+}$  as the data followed the same trends as in Figure 4.8 (Figure 4.10A and B). In view of our overall goal to use these chromophores for energy upconversion, it is quite notable that at higher

porphyrin concentrations PEPy fluorescence is completely quenched. Hence, it is important to keep porphyrin concentrations relatively low compared to PEPy concentrations for energy upconversion solutions. A steady state Stern-Volmer plot and  $\tau_0$  (1.3 ns)<sup>[6]</sup> yields a bimolecular quenching constant value of  $6.6 \times 10^{11} \text{ M}^{-1}\text{s}^{-1}$  (Table 4.1). No changes in the absorption spectrum of ZnTMPyP4 were observed upon addition of PEPy.



**Figure 4.10** Steady state fluorescence quenching of ZnTMPyP4 (4  $\mu\text{M}$ ) by PEPy in the concentration range 0 – 2.0  $\mu\text{M}$  in 9:1 (DMSO/H<sub>2</sub>O) at 25 °C.  $\lambda_{\text{ex}} = 430 \text{ nm}$  (A). Stern-Volmer plots for the fluorescence quenching of ZnTMPyP4 by PEPy at 25 °C and at 45 °C (B). Steady state fluorescence quenching of PEPy (0.25  $\mu\text{M}$ ) by ZnTMPyP4 in the quencher concentration range 0.0 – 200.0  $\mu\text{M}$ .  $\lambda_{\text{ex}} = 375 \text{ nm}$  (C), insert picture shows energy transfer from PEPy to ZnTMPyP4. A Stern-Volmer plot for the quenching of the fluorescence of PEPy (0.25  $\mu\text{M}$ ) by ZnTMPyP4 at 25 °C (D).

Conversely, ZnTMPyP4 quenches PEPy fluorescence at 417 nm (Figure 4.10C and D). Energy transfer also occurs from PEPy to ZnTMPyP4 at porphyrin concentrations higher than 50  $\mu\text{M}$ .

## 4.5 Analysis of Photon Upconversion

### 4.5.1 A typical energy upconversion analysis

EU experiments are typically done by exciting the donor at longer wavelength and monitoring the acceptor emission scan at shorter wavelength. The EU power dependence of upconversion emission intensities has been used here.<sup>[7]</sup> A quadratic power dependence is a feature of a TTA-based EU mechanism, which is due to the fluorescence emission caused by the bimolecular TTA step:<sup>[1, 7a]</sup>



The quadratic nature is due to the  $[\ ^3\text{A}^* ]^2$  term. As a result:

$$I_{FL} \propto (I_{EX})^2 \quad \text{eqn 4.13}$$

where  $I_{FL}$  is the upconverted fluorescence emission intensity and  $I_{EX}$  is the incident excitation power.

If a double logarithm plot is applied to the integrated upconversion emission intensity vs incident power, it yields a slope of 2.0:

$$\text{Log } I_{FL} = \text{Log } (I_{EX})^2 \quad \text{eqn 4.14}$$

$$\text{Hence, Log } I_{FL} = 2\text{Log } (I_{EX}) \quad \text{eqn 4.15}$$

In this case, the quadratic power dependence of the TTA based EU process is observed.<sup>[1, 8]</sup> Experimentally, the power dependence of EU can be measured using the integrated upconversion emission as a function of %T (percent light transmittance) or power density ( $\text{mW}/\text{cm}^2$ ) or laser pulse energy ( $\mu\text{J}$ ) depending on instrumentation available.

It is important to compare the efficiency of upconversion for our systems of interest. The observation of upconversion with DNA systems will show us that DNA does indeed act as a scaffold for bringing our chromophores of interest in to close proximity which is required for photon upconversion to take place in solution. This will then allow an investigation into how the efficiency of photon upconversion can be improved using DNA as a scaffold. Even though upconverted emission intensities of different systems at identical concentrations and under the same conditions can be used to give a relative comparison of the efficiencies of the process,<sup>[7b]</sup> quantum

yield measurements give absolute values of efficiency and are more accurate.<sup>[9]</sup> The quantum yield of upconversion can be defined as:

$$\Phi_{\text{up}} = \Phi_{\text{ISC}} \cdot \Phi_{\text{sens}} \cdot \Phi_{\text{TTA}} \cdot \Phi_{(\text{A})} \quad \text{eqn 4.16}$$

where  $\Phi_{\text{ISC}}$  is the efficiency of triplet excited state generation,  $\Phi_{\text{sens}}$  is the efficiency for sensitizing,  $\Phi_{\text{TTA}}$  is the the efficiency of TTA, and  $\Phi_{(\text{A})}$  is the quantum yield of the acceptor alone.

$\Phi_{\text{ISC}}$  is evaluated as a relative value from the phosphorescence intensity according to:

$$\Phi_{\text{ISC}} = \Phi_{\text{phos}} \quad \text{eqn 4.17}$$

Where,  $\Phi_{\text{phos}}$  is the quantum yield of phosphorescence of acceptor, obtained from literature or obtained experimentally.

The efficiency for sensitizing ( $\Phi_{\text{sens}}$ ) is calculated from the decrease of the emission band from the triplet-excited state of the donor:

$$\Phi_{\text{sens}} = 1 - (I/I_0) \quad \text{eqn 4.18}$$

where,  $I_0$  and  $I$  represent the integration of the phosphorescence from the donor in the absence and in the presence of acceptor, respectively.

Sing-Rachford and Castellano<sup>[10]</sup> recommend incorporating an additional multiplicative factor of 2 since the absorption of two photons is required for the observation of one upconverted photon; otherwise the limiting upconversion efficiency will be 50 % rather than 100 %, as described in earlier underestimated values. Hence, the corrected upconversion is:

$$\Phi_{\text{up}} = 2\Phi_{\text{ISC}} \cdot \Phi_{\text{sens}} \cdot \Phi_{\text{TTA}} \cdot \Phi_{(\text{A})} \quad \text{eqn 4.19}$$

The quantum yield of upconversion is determined by comparing the integrated upconverted fluorescence emission intensity to the fluorescence intensities of the acceptor alone as described by Tanaka *et al.*<sup>[9]</sup>

$$\Phi_{\text{up}} = 2\Phi_{(\text{A})} \cdot A_{\text{up}}/A_{(\text{A})} \cdot \varepsilon_{(\text{A}, \lambda_{\text{ex}})}/\varepsilon_{(\text{D}, \lambda_{\text{ex}})} \cdot c_{\text{D}}/c_{\text{A}} (\eta_1/\eta_2)^2 \quad \text{eqn 4.20}$$

where, D is the donor and A is the acceptor chromophore,  $\Phi_{(\text{A})}$  is the quantum yield of the fluorescence emission from the acceptor alone,  $A$  is the emission area calculated from the spectrum,  $\varepsilon$  is the molar extinct coefficient,  $c$  is the concentration, and  $\eta$  is the refractive index of each solvent.

Then the quantum yield of triplet-triplet annihilation ( $\Phi_{\text{TTA}}$ ) can be calculated from eqn 4.19.

#### 4.5.2 Experimental Requirements for Energy Upconversion

Photon upconversion through a TTA mechanism is quenched by the presence of oxygen, due to destruction of the generated triplet excited species of chromophores producing singlet oxygen. As a result, appropriate effective deaeration of the requisite solutions is an essential step for EU to occur. Several methods are available for degassing laboratory solutions. Freeze-pump-thaw, sonication and inert gas purging are the generally accepted methods of degassing. For our purposes we decided to degas solutions by argon purging in a sonicator for at least 30 minutes. To minimize solvent evaporation solutions were chilled to 10 °C. A simple home built set-up using an argon-filled balloon inserted into the EU solution in a chilled sonicator proved very effective and efficient, Figure 4.11 .



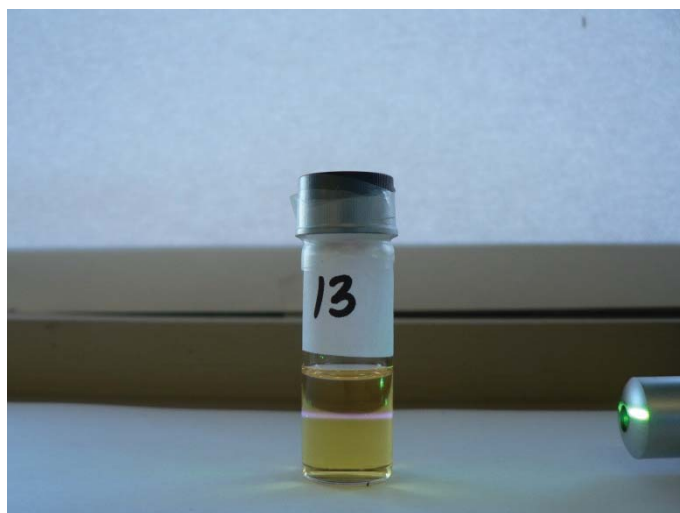
**Figure 4.11** Set up used for degassing solutions for energy upconversion experiments. Argon is bubbled from the balloon to the vial which is held in a sonicator at 10 °C.

In contrast to other EU mechanisms such as two photon absorption (TPA), sequential energy transfer upconversion (ETU) which specifically require excitation with coherent light and high power densities (see Section 1.3.1, Chapter 1), a TTA-based system can proceed on irradiation with low power non-coherent light sources, even including sunlight.<sup>[9]</sup> In our case, we excited the acceptor with a coherent light source (a commercial green laser), and then a continuous wave xenon arc lamp

source on a conventional fluorimeter fitted with an excitation monochromator. Light diffraction at the monochromator grating can occur as a first, second- or higher-order processes. As a result, when the monochromator is set at 500 nm, some 250 nm light can be present at the exit slit due to second-order diffraction.<sup>[2]</sup> The second order excitation combined with the continuous nature of the light can result in direct excitation of the acceptor. Therefore, we placed a 400 nm long-pass filter in the fluorimeter excitation beam before the sample to exclude all remnant high-energy photons from directly exciting the ground state singlet acceptor. The quadratic incident power dependence of the TTA-based EU system was achieved by placing a range of neutral density filters after the long-pass filter to modulate the intensity of the excitation beam. The exact percentage transmittance of the neutral density filters at 500 nm was measured using a UV-Vis spectrometer. The dual nature of the TTA process from the donor generally imposes a higher donor concentration requirement with respect to the acceptor.

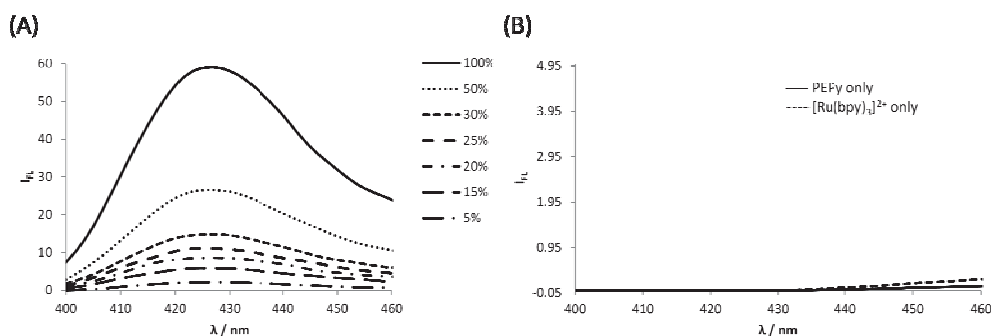
#### **4.5.3 [Ru(bpy)<sub>3</sub>]<sup>2+</sup> and TINA monomer (PEPy) in EU**

We evaluated EU using the inorganic chromophore [Ru(bpy)<sub>3</sub>]<sup>2+</sup> and PEPy. To the best of our knowledge, [Ru(bpy)<sub>3</sub>]<sup>2+</sup> and PEPy have never been studied for EU. We observed dynamic quenching of the [Ru(bpy)<sub>3</sub>]<sup>2+</sup> red fluorescence (Section 4.4.1), and the production of upconverted PEPy blue emission ( $\approx$  425 nm) upon green laser light excitation (532 nm) of [Ru(bpy)<sub>3</sub>]<sup>2+</sup> (Figure 4.12). The EU was observed in a deaerated DCM solution of [Ru(bpy)<sub>3</sub>]<sup>2+</sup> (46  $\mu$ M) and PEPy (4.6 mM). This result is a qualitative proof that EU occurs using these chromophores under these conditions.



**Figure 4.12** Green to blue upconversion from a deaerated DCM solution of  $[\text{Ru}(\text{bpy})_3]^{2+}$  (46  $\mu\text{M}$ ) and PEPy (4.6 mM). A commercial green laser pointer was used as the excitation source ( $\lambda_{\text{ex}} = 532 \text{ nm}$ , 5 mW peak power). Green light excitation is on the right (laser pointer) and blue fluorescence emission in the vial is in the center.

Next, a fluorimeter was used to record anti-Stokes emission spectra. Selective excitation at 500 nm of the deaerated DCM solutions containing both  $[\text{Ru}(\text{bpy})_3]^{2+}$  and PEPy using a conventional fluorimeter yielded a clearly observable upconverted fluorescence signal centred between 420 – 430 nm (Figure 4.13).

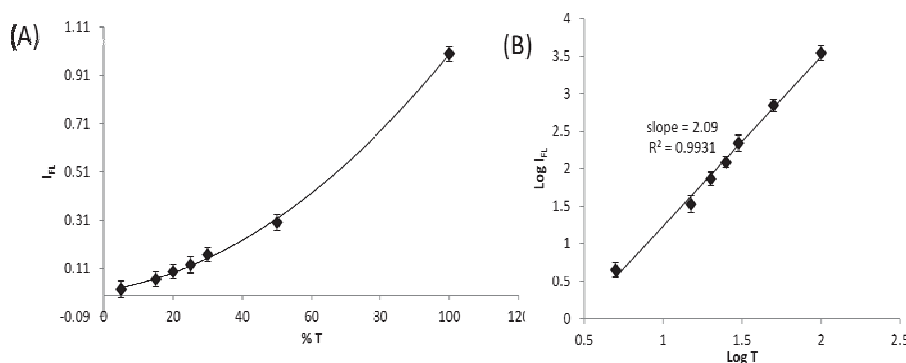


**Figure 4.13** Upconverted fluorescence emission spectra in a deaerated DCM solution of  $[\text{Ru}(\text{bpy})_3]^{2+}$  (46  $\mu\text{M}$ ) and PEPy (4.6 mM) measured as a function of neutral density filter percent transmission at 25 °C,  $\lambda_{\text{ex}} = 500 \text{ nm}$  (A). Fluorescence spectra of the individual chromophores after excitation at 500 nm (B).

The quadratic dependence of the intensity of the upconverted fluorescence on excitation power density was evaluated by systematically varying the incident optical power using neutral density filters (Figure 4.13). The total integrated emission was plotted as a function of the percentage transmittance of each filter at 500 nm to give an upward curved line indicative of the non linear excitation of TTA (Figure 4.14A). A double logarithm plot of the data in Figure 4.14A has a slope of 2.04 which means

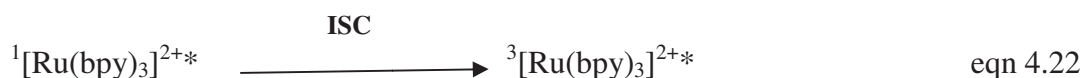


that it is a two-photon excitation process, expected for the bimolecular rate from eqn. 4.24.

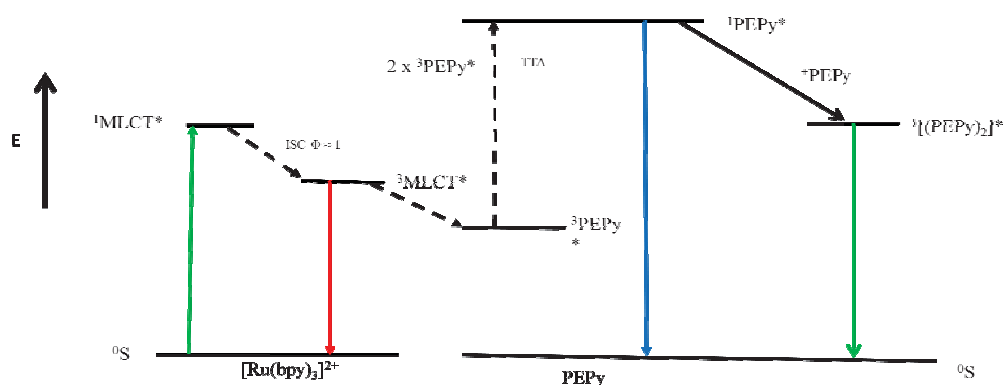


**Figure 4.14** (A) A plot of the normalized integrated fluorescence emission profiles in Figure 4.13 as a function of neutral density filter percent transmission. (B) A double logarithm plot of the data in A.

The optimum PEPy concentration for EU is the minimum concentration resulting in complete quenching of  $[\text{Ru}(\text{bpy})_3]^{2+}$  and determined by Stern-Volmer data (Figure 4.8). The lowest energy MLCT absorbance band has a maximum at about 450 nm and we selected 500 nm in order to effectively separate the excitation from the upconverted signal.<sup>[3]</sup> Long wavelength excitation of control samples at 500 nm containing the individual chromophores did not produce any signal in the 400 – 460 nm range. Almost complete quenching of 40 - 100  $\mu\text{M}$   $[\text{Ru}(\text{bpy})_3]^{2+}$  by PEPy was achieved in the mM concentration range. This indicates that a large excess of acceptor (PEPy) is required for efficient triplet energy transfer from the long wavelength light absorber ( $[\text{Ru}(\text{bpy})_3]^{2+}$ ), as described in Section 4.5.2. The sequence of reactions is as follows:

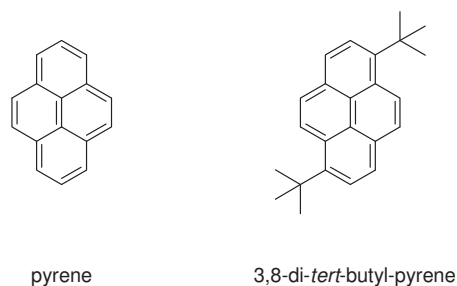


Excitation of  $[\text{Ru}(\text{bpy})_3]^{2+}$  (eqn. 4.21) sensitizes the triplet energy transfer from  $[\text{Ru}(\text{bpy})_3]^{2+}$  to PEPy ( $^3\text{PEPy}^*$  (eqn. 4.23) , which then undergoes annihilation (eqn. 4.24) producing higher energy singlet PEPy species ( $^1\text{PEPy}^*$ ) which eventually yields upconverted blue luminescence (eqn. 4.25). Intersystem crossing efficiency is close to unity for  $[\text{Ru}(\text{bpy})_3]^{2+}$ .<sup>[11]</sup> This sequence of reactions can be represented in a Jablonski diagram shown below (Figure 4.15).



**Figure 4.15** Qualitative Jablonski diagram of the upconversion process associated with  $[\text{Ru}(\text{bpy})_3]^{2+}$  triplet state sensitization of TINA monomer (PEPy) leading to singlet PEPy and PEPy singlet excimer fluorescence. <sup>a</sup>ISC is an intersystem crossing.

PEPy has the potential to form the undesirable excited dimer (excimer) under conditions which promote dynamic quenching of the PEPy excited state with another ground-state PEPy species, as has been established for pyrene.<sup>[1]</sup> This can significantly reduce the efficiency of EU (Figure 4.15). To reduce this process, we carefully selected concentrations at which no significant excimer formation was observed (data not shown). Excimer formation was significantly suppressed in PEPy in comparison to pyrene at the same concentrations. This is due to the steric bulk from the phenylethynyl group present on the first position of pyrene (Figure 4.16). Zhao and Castellano attributed excimer suppression with 1,6-di-*tert*-butyl pyrene to the steric hindrance from the two *tert*-butyl substituent in comparison to pyrene (Figure 4.16).<sup>[1]</sup>



**Figure 4.16** Structures of pyrene and 3,8-di-*tert*-butyl pyrene

The suppression of excimer formation in the case of pyrenyl derivatives is important as it minimizes long wavelength emission from the excimer.<sup>[1]</sup> This is crucial in our selection of TINA-modified DNA systems which are more likely to produce upconversion with the chromophores of interest.

#### 4.5.4 [Ru(bpy)<sub>3</sub>]<sup>2+</sup> and DPA in EU

Anthracenyl derivatives are good choices as acceptors for EU as demonstrated in Table 1.1, Chapter 1. Zhao and Castellano observed green-to-blue EU by the TTA mechanism between [Ru(bpy)<sub>3</sub>]<sup>2+</sup> and DPA using a green laser pointer and a conventional fluorimeter,<sup>[1]</sup> which was also observed in our case with a [Ru(bpy)<sub>3</sub>]<sup>2+</sup> - PEPy system in DCM, as described above in Section 4.5.3. The EU showed quadratic power dependence as expected of a TTA-based mechanism. Hence, we also considered using anthracene derivatives for modification of DNA as described in Chapter 5.

#### 4.5.5 ZnTMPyP4 and TINA monomer (PEPy) in EU

Next, we evaluated interactions between ZnTMPyP4 and PEPy. The chromophores were dissolved in 9:1 DMSO/ H<sub>2</sub>O and were degassed using the set-up described in the section above for 24 hours. The concentrations ranges were guided by Stern-Volmer analyses in Section 4.4.2 above. We explored several solutions in the concentration range of ZnTMPyP4 (5.0 – 200 μM) and PEPy (0.01 – 5 mM), but no EU was observed, even after prolonged degassing (24 hr). Possible explanations for this observation include: (i) PEPy upconverted fluorescence may be completely quenched by ZnTMPyP4, as it has been shown that high concentrations of porphyrin completely quench PEPy fluorescence in Section 4.4.2 (ii) Aqueous and DMSO solutions have high content of dissolved oxygen that quenches the triplet state (iii)

The singlet-triplet energy gap for ZnTMpyP4 may not be favorable for the energetics of upconversion with PEPy.

Although we did not observe any upconversion between ZnTMpyP4 and PEPy under our experimental conditions, we decided to continue our study with ZnTMpyP4 in DNA-templated EU because: (i) it is a well known ligand that interacts with DNA, and (ii) zinc metallated porphyrins and phthalocyanines have been used successfully as long wavelength absorbers in EU in combination with pyrene derivatives. In this regard, this system could be possibly used for EU as the interaction between PEPy and ZnTMpyP4 might be favorable for EU on the DNA template.

## 4.6 References

- [1] W. Zhao, F. N. Castellano, *The Journal of Physical Chemistry A* **2006**, *110*, 11440.
- [2] a) J. Lakowicz, *Principles of Fluorescence Spectroscopy*, Springer, **2006**. b) See also <http://hof-fluorescence-group.weebly.com/fluorescence-course.html>
- [3] B. M. Wilke, F. N. Castellano, *Journal of Chemical Education* **2013**, *90*, 786.
- [4] M. Eftink, L. Selvidge, *Biochemistry* **1982**, *21*, 117.
- [5] M. Asha Jhonsi, A. Kathiravan, G. Paramaguru, C. Manivannan, R. Renganathan, *Journal of Solution Chemistry* **2010**, *39*, 1520.
- [6] K. Kalyanasundaram, *Inorganic Chemistry* **1984**, *23*, 2453.
- [7] a) R. R. Islangulov, J. Lott, C. Weder, F. N. Castellano, *Journal of the American Chemical Society* **2007**, *129*, 12652; b) R. R. Islangulov, D. V. Kozlov, F. N. Castellano, *Chemical Communications* **2005**, 3776.
- [8] S. K. Sugunan, U. Tripathy, S. M. K. Brunet, M. F. Paige, R. P. Steer, *The Journal of Physical Chemistry A* **2009**, *113*, 8548.
- [9] K. Tanaka, K. Inafuku, Y. Chujo, *Chemical Communications* **2010**, *46*, 4378.
- [10] T. N. Singh-Rachford, F. N. Castellano, *Coordination Chemistry Reviews* **2010**, *254*, 2560.
- [11] L. S. Forster, *Coordination Chemistry Reviews* **2006**, *250*, 2023.

## 5 Arrangement of Chromophores on DNA using “Click Chemistry” for EU

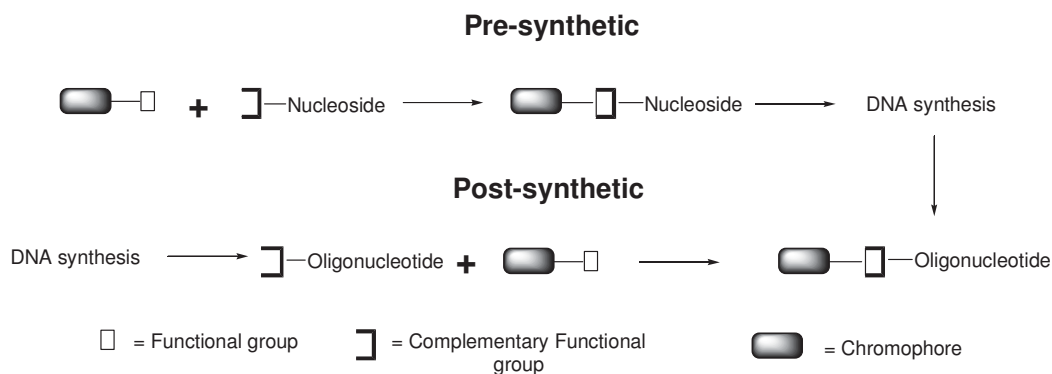
### 5.1 DNA Chemical Modification

Organic chromophores can be introduced into DNA by covalent or non-covalent attachment. Molecules may interact with DNA non covalently by electrostatic binding, or intercalating.<sup>[1]</sup> Intercalation occurs when ligands of an appropriate size and chemical nature fit themselves between base pairs of DNA. These ligands are mostly polycyclic, aromatic, and planar, and therefore often make good nucleic acid stains. The most exciting exploitation of intercalators is their interaction with nucleic bases via  $\pi$ - $\pi$  stacking.<sup>[2]</sup> DNA intercalators are used in chemotherapeutic treatment to inhibit DNA replication in rapidly growing cancer cells. By covalent attachment we can control the position of chromophores on the DNA.

#### 5.1.1 Covalent modification

Covalent attachment of organic chromophores into DNA structures can be achieved via modification of nucleotides (e.g. attachments to the base, sugar, or phosphate) or via entirely non-nucleosidic linkers.<sup>[2]</sup> The chromophore can be placed in the interior of nucleic bases or in the grooves of the nucleic acid complexes. The covalent attachment can be achieved through pre- or post-synthetic methods. In the pre-synthetic method (Figure 5.1) the organic chromophore is attached to a nucleoside which is then converted to a phosphoramidite or H-phosphonate. These are incorporated into the DNA structure during automated DNA synthesis. The phosphoramidite bearing the desired label needs to be stable enough to survive the harsh conditions employed during solid-phase synthesis (acidic and oxidative) and deprotection (strong alkaline conditions) of the DNA strand.<sup>[3]</sup> Furthermore, certain modifications are not available as a modified-CPG or phosphoramidite and must be attached to the oligonucleotide after the synthesis. Post-synthetic modifications are achieved using complementary functional groups. In the post-synthetic strategy (Figure 5.1), a small reactive group is introduced into DNA, which can then be conjugated to the desired functional molecule in a selective manner after DNA synthesis and deprotection.<sup>[3]</sup> Post-synthetic chemical modifications of

oligonucleotides (ONs) tend to result in lower yields than modifications introduced during synthesis. However, high purity DNA is usually obtained after purification using high-performance liquid chromatography (HPLC) with reverse phase columns or using denaturing polyacrylamide gel electrophoresis (PAGE).



**Figure 5.1** Representation for pre- and post-synthetic DNA modifications.

This research aims to employ covalent attachment of organic chromophores via both post and pre-synthetic approaches. A number of methods have been developed for post-synthetic covalent attachment of organic labels.<sup>[2, 4]</sup> The Cu<sup>I</sup> catalysed Huisgen 1,3-dipolar cycloaddition (CuAAC) reaction (Figure 5.2) between azides and terminal alkynes, and the isoxazole generating 1,3-dipolar cycloaddition of nitrile oxides and alkynes (Figure 5.3), both classified as “click chemistry”, have been being explored on DNA. The CuAAC reaction is well established,<sup>[5]</sup> and has been used in our laboratory for DNA functionalization.<sup>[6]</sup>

### 5.1.2 Click Chemistry on DNA

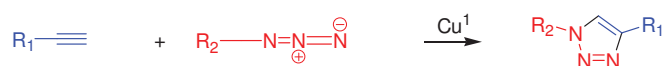
#### 5.1.2.1 Cu(I)-catalysed Huisgen 1,3-dipolar cycloaddition (CuAAC)

“Click chemistry” describes reactions tailored to generate substances quickly and reliably by joining small units together. “Click chemistry” is not a specific reaction; it is a concept that mimicks Nature. A “click” reaction is one that is wide in scope, is stereospecific, easy to perform, uses only readily available reagents, gives very high chemical yields, has no or inoffensive by-products, exhibits a large thermodynamic driving force to favor a reaction with a single reaction product, and provides simple product isolation among other factors. In several instances water is the ideal reaction solvent, providing the best yields and highest rates. Reaction work-up and

purification uses benign solvents and avoids chromatography.<sup>[7]</sup> Several reactions have been identified which fit the criteria:

- Cycloaddition reactions, such as the Huisgen 1,3-dipolar cycloaddition and the Diels-Alder reaction.
- Nucleophilic substitution especially to small strained rings like epoxy and aziridine compounds.
- Carbonyl chemistry of the non-aldol type.
- Addition reactions to carbon-carbon multiple bonds.<sup>[7]</sup>

The Cu(I)-catalyzed Huisgen 1,3-dipolar cycloaddition (CuAAC) of alkynes and azides (Figure 5.2) yielding 1,2,3-triazoles, is often referred to simply as the "click reaction". The Cu(I) catalyzed version is highly preferred as it offers a dramatic rate acceleration, complete conversion and the resulting triazole is stable to hydrolysis, oxidation and reduction.<sup>[8]</sup>



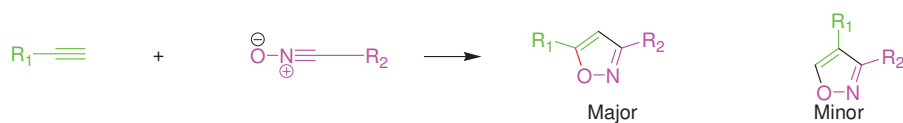
**Figure 5.2** General scheme for the Cu(I)-catalysed Huisgen 1,3-dipolar cycloaddition (CuAAC) reaction between azides and terminal alkynes.

#### 5.1.2.2 1,3- Dipolar cycloaddition of nitrile oxides and alkynes (NO/AC)

Recently, there has been significant interest in developing “click” reactions that do not require any metal catalyst while exhibiting all the beneficial properties of the CuAAC reaction.<sup>[9]</sup> The potential toxicity of metal catalysts used in organic synthesis is a major issue when the products are designed to be used for biological applications and other applications where metal interference is undesirable.<sup>[9-10]</sup> Metal free highly efficient Click reactions include reactions such as nucleophilic substitution, radical additions, Michael additions, as well as Diels–Alder and retro-Diels–Alder reactions.<sup>[9]</sup> The uncatalyzed isoxazole generated by nitrile oxide/alkyne cycloadditions (NO/AC) present an interesting prospect (Figure 5.3). Indeed, these reactions can be performed at relatively mild temperatures and are usually highly regioselective.<sup>[10]</sup> More importantly, this reaction enables modification of



oligonucleotides in solution and on solid supports.<sup>[11]</sup>

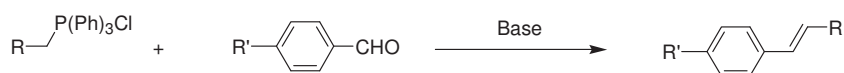


**Figure 5.3** General Scheme for the 1,3-Dipolar Cycloaddition of Nitrile Oxides and Alkynes.

## 5.2 Chapter Summary

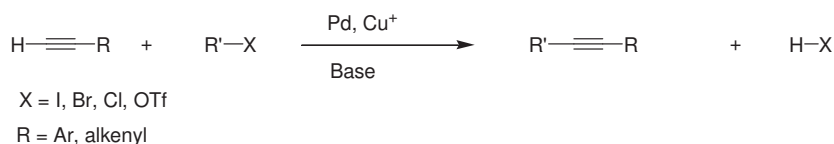
In this Chapter we describe our endeavours to covalently attach organic chromophores to DNA by “click chemistry.”<sup>[12]</sup> Here, we used the Cu(I)-catalyzed Huisgen 1,3-dipolar cycloaddition of alkynes and azides and the metal free isoxazole generating nitrile oxide/alkyne cycloaddition reactions to attach chromophores to DNA. In order to achieve this, azide or nitrile oxide functionalized chromophores are required to react with alkyne functionalized DNA. In the case of nitrile oxide/alkyne. Therefore, we aimed to obtain azide, oxime and hydroximinoyl chloride functionalized anthracenyl, pyrenyl and porphyrinic derivatives.

The syntheses of styryl linked organic chromophores were achieved via the Wittig reaction between a phosphonium salt and a substituted benzaldehyde (Figure 5.4)<sup>[13]</sup>.



**Figure 5.4** Generalized Wittig reaction

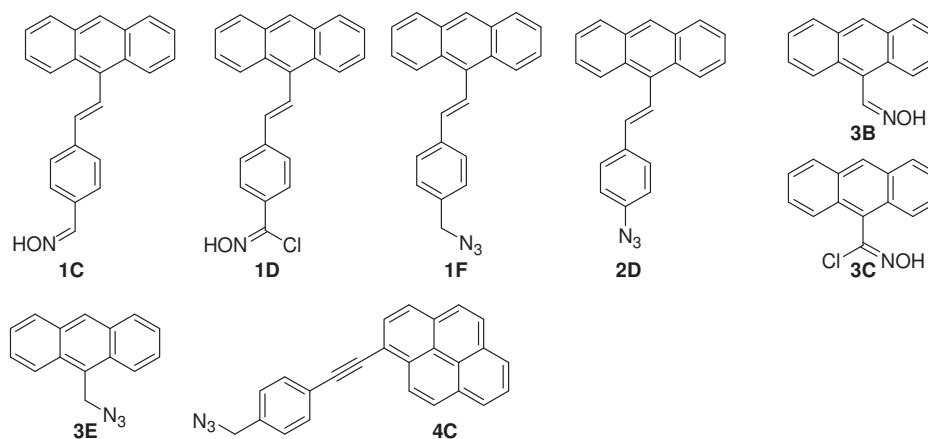
Alkyne linked chromophores were synthesized using a Sonogashira coupling of terminal alkynes with aryl or vinyl halides in the presence of a palladium catalyst, a copper(I) co-catalyst, and an amine base<sup>[14]</sup>(Figure 5.5).



**Figure 5.5** Generalized Sonogashira reaction.

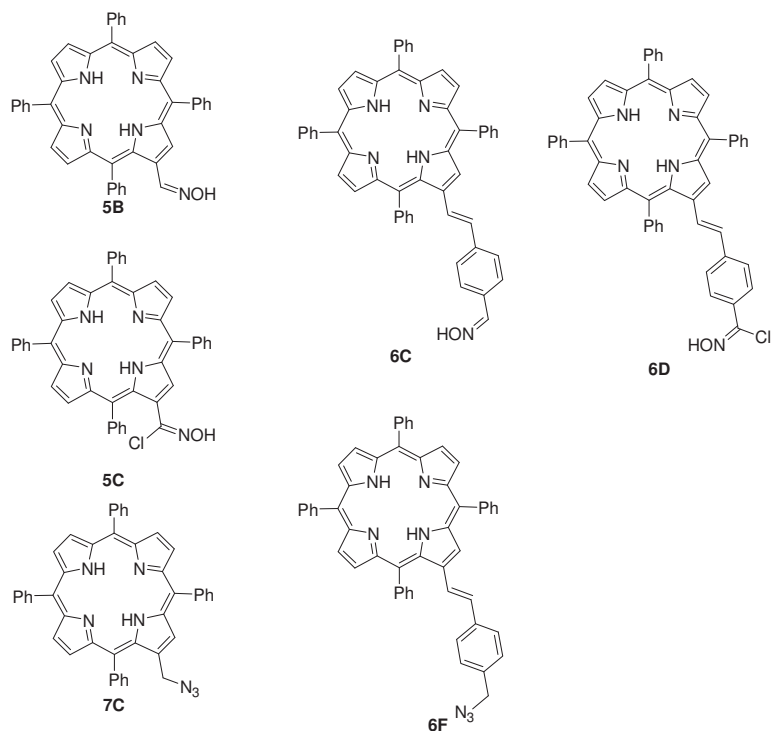
Oxime functionalized chromophores were synthesized by a condensation of an aldehyde or a ketone with hydroxylamine. The condensation of aldehydes with hydroxylamine gives aldoxime, and ketoxime is produced from ketones and hydroxylamine. Oximes were converted to hydroximinoyl chlorides by chlorination using *N*-chlorosuccinimide or chloroamine-T.<sup>[15]</sup> Appropriately functionalized compounds were converted to azides via nucleophilic substitution with sodium azide.<sup>[13]</sup>

The proposed target organic chromophores containing the required functional groups for “click chemistry” are all found below (Figure 5.6 and Figure 5.7). The proposed photoemitters are PAHs, particularly anthracenyl and pyrenyl derivatives. Styryl linked, ethynyl benzene linked and directly linked azide/oxime/hydroximinoyl chloride functionalities were explored.



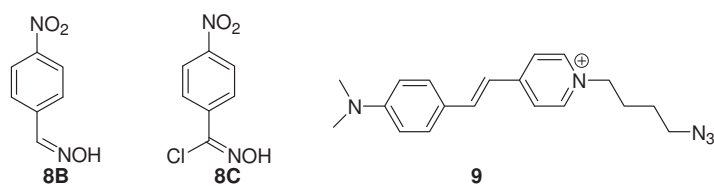
**Figure 5.6.** Structures of proposed PAH derivative chromophores for “click chemistry”.

Porphyrin derivatives; styryl linked and directly linked porphyrinic azides/oxime/hydroximinoyl chlorides were studied (Figure 5.7).



**Figure 5.7** Structures of proposed porphyrin derivative chromophores for “click chemistry”.

Easily synthesized 4-nitrobenzaldehyde derivatives i.e. 4-nitrobenzaldehyde oxime and 4-nitrobenzaldehyde hydroximinoyl chloride have been used as model compounds for nitrile oxide/alkyne “click chemistry” on DNA (Figure 5.8). The dye, 1-(4-azidobutyl)-4-[2-(4-dimethylaminophenyl)vinyl]pyridinium (**9**), synthesized previously in our lab was also investigated to verify already known CuAAC Click chemistry.

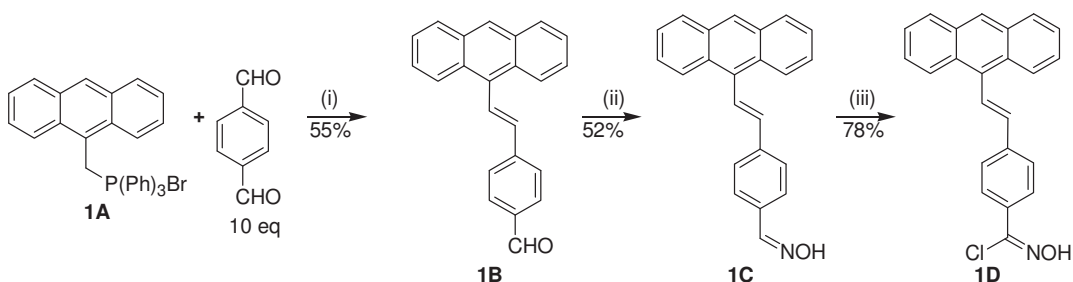


**Figure 5.8** Model compounds for “click chemistry” on DNA.

### 5.3 Synthesis of Organic Chromophores for DNA modification

#### 5.3.1 Synthesis of 1C and 1D

Compound **1B** was prepared by the Wittig reaction<sup>[16]</sup> between the 9-anthracene methylphosphonium salt (**1A**) and terephthalaldehyde (Figure 5.9), followed by isomerization with 3 equivalents of  $I_2$  at RT for 3 hours to yield the desired trans double bond (See experimental section 11.1.2.1).



**Figure 5.9** Compounds **1C** and **1D** synthesis route. Reaction conditions; (i)  $tBuOK$  (1.1 eq), THF, reflux, 3 h, then  $I_2$  (3 eq), THF, RT, 3 h; (ii)  $NH_2OH \cdot HCl$  (2.0 eq),  $NaOAc$  (2.0 eq),  $H_2O/EtOH/CHCl_3$ , 12 h; (iii)  $NCS$  (1.2 eq, DMF)

$^1H$  NMR spectroscopy showed two doublets at 7.10 and 8.00 ppm with equal  $^3J_{H-H}$  coupling constants of approximately 16 Hz from the two ethenyl protons and a singlet at 10.07 ppm from the carbonyl proton. IR spectroscopy showed that the carbonyl  $C=O$  stretch at  $1693\text{ cm}^{-1}$  was present in the IR-spectra of **1B**. This compound was isolated as a bright yellow-orange solid by silica gel column chromatography using a 7.5:2.5 DCM-hexane eluent. Compound **1B** was converted to the oxime **1C** with hydroxylamine in a slightly alkaline medium using a modified published method.<sup>[10]</sup> A  $CHCl_3:EtOH:H_2O$  mixture was used as a solvent in place of  $EtOH:H_2O$  to increase the solubility of the starting material **1B**. The integrity of the anthracene and trans double bond was shown by the  $^1H$  NMR spectra. NMR spectroscopy revealed two double peaks at 8.02 and 6.99 ppm. In addition to the ethenyl proton signals, the  $^1H$  NMR spectrum of **1C** also displayed the expected anthracene set of peaks between 7.50 and 8.50 ppm. The disappearance of the IR carbonyl stretch around  $1693\text{ cm}^{-1}$  was accompanied by an appearance of a  $C=N$  stretch at  $1601\text{ cm}^{-1}$  and a broad OH stretch at  $3273\text{ cm}^{-1}$  in **1C**. Chlorination of **1C** to **1D** was achieved using *N*-chlorosuccinimide in DMF.<sup>[15]</sup>

### 5.3.2 Synthesis of 1F

The synthesis of compound **1E** was accomplished by reduction of an aldehyde (**1B**) with sodium borohydride.<sup>[17]</sup> This was accompanied by a disappearance of the IR carbonyl stretch at  $1693\text{ cm}^{-1}$  and the appearance of the alcohol stretch at  $3308\text{ cm}^{-1}$ .

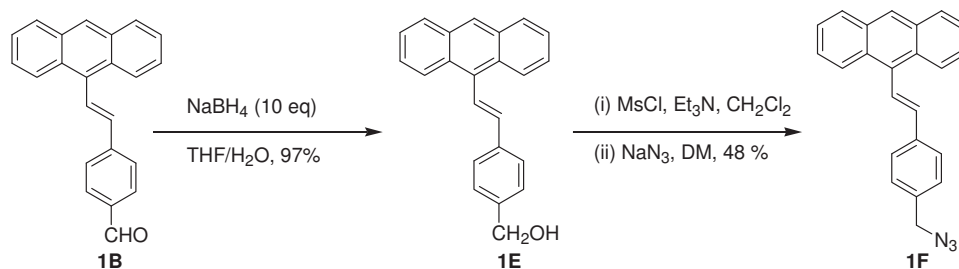


Figure 5.10 The synthesis of compound **1E** and **1F** with reaction conditions.

The desired azide functionalized compound **1F** was synthesized through nucleophilic substitution on **1E** using  $\text{NaN}_3$  as illustrated on Figure 5.10 above.<sup>[17]</sup> The alcohol IR stretch at  $3308\text{ cm}^{-1}$  was replaced by strong  $\text{N}_3$  stretch at  $2144\text{ cm}^{-1}$  in the product (See experimental section 11.1.2.5).

### 5.3.3 Synthesis of 2D

The synthesis of compound **2B** was achieved by a Wittig reaction<sup>[16]</sup> between the 9-anthracene methylphosphonium salt and 4-nitrobenzaldehyde (Figure 5.11). Reduction of **2B** with stannous chloride<sup>[18]</sup> yielded **2C** which has two distinctive amine IR stretches at  $3354$  and  $3459\text{ cm}^{-1}$  respectively (See experimental section 11.1.2.7).

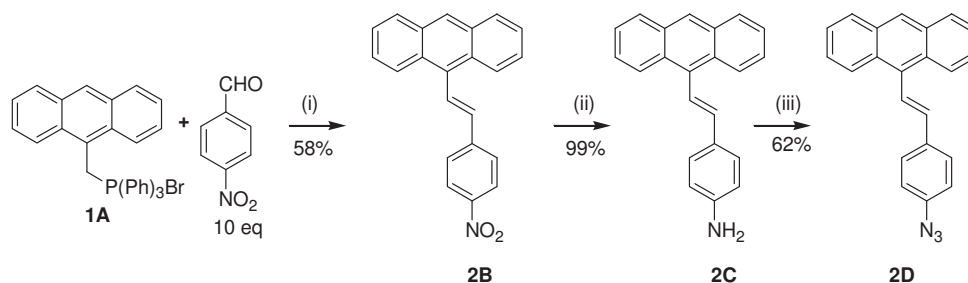
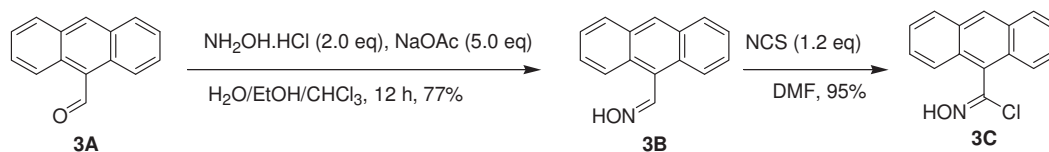


Figure 5.11 The synthesis of compound **2D**. Reaction conditions; (i)  $\text{tBuOK}$  (1.1 eq), THF, reflux, 3 h, then  $\text{I}_2$  (3 eq), THF, RT 3 h; (ii)  $\text{SnCl}_2$  (excess)/conc.  $\text{HCl}$ , EtOH, reflux, 12 h; (iii)  $\text{NaNO}_2$ ,  $\text{H}_2\text{SO}_4$ ,  $\text{NaN}_3$ , THF/ $\text{H}_2\text{O}$ .

After diazotization of compound **2C**, nucleophilic substitution with sodium azide<sup>[17]</sup> provided the desired azide functionalized compound **2D** with an IR stretch at 2141  $\text{cm}^{-1}$  (See experimental section 11.1.2.8).

### 5.3.4 Synthesis of **3B**

The commercially available compound **3A** was converted to the aldehyde oxime **3B** according to the modified literature method<sup>[10]</sup> as for **1C**.

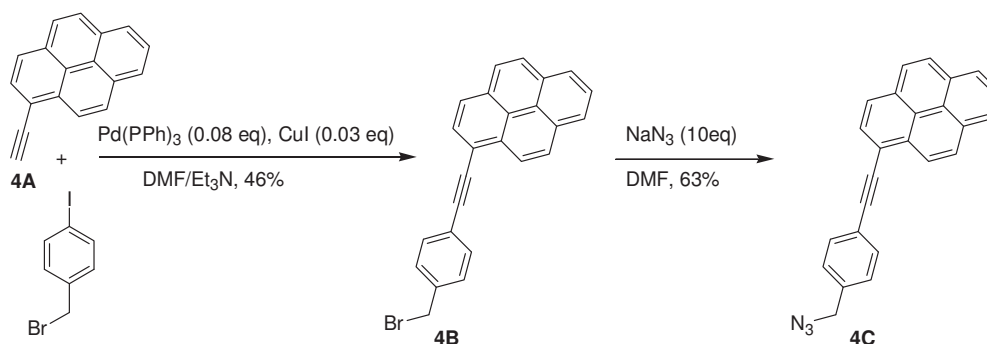


**Figure 5.12** Compound **3B** synthesis with reaction conditions. The synthesis conditions for compound **3C** are also shown.

The synthesis of **3C** was done under the same conditions as **1D** (Figure 5.12).<sup>[15]</sup>

### 5.3.5 Synthesis of **4C**

The synthesis of compound **4B** was achieved using Sonogashira conditions between 1-ethynylpyrene (**4A**) and 4-iodobenzyl bromide (Figure 5.13).<sup>[19]</sup>



**Figure 5.13** The synthesis of the ethynyl-linked azide functionalized **4C** via a Sonogashira coupling<sup>[19]</sup> followed by a nucleophilic substitution.<sup>[20]</sup>

The desired compound **4C** was prepared by a nucleophilic substitution with sodium azide using a modified published method.<sup>[20]</sup> The substitution of the bromine atom with the azido group was carried out in THF rather than acetone as reported,<sup>[20]</sup> to give **4C** confirmed by the appearance of an IR peak at 2097  $\text{cm}^{-1}$  assigned to a  $\text{N}=\text{N}=\text{N}$  stretch of the azide (see experimental section 11.1.2.11).

### 5.3.6 Synthesis of 5B and 5C

The aldehyde (Compound **5A**) was converted to the oxime (**5B**) under the same conditions as for **1C** (Figure 5.14).<sup>[10]</sup>

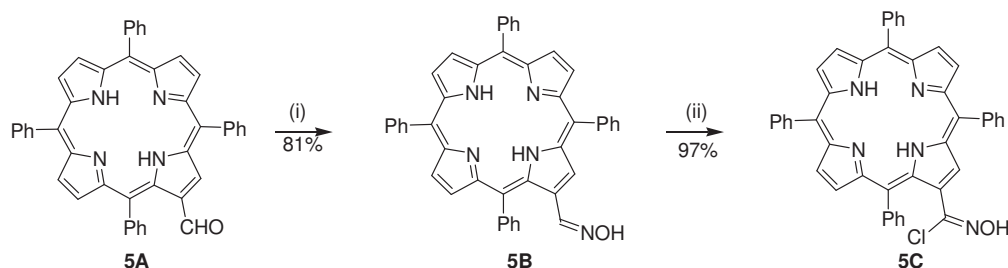


Figure 5.14 Synthesis of compounds **5B** and **5C**. (i)  $\text{NH}_2\text{OH}\cdot\text{HCl}$  (2.0 eq),  $\text{NaOAc}$  (5.0 eq),  $\text{H}_2\text{O}/\text{EtOH}$ , 12 h; (ii)  $\text{NCS}$  (1.2 eq),  $\text{DMF}$ .

Compound **5C** was synthesized under the same conditions as **1D**.

### 5.3.7 Synthesis of 6C and 6D

The styryl linked porphyrin **6B** was synthesized by the Wittig reaction of *meso*-tetraphenylporphyrin phosphonium salt (TPPPs, **6A**) and terephthalaldehyde.<sup>[16]</sup> This compound was purified by silica gel column chromatography.

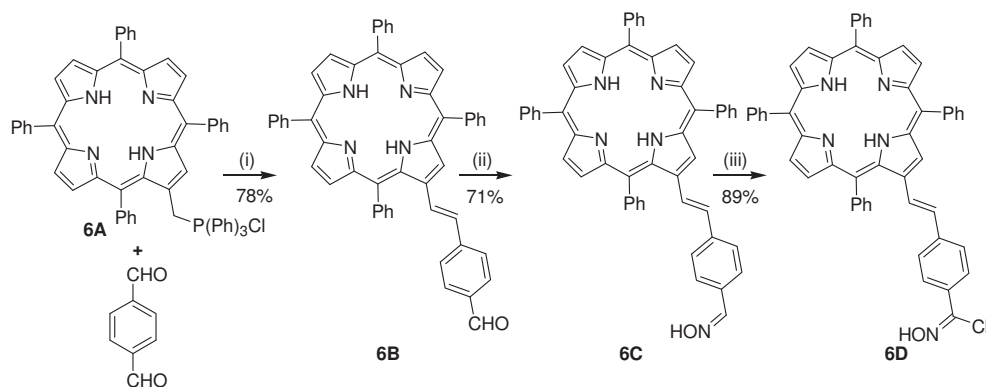


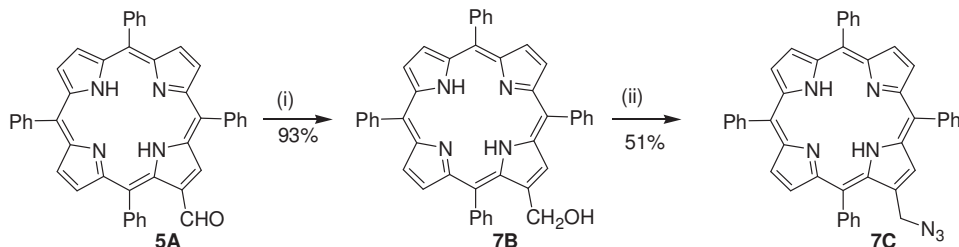
Figure 5.15 The synthesis of the styryl-linked porphyrins **6C** and **6D**. Reaction conditions; (i)  $\text{tBuOK}$  (1.1 eq),  $\text{THF}$ , reflux, 3 h; then  $\text{I}_2$  (3 eq),  $\text{THF}$ , RT, 3 h; (ii)  $\text{HONH}_2\cdot\text{HCl}$  (2.0 eq),  $\text{NaOAc}$  (5.0 eq),  $\text{H}_2\text{O}/\text{EtOH}/\text{CHCl}_3$ , 12 h; (iii)  $\text{NCS}$  (1.2 eq,  $\text{DMF}$ ).

Compound **6B** was converted to the desired oxime **6C** with hydroxylamine.<sup>[10]</sup>

Compound **6C** was chlorinated to **6D** using *N*-chlorosuccinimide (Figure 5.15, See experimental section 11.1.2.16).<sup>[15]</sup>

### 5.3.8 Synthesis of 7C

The alcohol **7B** was prepared via a sodium borohydride reduction<sup>[17]</sup> in a THF/H<sub>2</sub>O solvent mixture (Figure 5.16).

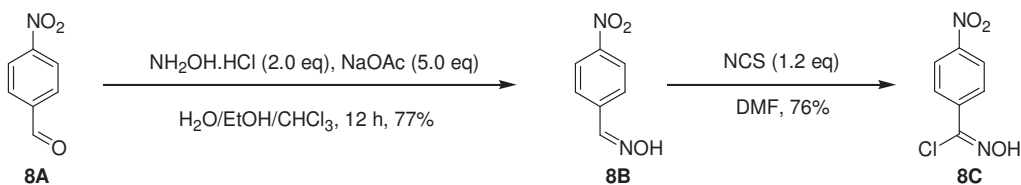


**Figure 5.16** The synthesis of compound **7C**. Reaction conditions; (i) NaBH<sub>4</sub> (10 eq), THF/H<sub>2</sub>O; (ii) MsCl, Et<sub>3</sub>N, CH<sub>2</sub>Cl<sub>2</sub> then NaN<sub>3</sub> (10 eq), THF.

We synthesized the desired azide functionalized porphyrin **7C** through nucleophilic substitution on **7B** using NaN<sub>3</sub> as illustrated on Figure 5.16 above (See experimental section 11.1.2.18).<sup>[17]</sup>

### 5.3.9 Synthesis of 8B and 8C

The commercially available aldehyde **8A** was converted to the oxime **8B** (Figure 5.17) with hydroxylamine in a slightly alkaline medium in an EtOH:H<sub>2</sub>O (9 : 1) as previously published.<sup>[10]</sup>



**Figure 5.17** The synthesis of compounds **8B** and **8C** with reaction conditions.

The hydroximinoyl chloride, **8C** was prepared by chlorination of **8B** using *N*-chlorosuccinimide.<sup>[15]</sup>

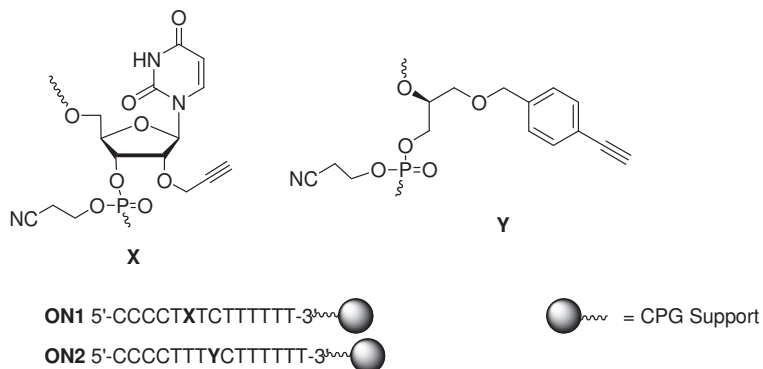
## 5.4 Post-synthetic DNA functionalization

### 5.4.1 DNA synthesis

DMT-off oligodeoxynucleotides on CPG solid support were synthesised on a MerMade 4 Automated DNA Synthesizer under standard conditions with hand coupling of the required functional group modified nucleoside phosphoramidites. A single insertion of the commercially available 2'-*O*-propargyl uridine (**X**) or the p-



ethynylbenzyl functionalized (*R*)-1-*O*-(4-ethynylbenzyl)glycerol (**Y**) synthesized in our lab, was used in the initial trial experiments to give **ON1** and **ON2** respectively (Figure 5.18). Solutions of 2'-*O*-propargyl uridine phosphoramidite or (*R*)-1-*O*-(4-ethynylbenzyl)glycerol phosphoramidite in activator (4,5-dicyanoimidazole (DCI) in dry acetonitrile) were coupled at the appropriate positions of DNA in the synthesis cycle (See experimental section 11.1.3).



**Figure 5.18** Oligodeoxynucleotides **ON1** and **ON2**. **ON1** has a single insertion of 2'-*O*-propargyl uridine (**X**) **ON2** has a single insertion of (*R*)-1-*O*-(4-ethynylbenzyl)glycerol (**Y**).

Oligonucleotide sequences bearing cytosine and thymine only (CT sequences) were selected as they are easy to deprotect and easily analysed by MALDI-TOF. These containing oligonucleotides were then evaluated in “click chemistry” to attach organic chromophores. All post-synthetic reactions were carried out on DNA bound to the CPG solid support.

#### 5.4.2 DNA modification

As mentioned previously, the “click reaction” is favored for post-synthetic attachment of organic chromophores to the triple bond functionalized DNA. We chose to initially investigate the post-synthetic oligonucleotide modification approach as opposed to the pre-synthetic method which involves time consuming preparation of modified phosphoramidites that, in most cases, also have limited stability.

CuAAC and NO/AC reactions between the CPG bound terminal alkyne functionalized oligonucleotides **ON1** and **ON2** with azide, oxime and hydroximinoyl chloride functionalized anthracenyl, pyrenyl and porphyrinic moieties (See Figures

5.6 and 5.7 for structures) were investigated. Metal free NO/AC chemistry was first attempted with model 4-nitrobenzaldehyde derivatives in order to validate feasibility of the reactions. For NO/AC “click chemistry”, the nitrile oxide was prepared in situ from the oxime/hydroximinoyl chloride precursor using *N*-chlorosuccinimide or chloramine-T as the dipole generating agent.<sup>[10, 21]</sup>

**Table 5.1** Nitrile oxide/alkyne cycloaddition (NO/AC) and Cu(I)-catalyzed Huisgen 1,3-dipolar cycloaddition (CuAAC) reactions attempted on **ON1** and **ON2**.

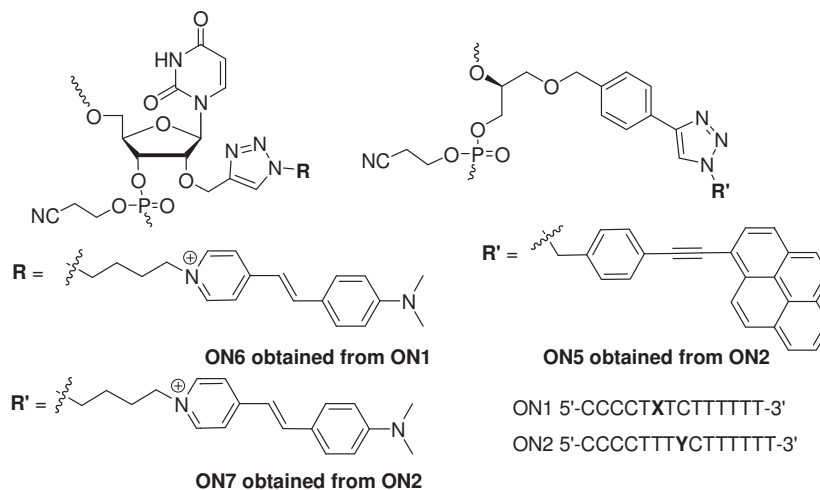
Reaction	Oligonucleotide	Chromophore	Reaction type	Reaction occurrence*
1	ON1	8B <sup>c</sup>	NO/AC <sup>a</sup>	Yes, <b>ON3</b>
2	ON1	8C <sup>d</sup>	NO/AC <sup>a</sup>	Yes, <b>ON3</b>
3	ON1	1C <sup>c</sup>	NO/AC <sup>a</sup>	No
4	ON1	1D <sup>d</sup>	NO/AC <sup>a</sup>	No
5	ON1	5B <sup>c</sup>	NO/AC <sup>a</sup>	No
6	ON1	6C <sup>c</sup>	NO/AC <sup>a</sup>	No
7	ON1	6D <sup>d</sup>	NO/AC <sup>a</sup>	No
8	ON1	3C <sup>c</sup>	NO/AC <sup>a</sup>	Yes, <b>ON4</b>
9	ON1	6C <sup>c</sup>	NO/AC <sup>a</sup>	No
10	ON1	6D <sup>d</sup>	NO/AC <sup>a</sup>	No
11	ON1	5B <sup>c</sup>	NO/AC <sup>a</sup>	No
12	ON1	4C <sup>e</sup>	CuAAC <sup>b</sup>	No
13	ON2	4C <sup>e</sup>	CuAAC <sup>b</sup>	Yes, <b>ON5</b>
14	ON1	9 <sup>e</sup>	CuAAC <sup>b</sup>	Yes, <b>ON6</b>
15	ON2	9 <sup>e</sup>	CuAAC <sup>b</sup>	Yes, <b>ON7</b>

<sup>a</sup>Nitrile oxide/alkyne cycloaddition. <sup>b</sup>Cu(I)-catalyzed Huisgen 1,3-dipolar cycloaddition. <sup>c</sup>Oxime, <sup>d</sup>Hydroximinoyl chloride.

<sup>e</sup>Organic azide, See Insert in appendix for chromophore structures. \*As observed in denaturing 20% PAGE.

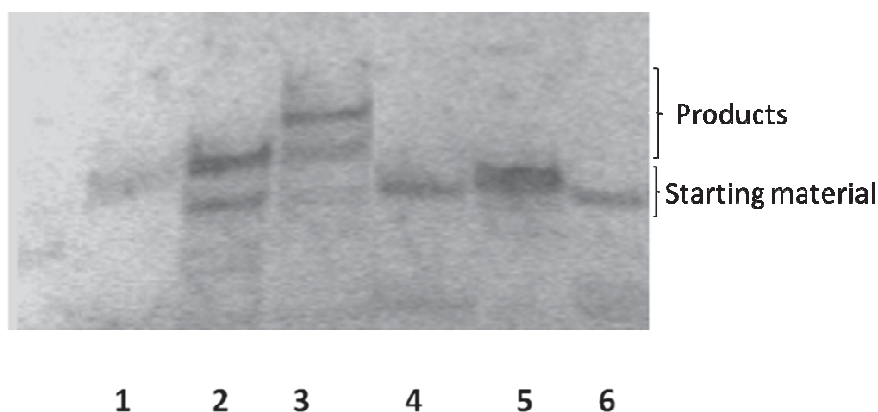
Numerous conditions were attempted for the post-synthetic attachment of organic molecules to DNA through “click chemistry” using ambient conditions as well as microwave irradiation. The CuAAC method has been used extensively in our laboratory.<sup>[22]</sup> The commonly used method involves the shaking of the reaction mixture containing an oligonucleotide bound to a CPG support, organic azide, CuSO<sub>4</sub> and sodium ascorbate at room temperature. The required Cu<sup>I</sup> catalyst is produced from the *in situ* reduction of Cu<sup>II</sup> with sodium ascorbate. Alternatively, CuBr could be used.<sup>[22]</sup> However, CuSO<sub>4</sub>·5H<sub>2</sub>O is easier to handle due to its greater solubility in water. Stephenson<sup>[22]</sup> reported low yields using the room temperature CuAAC reaction for azide functionalized porphyrins with ONs bearing 2'-*O*-propargyl nucleotides and then employed focused microwave irradiation which resulted in full conversion of the starting ONs as indicated by denaturing PAGE of

the ONs cleaved from the CPG support. A similar approach was employed in our case to modify **ON1** and **ON2** with azide functionalized chromophores.



**Figure 5.19** Organic chromophore modified ONs obtained using the post-synthetic CuAAC reaction. The modifications are on **X (ON1)** and **Y (ON2)**.

The model azide functionalized dye, **9** (Figure 5.8) reacted with both the 2'-*O*-propargyl uridine (**ON1**) and the *p*-ethynylbenzyl functionalized **ON2** to give **ON6** and **ON7** as observed in denaturing 20% PAGE after ONs were cleaved from the solid supports (Figure 5.19). The azide functionalized pyrenyl derivative only reacted with **ON2** (Figure 5.19). Reaction occurrence between ONs and the chromophores was checked using 20% denaturing PAGE followed by developing of ONs with Stains-All dye (Figure 5.20).



**Figure 5.20** Denaturing 20% PAGE (7 M urea) of chromophore modified oligonucleotides (by CuAAC) stained with Stains-All<sup>®</sup> dye and destained with H<sub>2</sub>O. Lane 1 is **ON6**, lane 2 is **ON5**, lane 3 is **ON7**, lane 4 is failed reaction 12 (Table 5.1), lane 5 is **ON2** and lane 6 is **ON1**.

It is important to note that studies have been carried out to establish feasibility of reactions, as well as determine which groups react better than others. The extent of reactions as well as reaction yields were determined using a qualitative assessment. The reaction of **ON1** with compound **9** results in an estimated complete conversion according to denaturing PAGE. However, **ON1** does not react with **4C**. In contrast, **ON2** reacts with both **9** and **4C** albeit with estimated incomplete reactions. It is postulated that the bulged insertion of the TINA monomer may make the triple bond more available for reaction with compound **9**.

Although the CuAAC reaction is well established, high yielding and efficient, the presence of copper poses the threat of metallation/transmetallation of porphyrin moieties and can also possibly degrade DNA in the presence of oxygen through generation of highly reactive oxygen species (ROS). Hence, proper precautions have to be taken during CuAAC chemistry for DNA modification. We decided to explore metal-free nitrile oxide/azide cycloaddition (NO/AC) chemistry on DNA.<sup>[9-11, 21, 23]</sup>

A range of conditions were attempted for the NO/AC reaction using two model compounds, 4-nitrobenzaldehyde oxime (**8B**) and 4-nitrobenzaldehyde hydroximinoyl chloride (**8C**), Table 5.1. Both the oxime functionalized **8B** and the hydroximinoyl chloride functionalized **8C** reacted with the 2'-*O*-propargyl uridine functionalized **ON1** to give **ON3** (Figure 5.21). A chromophore of interest, 9-anthraldehyde oxime (**3B**) also reacted with **ON1** to give **ON4** (Figure 5.21). The oxime (**1C**) and hydroximinoyl chloride (**1D**) functionalized styryl linked anthracenyl derivatives as well as both the oxime functionalized porphyrins (**5B** and **6C**) and hydroximinoyl chloride functionalized porphyrin **6D** did not react with **ON1** (Table 5.1).

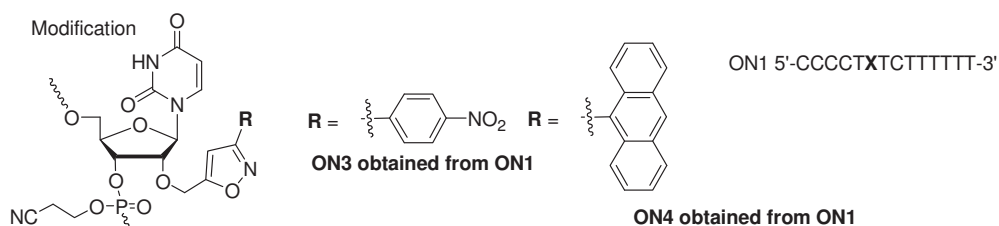


Figure 5.21 Oligonucleotides modified via NO/AC reaction. The modification is on **X** (**ON1**).

A summary of the NO/AC reactions attempted including chromophores, reagents, conditions, and reaction times are shown in Table 5.2.

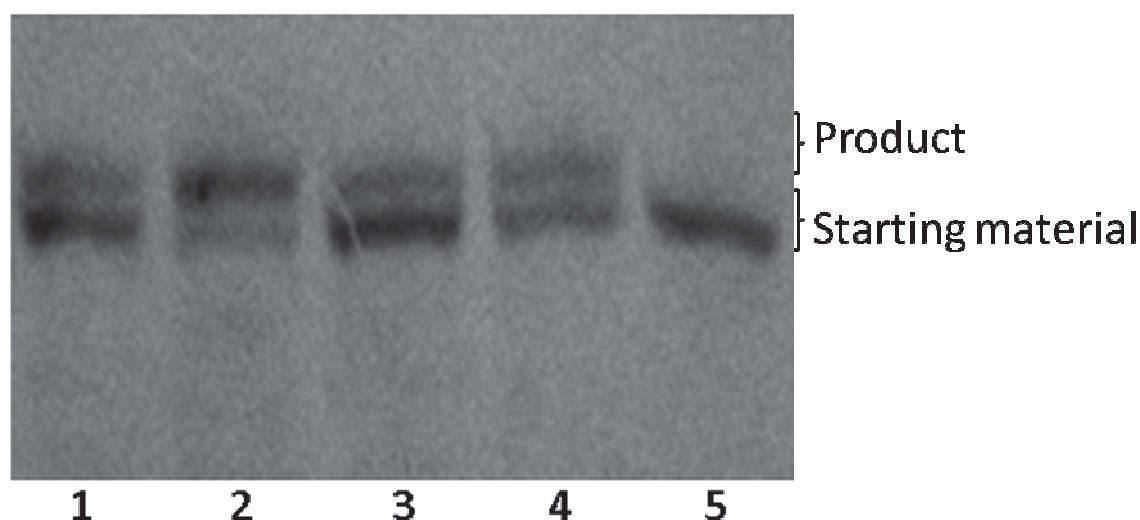
**Table 5.2** NO/AC reaction conditions attempted on **ON1**. Note structures of chromophores are in Figures 5.6 - 5.8.

Reaction	Chromophore	Reagents; Conditions; Duration	Reaction Occurrence*	Reaction progress
1	8B <sup>a</sup>	NCS, DMF, 0.1 M NaHCO <sub>3</sub> (aq), RT; Overnight	Yes	Incomplete
2	8C <sup>b</sup>	1:1 ACN/H <sub>2</sub> O, RT; Overnight	Yes	Incomplete
3	8C <sup>b</sup>	1:1 DMF/Et <sub>3</sub> N, RT; Overnight	No	N/A
4	8C <sup>b</sup>	1:1 ACN/0.1 M NaHCO <sub>3</sub> (aq), RT; Overnight	Yes	Complete
5	8C <sup>b</sup>	1:1 ACN/0.1 M NaHCO <sub>3</sub> (aq); microwave (70 °C, 1 h)	Yes	Incomplete
6	8C <sup>b</sup>	3:1 ACN/0.1 M NaHCO <sub>3</sub> (aq); Overnight	Yes	Incomplete
7	8C <sup>b</sup>	1:1 ACN/saturated NaHCO <sub>3</sub> (aq); 1 h	Yes	Incomplete
8	1C <sup>a</sup>	NCS, DMF, 0.1 M NaHCO <sub>3</sub> (aq), RT; Overnight	No	N/A
9	1D <sup>b</sup>	1:1 ACN/ H <sub>2</sub> O, RT; Overnight	No	N/A
10	1D <sup>b</sup>	1:1 ACN/ 0.1 M NaHCO <sub>3</sub> (aq), RT; Overnight	No	N/A
11	1D <sup>b</sup>	9:1 DMF/ saturated NaHCO <sub>3</sub> (aq), RT; Overnight	No	N/A
12	1D <sup>b</sup>	9:1 DMF/ Et <sub>3</sub> N RT; Overnight	No	N/A
13	1D <sup>b</sup>	1:1 ACN/ saturated NaHCO <sub>3</sub> (aq), RT; Overnight	No	N/A
14	6C <sup>a</sup>	NCS, DMF, 0.1 M NaHCO <sub>3</sub> (aq), RT; Overnight	No	N/A
15	6D <sup>b</sup>	1:1 ACN/ 0.1 M NaHCO <sub>3</sub> (aq), RT; Overnight	No	N/A
16	3B <sup>a</sup>	NCS, EtOH, 4% NaHCO <sub>3</sub> (aq), RT; Overnight	Yes	Incomplete
17	3B <sup>a</sup>	NCS, DMF, 0.1 M NaHCO <sub>3</sub> (aq), RT; Overnight	Yes	Inconclusive
18	1C <sup>a</sup>	NCS, 9:1 EtOH, saturated NaHCO <sub>3</sub> (aq), RT; Overnight	No	N/A
19	5B <sup>a</sup>	NCS, 9:1 EtOH, saturated NaHCO <sub>3</sub> (aq), RT; Overnight	No	N/A
20	5B <sup>a</sup>	NCS, 9:1 EtOH, saturated NaHCO <sub>3</sub> (aq); microwave (70 °C, 20 min)	No	N/A
21	5B <sup>a</sup>	NCS, 9:1 EtOH, saturated NaHCO <sub>3</sub> (aq); 56 °C, Overnight	No	N/A

<sup>a</sup>Oxime. <sup>b</sup>Hydroximinoyl chloride. \* As observed in denaturing 20% PAGE.

We have not been able to react some organic chromophores of interest (**1C**, **1D**, **6C**, **6D**) (Figures 5.6 and 5.7) with **ON1** under the reaction conditions tried (Table 5.2). Initial attempts to react **ON1** with **1C** using a reported modified method<sup>[23]</sup> through NO/AC chemistry using NCS, DMF, and NaHCO<sub>3</sub>(aq) to generate nitrile oxide *in situ* at room temperature was unsuccessful, reaction 8 (Table 5.2). Reaction times

were varied from 20 min to 12 hours with no success. We believed the reaction did not take place because the nitrile oxide was not produced in the solution. This was confirmed by running TLCs of the reaction supernatants alongside pre-formed hydroximinoyl chloride, which showed that hydroximinoyl chloride had been formed, but no further reaction occurred to produce nitrile oxide. An alternative failed reaction (entry 9 on Table 5.2) between **ON1** and **1D** in ACN/H<sub>2</sub>O confirmed that no nitrile oxide had been generated. To determine conditions under which the required reactive nitrile oxide is generated, we decided to perform the NO/AC reaction using 4-nitrobenzaldehyde derivatives (**8B** and **8C**). Both compounds **8B** and **8C** provided **ON3**, but according to the denaturing PAGE analysis the reactions were incomplete (Figure 5.22).

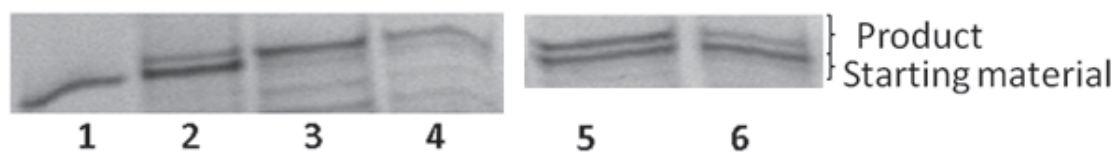


**Figure 5.22** Denaturing 20% PAGE (7 M urea) of 4-nitrobenzonitrile oxide modified oligonucleotides (**ON3**, modified by NO/AC) stained with Stains-All<sup>®</sup> dye and destained with H<sub>2</sub>O. Lane 1 – **8C**, **ON1**, 1:1 ACN/H<sub>2</sub>O, RT (20 min). Lane 2 – **8C**, **ON1**, 1:1 ACN/H<sub>2</sub>O, RT (1 h). Lane 3 – **8B**, **ON1**, NCS, DMF, 0.1 M NaHCO<sub>3</sub>, RT (30 min). Lane 4 – **8B**, **ON1**, NCS, DMF, 0.1 M NaHCO<sub>3</sub>, RT (1 h). Lane 5 – unmodified **ON1**.

In an attempt to drive the NO/AC reaction to completion it was decided to use a base on hydroximinoyl chloride reactions in order to optimize the formation of the required nitrile oxide. Et<sub>3</sub>N and HCO<sub>3</sub><sup>-</sup>, reported previously in the generation of nitrile oxides, were used.<sup>[15, 24]</sup> Unfortunately, addition of Et<sub>3</sub>N did not help the NO/AC reaction to take place (reactions 3 and 12, Table 5.2). The absence of both hydroximinoyl chloride and nitrile oxide in the supernatant (as observed by TLC and

MALDI-TOF MS) suggested a possible decomposition of nitrile oxide before NO/AC reaction could occur. This led us to explore  $\text{HCO}_3^-$  as a base in hydroximinoyl chloride NO/AC chemistry.

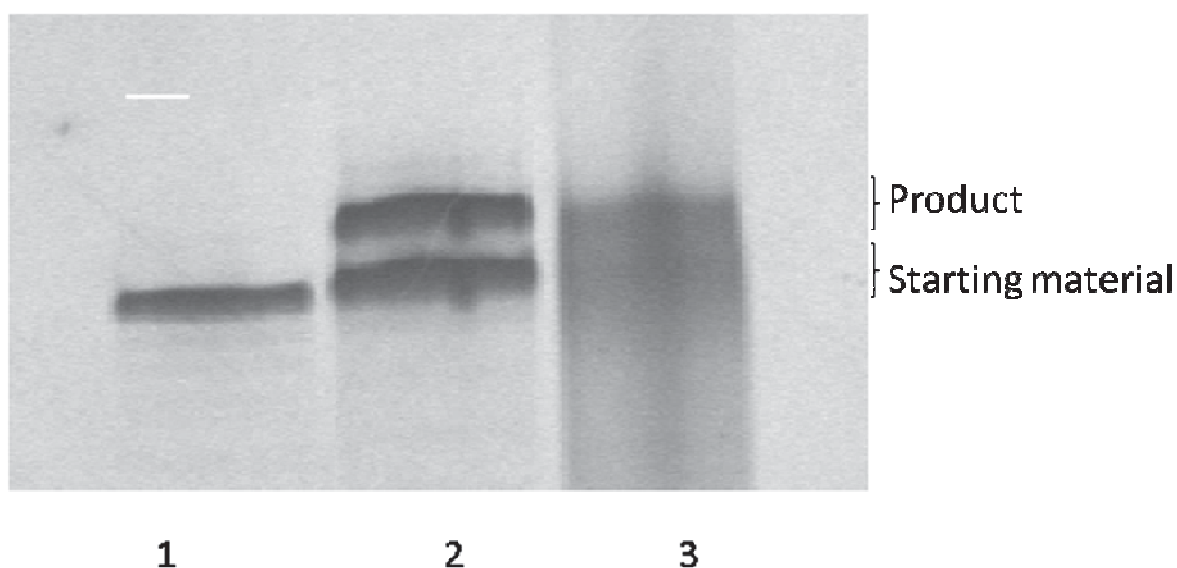
The hydroximinoyl chloride,  $\text{HCO}_3^-$  assisted NO/AC reaction led to full conversion of **ON1** to **ON3** when compound **8C** reacts with **ON1** in 1:1 ACN/0.1 M  $\text{NaHCO}_3(\text{aq})$  at room temperature overnight (Figure 5.23). Other conditions which resulted in NO/AC reaction but with no completion are illustrated in Table 5.2 (see Gels in Figure 5.3). Even though it was also established that the use of microwave irradiation did not improve the reaction, its use did not in any way impede the reaction. However, the  $\text{HCO}_3^-$  assisted NO/AC reaction failed using the styryl linked anthracenyl hydroximinoyl chloride **1D** and the styryl linked porphyrinic hydroximinoyl chloride **6D** with **ON1**.



**Figure 5.23** Denaturing 20% PAGE (7 M urea) of 4-nitrobenzonitrile oxide modified oligonucleotides (**ON3**, modified by NO/AC) stained with Stains-All<sup>®</sup> dye and destained with  $\text{H}_2\text{O}$ . Lane 1 – unmodified **ON1**. Lane 2 – **8C**, **ON1**, 1:1 ACN/0.1 M  $\text{NaHCO}_3$ , microwave (20 min), RT (1 h). Lane 3 – **8C**, **ON1**, 1:1 ACN/0.1 M  $\text{NaHCO}_3$ , Overnight. Lane 4 - **8C**, **ON1**, 1:1 ACN/0.1 M  $\text{NaHCO}_3$ , RT (1 h), 1:1 ACN/0.1 M  $\text{NaHCO}_3$ , Overnight. Lane 5 - **8C**, **ON1**, 3:1 ACN/0.1 M  $\text{NaHCO}_3$ , 1 h. Lane 6 - **8C**, **ON1**, 2:1 ACN/saturated  $\text{NaHCO}_3(\text{aq})$ , 1 h.

On the other hand, 9-anthraldehyde oxime (**3B**), with the oxime group directly linked to anthracene, was successfully reacted with **ON1** using NO/AC chemistry with a 50 % yield on conversion according to PAGE. The  $\text{NCS}/\text{DMF}/\text{NaHCO}_3(\text{aq})$  method which was used successfully with **8B** resulted in DNA degradation when **3B** was used (Figure 5.24) as seen by denaturing PAGE. A variation of the oxime NO/AC reaction,<sup>[10, 21, 25]</sup> using a different solvent system replacing DMF with EtOH in a  $\text{NCS}/\text{EtOH}/\text{NaHCO}_3(\text{aq})$  system also proved successful with **3B** and **ON1**, but the reaction did not go to completion (Figure 5.24).





**Figure 5.24** Denaturing 20% PAGE (7 M urea) of 4-nitrobenzonitrile oxide modified oligonucleotides (**ON3**, modified by NO/AC) stained with Stains-All<sup>®</sup> dye and destained with H<sub>2</sub>O. Lane 1 – unmodified **ON1**. Lane 2 – **3B**, **ON1**, NCS/1:1 EtOH 4% NaHCO<sub>3</sub>, RT, Overnight. Lane 3 – **3B**, **ON1**, NCS/DMF EtOH/0.1 M NaHCO<sub>3</sub>, RT, Overnight.

Taking into account that none of the porphyrin derivatives reacted with ONs bearing terminal alkynes in metal-free NO/AC chemistry led us to reconsider our approach in the design of DNA-based EU systems. We decided to use DNAs modified with PAHs as acceptors for EU with porphyrins and ruthenium polypyridyl complexes as donors, in a non-covalent supramolecular approach (See Figure 3.8).

## 5.5 Conclusions

We synthesized several anthracenyl, pyrenyl and porphyrinic derivatives having the azido, oxime and hydroximinoyl chloride functional groups required to perform “click chemistry” with terminal alkyne groups on oligonucleotides. Model nitrobenzaldehyde derivatives were also synthesized.

Microwave assisted CuAAC reactions were successfully carried out on both the 2'-*O*-propargyl uridine (**ON1**) and (*R*)-1-*O*-(4-ethynylbenzyl)glycerol (**ON2**) functionalized DNA with several azido-derivatives of organic chromophores.



We found optimum conditions required to perform the metal-free nitrile oxide/azide cycloaddition (NO/AC) reaction using various oximes and hydroximinoyl chlorides on **ON1**. The use of  $\text{NaHCO}_3^-$  as a base proved to be important for the reaction. The use of a microwave did not either improve or impede the reaction. None of the porphyrin derivatives reacted with ONs bearing terminal alkynes in metal-free NO/AC chemistry. We can conclude that the reactivity of oximes and hydroximinoyl chlorides is considerably reduced in the structure of the porphyrin. We can conclude that the reactivity of oximes and hydroximinoyl chlorides is considerably reduced in the structure of the bulky porphyrin in comparison with corresponding 4-nitrobenzaldehyde derivatives.

## 5.6 References

- [1] A. D. Richards, A. Rodger, *Chemical Society Reviews* **2007**, 36, 471.
- [2] V. V. Filichev, E. B. Pedersen, T. P. Begley, *DNA-Conjugated Organic Chromophores in DNA Stacking Interactions*, John Wiley & Sons Inc., New York, **2009**, 1, 493.
- [3] P. M. E. Gramlich, C. T. Wirges, A. Manetto, T. Carell, *Angewandte Chemie International Edition* **2008**, 47, 8350.
- [4] H.-A. Wagenknecht, *Angewandte Chemie International Edition* **2009**, 48, 2838.
- [5] J.-F. Lutz, *Angewandte Chemie International Edition* **2007**, 46, 1018.
- [6] A. W. I. Stephenson, N. Bomholt, A. C. Partridge, V. V. Filichev, *ChemBioChem* **2010**, 11, 1833.
- [7] H. C. Kolb, K. B. Sharpless, *Drug Discovery Today* **2003**, 8, 1128.
- [8] a)V. V. Rostovtsev, L. G. Green, V. V. Fokin, K. B. Sharpless, *Angewandte Chemie International Edition* **2002**, 41, 2596; b)C. W. Tornøe, C. Christensen, M. Meldal, *The Journal of Organic Chemistry* **2002**, 67, 3057.
- [9] C. R. Becer, R. Hoogenboom, U. S. Schubert, *Angewandte Chemie International Edition* **2009**, 48, 4900.
- [10] I. Singh, F. Heaney, *Organic & Biomolecular Chemistry* **2010**, 8, 451.
- [11] K. Gutmiedl, C. T. Wirges, V. Ehmke, T. Carell, *Organic Letters* **2009**, 11, 2405.
- [12] S. H. Weisbrod, A. Marx, *Chemical Communications* **2008**, 5675.
- [13] K. C. Kumara Swamy, V. Srinivas, K. V. P. Pavan Kumar, K. Praveen Kumar, *Synthesis* **2007**, 2007, 893.
- [14] K. Sonogashira, Y. Tohda, N. Hagihara, *Tetrahedron Letters* **1975**, 16, 4467.
- [15] K.-C. Liu, B. R. Shelton, R. K. Howe, *The Journal of Organic Chemistry* **1980**, 45, 3916.
- [16] I. Cade, N. J. Long, A. J. P. White, D. J. Williams, *Journal of Organometallic Chemistry* **2006**, 691, 1389.
- [17] F. Xie, K. Sivakumar, Q. Zeng, M. A. Bruckman, B. Hodges, Q. Wang, *Tetrahedron* **2008**, 64, 2906.
- [18] V. K. Jain, S. S. Sait, P. Shrivastav, Y. K. Agrawal, *Talanta* **1997**, 45, 397.
- [19] V. V. Filichev, H. Gaber, T. R. Olsen, P. T. Jørgensen, C. H. Jessen, E. B. Pedersen, *European Journal of Organic Chemistry* **2006**, 2006, 3960.
- [20] J.-M. Barbe, G. Canard, S. Brandès, R. Guillard, *European Journal of Organic Chemistry* **2005**, 2005, 4601.

- [21] T. N. Singh-Rachford, F. N. Castellano, *The Journal of Physical Chemistry Letters* **2009**, *1*, 195.
- [22] A. W. Stephenson, PhD Thesis, Massey University (Palmerston North), **2010**.
- [23] K. Gutsmedl, D. Fazio, T. Carell, *Chemistry – A European Journal* **2010**, *16*, 6877.
- [24] A. R. Katritzky, M. A. C. Button, S. N. Denisenko, *Journal of Heterocyclic Chemistry* **2000**, *37*, 1505.
- [25] I. Singh, F. Heaney, *Chemical Communications* **2011**, *47*, 2706.

## 6 Interactions of TINA-modified DNA Duplexes with a Zinc Cationic Porphyrin

### 6.1 Introduction

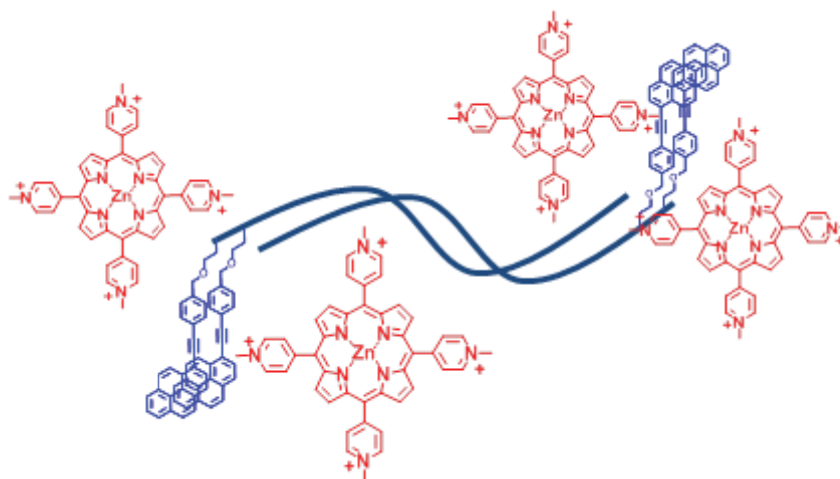
In the previous chapter it was identified that the porphyrin covalent attachment to DNA is problematic. At this stage we decided to focus on the systems in which the acceptor molecule (TINA) is attached to DNA and the donor (porphyrin or  $[\text{Ru}(\text{bpy})_3]^{2+}$ ) is present in solution. In this way, we can take an advantage of the supramolecular approach, in which donors interact with DNA and thus can be brought into the close proximity to the acceptor. Such an arrangement of chromophores is rare in the literature and requires a thorough biophysical analysis.

The supramolecular interactions of unmodified DNA with small molecules or ligands have been a subject of intense research for several decades.<sup>[1]</sup> This was mainly driven by the search for possible drugs that interfere with biological processes on DNA.<sup>[2]</sup> The majority of the studies devoted to the interaction of ligands and DNA have been performed using cheap, commercially available DNAs of biological origin, such as salmon testes DNA (stDNA) and calf thymus DNA (ctDNA). These DNA duplexes are long (ca 2000 base-pairs) with an even distribution of nucleotides, which preferentially adopt a B-type DNA helix. In contrast, DNA and RNA sequences with the length of 5-50 nucleotides can be designed to fold into topologies different from the classical A- and B-type DNA helices, which include DNA triplexes, G-quadruplexes, parallel duplexes, i-motifs and so on. It can be expected that interactions of ligands with such structures, especially if other organic chromophores are attached to DNA, are different from interactions with the long DNA duplex.

Recent advances in DNA chemistry allow us to introduce functional entities in any desired position along the DNA helix.<sup>[3]</sup> This forms a foundation for the creation of supramolecular helical nanoarrays based on DNA.<sup>[4]</sup> Combination of the supramolecular and covalent anchoring strategies has several advantages.<sup>[5]</sup> Firstly, interactions of ligands based on aromatic molecules with DNA possessing organic chromophores can lead to novel photoactive materials because properties of

individual components may change after complex formation. Secondly, covalent attachment of certain compounds to DNA still remains challenging, requires significant effort and is time-consuming. Moreover, creation of the tether in the desired molecule for the attachment to the DNA can, and often does, change the spectroscopic properties of the molecule, which is usually detrimental for the desired array. Thirdly, various fluorophores are either commercially available as DNA phosphoramidites or can be synthesised and attached to the DNA in a timely manner using available procedures. Fourthly, such systems can be quickly designed, self-assembled and evaluated spectrophotometrically using commercially available ligands and modified DNA. Finally, a prototype of photo-optical devices can be easily fabricated if needed.

In this chapter we describe the interactions of a cationic porphyrin, ZnTMpyP4, the  $\text{Zn}^{2+}$  derivative of 5,10,15,20-tetrakis-(1-methyl-4-pyridyl)-21*H*,23*H*-porphine (Figure 6.2B), which is one of the most studied DNA ligands,<sup>[1e, 6]</sup> with synthetic DNA duplexes bearing the TINA monomer, Figure 6.1 and Figure 6.2B). TINA has been used recently to modify DNA duplexes, triplexes and G-quadruplexes.<sup>[7]</sup> ZnTMpyP4, DNA duplexes, and the TINA monomer do not have significant overlaps in the UV-Vis spectrum and hence each of them can be easily monitored in the mixture using a variety of spectrophotometric methods. In addition, ZnTMpyP4 and TINA are highly fluorescent, which makes it easy to determine the change in their environment in the mixture by fluorescence spectroscopy. This model study shows that a free porphyrin in solution preferentially interacts with pyrenes of the TINA molecule and this interaction is dependent on the number of TINAs in the DNA duplex.



**Figure 6.1** A schematic representation of TINA-modified DNA duplex with ZnTMPyP4.

## 6.2 Chapter Summary

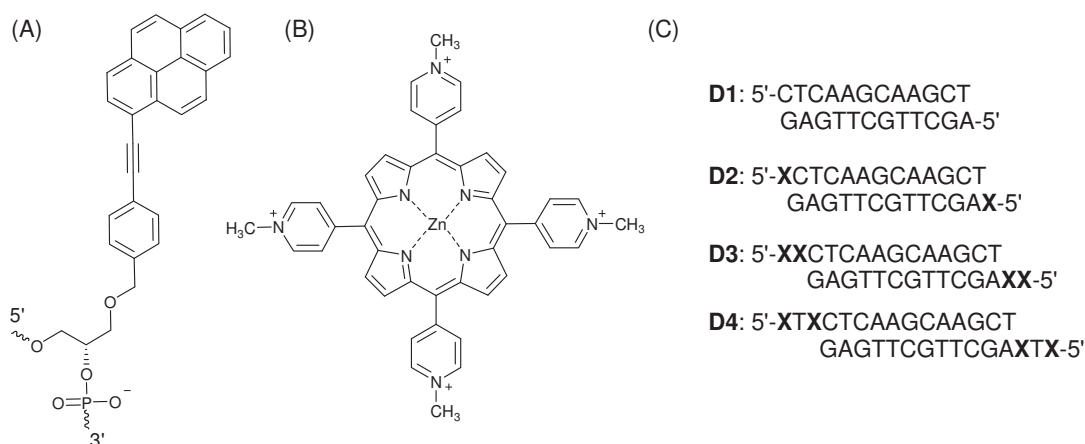
The attachment of one and two TINA monomers at the 5'-end of the 12-mer duplex led to decreased thermal stability at a low (50 mM NaCl) salt concentration. This was circumvented by using buffers with high (1.0 M NaCl) salt concentrations, although the duplex with a three-unit 5'-tail (TINA-thymidine-TINA) was less stable than the unmodified DNA. UV-Vis and fluorescence spectroscopy studies indicate that the cationic porphyrin ZnTMPyP4 has a greater affinity to TINA-modified duplexes than to the unmodified 12-mer duplex at both low and high salt concentrations. An increase in duplex thermal stability (up to  $\Delta T_m +23\text{ }^{\circ}\text{C}$ ) was more pronounced upon addition of the porphyrin to duplexes having two TINA monomers at 5'-ends than for an unmodified duplex and a duplex with a single TINA monomer at each 5'-end.

Complex formation resulted in a bathochromic shift observed in the UV-Vis spectra for the porphyrin Soret and Q-bands (up to 8 nm) which was also accompanied by changes in their intensities. Energy transfer from TINA to the porphyrin shown by fluorescence excitation spectra was accompanied by changes in both TINA and porphyrin emission intensities. TINA fluorescence for both the monomer and excited dimer was quenched when duplexes were further titrated with the porphyrin, which was attributed to the formation of the ground state complex (major component) and collisional quenching (minor component). Porphyrin fluorescence quenching by  $\text{K}_4\text{Fe}(\text{CN})_6$  show that TINA-modified duplexes protect the porphyrin from

quenching slightly better than the unmodified duplex but not to the extent of the porphyrin protection shown by stDNA.

### 6.3 DNA Duplex Design

TINA-modified duplexes based on a dodecameric sequence **D1** (Figure 6.2C) were synthesised for our study. It has been shown that incorporation of TINA as a bulge in the middle of the Watson-Crick-type duplex is detrimental for the duplex stability ( $\Delta T_m = -8.0 \dots -15.5$  °C).<sup>[8]</sup> Instead, chromophore attachment to the 5'-terminal position on the DNA does not disrupt duplex formation and can potentially maximize the interaction between the phenylethynylpyrene moieties with the cationic porphyrin ZnTMpyP4. The use of TINA in the middle of the DNA duplex inserted as a bulge (the intercalating mode) might shield pyrene and prevent its interaction with ZnTMpyP4. Therefore, we decided to use TINA at the end of the duplex; in this mode TINA is exposed to the environment and only partly shielded by the terminal nucleobases. We hypothesized that by increasing the content of lipophilic pyrene moieties at the ends of the duplex the porphyrin-DNA interaction will become stronger and the cationic porphyrin will reside next to the TINA. This will lead to the supramolecular complex with significantly increased duplex stability, whereas spectroscopic properties of TINA and a porphyrin will be altered giving a rise to the new photonic system Single and double 5'-TINA modifications as well as a double TINA modification with a thymidine sandwiched between two TINA monomers were employed (Figure 6.2C).



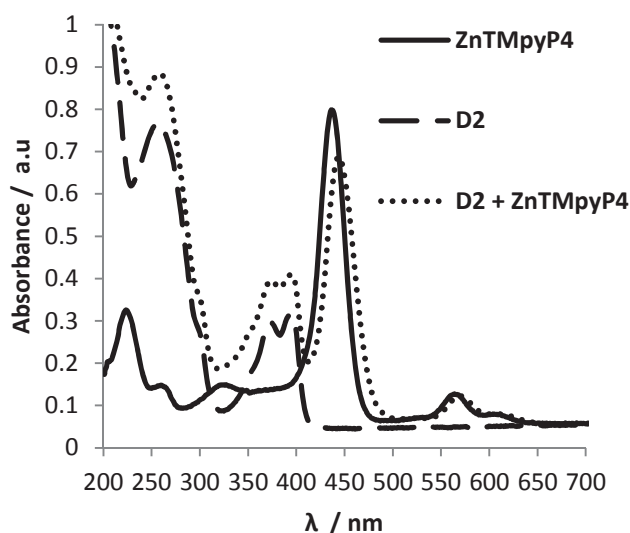
**Figure 6.2** Structures of twisted intercalating nucleic acid monomer (TINA, monomer **X**, A), a cationic porphyrin (B) and TINA-modified duplexes used in the present study (C).

Several DNA systems based on multiple insertions of pyrenes at terminal positions have been designed in the past and used for detection of DNA and RNA sequences.<sup>[9]</sup> The appropriate duplexes (1.0  $\mu\text{M}$ ) in the present study were prepared in a 10 mM sodium phosphate buffer (pH 7.0, 0.1 mM EDTA) in the absence and in the presence of 10  $\mu\text{M}$  ZnTMpyP4 (Figure 6.2B). It has been shown that cationic porphyrins interact differently with DNA depending on the salt concentration, *i.e.* they intercalate between nucleobases in the high salt and bind to the phosphate backbone in the low salt.<sup>[1e, 1g, 6, 10]</sup>

#### 6.4 UV-Vis Spectroscopy of porphyrin/TINA-DNA complexes

UV-Vis spectroscopy is an excellent, well studied technique for determining ligand interaction with DNA.<sup>[1h]</sup> In our case, initial evidence of interaction between the DNA duplexes with ZnTMpyP4 was provided by UV-vis spectroscopy. Typical spectra for UV-vis trends are illustrated with data for **D2** and ZnTMpyP4 in Figure 6.3. Duplex **D2**, containing terminal 5' TINA modifications, exhibits the 260 nm absorbance band attributed to absorbance of nucleobases and the pyrenyl moiety has maxima at 373 nm and 396 nm. The pyrenyl moiety peaks resemble the free pyrene peaks,<sup>[11]</sup> red-shifted due to conjugation with the ethynylphenyl group. The ZnTMpyP4 Soret and the most prominent Q-band appear at 436 nm and 564 nm respectively.<sup>[6]</sup> It is interesting to note that the addition of ZnTMpyP4 to **D2** caused both, a bathochromic shift in the Soret band ( $\Delta\lambda = +8$  nm, Table 6.1) and Q-band ( $\Delta\lambda = +3$  nm, Table 6.1), and a hypochromic shift in the Soret band ( $H = -13.8$  %) and Q-band ( $H = -3.8$  %). This is in agreement with trends and ranges of changes described in the literature.<sup>[1h, 10]</sup>





**Figure 6.3** UV-Vis absorption spectra of free ZnTMpyP4 (10  $\mu$ M), free **D2** (1.0  $\mu$ M), and **D2** in the presence of ZnTMpyP4. Conditions: 25  $^{\circ}$ C, 10 mM sodium phosphate buffer, pH = 7, 0.1 mM EDTA, 50 mM NaCl. See Table 6.1 for more examples.

A hyperchromic shift in the absorbance of TINA in the presence of ZnTMpyP4 provides evidence of the participation of the TINA monomer in the interaction of the duplex with the metalloporphyrin (Figure 6.3). A percentage hyperchromicity of 29.3 % (396 nm peak) and 32.8 % (373 nm) was observed (Table 6.2). However, no bathochromic or hypsochromic shifts were seen for the TINA molecule.

**Table 6.1** UV-Vis absorption data for ZnTMpyP4 bound to duplexes.<sup>a</sup>

Complex	Soret band, nm	Soret band, % $\Delta A^b$	Q-band, nm	Q band, % $\Delta A$
ZnTMpyP4 <sup>L</sup>	436	-	564	-
ZnTMpyP4 <sup>H</sup>	438	-	565	-
<b>D1</b> + ZnTMpyP4 <sup>L</sup>	437	+7.5	564	-4.6
<b>D1</b> + ZnTMpyP4 <sup>H</sup>	438	+7.5	566	+6.8
<b>D2</b> + ZnTMpyP4 <sup>L</sup>	444	-13.8	567	-3.8
<b>D2</b> + ZnTMpyP4 <sup>H</sup>	444	-23.3	571	-4.4
<b>D3</b> + ZnTMpyP4 <sup>L</sup>	444	-24.9	565	-34.2
<b>D3</b> + ZnTMpyP4 <sup>H</sup>	439	+11.3	565	+10.9
<b>D4</b> + ZnTMpyP4 <sup>L</sup>	438	+1.6	568	-14.7
<b>D4</b> + ZnTMpyP4 <sup>H</sup>	438	-10.7	568	-22.2

<sup>a</sup> ZnTMpyP4 = 10  $\mu$ M, duplex = 1.0  $\mu$ M, 10 mM sodium phosphate buffer, 0.1 mM EDTA, pH = 7.0 in the presence of 50 mM (superscript L) and 1.0 M NaCl (superscript H), 25  $^{\circ}$ C. <sup>b</sup> %  $\Delta A = [(A_{\text{free}} - A_{\text{bound}})/A_{\text{free}}] \times 100$ .  $A_{\text{free}}$  and  $A_{\text{bound}}$  are the absorbances of free and bound porphyrin, respectively.<sup>[1h, 10]</sup>

It is noteworthy that in all duplex-ZnTMpyP4 systems investigated some changes were observed in the porphyrin (Table 6.1) and TINA (Table 6.2) UV-Vis absorbance spectra. Even though in all the systems a bathochromic shift in the Soret

and Q- bands of the ZnTMpyP4 were observed, the largest shifts occurred with TINA modified duplexes **D2** and **D3** from 436 to 444 nm for the Soret band and from 564 to 571 nm for the Q-band. In agreement with the melting stability and binding affinity data (discussed below) this leads us to postulate that the presence of TINA either improves the association of the duplex with the porphyrin or at the very least TINA plays a role in the interaction. In addition, the intensities of the Soret band and Q-band of the porphyrin are altered in the presence of all duplexes. However, it is worth noting that in the systems studied, both hyperchromic and hypochromic intensity changes in the Soret and Q-bands were observed, therefore highlighting the possibility of different modes of interaction (Table 6.1).

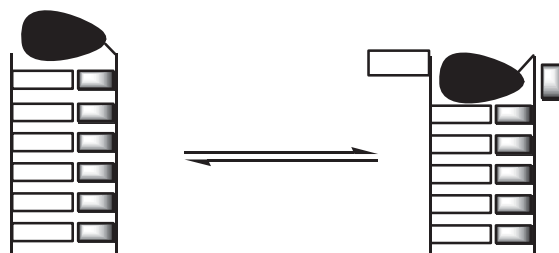
**Table 6.2** UV-Vis absorption parameters for the pyrenyl moiety of TINA on duplexes bound to ZnTMpyP4. %  $\Delta A$  was calculated as in Table 6.1.

Duplex	% $\Delta A$ (396 nm)	% $\Delta A$ (373 nm)
<b>D2<sup>L</sup></b>	+29.3	+32.8
<b>D2<sup>H</sup></b>	+28.7	+31.8
<b>D3<sup>L</sup></b>	*NV	+34.0
<b>D3<sup>H</sup></b>	*NV	+95.1
<b>D4<sup>L</sup></b>	+3.1	+4.2
<b>D4<sup>H</sup></b>	+22.3	+18.8

Conditions are the same as in Table 6.1. \*There is no peak at 396 nm, so no value to report.

## 6.5 DNA Melting Studies

The melting temperatures of duplexes were monitored at 260 nm (Table 6.3). We compared the effect of adding ligand to all duplexes. Quite surprising results were obtained upon melting of the DNA duplexes with TINA at different salt concentrations and a notable difference in the duplex thermal stabilities was observed upon addition of the porphyrin (Table 6.3). At low salt concentration all modified duplexes had decreased thermal stability ( $\Delta T_m = - 5.5 \dots - 20.0$  °C) in comparison with unmodified duplex **D1**. On the other hand, TINA insertion led to increased  $T_m$  values at high salt concentration except duplex **D4**. The destabilizing effect can be explained by increased electrostatic repulsion caused by additional phosphates present in the overhang and by increased breathing of terminal base-pairs at low salt concentration. Breathing can result in the situation when an organic chromophore attached at the 5'-end disrupts terminal base-pairing and interacts with the next base-pairing (Figure 6.4).<sup>[12]</sup>



**Figure 6.4** Schematic representation of different positioning of an organic chromophore attached at the end of the duplex at low salt concentration.

Addition of the porphyrin to duplexes in the absence of TINA and with one TINA on each strand had a marginal effect on the thermal stabilities of these duplexes (**D1** and **D2**, respectively). However,  $T_m$  values of duplexes with two TINAs at both ends changed considerably upon porphyrin addition. Thus, the striking increase in  $T_m$  by 23 °C was seen for the duplex **D4** at high salt concentration.

**Table 6.3** Melting temperatures of duplexes in the absence and presence of ZnTMpyP4 at 260 nm<sup>a</sup> and binding constants of unmodified and TINA modified duplexes with ZnTPpyP4 obtained by Scatchard analysis of fluorescence titration data at 664 nm.

Duplex	$T_{m\ 260} / \Delta T_m$ (°C)		$K_a$ (M <sup>-1</sup> )	$N$
	No ZnTMpyP4	ZnTMpyP4 present		
<b>D1</b> <sup>L</sup>	59.0	56.5 / -2.5	$1.2 \pm 0.1 \times 10^5$	4.4
<b>D2</b> <sup>L</sup>	52.5	50.0 / -2.5	$2.0 \pm 0.3 \times 10^5$	4.8
<b>D3</b> <sup>L</sup>	39.0	48.0 / +9.0	$2.3 \pm 0.1 \times 10^6$	5.8
<b>D4</b> <sup>L</sup>	45.0	46.5 / +1.5	$3.1 \pm 0.2 \times 10^5$	6.6
<b>D1</b> <sup>H</sup>	54.5	56.0 / +1.5	$1.9 \pm 0.2 \times 10^4$	3.5
<b>D2</b> <sup>H</sup>	64.0	64.0 / 0.0	$8.4 \pm 0.4 \times 10^4$	3.8
<b>D3</b> <sup>H</sup>	62.0	68.0 / +6.0	$4.4 \pm 0.3 \times 10^4$	4.1
<b>D4</b> <sup>H</sup>	42.0	65.0 / +23.0	$3.2 \pm 0.2 \times 10^4$	4.6

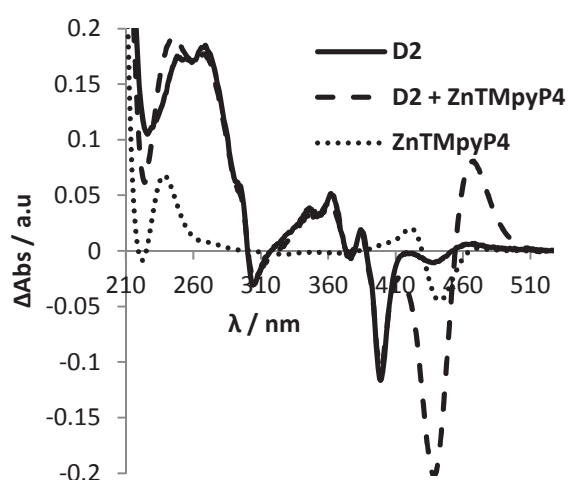
<sup>a</sup>Conditions: ZnTMpyP4 = 10 μM, duplex = 1.0 μM, 10 mM sodium phosphate buffer, 0.1 mM EDTA, pH = 7.0 in the presence of 50 mM (°) and 1.0 M NaCl (°). All melting temperatures are within the uncertainty of  $\pm 0.5$  °C as determined by repetitive experiments.  $\Delta T_m$  was calculated as  $T_m$  (ZnTMpyP4 present) –  $T_m$  (no ZnTMpyP4). <sup>b</sup>Binding constant of st DNA with ZnTPpyP4 was found to be  $1.6 \pm 0.3 \times 10^6$  (low salt) which closely resemble previously reported values for DNA-porphyrin complexes.<sup>[10, 13]</sup>  $N$  is the number of porphyrins bound to the duplex at saturation point (see Appendix Section 12.2.2).

It is interesting to compare UV-Vis thermal stability data with the binding constants determined by Scatchard analysis of fluorescence titration data at 664 nm (Table 6.3).<sup>[14]</sup> In general, the affinity of DNA for the porphyrin decreases from low salt to high salt concentration buffer.<sup>[13]</sup> This is attributed to competition for binding sites between the porphyrin and the metal cation (Na<sup>+</sup>) at high salt concentrations. A more interesting observation is the higher affinity for the porphyrin by TINA modified duplexes (**D2-D4**) compared to unmodified DNA (**D1**) both at high and low salt

concentrations. Addition of TINA increases the number of porphyrins bound to the duplex at saturation point. However, only one complex had a binding affinity comparable with the  $K_a$  value for the porphyrin-st DNA assembly ( $1.6 \times 10^6 \text{ M}^{-1}$ ), i.e. **D3** + ZnTMpyP4 ( $2.3 \times 10^6 \text{ M}^{-1}$ ). This correlates with an increase in the duplex thermal stability by 9 °C upon addition of the porphyrin to the duplex **D3**.

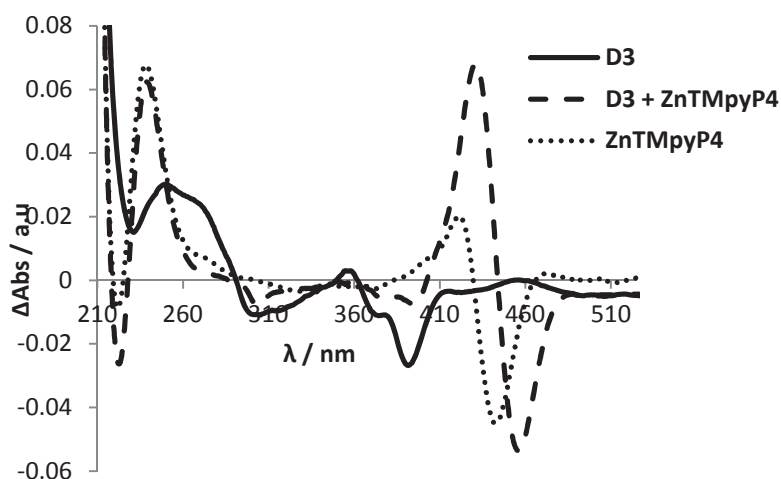
## 6.6 Thermal Difference Spectra (TDS) of porphyrin/TINA-DNA complexes

The participation of TINA in DNA folding is illustrated by TDS profiles, which are characterized by negative peaks at ~373 and ~396 nm in addition to the expected B-DNA positive peaks around 260 nm and a negative peak at ~300 nm (Figure 6.5 and Figure 6.6). The appearance of peaks around 435 and 460 nm when ZnTMpyP4 was added to all duplexes indicates porphyrin-DNA interaction and the sign of these peaks was dependent on the number of TINA molecules present in the duplex. Thus, ZnTMpyP4 interaction with unmodified **D1** and single TINA-modified **D2** (Figure 6.5) caused a negative peak at 435 nm and a positive peak at 460 nm. An opposite sign of these peaks was observed for the mixtures of the porphyrin with duplexes having two TINA molecules at both ends of the duplex (**D3** (Figure 6.6) and **D4**) at both low and high salt concentrations. In addition sharp negative and positive peaks at 215 and 235 nm were observed instead of a broad positive peak between 215 and 290 nm seen for the duplex **D2**.



**Figure 6.5** Thermal difference spectra of **D2** in the absence and presence of ZnTMpyP4. See DNA and chromophore concentrations, as well as buffer conditions in Figure 6.3.

Further evidence for the porphyrin interaction with TINA monomers is provided by a significant decrease in the TINA TDS signal for **D3** (Figure 6.6) and **D4** in the presence of ZnTMPyP4, which does not happen for **D1** and **D2**. We also observed that the magnitude of the decrease is greater for **D3** than **D4** (data not shown), which suggests that the presence of a thymidine in-between the TINA molecules decreases the efficiency of the  $\pi$ - $\pi$  stacking interactions between the porphyrin and the phenylethynylpyrene. This contrasts with the results of thermal stability studies because the most dramatic thermal stabilization caused by the porphyrin was observed for the duplex **D4** at 1M NaCl. However, insignificant changes in the intensity of the pyrene excimer band in the fluorescence spectra of **D4** upon porphyrin addition are indicative of decreased communication efficiency between the porphyrin and TINA in comparison with **D3** (see Table 6.4).

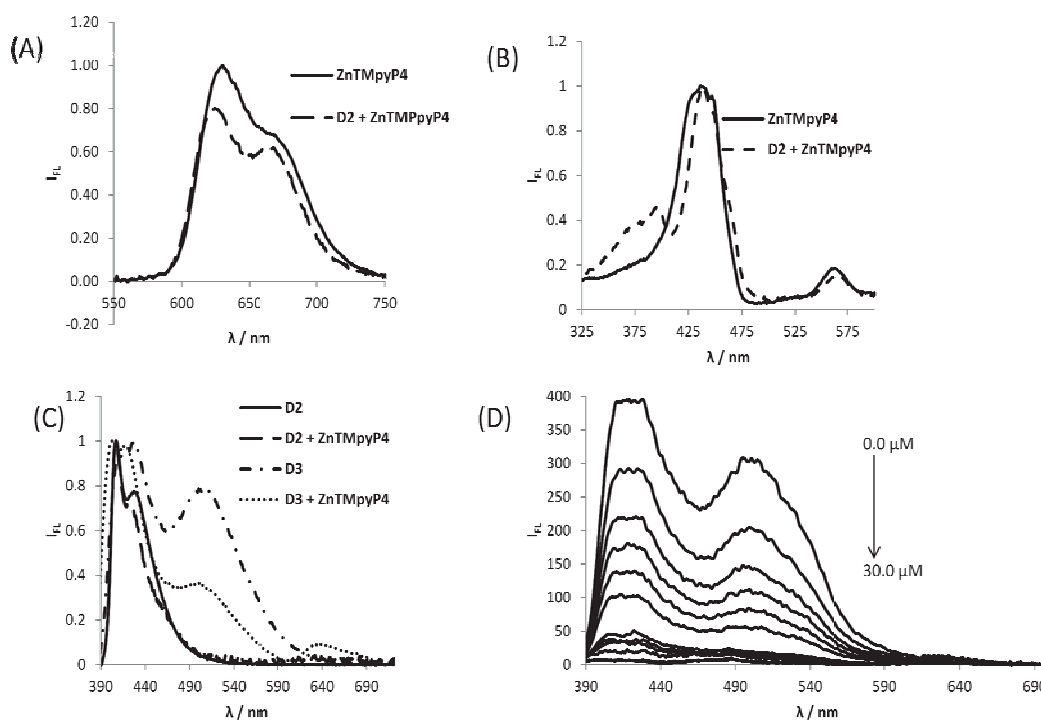


**Figure 6.6** Thermal difference spectra of **D3** in the absence and presence of ZnTMPyP4. See DNA and chromophore concentrations, as well as buffer conditions in Figure 6.3.

## 6.7 Fluorescence Spectroscopy of porphyrin/TINA-DNA complexes

The effect of duplexes on ZnTMPyP4 fluorescence emission spectra is illustrated on Figure 6.7A, where binding of the porphyrin to **D2** leads to an increase in the red-shifted component of the fluorescence signal at 668 nm and a shift in the blue component from 629 nm to 624 nm. The changes in fluorescence band shape and position are in agreement with ZnTMPyP4 bound to the outside of poly(dG:dC).<sup>[1e]</sup> The involvement of the phenylethynylpyrene in interaction with ZnTMPyP4 is further confirmed by a transfer of energy from TINA to porphyrin (bands at 373 and

396 nm) in the presence of the TINA modified duplex, as illustrated in Figure 6.7B (fluorescence excitation spectra, dashed line **D2** + ZnTMPyP4). Energy transfer is also accompanied by a porphyrin emission band at 631 nm following the TINA excitation at 375 nm in the TINA-DNA/porphyrin complexes (Figure 6.7C, dotted line). These spectral bands were not observed with the porphyrin alone.



**Figure 6.7** (A) Normalized fluorescence emission spectra of ZnTMPyP4 in the absence (solid line) and presence of **D2**;  $\lambda_{\text{ex}} = 436$  nm. (B) Normalized fluorescence excitation spectra of ZnTMPyP4 in the absence (solid line) and presence of **D2**;  $\lambda_{\text{em}} = 630$  nm. (C) Normalized fluorescence emission spectra of **D2** and **D3** in the absence and presence of ZnTMPyP4;  $\lambda_{\text{ex}} = 375$  nm. (D) Quenching of fluorescence emission spectra of TINA on **D3** (1.0  $\mu\text{M}$ ) with increasing concentration (0.0  $\mu\text{M}$  to 30  $\mu\text{M}$ ) of ZnTMPyP4;  $\lambda_{\text{ex}} = 375$  nm. Buffer is the same as for Figure 6.3.

The effect of ZnTMPyP4 on the TINA fluorescence emission is shown in Figure 6.7C. The monomeric TINA emission bands appear around 407 nm and 427 nm. In both TINA modified duplexes (**D2** and **D3**), the intensity of the red-shifted band around 427 nm decreases in the presence of the porphyrin. The presence of two TINA residues at the 5'-ends of the duplex results in the formation of a red-shifted excited dimer (excimer) at around 500 nm (Figure 6.7C, Table 6.4, **D3** and **D4** both in the absence and presence of ZnTMPyP4). It is interesting that binding of the

porphyrin to DNA disrupts the excimer as shown by the decrease in the ratio of the excimer to monomer in Table 6.4.

**Table 6.4** Fluorescence emission characteristics of TINA and TINA-porphyrin complexes upon excitation of TINA at 375 nm.<sup>a</sup>

Duplex	TINA emission ( $\lambda_{\text{max}}$ , nm)		Porphyrin emission ( $\lambda_{\text{max}}$ , nm)	TINA, $I_{\text{ex}}/I_{\text{m}}$ <sup>b</sup>
	Monomer	Excimer		
<b>D2<sup>L</sup></b>	407;427	-	-	-
<b>D2<sup>H</sup></b>	407;427	-	-	-
<b>D2 + ZnTMpyP4<sup>L</sup></b>	407	-	-	-
<b>D2 + ZnTMpyP4<sup>H</sup></b>	407;427	-	-	-
<b>D3<sup>L</sup></b>	415;427	506	-	0.77
<b>D3<sup>H</sup></b>	415;429	506	-	1.3
<b>D3 + ZnTMpyP4<sup>L</sup></b>	403;415	502	631	0.42
<b>D3 + ZnTMpyP4<sup>H</sup></b>	404	498	629	0.82
<b>D4<sup>L</sup></b>	407;427	506	-	0.55
<b>D4<sup>H</sup></b>	409;427	507	-	0.48
<b>D4 + ZnTMpyP4<sup>L</sup></b>	407	495	632	0.45
<b>D4 + ZnTMpyP4<sup>H</sup></b>	407	505	632	0.44

<sup>a</sup> Conditions, see Table 6.1. <sup>b</sup>  $I_{\text{ex}}/I_{\text{m}} = I_{\text{excimer}(500\text{nm})}/I_{\text{monomer}(405\text{nm})}$ .

Further titration of TINA-duplexes by the porphyrin results in complete quenching of both monomeric and excimer TINA fluorescence (Figure 6.7D).

### 6.7.1 Stern-Volmer Analysis

The quenching mechanisms of TINA's monomeric and excimer fluorescence were determined by the Stern–Volmer method.<sup>[15]</sup> Fluorescence quenching data are usually analysed by the Stern–Volmer equation:

$$F_0/F = 1 + K_{SV}[Q] \quad \text{eqn 6.1}$$

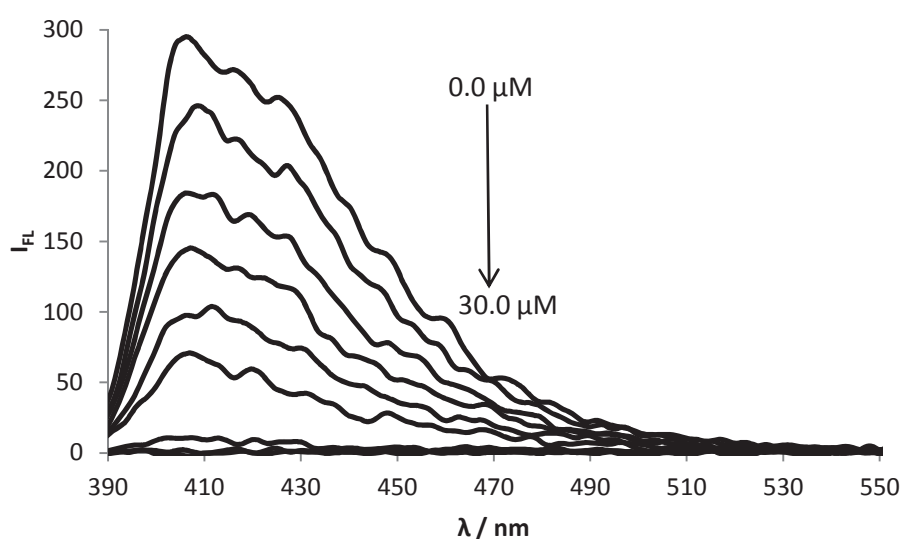
where  $F_0$  and  $F$  are the fluorescence intensities observed in the absence and presence, respectively, of a quencher,  $[Q]$  is the quencher concentration and  $K_{SV}$  is the Stern–Volmer quenching constant. In the simplest cases, then, a plot of  $F_0/F$  versus  $[Q]$  should yield a straight line with a slope equal to  $K_{SV}$ . This could be due to a case of purely collisions between the fluorophore in the excited state and the quencher (dynamic quenching), where  $K_{SV} = K_D$  (dynamic quenching constant), or alternatively static quenching occurring as a result of the formation of a non-

fluorescent ground state complex between the fluorophore and the quencher and  $K_{SV} = K_S$  (static quenching constant).

Interestingly, in all our studies with the TINA monomer and excimer quenched by ZnTMPyP4, a plot of  $F_0/F$  versus  $[Q]$  yields an upward curvature due to the  $[Q]^2$  term:

$$F_0/F = (1 + K_D[Q]) (1 + K_S[Q]) \quad \text{eqn 6.2}$$

In our present study, the TINA fluorescence quenching by ZnTMPyP4 was followed at a duplex concentration of  $1.0 \mu\text{M}$ , as shown on Figure 6.8 for **D2** and Figure 6.7D for **D3**.

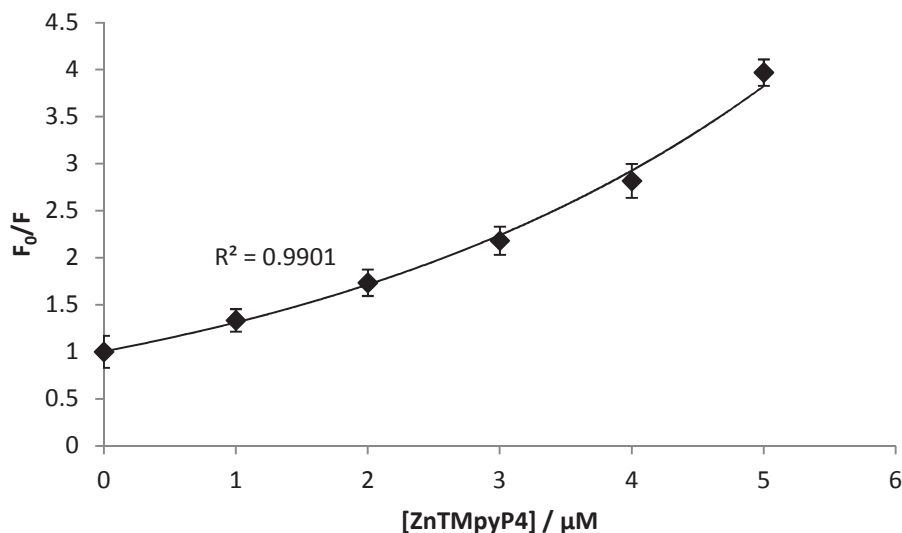


**Figure 6.8** Fluorescence emission spectra of the TINA on **D2** ( $1.0 \mu\text{M}$ ) with increasing concentration ( $0.0 \mu\text{M}$  to  $30 \mu\text{M}$ ) of ZnTMPyP4;  $\lambda_{\text{ex}} = 375 \text{ nm}$ . Buffer conditions are the same as for Figure 6.3.

ZnTMPyP4 quenches both monomer and excimer fluorescence for all duplexes studied, including **D4**, albeit to varying degrees. Quite noteworthy is the fact that at high concentrations of ZnTMPyP4 ( $\geq 10 \mu\text{M}$ ) complete quenching of both monomer and excimer TINA fluorescence is observed.

More significantly, a Stern–Volmer plot of  $F_0/F$  versus ZnTMPyP4 concentration for both monomer and excimer quenching yields an upward curved line for all duplexes studied, as exemplified by Figure 6.9 below for the **D2** TINA monomer quenching. This leads us to conclude that quenching of both the TINA monomer and excimer occurs by a combination of collisional encounters with ZnTMPyP4 and by ground state complex formation with the same quencher.<sup>[15]</sup>





**Figure 6.9** A Stern-Volmer plot of the quenching of TINA monomer fluorescence on **D2** (1.0 μM) with increasing concentration (0.0 μM to 5 μM) of ZnTMPyP4;  $\lambda_{\text{ex}} = 375$  nm. Buffer conditions are the same as for Figure 6.3.

In order to quantify the dynamic and static portions of the observed quenching we used the modified form of the Stern–Volmer equation. Expanding eqn 6.2 yields:

$$F_0/F = 1 + (K_D + K_S)[Q] + K_D K_S [Q]^2 \quad \text{eqn 6.3}$$

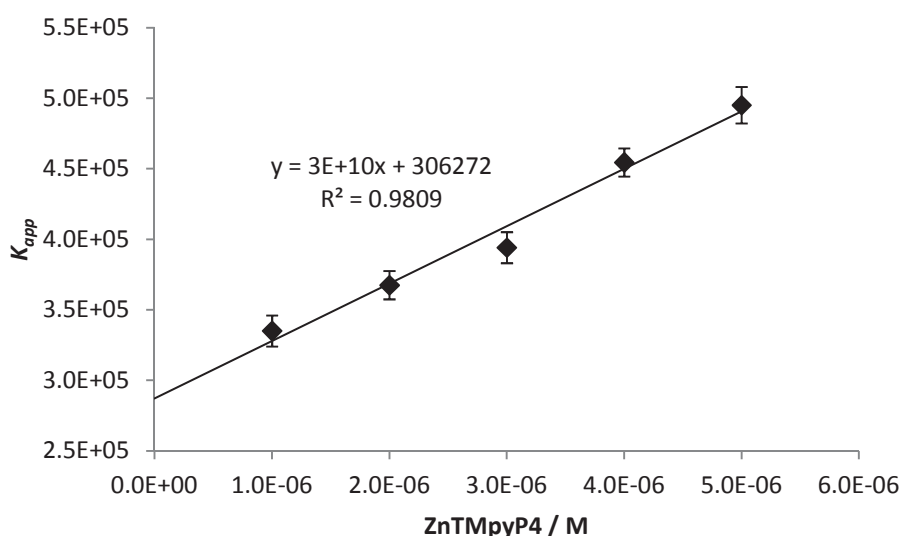
and

$$F_0/F = 1 + K_{\text{app}}[Q]; K_{\text{app}} \text{ is the apparent quenching constant} \quad \text{eqn 6.4}$$

where

$$K_{\text{app}} = [(F_0/F) - 1](1/[Q]) = (K_D + K_S) + K_D K_S [Q] \quad \text{eqn 6.5}$$

A plot of  $K_{\text{app}}$  versus  $[Q]$  yields a straight line, as shown on Figure 6.10 below for **D2** TINA monomer quenching, with a y-intercept of  $K_D + K_S$  and a gradient of  $K_S K_D$ .



**Figure 6.10** A modified Stern-Volmer plot for the quenching of TINA monomer fluorescence on **D2** (1.0  $\mu$ M) with increasing concentration (0.0  $\mu$ M to 5.0  $\mu$ M) of ZnTMPyP4;  $\lambda_{ex}$  = 375 nm. Buffer conditions are the same as for Figure 6.3.

Rearranging slope ( $S$ ) =  $K_D K_S$  and y-intercept ( $I$ ) =  $K_D + K_S$ , yields the quadratic equation:<sup>[15]</sup>

$$K_S^2 - K_S I + S = 0 \quad \text{eqn 6.6}$$

We determined  $K_S$  and  $K_D$  values (Table 6.5) by comparing the solutions to the quadratic equation to  $K_a$  values obtained by Scatchard analysis (Table 6.3), assuming that  $K_a$  values should be close or equal to  $K_S$  values.<sup>[15]</sup>

Therefore, Stern-Volmer analysis of the TINA-fluorescence quenching indicates that both static and dynamic interactions between the TINA-duplexes and the porphyrin are responsible for quenching. Extraction of static and dynamic quenching constants show that formation of a ground state complex is dominant over diffusion controlled interactions except for the complex **D4** + ZnTMPyP4 in which both mechanisms contribute nearly equally to quenching (Table 6.5).

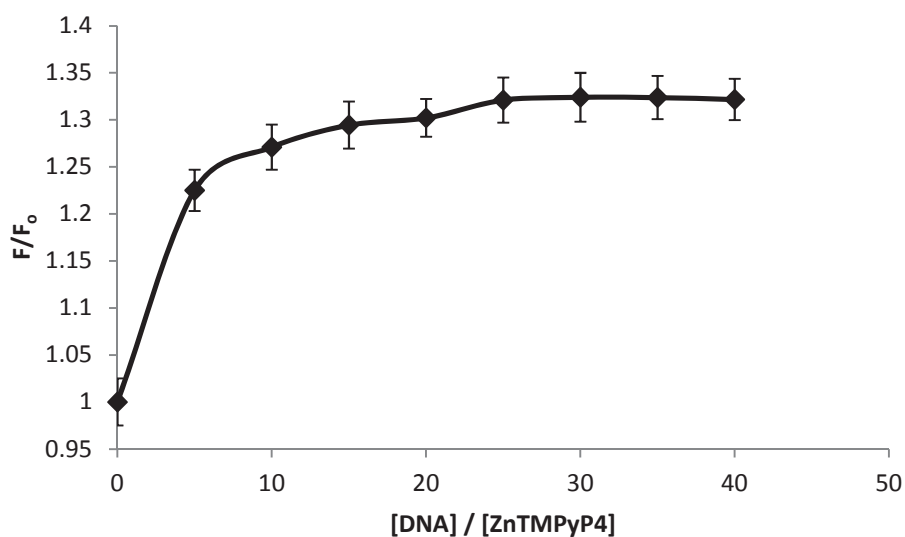
**Table 6.5** Stern–Volmer static quenching constants,  $K_S$  and dynamic quenching constants,  $K_D$  for the monomer and excimer of TINA-modified duplexes quenched by ZnTMPyP4.<sup>a</sup>

Duplex	$K_{S(mon)}, M^{-1}$	$K_{D(mon)}, M^{-1}$	$K_{S(ex)}, M^{-1}$	$K_{D(ex)}, M^{-1}$
<b>D2<sup>L</sup></b>	$2.9 \times 10^5$	$1.0 \times 10^4$	-	-
<b>D3<sup>L</sup></b>	$3.1 \times 10^5$	$1.3 \times 10^4$	$3.0 \times 10^5$	$3.4 \times 10^4$
<b>D4<sup>L</sup></b>	$1.5 \times 10^5$	$2.6 \times 10^4$	$2.8 \times 10^5$	$1.8 \times 10^5$

<sup>a</sup> Conditions, see Table 6.1.  $K_S$  and  $K_D$  values are reported within 2 % error.

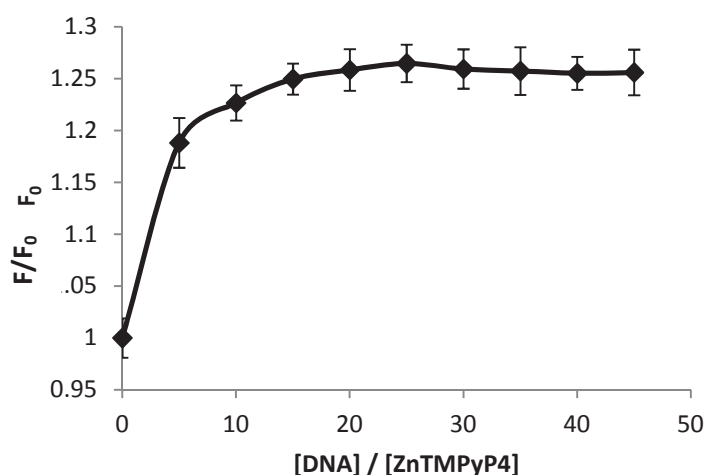
### 6.7.2 $K_4Fe(CN)_6$ – ZnTMPyP4 Quenching Studies

To evaluate the engagement of the porphyrin in the complex with DNA we compared quenching of porphyrin fluorescence by  $[Fe(CN)_6]^{4-}$  in the presence of stDNA and TINA-modified duplexes. We followed ZnTMPyP4 fluorescence in the presence of increasing amounts of duplexes, and the subsequent quenching of porphyrin fluorescence by  $K_4Fe(CN)_6$ . Upon addition of stDNA the ZnTMPyP4 emission intensity grows steadily to around 1.3 (Figure 6.11), which is similar to the value obtained when stDNA was added to the  $[Ru(bpy)_3]^{2+}$  complex (1.06).<sup>[16]</sup>



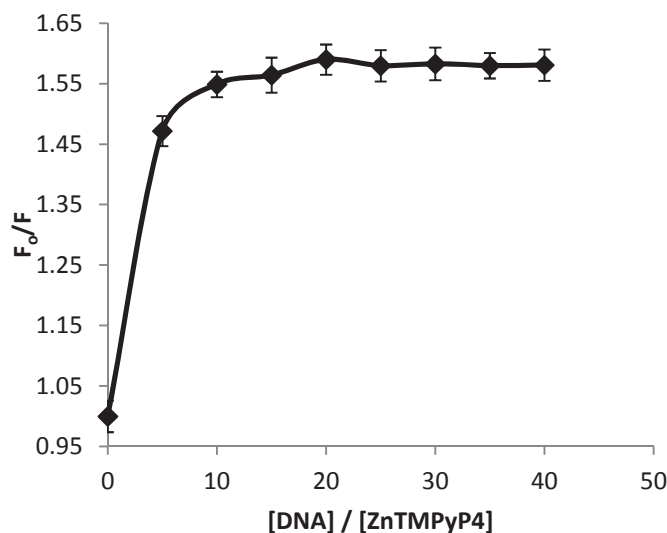
**Figure 6.11** Plot of the relative fluorescence emission intensity of ZnTMPyP4 *versus* the stDNA: ZnTMPyP4 ratio. [ZnTMPyP4] = 4  $\mu$ M;  $\lambda_{em}$  = 630 nm. Buffer conditions are the same as for Figure 6.3.

Addition of unmodified synthetic DNA (**D1**) also results in emission enhancement of ZnTMPyP4 steady state fluorescence to approximately 1.25, Figure 6.12 below.



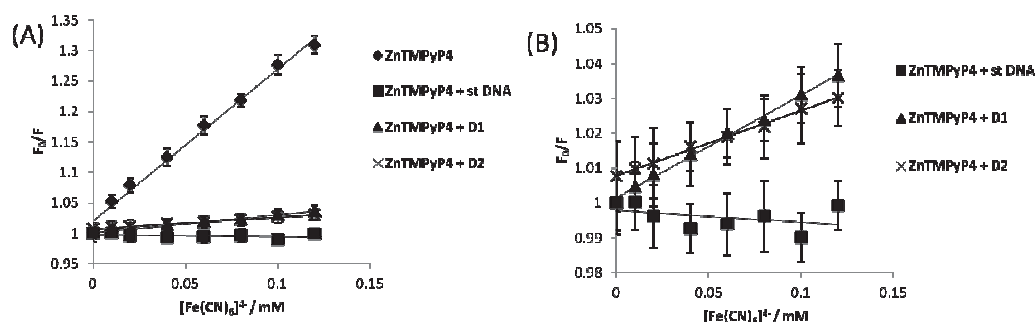
**Figure 6.12** Plot of the relative fluorescence emission intensity of ZnTMPyP4 *versus* the **D1**: ZnTMPyP4 ratio. [ZnTMPyP4] = 4  $\mu$ M;  $\lambda_{em}$  = 630 nm. Buffer conditions are the same as for Figure 6.3.

In contrast, addition of the TINA-modified DNA to ZnTMPyP4 led to a decrease in the fluorescence of the porphyrin, which is a confirmation of porphyrin fluorescence quenching by TINA. So we decided to invert the relative fluorescence and express it as  $F_0/F$ , as shown in Figure 6.13, where ZnTMPyP4 fluorescence is quenched by as much as around 1.6.



**Figure 6.13** Plot of the relative fluorescence emission intensity of ZnTMPyP4 versus the **D2**: ZnTMPyP4 ratio. [ZnTMPyP4] = 4  $\mu$ M;  $\lambda_{em}$  = 630 nm. Buffer conditions are the same as for Figure 6.3.

$[\text{Fe}(\text{CN})_6]^{4-}$  has been used to compare the extent of binding of  $\text{Ru}^{2+}$  complexes to native DNAs.<sup>[17]</sup> Positively charged  $\text{Ru}^{2+}$  complex ions are readily quenched by  $[\text{Fe}(\text{CN})_6]^{4-}$ , whereas a DNA-bound complex is protected within the hydrophobic environment as the quencher is repelled by the negative DNA phosphate backbone leading to reduced quenching. A Stern-Volmer plot results in a smaller gradient when the extent of protection is greater. The positively charged ZnTMPyP4 is readily quenched by  $[\text{Fe}(\text{CN})_6]^{4-}$ , Figure 6.14. Similar to the scenario with  $\text{Ru}^{2+}$  complexes, the presence of native stDNA causes diminished quenching of ZnTMPyP4, which in our case gives us a gradient of nearly equal to zero (gradient - 0.032, correlation coefficient 0.998), compared to ZnTMPyP4 alone where the slope is higher (gradient 2.50, correlation coefficient 0.991).



**Figure 6.14** Fluorescence quenching curves of ZnTMPyP4 with increasing concentration of a quencher,  $[\text{Fe}(\text{CN})_6]^{4-}$  in the absence and presence of DNA (A). The three bottom lines are expanded in B.  $[\text{ZnTMPyP4}] = 4 \mu\text{M}$ ,  $\text{DNA}:\text{ZnTMPyP4} = 20:1$ . Buffer conditions are the same as for Figure 6.3.

In the presence of the unmodified shorter strand synthetic **D1**, protection from quenching of ZnTMPyP4 fluorescence occurs too but to a lesser extent (gradient 0.29, correlation coefficient 0.996). However, in the presence of TINA modifications, there is a marginal improvement in the protection of porphyrin fluorescence from  $[\text{Fe}(\text{CN})_6]^{4-}$  (Figure 6.14), (**D2**, gradient 0.19, correlation coefficient 0.996), Table 6.6.

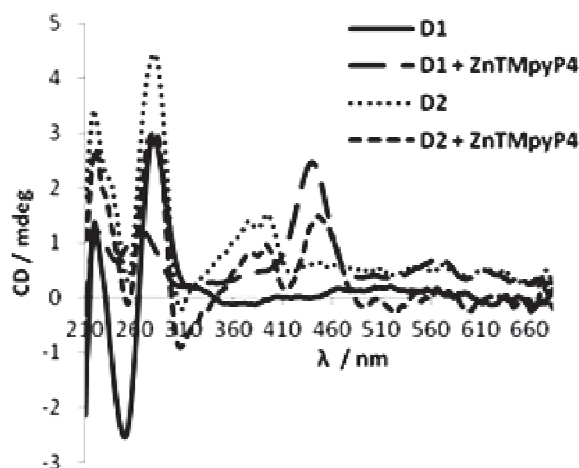
**Table 6.6** Slopes of ZnTMPyP4 in absence and presence of DNA duplexes. ZnTMPyP4 = 10  $\mu\text{M}$ , duplex = 1.0  $\mu\text{M}$ , 10 mM sodium phosphate buffer, 0.1 mM EDTA, pH = 7.0 in the presence of 50 mM NaCl (superscript L)

Duplex	Slope	$R^2$ value
<sup>L</sup> No DNA	2.50	0.991
<sup>L</sup> D1	0.29	0.996
<sup>L</sup> D2	0.19	0.996
<sup>L</sup> D3	0.21	0.997
<sup>L</sup> D4	0.17	0.995
<sup>L</sup> stDNA	-0.032	0.998

In summary, porphyrin fluorescence is completely protected by stDNA whereas the TINA-modified and unmodified duplexes are not as effective as stDNA. This may be explained by the efficient repelling of  $[\text{Fe}(\text{CN})_6]^{4-}$  ions from the negatively charged phosphates of stDNA, which is much longer than short DNA duplexes **D1-D4**.

## 6.8 Circular Dichroism of porphyrin/TINA-DNA complexes

The CD spectra of B-DNA are characterised by bands with positive ellipticities at 220 and 280 nm and a band with negative ellipticity at 255 nm (**D1**, Figure 6.15).<sup>[18]</sup> Duplex **D2** (Figure 6.15) contains extra positive bands at 373 nm and 396 nm attributed to the presence of the TINA monomer in the sequence.



**Figure 6.15** CD spectra of **D1** and **D2** in the absence and in the presence of ZnTMpyP4. Conditions: ZnTMpyP4 = 10  $\mu$ M, **D2** = 1.0  $\mu$ M, room temperature, 10 mM sodium phosphate, 0.1 mM EDTA, 1.0 M NaCl, pH = 7.0.

The addition of ZnTMpyP4 to **D1** and **D2** results in positive induced CD signals both at the Soret and Q-bands, which is similar to CD signals reported for a porphyrin bound in the groove of stDNA.<sup>[19]</sup> The porphyrin signal intensity is lower for complexes with TINA-modified duplexes than that observed for **D1** + ZnTMpyP4. This shows that the chirality transfer from DNA to the porphyrin is dependent on the presence of the TINA molecule which is also chiral. On the other hand, the intensity of the TINA CD signal decreases in the presence of porphyrin for TINA-modified duplexes except **D2** in the low salt concentration solution (Table 6.7). Thus, TINA CD signals completely disappeared after the addition of the porphyrin to duplex **D3** indicating that the TINA monomers interact with the achiral porphyrin whereas the influence of the chiral DNA is minimized.

**Table 6.7** Characteristic bands in CD spectra of duplexes in the absence and presence of ZnTMpyP4.

Duplex	Porph. CD ( $\lambda$ , nm)	Porph. $\Delta\epsilon$ ( $M^{-1}cm^{-1}$ )	TINA CD ( $\lambda$ , nm)	TINA $\Delta\epsilon$ ( $M^{-1}cm^{-1}$ )
D1 + <b>ZnTMpyP4<sup>L</sup></b>	440	+61	-	-
D1 + <b>ZnTMpyP4<sup>H</sup></b>	439	+54	-	-
D2 <sup>L</sup>	-	-	373;395	+37;+33
D2 <sup>H</sup>	-	-	375;395	+43;+45
D2 + <b>ZnTMpyP4<sup>L</sup></b>	436	+57	374;393	+58;+60
D2 + <b>ZnTMpyP4<sup>H</sup></b>	446	+45	377;393	+25;+29
D3 <sup>L</sup>	-	-	394	+9
D3 <sup>H</sup>	-	-	402	+6
D3 + <b>ZnTMpyP4<sup>L</sup></b>	441	+27	-	-
D3 + <b>ZnTMpyP4<sup>H</sup></b>	440	+5	-	-
D4 <sup>L</sup>	-	-	379;400	+35;+42
D4 <sup>H</sup>	-	-	389	+14
D4 + <b>ZnTMpyP4<sup>L</sup></b>	440	+23	398	+8
D4 + <b>ZnTMpyP4<sup>H</sup></b>	440	+15	398	+7

Conditions: see Table 6.1

## 6.9 Conclusions and Future Directions

Incorporation of TINA at the 5'-end of the DNA duplex results in the formation of supramolecular assemblies with the cationic porphyrin ZnTMpyP4. It is important that optical properties of individual components are changing as a result of electronic interactions between the TINA monomer and the porphyrin. Analysis of the TINA fluorescence quenching by the porphyrin reveals that these components interact mainly through ground state complex formation rather than via collisional encounters, although diffusion controlled interactions still play an important role.

Porphyrin binding to the short DNA duplexes is less efficient than to the DNAs of a biological origin. Insertion of TINA monomer(s) at the 5'-end improves this characteristic, however only one modified duplex **D3** had a  $K_a$  value of similar magnitude to the  $K_a$  of the porphyrin-stDNA complex at low salt concentration. This result has been attributed to breathing of terminal base-pairs, which is more substantial at low rather than at high salt concentration. This means that the binding affinity can be improved further by increasing the length of the duplex, allocating

more than two organic chromophores in the grooves or by using a different DNA scaffold in which DNA breathing is minimized and that allows association of several chromophores at once, G-quadruplexes for example.<sup>[20]</sup>

In contrast to the ligands in solution, the binding of the porphyrin to the TINA-modified duplexes alters the spectroscopic signals of both TINA and ZnTMpyP4, albeit to different extents. As such this study offers a new insight into utilizing organic chromophore-modified DNA as a supramolecular scaffold for the organization of functional molecules. It shows the possibility to increase communication between ligands and chromophores with predetermined positions on DNA. We decided to extend the study to the organization of tris(bipyridine)ruthenium(II),  $[\text{Ru}(\text{bpy})_3]^{2+}$  on TINA-modified DNA duplexes, as well as both ZnTMpyP4 and  $[\text{Ru}(\text{bpy})_3]^{2+}$  on TINA-modified G-quadruplexes.



## 6.10 References

- [1] a)R. J. Fiel, J. C. Howard, E. H. Mark, N. D. Gupta, *Nucleic Acids Research* **1979**, *6*, 3093; b)C. Bonechi, A. Donati, M. P. Picchi, C. Rossi, E. Tiezzi, *Colloids and Surfaces A: Physicochemical and Engineering Aspects* **1996**, *115*, 89; c)B. G. Feuerstein, N. Pattabiraman, L. J. Marton, *Nucleic Acids Research* **1989**, *17*, 6883; d) A. Kirsch-De Mesmaeker, G. Orellana, J. K. Barton, N. J. Turro, *Photochemistry and Photobiology* **1990**, *52*, 461; e)J. M. Kelly, M. J. Murphy, D. J. McConnell, C. Ohuigin, *Nucleic Acids Research* **1985**, *13*, 167; f)J.-O. Kim, Y.-A. Lee, B. H. Yun, S. W. Han, S. T. Kwag, S. K. Kim, *Biophysical Journal* **2004**, *86*, 1012; g)M. J. Morris, K. L. Wingate, J. Silwal, T. C. Leeper, S. Basu, *Nucleic Acids Research* **2012**; h)N. Nagesh, V. K. Sharma, A. Ganesh Kumar, E. A. Lewis, *Journal of Nucleic Acids* **2010**, *2010*; i)J. A. Strickland, D. L. Banville, W. D. Wilson, L. G. Marzilli, *Inorganic Chemistry* **1987**, *26*, 3398.
- [2] a)L. P. G. Wakelin, M. J. Waring, *Journal of Molecular Biology* **1980**, *144*, 183; b)G. Luck, K. E. Reinert, B. Baguley, C. Zimmer, *Journal of Biomolecular Structure & Dynamics* **1987**, *4*, 1079; c)K. Duskova, S. Sierra, M. J. Fernandez, L. Gude, A. Lorente, *Bioorganic & Medicinal Chemistry* **2012**, *20*, 7112; d)A. D. R. Pontinha, S. Sparapani, S. Neidle, A. M. Oliveira-Brett, *Bioelectrochemistry* **2013**, *89*, 50.
- [3] a)V. V. Filichev, E. B. Pedersen, T. P. Begley, *DNA-Conjugated Organic Chromophores in DNA Stacking Interactions*, John Wiley & Sons Inc., New York, **2009**, *1*, 493; b)P. M. E. Gramlich, C. T. Wirges, A. Manetto, T. Carell, *Angewandte Chemie International Edition* **2008**, *47*, 8350.
- [4] H.-A. Wagenknecht, *Angewandte Chemie International Edition* **2009**, *48*, 2838.
- [5] B. Albinsson, J. K. Hannestad, K. Borjesson, *Coordination Chemistry Reviews* **2012**, *256*, 2399.
- [6] F. Qu, N.-Q. Li, *Electroanalysis* **1997**, *9*, 1348.
- [7] a)O. Doluca, A. S. Boutorine, V. V. Filichev, *ChemBioChem* **2011**, *12*, 2365; b)V. V. Filichev, E. B. Pedersen, *Journal of the American Chemical Society* **2005**, *127*, 14849; c)I. Géci, V. V. Filichev, E. B. Pedersen, *Bioconjugate Chemistry* **2006**, *17*, 950; d)E. B. Pedersen, J. T. Nielsen, C. Nielsen, V. V. Filichev, *Nucleic Acids Research* **2011**, *39*, 2470; e)M. Paramasivam, S. Cogoi, V. V. Filichev, N. Bomholt, E. B. Pedersen, L. E. Xodo, *Nucleic Acids Research* **2008**, *36*, 3494; f)U. V. Schneider, N. D. Mikkelsen, N. Jøhnik, L. M. Okkels, H. Westh, G. Lisby, *Nucleic Acids Research* **2010**, *38*, 4394.
- [8] A. W. I. Stephenson, N. Bomholt, A. C. Partridge, V. V. Filichev, *ChemBioChem* **2010**, *11*, 1833.

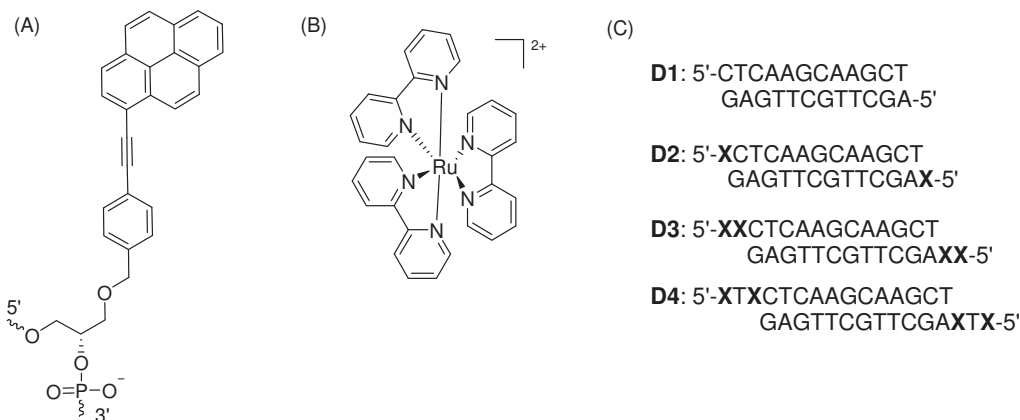
- [9] a)E. Kostenko, M. Dobrikov, D. Pyshnyi, V. Petyuk, N. Komarova, V. Vlassov, M. Zenkova, *Nucleic Acids Res* **2001**, 29, 3611; b)K. Yamana, T. Iwai, Y. Ohtani, S. Sato, M. Nakamura, H. Nakano, *Bioconjugate Chemistry* **2002**, 13, 1266; c)K. Yamana, Y. Ohshita, Y. Fukunaga, M. Nakamura, A. Maruyama, *Bioorganic & Medicinal Chemistry* **2008**, 16, 78; d)D. S. Novopashina, O. S. Totskaya, S. A. Kholodar, M. I. Meshchaninova, A. G. Ven'yaminova, *Russian Journal of Bioorganic Chemistry* **2008**, 34, 602; e)P. Conlon, C. Y. J. Yang, Y. R. Wu, Y. Chen, K. Martinez, Y. M. Kim, N. Stevens, A. A. Marti, S. Jockusch, N. J. Turro, W. H. Tan, *Journal of the American Chemical Society* **2008**, 130, 336.
- [10] L. R. Keating, V. A. Szalai, *Biochemistry* **2004**, 43, 15891.
- [11] a)R. Borsdorf, *Crystal Research and Technology* **1987**, 22, K158; b)R. Dabestani, I. N. Ivanov, *Photochemistry and Photobiology* **1999**, 70, 10.
- [12] J. Tuma, W. H. Connors, D. H. Stitelman, C. Richert, *Journal of the American Chemical Society* **2002**, 124, 4236.
- [13] J. A. Strickland, L. G. Marzilli, K. M. Gay, W. D. Wilson, *Biochemistry* **1988**, 27, 8870.
- [14] G. G. Hammes, *Spectroscopy for the Biological Sciences*, Wiley, **2005**.
- [15] J. Lakowicz, *Principles of Fluorescence Spectroscopy*, Springer, **2006**.
- [16] A. M. Pyle, J. P. Rehmman, R. Meshoyrer, C. V. Kumar, N. J. Turro, J. K. Barton, *Journal of the American Chemical Society* **1989**, 111, 3051.
- [17] Y. Xiong, X.-F. He, X.-H. Zou, J.-Z. Wu, X.-M. Chen, L.-N. Ji, R.-H. Li, J.-Y. Zhou, K.-B. Yu, *Journal of the Chemical Society, Dalton Transactions* **1999**, 19, 101.
- [18] J. Kypr, I. Kejnovská, D. Renčiuk, M. Vorlíčková, *Nucleic Acids Research* **2009**, 37, 1713.
- [19] R. F. Pasternack, *Chirality* **2003**, 15, 329.
- [20] J. Jayawickramarajah, D. M. Tagore, L. K. Tsou, A. D. Hamilton, *Angewandte Chemie-International Edition* **2007**, 46, 7583.



## 7 Interactions of TINA-modified DNA Duplexes with $[\text{Ru}(\text{bpy})_3]^{2+}$

### 7.1 Introduction

In light of the results from Chapter 4 we decided to extend our study to investigate the interactions of racemic  $[\text{Ru}(\text{bpy})_3]^{2+}$  with synthetic DNA duplexes modified with the TINA monomer, the same ones used in Chapter 6. In Chapter 4 we observed that our chromophores of interest PEPy and  $[\text{Ru}(\text{bpy})_3]^{2+}$  interact when freely in solution and photon upconversion was observed in DCM.



**Figure 7.1** Structures of twisted intercalating nucleic acid monomer (TINA monomer) **X**, (A),  $[\text{Ru}(\text{bpy})_3]^{2+}$  (B) and TINA-modified duplexes used in this study (C).

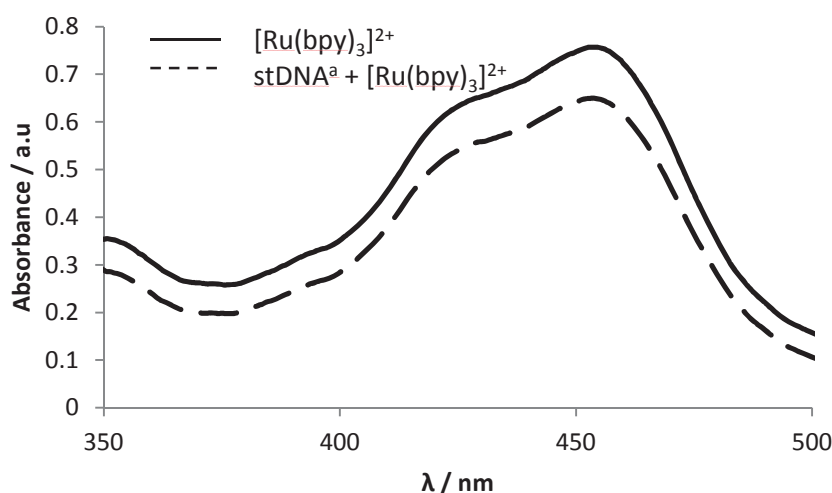
Short-stranded DNA duplexes **D1** – **D4**, bearing 5'-end TINA insertions, were prepared at 1.0  $\mu\text{M}$  concentration in 10 mM sodium phosphate buffer (pH 7.0, 0.1 mM EDTA) in the presence of low (50 mM NaCl) and high (1.0 M NaCl) salt concentration. Various spectroscopic techniques were used to study the properties of the DNAs in the absence and presence of  $[\text{Ru}(\text{bpy})_3]^{2+}$ .

### 7.2 stDNA - $[\text{Ru}(\text{bpy})_3]^{2+}$ studies

The binding of organometallic complexes, particularly ruthenium polypyridyl complexes to long stranded DNA duplexes of biological origin has been extensively investigated.<sup>[1]</sup> The significant interest in these compounds has been prompted by the fact that metallointercalators have been useful in probing DNA secondary structure and for their potential use in anti-cancer therapy.<sup>[2]</sup> Earlier studies of metallointercalators focused on square-planar platinum(II) having aromatic

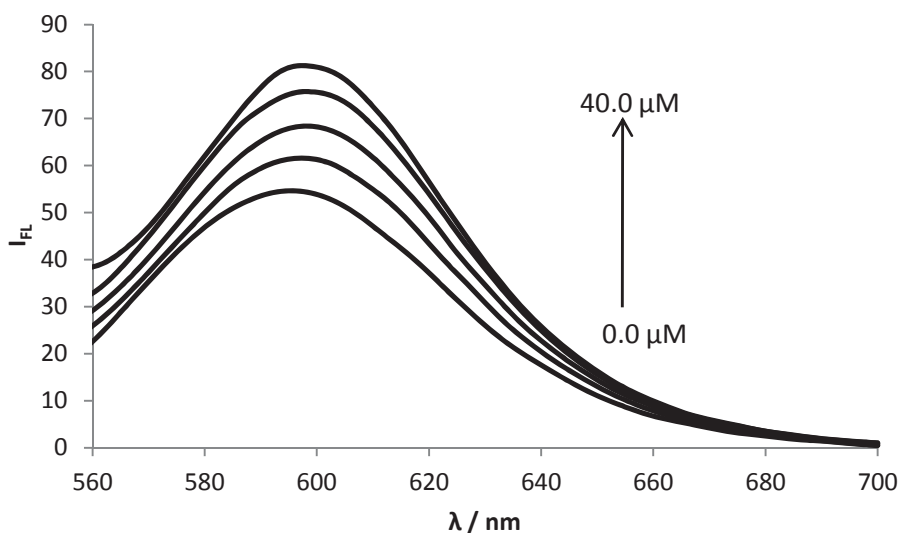
terpyridyl or phenanthroline ligands.<sup>[2a]</sup>  $[\text{Ru}(\text{bpy})_3]^{2+}$  is particularly convenient for monitoring DNA binding processes due to its strong absorption in the visible region and its strong fluorescence. As a result of  $[\text{Ru}(\text{bpy})_3]^{2+}$  binding to DNA, the perturbation of spectroscopic properties is usually observed.<sup>[3]</sup>  $[\text{Ru}(\text{bpy})_3]^{2+}$  has  $\pi$ - $\pi^*$  intra-ligand UV absorption bands around 211 nm, 244 nm, 289 nm, a MLCT visible absorption band around 450 nm, and fluoresces around 600 nm from the  $^3\text{MLCT}$  state to the ground state. In this investigation we explored the perturbations on the 289 nm absorption band, the 450 nm absorption band and the 600 nm emission band, but paid particular emphasis to the 450 nm and 600 nm bands since the 289 nm band overlaps with the 260 nm absorption band from DNA nucleobases.

We performed a preliminary study of the biological stDNA interaction with  $[\text{Ru}(\text{bpy})_3]^{2+}$  as a guide to find the optimal conditions for our relevant TINA-modified samples using UV-Vis, CD, and fluorescence spectroscopy. The  $[\text{Ru}(\text{bpy})_3]^{2+}$  optical changes that were observed upon stDNA binding resemble previously reported trends.<sup>[2-3]</sup> The addition of stDNA to  $[\text{Ru}(\text{bpy})_3]^{2+}$  in a low salt buffer resulted in a hypochromic shift (23 %) in the MLCT absorption band, Figure 7.2.<sup>[4]</sup> Barton *et al* suggested that stacking interactions with the base pairs are responsible for hypochromic shifts in the  $\pi$ - $\pi^*$  interactions.<sup>[2a]</sup>



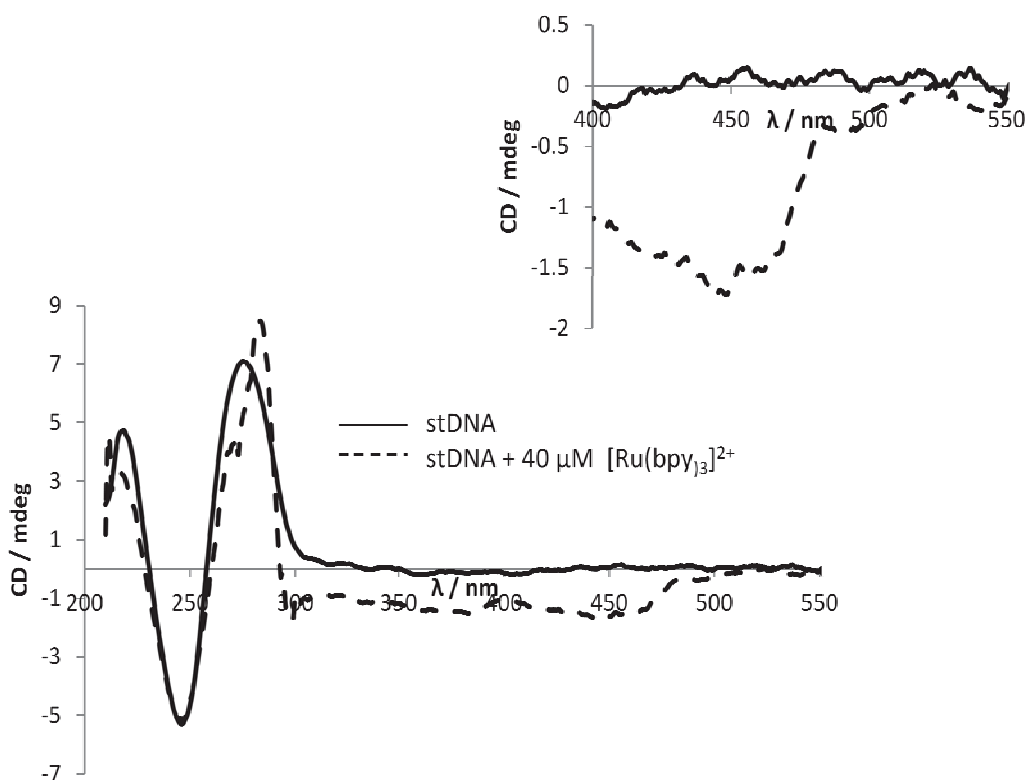
**Figure 7.2** The effect of stDNA<sup>a</sup> on the  $[\text{Ru}(\text{bpy})_3]^{2+}$  UV-Vis absorption spectrum. Conditions:  $[\text{Ru}(\text{bpy})_3]^{2+} = 100 \mu\text{M}$ , stDNA<sup>a</sup> = 1.0  $\mu\text{M}$ , 25 °C, pH = 7.0, 10 mM sodium phosphate buffer, 0.1 mM EDTA, 50 mM NaCl.

The fluorescence emission of  $[\text{Ru}(\text{bpy})_3]^{2+}$  was gradually increased with increasing stDNA concentration (Figure 7.3).<sup>[2-3, 5]</sup> Similar to what was mentioned in Chapter 6, enhanced emission reflects decreased mobility of  $[\text{Ru}(\text{bpy})_3]^{2+}$  when bound to the duplex.<sup>[2a]</sup>



**Figure 7.3** Fluorescence emission enhancement of  $[\text{Ru}(\text{bpy})_3]^{2+}$  (5  $\mu\text{M}$ ) upon addition of stDNA (0.0 – 40.0  $\mu\text{M}$ ). Buffer conditions are the same as in Figure 7.2.  $\lambda_{\text{ex}} = 500 \text{ nm}$ .

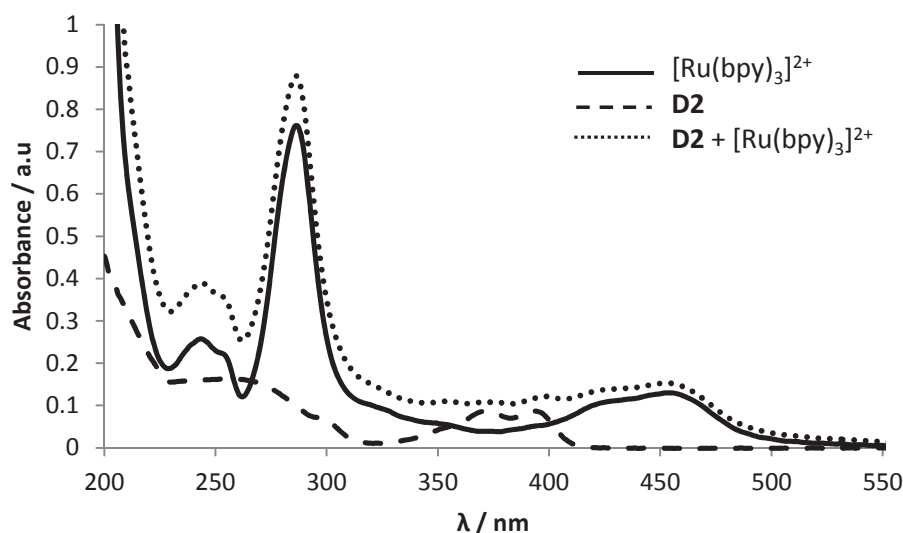
CD spectroscopy provided further evidence of binding of  $[\text{Ru}(\text{bpy})_3]^{2+}$  to stDNA through an induced CD signal (ICD) in the visible absorption band of the complex ( $\approx 450 \text{ nm}$ ) indicating transfer of chirality from DNA to  $[\text{Ru}(\text{bpy})_3]^{2+}$ , Figure 7.4. We noted that at concentrations of up to 40  $\mu\text{M}$   $[\text{Ru}(\text{bpy})_3]^{2+}$  it required 24 hours for complete binding to occur whereas with 100  $\mu\text{M}$  it took 1 hr, as shown by an appearance of an ICD signal. These findings were used to design experiments using TINA-modified duplexes.



**Figure 7.4** CD spectra of stDNA (0.02  $\mu\text{M}$ ) in the absence and presence of  $[\text{Ru}(\text{bpy})_3]^{2+}$  (40  $\mu\text{M}$ ), insert shows zoomed 400 – 550 nm region. Buffer conditions are the same as in Figure 7.2.

### 7.3 UV-Vis Spectroscopy of $[\text{Ru}(\text{bpy})_3]^{2+}$ /TINA-DNA complexes

The UV-Vis spectra of  $[\text{Ru}(\text{bpy})_3]^{2+}$  in the absence and presence of the TINA-modified DNA duplexes were analyzed and hyperchromic shifts in the MLCT band were observed (Figure 7.5) as opposed to stDNA with  $[\text{Ru}(\text{bpy})_3]^{2+}$  as discussed earlier (Figure 7.2). The increase in the MLCT absorbance band was attributed to a change in the  $[\text{Ru}(\text{bpy})_3]^{2+}$  environment where TINA affects the normal stacking interactions between the base pairs and  $[\text{Ru}(\text{bpy})_3]^{2+}$  seen with long biological DNAs. In the case of TINA-modified duplexes,  $[\text{Ru}(\text{bpy})_3]^{2+}$  is drawn more to the lipophilic TINA than to the base pairs. The increase in the  $\pi$ - $\pi^*$  intraligand absorption band on DNA binding is a result of an additive effect due to an overlap with the 260 nm band from DNA nucleobases.



**Figure 7.5** UV-Vis absorption spectra of free  $[\text{Ru}(\text{bpy})_3]^{2+}$  (40  $\mu\text{M}$ ), free **D2** (1.0  $\mu\text{M}$ ), and **D2** in the presence of  $[\text{Ru}(\text{bpy})_3]^{2+}$ . Buffer conditions are the same as in Figure 7.2, except  $\text{NaCl} = 1.0 \text{ M}$ .

Increase in concentration of  $\text{NaCl}$  from 50 mM to 1 M generally results in an increase of the visible absorption band (Table 7.1). This is due to competition with  $\text{Na}^+$  for the polyphosphate backbone on DNA, which in turn negatively impacts on the  $[\text{Ru}(\text{bpy})_3]^{2+}$  interaction with nucleobases. This effect was not seen on the intra-ligand band. This further supports the observation that the intensity increase in the ligand-ligand band is due to an additive effect of the overlapping 260 nm and 289 nm bands rather than as a result of binding. Furthermore, a dramatic increase in the MLCT band with two TINAs attached, **D3** and **D4**, both in low and high salt concentration solutions is important as it is an indicator of more TINA- $[\text{Ru}(\text{bpy})_3]^{2+}$  attraction as the number of TINAs increase. However, no bathochromic or hypsochromic shifts were observed.

The TINA absorption was also perturbed on addition of  $[\text{Ru}(\text{bpy})_3]^{2+}$ . In all duplexes studied the 373 nm band disappeared after addition of  $[\text{Ru}(\text{bpy})_3]^{2+}$  (Table 7.2). For **D3** both the 373 nm and 396 nm peaks disappeared. Duplex **D2** had slight bathochromic shifts in the 396 nm peak to 399 nm (low salt) and 398 nm (high salt) and hypochromic shifts (-64.1 % low salt, -78.5 % high salt). Duplexes **D3** and **D4** showed hyperchromic shifts ( $\approx 30 \%$ ). The extent of the shifts were higher in the high salt concentration.



**Table 7.1** UV-Vis absorption data for [Ru(bpy)<sub>3</sub>]<sup>2+</sup> bound to duplexes.<sup>a</sup>

Complex	MLCT band , nm	MLCT band, % $\Delta A^b$	L-L band, nm	L-L band, % $\Delta A^b$
<sup>L</sup> [Ru(bpy) <sub>3</sub> ] <sup>2+</sup>	454	-	286	-
<sup>H</sup> [Ru(bpy) <sub>3</sub> ] <sup>2+</sup>	453	-	286	-
<sup>L</sup> D1 + [Ru(bpy) <sub>3</sub> ] <sup>2+</sup>	453	+2.1	286	+10.6
<sup>H</sup> D1 + [Ru(bpy) <sub>3</sub> ] <sup>2+</sup>	453	+5.6	285	+12.6
<sup>L</sup> D2 + [Ru(bpy) <sub>3</sub> ] <sup>2+</sup>	453	+1.2	285	+14.0
<sup>H</sup> D2+ [Ru(bpy) <sub>3</sub> ] <sup>2+</sup>	453	+6.3	286	+14.0
<sup>L</sup> D3+ [Ru(bpy) <sub>3</sub> ] <sup>2+</sup>	453	+22.7	285	+11.0
<sup>H</sup> D3+ [Ru(bpy) <sub>3</sub> ] <sup>2+</sup>	454	+27.9	286	+8.0
<sup>L</sup> D4+ [Ru(bpy) <sub>3</sub> ] <sup>2+</sup>	454	+24.1	286	+18.6
<sup>H</sup> D4+ [Ru(bpy) <sub>3</sub> ] <sup>2+</sup>	453	+36.4	286	+18.1

<sup>a</sup> [Ru(bpy)<sub>3</sub>]<sup>2+</sup> = 40  $\mu$ M, duplex = 1.0  $\mu$ M, 10 mM sodium phosphate buffer, 0.1 mM EDTA, pH = 7.0 in the presence of 50 mM (superscript L) and 1.0 M NaCl (superscript H), 25 °C. <sup>b</sup> %  $\Delta A$  = [(A<sub>free</sub> - A<sub>bound</sub>) / A<sub>free</sub>] × 100. A<sub>free</sub> and A<sub>bound</sub> are the absorbances of free and bound [Ru(bpy)<sub>3</sub>]<sup>2+</sup>, respectively.<sup>[6]</sup>

**Table 7.2** UV-Vis absorption parameters for the pyrenyl moiety of TINA on duplexes bound to [Ru(bpy)<sub>3</sub>]<sup>2+</sup>. %  $\Delta A$  was calculated as in Table 7.1.

Duplex	$\lambda_{max}$	% $\Delta A$ ( $\approx$ 396 nm)	% $\Delta A$ ( $\approx$ 373 nm)
<sup>L</sup> D2	373;396	-	-
<sup>H</sup> D2	373;396	-	-
<sup>L</sup> D3	371;392	-	-
<sup>H</sup> D3	373;396	-	-
<sup>L</sup> D4	371	-	-
<sup>H</sup> D4	394	-	-
<sup>L</sup> D2 + [Ru(bpy) <sub>3</sub> ] <sup>2+</sup>	399	-64.1	*NV
<sup>H</sup> D2+ [Ru(bpy) <sub>3</sub> ] <sup>2+</sup>	398	-78.5	*NV
<sup>L</sup> D3+ [Ru(bpy) <sub>3</sub> ] <sup>2+</sup>	395	+33.1	*NV
<sup>H</sup> D3+ [Ru(bpy) <sub>3</sub> ] <sup>2+</sup>	*NV	*NV	*NV
<sup>L</sup> D4+ [Ru(bpy) <sub>3</sub> ] <sup>2+</sup>	394	+25.6	*NV
<sup>H</sup> D4+ [Ru(bpy) <sub>3</sub> ] <sup>2+</sup>	399	+30.6	*NV

Buffer conditions are the same as in Table 7.1. \*NV - there is no peak at 396 nm (no value to report).

## 7.4 DNA Melting Studies

The effect of TINA and salt concentration on DNA meltings at 260 nm have already been discussed in Chapter 6. We followed DNA meltings at 260 nm at 40  $\mu$ M and 100  $\mu$ M of [Ru(bpy)<sub>3</sub>]<sup>2+</sup>, Table 7.3. Addition of [Ru(bpy)<sub>3</sub>]<sup>2+</sup> destabilized unmodified duplex **D1** at both low and high salt concentrations. We think that this is due to [Ru(bpy)<sub>3</sub>]<sup>2+</sup> stacking interactions with nucleobases thereby destabilizing the duplex. Increasing [Ru(bpy)<sub>3</sub>]<sup>2+</sup> concentration to 100  $\mu$ M slightly restores the stability of **D1**, particularly in high salt conditions where stability is returned to the pre-[Ru(bpy)<sub>3</sub>]<sup>2+</sup> value.

**Table 7.3** UV-Vis melting temperatures of duplexes in the absence and presence of  $[\text{Ru}(\text{bpy})_3]^{2+}$  at 260 nm.

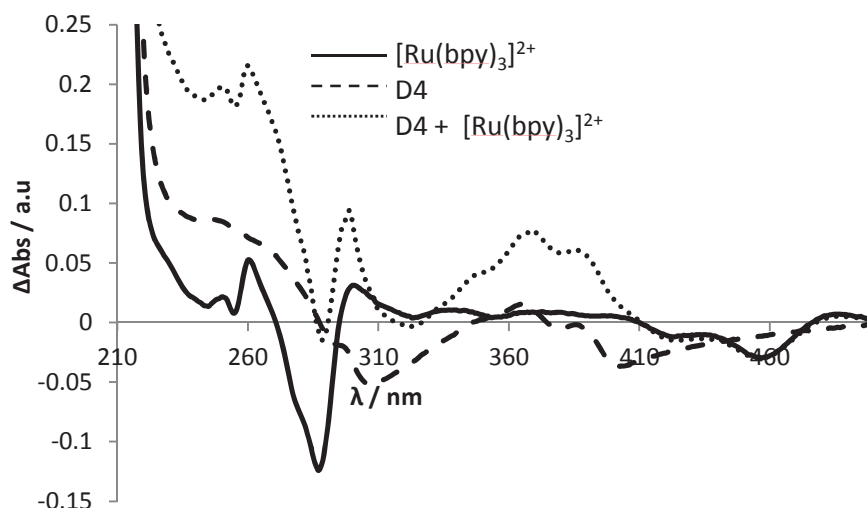
Duplex	$T_{m\ 260} / \Delta T_m$		
	No $[\text{Ru}(\text{bpy})_3]^{2+}$	40 $\mu\text{M}$ $[\text{Ru}(\text{bpy})_3]^{2+}$	100 $\mu\text{M}$ $[\text{Ru}(\text{bpy})_3]^{2+}$
<b>D1<sup>L</sup></b>	59.0	40.0 / -19.0	43.0 / -16.0
<b>D1<sup>H</sup></b>	54.5	51.5 / -3.0	55.0 / +0.5
<b>D2<sup>L</sup></b>	52.5	54.0 / +1.5	60.0 / +7.5
<b>D2<sup>H</sup></b>	64.0	64.0 / 0.0	67.5 / +3.5
<b>D3<sup>L</sup></b>	39.0	58.0 / +19.0	61.5 / +22.5
<b>D3<sup>H</sup></b>	62.0	56.0 / -6.0	63.0 / +1.0
<b>D4<sup>L</sup></b>	45.0	60.0 / +15.0	64.5 / +19.5
<b>D4<sup>H</sup></b>	42.0	80.0 / +38.0	83.0 / +41.0

Duplex = 1.0  $\mu\text{M}$ , 10 mM sodium phosphate buffer, 0.1 mM EDTA, pH = 7.0 in the presence of 50 mM (superscript L) and 1.0 M NaCl (superscript H), 25 °C.  $\Delta T_m$  is calculated as  $T_m(\text{R}) - T_m(\text{N})$ .  $T_m(\text{R})$  and  $T_m(\text{N})$  are melting temperatures in the presence and absence of  $[\text{Ru}(\text{bpy})_3]^{2+}$ , respectively.

More exciting is the fact that addition of  $[\text{Ru}(\text{bpy})_3]^{2+}$  stabilizes all TINA-modified duplexes in both high and low salt concentrations, except for **D3** at high salt concentration. In agreement with unmodified **D1**, increasing  $[\text{Ru}(\text{bpy})_3]^{2+}$  concentration further stabilizes the TINA-modified duplexes. At the higher concentration of  $[\text{Ru}(\text{bpy})_3]^{2+}$  (100  $\mu\text{M}$ ) duplexes were more thermally stable.

## 7.5 UV-Vis thermal difference spectra (TDS) of $[\text{Ru}(\text{bpy})_3]^{2+}$ /TINA-DNA complexes

Marked changes in the TDS profiles (described in Section 3.6.4) of the duplexes studied in the presence of  $[\text{Ru}(\text{bpy})_3]^{2+}$  were quite useful in our analyses, see Figure 7.6.  $[\text{Ru}(\text{bpy})_3]^{2+}$  alone exhibits two prominent negative TDS peaks around 290 nm and 450 nm. The most significant observation was the appearance of a negative TDS peak around 450 nm in all duplexes in the presence of  $[\text{Ru}(\text{bpy})_3]^{2+}$ , as opposed to porphyrin studies in Chapter 6 where both negative and positive peaks were observed in the porphyrin region. There was no sign change on the TDS peak at around 450 nm on adding  $[\text{Ru}(\text{bpy})_3]^{2+}$  to all duplexes. There was a decrease in the intensity of the  $[\text{Ru}(\text{bpy})_3]^{2+}$  peak in the presence of **D2** and **D3** (See Appendix, Chapter 12, Figures 12.12 and 12.13), but no such change was observed with **D4**, Figure 7.6.



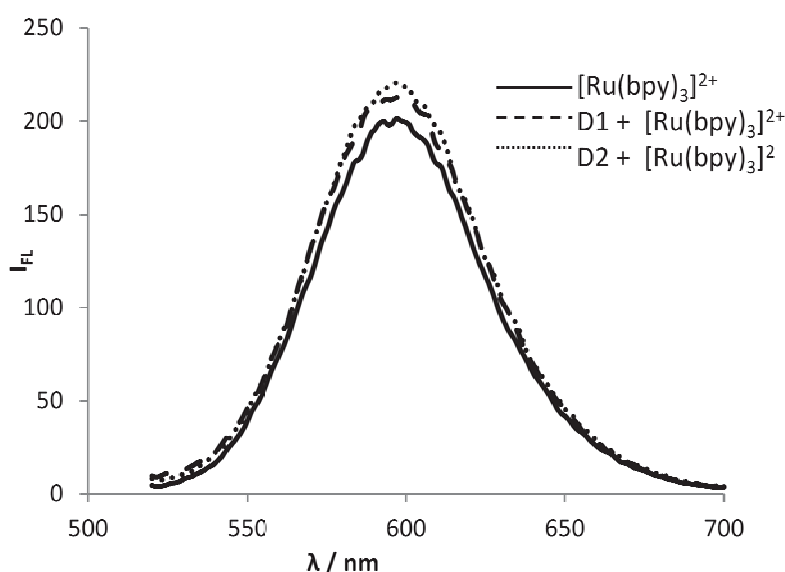
**Figure 7.6** Changes in thermal difference spectrum of **D4** on addition of  $[\text{Ru}(\text{bpy})_3]^{2+}$  (40  $\mu\text{M}$ ). Buffer conditions are the same as in Figure 7.5.

Addition of one TINA-modified **D1** led to the disappearance of the negative  $[\text{Ru}(\text{bpy})_3]^{2+}$  peak around 290 nm. On the other hand, in the presence of the doubly TINA-modified duplexes **D2** and **D3** the 290 nm negative peak is present, albeit at lower intensities in both cases (See Appendix, Chapter 12, Figures 12.12 and 12.13). This may suggest that  $[\text{Ru}(\text{bpy})_3]^{2+}$  participates differently in the duplex folding in the presence of two TINAs compared to one TINA. The positive DNA peak around 260 nm increases significantly in intensity in the presence of  $[\text{Ru}(\text{bpy})_3]^{2+}$  in all duplexes, except **D2**. This is partly a result of the presence of two  $[\text{Ru}(\text{bpy})_3]^{2+}$  positive peaks in the same region, but this cannot entirely account for the big increase.

Major decreases were observed in the intensities of TINA peaks in the range of 300 - 420 nm in the presence of  $[\text{Ru}(\text{bpy})_3]^{2+}$  for **D2** and **D3** in a low salt concentration, but for **D4** there was an increase, Figure 7.6. These changes suggested that  $[\text{Ru}(\text{bpy})_3]^{2+}$  interacts with TINA and plays a major role as it is in close proximity to the TINA during duplex folding and unfolding.

## 7.6 Fluorescence Spectroscopy of $[\text{Ru}(\text{bpy})_3]^{2+}$ /TINA-DNA complexes

The binding of  $[\text{Ru}(\text{bpy})_3]^{2+}$  to unmodified DNA and all the modified duplexes resulted in  $[\text{Ru}(\text{bpy})_3]^{2+}$  fluorescence emission enhancement due to protection of the  $[\text{Ru}(\text{bpy})_3]^{2+}$  by the duplex from water quenching, in agreement with binding to stDNA described in Section 7.2. <sup>[2a]</sup> In the presence of TINA, the degree of fluorescence enhancement is generally higher (Figure 7.7).



**Figure 7.7** Fluorescence emission enhancement of  $[\text{Ru}(\text{bpy})_3]^{2+}$  (40  $\mu\text{M}$ ) upon addition of short duplex DNA (1.0  $\mu\text{M}$ ),  $\lambda_{\text{ex}} = 500$  nm. Buffer conditions are the same as in Figure 7.2.

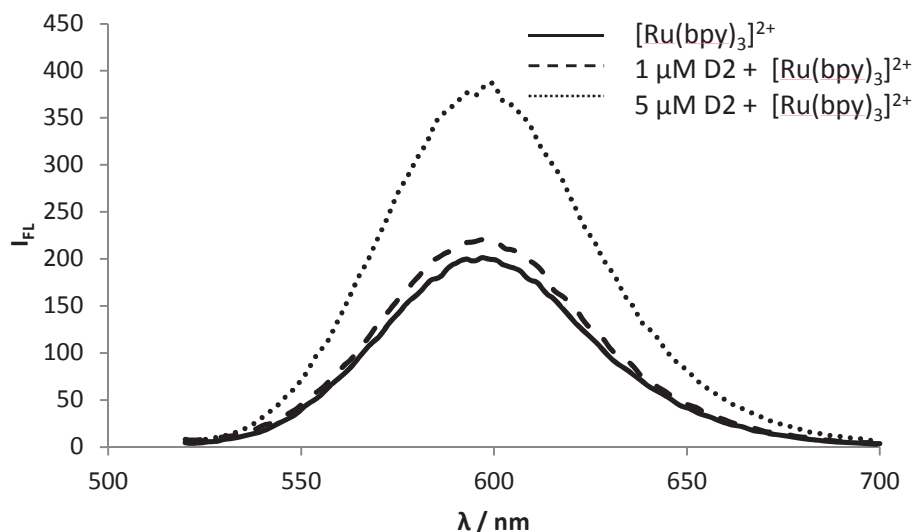
The fluorescence enhancements in the presence of the TINA-modified duplexes range from 8 – 17 %. The largest  $[\text{Ru}(\text{bpy})_3]^{2+}$  fluorescence enhancement of 17% was observed with **D2** at a low salt concentration (Table 7.4). In general, the fluorescence enhancement is greater in the low salt concentration, which may be explained by competition for binding sites with  $\text{Na}^+$  in higher salt concentrations.

**Table 7.4** Fluorescence emission data for  $[\text{Ru}(\text{bpy})_3]^{2+}$  bound to duplexes,  $\lambda_{\text{ex}} = 500 \text{ nm}$ .

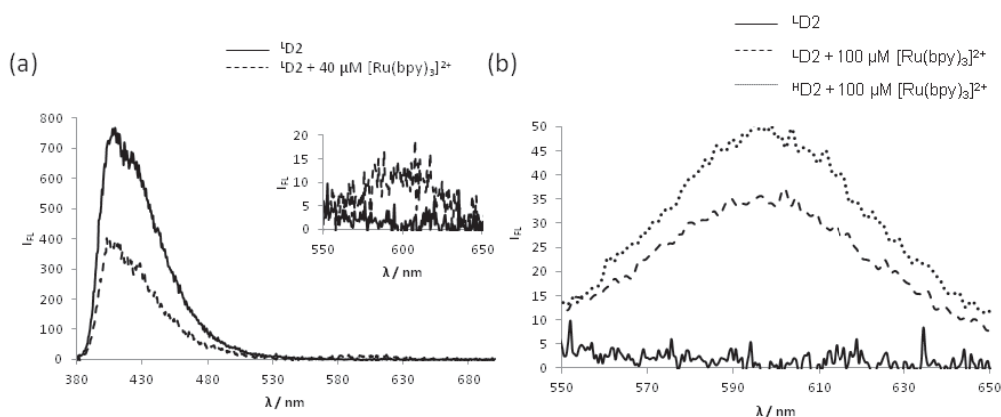
Complex	$\lambda_{\text{max}}, \text{nm}$	Fluorescence enhancement, %
$^{\text{L}}[\text{Ru}(\text{bpy})_3]^{2+}$	598	-
$^{\text{H}}[\text{Ru}(\text{bpy})_3]^{2+}$	596	-
$^{\text{L}}\text{D1} + [\text{Ru}(\text{bpy})_3]^{2+}$	596	9
$^{\text{H}}\text{D1} + [\text{Ru}(\text{bpy})_3]^{2+}$	597	4
$^{\text{L}}\text{D2} + [\text{Ru}(\text{bpy})_3]^{2+}$	599	17
$^{\text{H}}\text{D2} + [\text{Ru}(\text{bpy})_3]^{2+}$	596	8
$^{\text{L}}\text{D3} + [\text{Ru}(\text{bpy})_3]^{2+}$	597	11
$^{\text{H}}\text{D3} + [\text{Ru}(\text{bpy})_3]^{2+}$	600	10
$^{\text{L}}\text{D4} + [\text{Ru}(\text{bpy})_3]^{2+}$	599	10
$^{\text{H}}\text{D4} + [\text{Ru}(\text{bpy})_3]^{2+}$	599	8

Conditions are the same as in Table 7.1.

The emission intensities of  $[\text{Ru}(\text{bpy})_3]^{2+}$  further increased when the concentrations of the duplexes were increased from  $1 \mu\text{M}$  to  $5 \mu\text{M}$ , clearly indicating that at a higher DNA concentration the  $[\text{Ru}(\text{bpy})_3]^{2+}$  is in a more hydrophobic environment interacting with DNA to a greater extent than the aqueous phase, Figure 7.8. The increase in fluorescence intensities of  $[\text{Ru}(\text{bpy})_3]^{2+}$  in the presence of  $5 \mu\text{M}$  DNA make the fluorescence enhancement trend described above clearer (Figure 7.8).

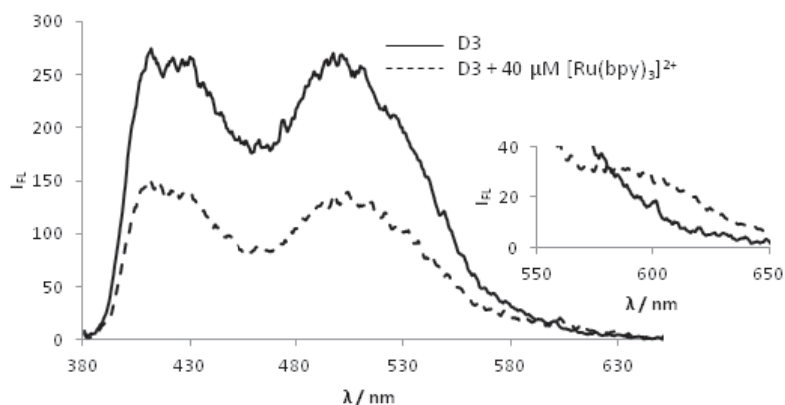
**Figure 7.8** Fluorescence emission enhancement of  $[\text{Ru}(\text{bpy})_3]^{2+}$  ( $40 \mu\text{M}$ ) with increasing DNA concentration,  $\lambda_{\text{ex}} = 500 \text{ nm}$ . Buffer conditions are the same as in Figure 7.2.

The presence of  $[\text{Ru}(\text{bpy})_3]^{2+}$  quenches the TINA fluorescence, Figure 7.9A. Upon increasing the  $[\text{Ru}(\text{bpy})_3]^{2+}$  concentration, further TINA emission quenching occurs, accompanied by energy transfer to the  $[\text{Ru}(\text{bpy})_3]^{2+}$  complex as shown by the appearance of a  $[\text{Ru}(\text{bpy})_3]^{2+}$  emission peak around 600 nm upon TINA excitation at 375 nm, Table 7.5. Another interesting result was the improved intensity of energy transfer at a higher salt concentration, Figure 7.9B, which we attribute to an increase in competition for polyphosphates with  $\text{Na}^+$  leading to increased association of  $[\text{Ru}(\text{bpy})_3]^{2+}$  with the lipophilic TINA moieties.



**Figure 7.9** Fluorescence quenching of TINA **D2** by  $[\text{Ru}(\text{bpy})_3]^{2+}$  (A), insert picture shows a  $[\text{Ru}(\text{bpy})_3]^{2+}$  energy transfer from TINA excitation. (B) TINA -  $[\text{Ru}(\text{bpy})_3]^{2+}$  energy transfer in low salt (50 mM NaCl)<sup>L</sup> and high salt (1 M NaCl)<sup>H</sup> buffer. Buffer = 10 mM sodium phosphate, 0.1 mM EDTA, pH = 7.0,  $\lambda_{\text{ex}}$  = 375 nm.

In the presence of two TINAs, the  $[\text{Ru}(\text{bpy})_3]^{2+}$  complex quenches both monomer and excimer fluorescence followed by energy transfer as with **D2**, Figure 7.10. As with porphyrin in Chapter 6, the binding of  $[\text{Ru}(\text{bpy})_3]^{2+}$  to DNA disrupts the excimer as shown by the decrease in the ratio of the excimer to monomer (See Table 7.5).



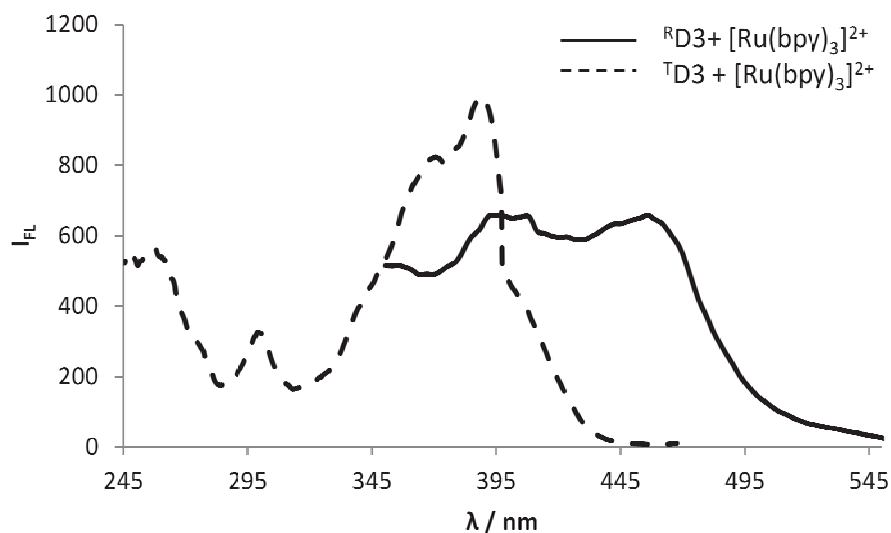
**Figure 7.10** Fluorescence quenching of TINA **D3** (1.0  $\mu\text{M}$ ) by  $[\text{Ru}(\text{bpy})_3]^{2+}$  (A). Insert picture shows a  $[\text{Ru}(\text{bpy})_3]^{2+}$  energy transfer from TINA excitation,  $\lambda_{\text{ex}} = 375 \text{ nm}$ . Buffer conditions are the same as for Figure 7.2.

**Table 7.5** Fluorescence emission characteristics of TINA and TINA- $[\text{Ru}(\text{bpy})_3]^{2+}$  complexes upon excitation of TINA at 375 nm.

Duplex	TINA emission ( $\lambda_{\text{max}}$ , nm)		$[\text{Ru}(\text{bpy})_3]^{2+}$ emission ( $\lambda_{\text{max}}$ , nm)	TINA, $I_{\text{ex}}/I_{\text{m}}$
	Monomer	Excimer		
<b>D2<sup>L</sup></b>	407;427	-	-	-
<b>D2<sup>H</sup></b>	407;427	-	-	-
<b>D2<sup>L</sup> + <math>[\text{Ru}(\text{bpy})_3]^{2+}</math></b>	408	-	602	-
<b>D2<sup>H</sup> + <math>[\text{Ru}(\text{bpy})_3]^{2+}</math></b>	406	-	599	-
<b>D3<sup>L</sup></b>	415;427	498	-	0.77
<b>D3<sup>H</sup></b>	415;429	492	-	1.3
<b>D3<sup>L</sup> + <math>[\text{Ru}(\text{bpy})_3]^{2+}</math></b>	403;415	498	600	0.70
<b>D3<sup>H</sup> + <math>[\text{Ru}(\text{bpy})_3]^{2+}</math></b>	404	500	593	0.26
<b>D4<sup>L</sup></b>	407;427	501	-	0.55
<b>D4<sup>H</sup></b>	409;427	496	-	0.48
<b>D4<sup>L</sup> + <math>[\text{Ru}(\text{bpy})_3]^{2+}</math></b>	407	503	596	0.32
<b>D4<sup>H</sup> + <math>[\text{Ru}(\text{bpy})_3]^{2+}</math></b>	407	500	598	0.18

Buffer conditions, see Table 7.1.  $I_{\text{ex}}/I_{\text{m}} = I_{\text{excimer}(500\text{nm})}/I_{\text{monomer}(405 \text{ nm})}$

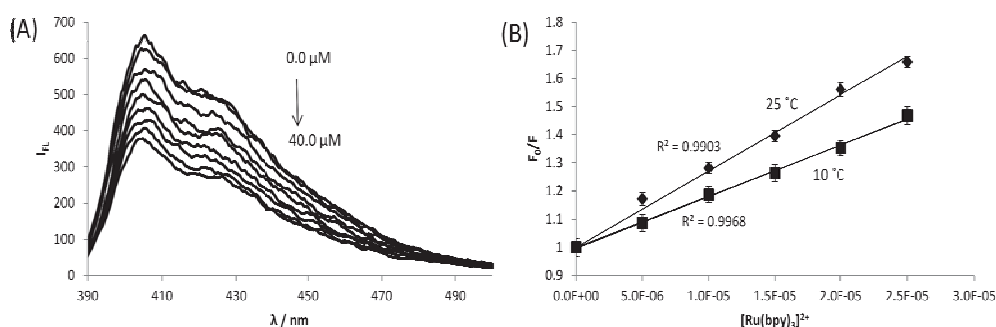
According to the excitation spectra, energy transfer from the TINA to the  $[\text{Ru}(\text{bpy})_3]^{2+}$  complex was observed (Figure 7.11). Energy transfer was also observed from DNA bases to the TINA ( $\sim 260 \text{ nm}$  peak, Figure 7.11).



**Figure 7.11** Fluorescence excitation spectra for **D3** (1.0  $\mu\text{M}$ ) in presence of  $[\text{Ru}(\text{bpy})_3]^{2+}$  (40  $\mu\text{M}$ ) at  $[\text{Ru}(\text{bpy})_3]^{2+}$  600 nm emission<sup>R</sup>, and TINA 490 nm<sup>T</sup> emission. Superscript R denotes  $[\text{Ru}(\text{bpy})_3]^{2+}$  emission and superscript T denotes TINA emission. Buffer conditions are the same as for Figure 7.2.

### 7.6.1 Stern-Volmer Analyses

As with  $\text{ZnTMpyP4}$ ,  $[\text{Ru}(\text{bpy})_3]^{2+}$  quenches both the TINA monomer and excimer fluorescence at concentrations of 1.0  $\mu\text{M}$  for all duplexes. However,  $[\text{Ru}(\text{bpy})_3]^{2+}$  does not quench the monomer or excimer completely even at elevated concentrations ( $\geq 10$   $\mu\text{M}$ ), Figure 7.12. Stern-Volmer analyses yielded straight lines for the monomer and excimer quenching indicating only one mode of quenching which could either be static or dynamic (See Section 4.3 in Chapter 4 for a theoretical account).



**Figure 7.12** (A) Fluorescence emission quenching of TINA monomer on **D2** (1.0  $\mu\text{M}$ ) with increasing concentration (0.0 to 40  $\mu\text{M}$ ) of  $[\text{Ru}(\text{bpy})_3]^{2+}$ ;  $\lambda_{\text{ex}} = 375$  nm. Buffer conditions are the same as for Figure 7.2. (B) Stern-Volmer plots for TINA-containing duplex **D2** (1.0  $\mu\text{M}$ ) quenching by  $[\text{Ru}(\text{bpy})_3]^{2+}$  at 25  $^{\circ}\text{C}$  and 10  $^{\circ}\text{C}$ .



The extent of excimer quenching is significantly higher than for monomer quenching for both **D3** and **D4** ( $\approx 2$  fold), Table 7.6. Excimer quenching, as opposed to monomer quenching, is desirable for photon upconversion applications as it suppresses long wavelength emission. Interestingly, the amount of monomer quenching is similar for all duplexes.

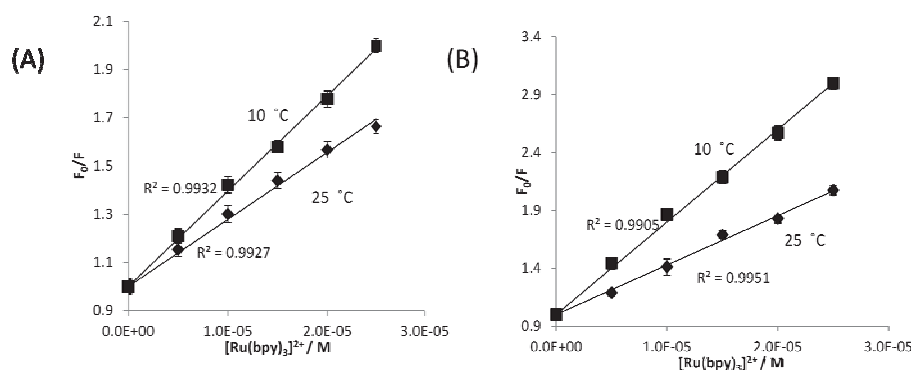
**Table 7.6** Stern–Volmer quenching constants,  $K_{SV}$  for the monomer and excimer of TINA-modified duplexes quenched by [Ru(bpy)<sub>3</sub>]<sup>2+</sup>. [Ru(bpy)<sub>3</sub>]<sup>2+</sup> = 40  $\mu$ M, duplex = 1.0  $\mu$ M, 10 mM sodium phosphate buffer, 0.1 mM EDTA, pH = 7.0 in the presence of 50 mM NaCl, 25 °C.

Duplex	$K_{SV(\text{mon})}$ , M <sup>-1</sup>	$K_{S(\text{ex})}$ , M <sup>-1</sup>	$K_a$ , M <sup>-1</sup>
<b>D2</b>	<sup>D</sup> $3.2 \times 10^4$	-	
<b>D3</b>	<sup>S</sup> $2.6 \times 10^4$	$4.1 \times 10^4$	$6.7 \times 10^4$
<b>D4</b>	<sup>S</sup> $2.3 \times 10^4$	$4.2 \times 10^4$	$6.5 \times 10^4$

Superscript S denotes static quenching and superscript D denotes dynamic quenching.  $K_a = K_{s(\text{mon})} + K_{s(\text{ex})}$ .  $K_{SV}$ ,  $K_S$  and  $K_a$  values are reported within 1 % error.

We established the mode of quenching of the TINA by [Ru(bpy)<sub>3</sub>]<sup>2+</sup> through temperature dependence measurements. Single TINA modified **D2** monomer was quenched with [Ru(bpy)<sub>3</sub>]<sup>2+</sup> by a dynamic mechanism (Figure 7.12). The presence of two TINAs on the DNA (**D3** and **D4**) led to significant results where both the monomer and excimer experienced static quenching by [Ru(bpy)<sub>3</sub>]<sup>2+</sup> (data shown for **D3** in Figure 7.3). The static quenching constants for monomer and excimer were used to determine the association constant ( $K_a$ ) for complex formation between the DNAs and the [Ru(bpy)<sub>3</sub>]<sup>2+</sup> complex (Table 7.6) using the equation below:

$$K_a = K_{s(\text{mon})} + K_{s(\text{ex})} \quad \text{eqn 7.1}$$

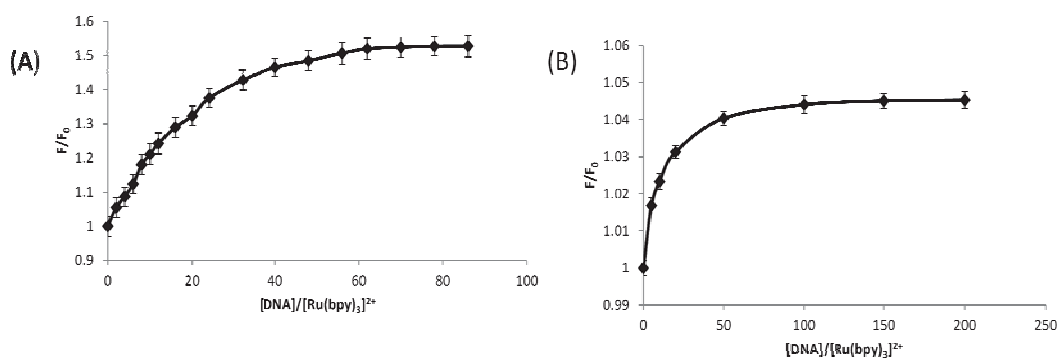


**Figure 7.13** Stern-Volmer plots for TINA **D3** (1.0  $\mu$ M) monomer (A) and excimer (B) quenching by [Ru(bpy)<sub>3</sub>]<sup>2+</sup> at 25 °C and 10 °C.  $\lambda_{\text{ex}}$  = 375 nm. Conditions are the same as for Figure 7.2.

Static quenching of the TINA by  $[\text{Ru}(\text{bpy})_3]^{2+}$  in the double TINA modification indicates the influence of proper chromophore arrangement on the DNA in the interaction of desirable chromophores (Figure 7.13). This is a clear indication of a change from dynamic quenching for free chromophores in solution (and with **D2**) to a ground state complex formation between  $[\text{Ru}(\text{bpy})_3]^{2+}$  and TINA facilitated by DNA on the duplexes **D3** and **D4**.

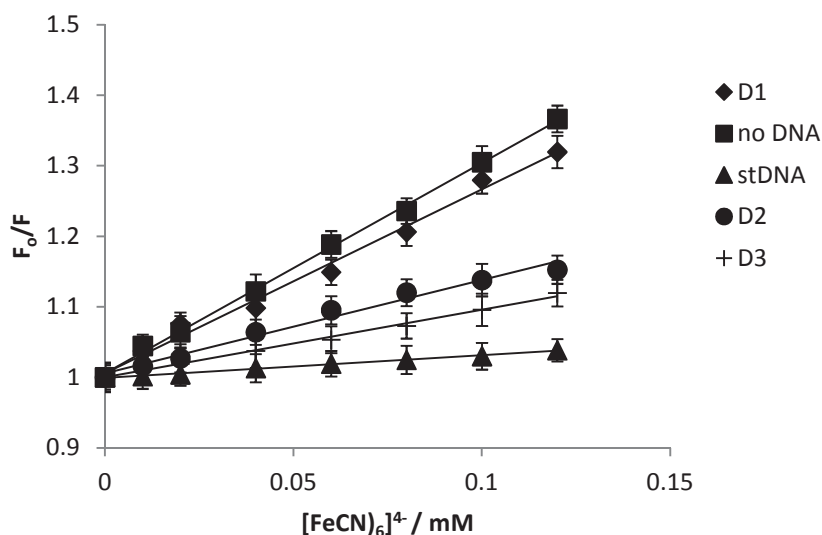
### 7.6.2 $\text{K}_4\text{Fe}(\text{CN})_6$ - $[\text{Ru}(\text{bpy})_3]^{2+}$ Fluorescence Quenching Studies

We evaluated how strongly the  $[\text{Ru}(\text{bpy})_3]^{2+}$  complex interacts with the DNA duplexes by how efficiently it is protected from quenching by  $[\text{Fe}(\text{CN})_6]^{4-}$  by the method outlined in Section 6.7.2 in Chapter 6. Initial trials using methyl viologen ( $\text{MV}^+$ ) as a quencher were unsuccessful in the presence of DNA. Free  $[\text{Ru}(\text{bpy})_3]^{2+}$  and  $\text{ZnTMpyP4}$  were quenched by free  $\text{MV}^+$  in solution, but in the presence of DNA no appreciable quenching was seen for any of the duplexes.  $\text{MV}^+$  has been well documented to interact with DNA,<sup>[7]</sup> possibly competing with chromophores of interest for DNA binding sites, hence we decided to use  $\text{K}_4\text{Fe}(\text{CN})_6$  which does not interfere with DNA.



**Figure 7.14** Plots of relative emission intensity versus stDNA:  $[\text{Ru}(\text{bpy})_3]^{2+}$  ratio (A) and relative emission intensity versus **D1**:  $[\text{Ru}(\text{bpy})_3]^{2+}$  ratio (B).  $[\text{Ru}(\text{bpy})_3]^{2+} = 1.0 \mu\text{M}$ . Buffer conditions are the same as in Figure 7.2.

Titration of  $1 \mu\text{M}$   $[\text{Ru}(\text{bpy})_3]^{2+}$  with stDNA resulted in an emission enhancement of up to around 1.50, more than that for short stranded **D1** ( $\approx 1.04$ ), Figure 7.14. TINA-containing short stranded duplexes **D2**, **D3** and **D4** caused emission enhancements higher than **D1** but smaller than stDNA and the values were 1.22, 1.41 and 1.36, respectively.



**Figure 7.15** Stern-Volmer plots of quenching of  $[\text{Ru}(\text{bpy})_3]^{2+}$  fluorescence with increasing concentration of a quencher,  $[\text{Fe}(\text{CN})_6]^{4-}$  in the absence and presence of DNAs.  $[\text{Ru}(\text{bpy})_3]^{2+} = 1 \mu\text{M}$ , DNA:  $[\text{Ru}(\text{bpy})_3]^{2+} = 40:1$ . Buffer conditions are the same as in Figure 7.2.

As shown in Figure 7.15, in the absence of DNA,  $[\text{Ru}(\text{bpy})_3]^{2+}$  was efficiently quenched by  $[\text{Fe}(\text{CN})_6]^{4-}$ , resulting in a linear Stern-Volmer plot (slope 2.98, correlation coefficient 0.998, Table 7.7). In the presence of long stDNA, the slope of the plot is markedly decreased (slope 0.32, correlation coefficient 0.996). This is in contrast to short unmodified **D1** (slope 2.61, correlation coefficient 0.990) which exhibited only a marginal decrease. The presence of the TINA in duplexes **D2-D4** caused a significant decrease in the slopes (Table 7.7), approaching that of stDNA which is nearly equal to zero.

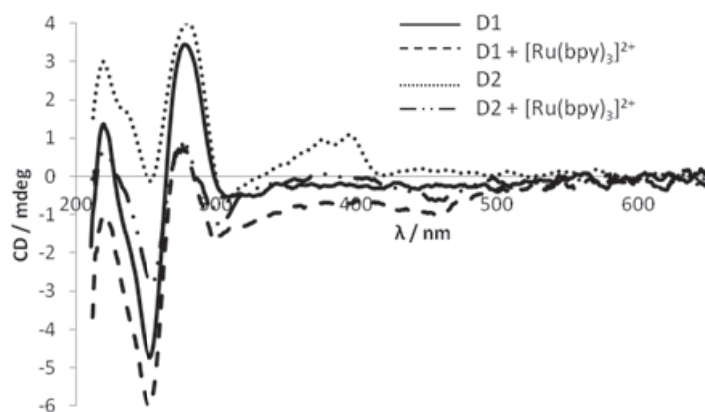
**Table 7.7** Slopes of plots on Figure 7.15, representing quenching efficiency of  $[\text{Ru}(\text{bpy})_3]^{2+}$  fluorescence by  $[\text{Fe}(\text{CN})_6]^{4-}$  in the presence of DNA duplexes.

Duplex	Slope	$R^2$ value
No DNA	2.98	0.998
<b>D1</b>	2.61	0.990
<b>D2</b>	1.33	0.983
<b>D3</b>	0.96	0.995
<b>D4</b>	1.06	0.994
stDNA	0.32	0.996

The results in Table 7.7 imply that the presence of TINA improves the engagement of  $[\text{Ru}(\text{bpy})_3]^{2+}$  within the DNA structure for short-stranded DNA duplexes.

## 7.7 Circular Dichroism of $[\text{Ru}(\text{bpy})_3]^{2+}$ /TINA-DNA complexes

In the presence of  $[\text{Ru}(\text{bpy})_3]^{2+}$ , both unmodified and modified duplexes develop a negative induced CD signal in the  $[\text{Ru}(\text{bpy})_3]^{2+}$  MLCT band around 450 nm, an increase in the negative peak around 250 nm, and a new negative peak around 300 nm. The appearance of a negative induced  $[\text{Ru}(\text{bpy})_3]^{2+}$  signal, is indicative of complex formation, usually by intercalation.<sup>[8]</sup> A negative band appearing in the 290 – 300 nm is further evidence of interaction between the ligand and DNA. Upon binding to the TINA-modified **D2** duplex, the  $[\text{Ru}(\text{bpy})_3]^{2+}$  complex produced a decrease in the negative ICD magnitude ( $\approx 64\%$ ) and a red shift of 9 nm from 460 nm as compared to unmodified **D1**.



**Figure 7.16** CD spectra of 1.0  $\mu\text{M}$  **D1** and **D2** in the absence and in the presence of  $[\text{Ru}(\text{bpy})_3]^{2+}$ . Conditions are same as in Figure 7.2.

The intensity of the positive TINA signals at 371 and 395 nm decrease upon  $[\text{Ru}(\text{bpy})_3]^{2+}$  binding. This, just like in the case of porphyrin, indicates that the TINA monomers interact with  $[\text{Ru}(\text{bpy})_3]^{2+}$ .

## 7.8 Conclusions

In contrast to ZnTMPyP4/TINA-modified complexes, in which both dynamic and static mechanism of interaction were realized, the use of two TINAs at the end of DNA duplexes converted the purely dynamic mode seen with one TINA to the static mode of  $[\text{Ru}(\text{bpy})_3]^{2+}$ -TINA interactions. Despite the fact that both ZnTMPyP4 and  $[\text{Ru}(\text{bpy})_3]^{2+}$  are positively charged, it shows that the nature of the ligand plays an important role in the interaction with the dyes covalently attached to DNA. We assume that four positive charges of ZnTMPyP4 located at the periphery of the molecule prevent the porphyrin to form a ground state complex with the TINA because it might migrate from the TINA to phosphates of DNA and back.

In the case of  $[\text{Ru}(\text{bpy})_3]^{2+}$ , as soon as two TINAs are present at the end of the duplex, the ligand is sandwiched and its mobility is significantly diminished. However, the TINA fluorescence is not completely quenched by the  $[\text{Ru}(\text{bpy})_3]^{2+}$  complex and the TINA excimer band disappears faster than the monomer band. This suggests that the  $[\text{Ru}(\text{bpy})_3]^{2+}$ /TINA-DNA system might be more suitable for EU than that of the ZnTMPyP4/TINA-DNA system.

## 7.9 References

- [1] a)R. Pasternack, E. Gibbs, T. Tullius, in *ACS Symposium Series, Vol. 402*, **1989**, 59;  
b)C. S. Chow, J. K. Barton, *Methods in enzymology* **1992**, 212, 219.
- [2] a)J. K. Barton, A. Danishefsky, J. Goldberg, *Journal of the American Chemical Society* **1984**, 106, 2172; b)Z.-Z. Li, Z.-H. Liang, H.-L. Huang, Y.-J. Liu, *Journal of Molecular Structure* **2011**, 1001, 36.
- [3] Y. Xiong, X.-F. He, X.-H. Zou, J.-Z. Wu, X.-M. Chen, L.-N. Ji, R.-H. Li, J.-Y. Zhou, K.-B. Yu, *Journal of the Chemical Society, Dalton Transactions* **1999**, 19.
- [4] S. A. Tysoe, R. J. Morgan, A. D. Baker, T. C. Strekas, *The Journal of Physical Chemistry* **1993**, 97, 1707.
- [5] S. Satyanarayana, J. C. Dabrowiak, J. B. Chaires, *Biochemistry* **1993**, 32, 2573.
- [6] a)L. R. Keating, V. A. Szalai, *Biochemistry* **2004**, 43, 15891; b)N. Nagesh, V. K. Sharma, A. Ganesh Kumar, E. A. Lewis, *Journal of nucleic acids* **2009**, 2010, 2275.
- [7] a)C. D. Poy, M. L. Cornélio, *Eclética Química* **1998**, 23, 99; b)A. M. Brun, A. Harriman, *Journal of the American Chemical Society* **1994**, 116, 10383.
- [8] Y. J. Jang, B.-H. Kwon, B.-H. Choi, C. H. Bae, M. S. Seo, W. Nam, S. K. Kim, *Journal of inorganic biochemistry* **2008**, 102, 1885.



## 8 Interactions of TINA-modified G-quadruplexes with [Ru(bpy)<sub>3</sub>]<sup>2+</sup> and ZnTMpyP4

### 8.1 Introduction

G-quadruplexes, higher order secondary structures of DNA are formed from guanine-rich sequences. Their significance has risen recently due to their capability to interact with intracellular proteins.<sup>[1]</sup> Many ligands have been synthesized with varying degrees of affinity and selectivity for G-quadruplexes both *in vivo* and *in vitro*. Therefore, understanding and elucidating G-quadruplex DNA/ligand interactions qualitatively and quantitatively using efficient, reliable, robust, cheap and readily available laboratory techniques is needed if their potential applications for bio/nanotechnology, drug design and molecular biology are to be maximized. The interactions of G-quadruplex DNAs with ligands, such as porphyrins, has been studied extensively by various biophysical methods.<sup>[2]</sup> Common spectroscopic methods, UV-vis, fluorescence, circular dichroism (CD) and nuclear magnetic resonance (NMR), provide valuable information on the nature of the DNA-ligand complex.<sup>[2-3]</sup> Other techniques such as isothermal titration calorimetry (ITC) provides thermodynamic data, X-ray crystallography gives detailed structural information and molecular modelling can predict the most stable structure and interaction energy.<sup>[2]</sup>

Most of the recent work on G-quadruplex-ligand interactions has been focused on ligands which can be potentially used as anti-tumor agents and utilize unmodified G-quadruplex structures.<sup>[3-4]</sup> A large number of proteins, mostly from ciliates and yeast, have been reported to bind to G-quadruplex structures.<sup>[4b]</sup> Several studies have been carried out which show that a wide variety of small molecules like cationic porphyrins and perylenes interact with G-quadruplexes *in vitro*.<sup>[4b]</sup> G-Quadruplex DNAs are an interesting proposition for us as they give us versatility since they form structures of extraordinary stability, are stabilized by coordinating monovalent cations, form a wide variety of geometries depending on their molecularity and strand orientation, can interact with small molecules that can facilitate their formation and/or stabilization. In addition organic chromophores can be attached to them covalently.



In our study, we decided to use G-quadruplexes modified with pyrene-containing TINA molecules at various positions and investigate how the presence of the DNA affects interaction of the TINA with either a cationic porphyrin (ZnTMpyP4) or a ruthenium polypyridyl complex, ([Ru(bpy)<sub>3</sub>]<sup>2+</sup>). Previous studies have shown that inserting pyrene-containing TINA molecules on G-rich oligonucleotides still results in G-quadruplex structure formation, with improved thermodynamic stabilities.<sup>[5]</sup> A recent study showing energy transfer between a coumarin-modified G-quadruplex and a cationic porphyrin indicates the potential of G-quadruplex DNA to provide a scaffold for systematic assembly of multiple chromophores for photonic applications.<sup>[6]</sup>

## 8.2 G-Quadruplex Design

We decided to insert the TINA monomer at various positions in the d(TG4T) sequence from the *Tetrahymena* telomere, between T and G, at the 5'-end and in the middle of the G-tract.<sup>[1]</sup>

**Table 8.1** G-Quadruplex sequences used in this chapter and their abbreviations

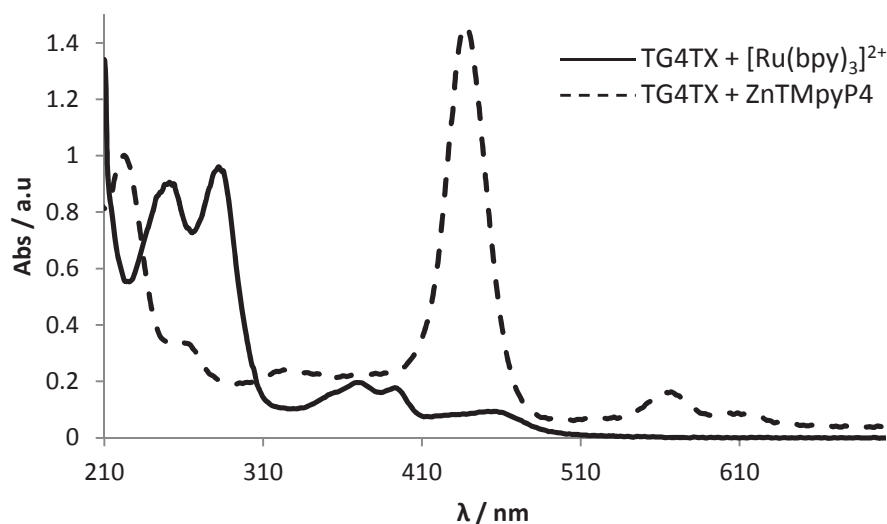
Abbreviation	Sequence
<b>TG4T</b>	5'-dTGGGGT
<b>TG4TX</b>	5'-d <b>X</b> TGGGGT <sup>a</sup>
<b>TG4XT</b>	5'-dT <b>X</b> GGGGT <sup>a</sup>
<b>TG3XG3T</b>	5'-dTGGG <b>X</b> GGGT <sup>a</sup>

<sup>a</sup> X refers to the TINA monomer.

The required oligonucleotide sequences were synthesized on an automated DNA synthesizer using phosphoramidite chemistry as described in Section 3.5 in Chapter 3. Oligonucleotides were purified using reverse-phase HPLC, where necessary. G-quadruplexes (10 μM strand concentration) were prepared by incubating the single strands in 10 mM sodium phosphate buffer (pH 7.0, 0.1 mM EDTA) in the presence of 50 mM NaCl at 90 °C for 30 min followed by slow cooling to 20 °C overnight.

### 8.3 UV-Vis Spectroscopy of $[\text{Ru}(\text{bpy})_3]^{2+}$ / G-Quadruplex complexes

A decrease in the intensity of the MLCT  $[\text{Ru}(\text{bpy})_3]^{2+}$  band was observed in the presence of unmodified **TG4T**, which is usually indicative of a binding mode that involves stacking interactions between the chromophore and the DNA base pairs.<sup>[7]</sup> In contrast, TINA-modified G-quadruplexes caused an increase in the MLCT intensity, as was earlier observed with the TINA-modified duplexes (See Appendix, Chapter 12, Table 12.2). This suggests an alternative or an additional binding mode initiated by the TINA. TINA absorption peaks were retained with  $[\text{Ru}(\text{bpy})_3]^{2+}$  present (Figure 8.1), only intensity increases observed are due to an additive effect from  $[\text{Ru}(\text{bpy})_3]^{2+}$  absorptions in the regions of interest.

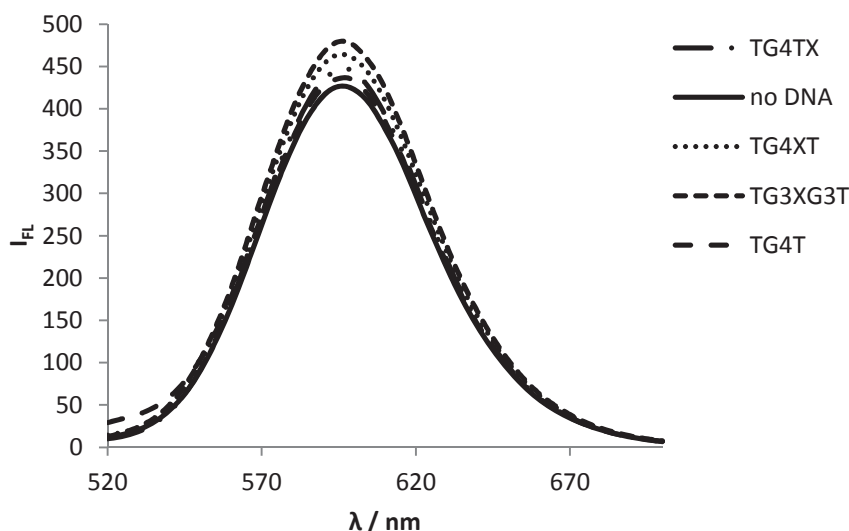


**Figure 8.1** UV-Vis absorption spectrum of **TG4TX** (10  $\mu\text{M}$  strand concentration) in the presence of  $[\text{Ru}(\text{bpy})_3]^{2+}$  (40  $\mu\text{M}$ , solid line) and  $\text{ZnTMpyP4}$  (40  $\mu\text{M}$ , dashed line). Conditions: 10 mM sodium phosphate buffer (pH 7.0), 0.1 mM EDTA, 50 mM NaCl, 25  $^{\circ}\text{C}$ .

In the presence of all G-quadruplexes, hypochromic and slight bathochromic shifts were observed in the  $\text{ZnTMpyP4}$  Soret and the largest Q-band. The extent of hypochromicity was greater with TINA-modified G-quadruplexes than with **TG4T** (See Appendix, Chapter 12, Table 12.2).

## 8.4 Fluorescence Spectroscopy of $[\text{Ru}(\text{bpy})_3]^{2+}$ /G-Quadruplex complexes

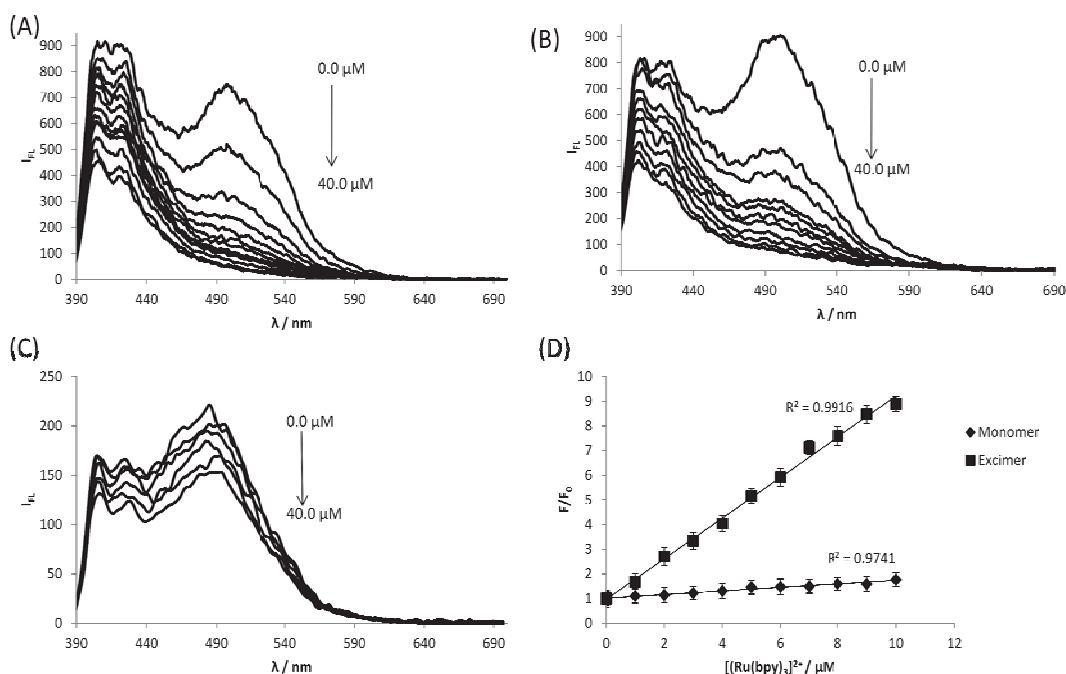
TINA-containing G-quadruplexes caused a slight increase in emission intensity of  $[\text{Ru}(\text{bpy})_3]^{2+}$  than **TG4T**, with the largest increase occurring in the presence of **TG3XG3T** (10 %), Figure 8.2.



**Figure 8.2** Effects of adding G-quadruplexes at 10  $\mu\text{M}$  strand concentration on fluorescence emission spectra of  $[\text{Ru}(\text{bpy})_3]^{2+}$  (40  $\mu\text{M}$ ). Buffer conditions are the same as in Figure 8.1.  $\lambda_{\text{ex}} = 500 \text{ nm}$ .

The TINA monomer and excimer fluorescence emissions observed in all G-quadruplexes were quenched by  $[\text{Ru}(\text{bpy})_3]^{2+}$  (Figure 8.3). Interestingly, excimer quenching far exceeds monomer quenching for **TG4TX** and **TG4XT** ( $\approx 10$  fold for both), in agreement with duplex **D4** in Chapter 7, whereas it is only approximately two-fold for **TG3XG3T**, resembling **D3** (Table 8.2 - See  $K_S$  values for excimer in comparison to monomer). In addition, the excimer fluorescence was completely quenched at high concentrations of  $[\text{Ru}(\text{bpy})_3]^{2+}$  ( $\geq 20 \mu\text{M}$ ) for **TG4TX** and **TG4XT**, where the TINA is located outside the G-tract (Figure 8.3A and B). On the other hand, with the TINA in the middle of the G-tract (**TG3XG3T**), the excimer peak is more prominent than the monomer and even at high concentrations of  $[\text{Ru}(\text{bpy})_3]^{2+}$  the excimer is not completely quenched (Figure 8.3B). This suggests that TINA-TINA interactions are protected by neighbouring guanines in **TG3XG3T**, whereas a TINA placed outside of the guanine tracts is more susceptible to interacting with  $[\text{Ru}(\text{bpy})_3]^{2+}$ . However, for each G-quadruplex the TINA's

monomer fluorescence is not completely quenched. These results suggest that positioning TINA outside the G-tract is better suited for photon upconversion applications.



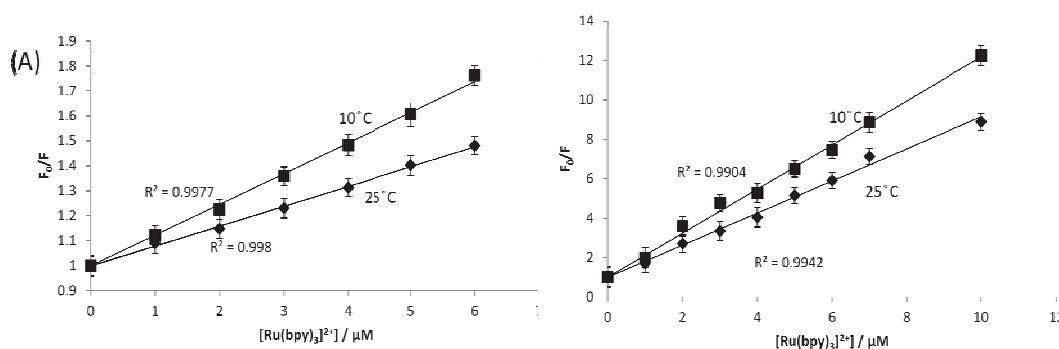
**Figure 8.3** Quenching of the TINA fluorescence upon addition of [Ru(bpy)<sub>3</sub>]<sup>2+</sup> to (A) **TG4TX**, (B) **TG4XT** and (C) **TG3XG3T**. (D) Stern-Volmer plots for steady state fluorescence quenching of **TG4TX** monomer and excimer by [Ru(bpy)<sub>3</sub>]<sup>2+</sup>. Conditions are the same as in Figure 8.1, λ<sub>ex</sub> = 375 nm.

**Table 8.2** Stern–Volmer quenching constants ( $K_{SV}$ ) for the monomer and excimer of TINA-modified G-quadruplexes quenched by [Ru(bpy)<sub>3</sub>]<sup>2+</sup>, as well as association constants ( $K_a$ ) for the DNA and [Ru(bpy)<sub>3</sub>]<sup>2+</sup>. Conditions: 10 mM sodium phosphate buffer (pH 7.0), 0.1 mM EDTA, 50 mM NaCl, 25 °C.  $K_a = K_{S(mon)} + K_{S(ex)}$ .  $K_S$  and  $K_o$  values are reported within 2.5 % error.

G-Quadruplex	$K_{S(mon)}, M^{-1}$	$K_{S(ex)}, M^{-1}$	$K_a, M^{-1}$
<b>TG4TX</b>	$7.1 \times 10^4$	$8.3 \times 10^5$	$8.3 \times 10^5$
<b>TG4XT</b>	$4.4 \times 10^4$	$4.0 \times 10^5$	$4.84 \times 10^5$
<b>TG3XG3T</b>	$1.6 \times 10^4$	$3.7 \times 10^4$	$5.3 \times 10^5$

The Stern-Volmer plots are linear in all cases for monomer and excimer, indicating that only one mode of quenching is realized (Figure 8.3D for **TG4TX**). Temperature dependence of TINA fluorescence quenching proved that all monomer and excimer signals are quenched by a static mechanism (Figure 8.4 for **TG4TX**). The association constant ( $K_a$ ) was obtained as a sum of monomer and excimer static

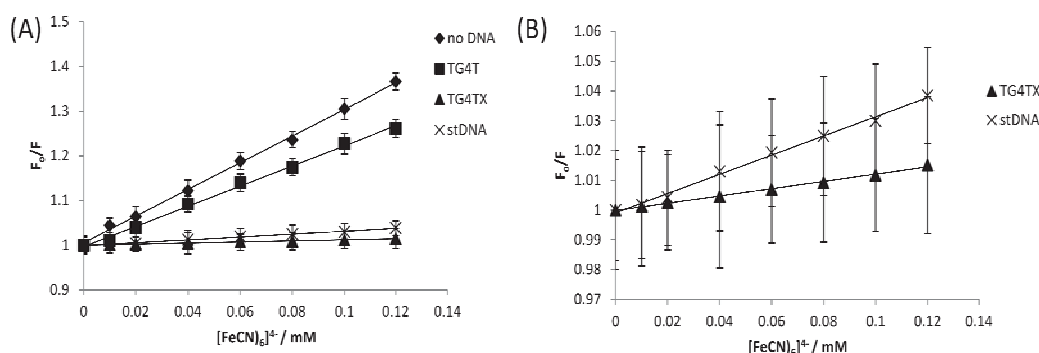
quenching constants (Table 8.2). **TG4TX** had the highest binding constant to  $[\text{Ru}(\text{bpy})_3]^{2+}$ , which is one order of magnitude higher than that obtained for TINA-modified duplexes.



**Figure 8.4** Stern-Volmer plots for **TG4TX** (1.0  $\mu\text{M}$ ) monomer (A) and excimer (B) quenching by  $[\text{Ru}(\text{bpy})_3]^{2+}$  at 25 °C and 10 °C. Conditions are the same as in Figure 8.1.  $\lambda_{\text{ex}} = 375 \text{ nm}$ .

#### 8.4.1 $\text{K}_4\text{Fe}(\text{CN})_6$ – $[\text{Ru}(\text{bpy})_3]^{2+}$ Quenching Studies

Studies of quenching of  $[\text{Ru}(\text{bpy})_3]^{2+}$  by  $\text{K}_4\text{Fe}(\text{CN})_6$ , as described earlier in Chapter 6, demonstrated that TINA containing G-quadruplexes dramatically increase the protection of  $[\text{Ru}(\text{bpy})_3]^{2+}$  from  $[\text{Fe}(\text{CN})_6]^{4-}$  quenching (Figure 8.5, Table 8.3), in comparison to TINA-modified duplexes and **TG4T**. Unmodified G-quadruplex **TG4T** only marginally protects  $[\text{Ru}(\text{bpy})_3]^{2+}$  (slope 2.25, correlation coefficient 0.997), whilst **TG4TX** markedly decreases the slope (slope 0.12, correlation coefficient 0.995, Figure 8.5). It is quite exciting that in the presence of TINA-modified G-quadruplexes, protection of  $[\text{Ru}(\text{bpy})_3]^{2+}$  is comparable to that in the presence of stDNA, which was not the case for the TINA-modified duplexes.



**Figure 8.5** Stern-Volmer fluorescence quenching curves of  $[\text{Ru}(\text{bpy})_3]^{2+}$  with increasing concentration of quencher,  $[\text{Fe}(\text{CN})_6]^{4-}$  in the absence and presence of G-quadruplexes (A). The two bottom lines are expanded in B.  $[\text{Ru}(\text{bpy})_3]^{2+} = 1.0 \mu\text{M}$ , DNA:  $[\text{Ru}(\text{bpy})_3]^{2+} = 40:1$ . Conditions are the same as in Figure 8.1.

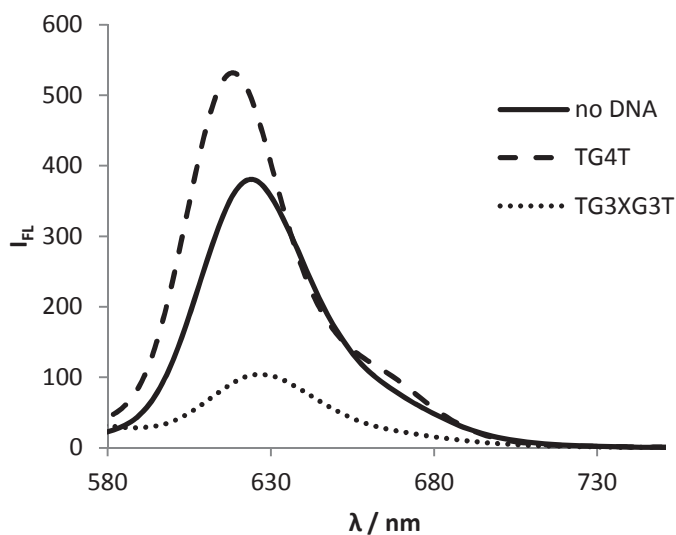
**Table 8.3** Slopes of plots on Figure 8.5, representing quenching efficiency of [Ru(bpy)<sub>3</sub>]<sup>2+</sup> fluorescence by [Fe(CN)<sub>6</sub>]<sup>4-</sup> after adding the corresponding G-quadruplex structures. Conditions are the same as in Table 8.2.

Duplex	Slope	R <sup>2</sup> value
No DNA	2.98	0.998
TG4T	2.25	0.997
TG4TX	0.12	0.995
TG4XT	0.26	0.996
TG3XG3T	0.08	0.999
stDNA	0.32	0.996

With these findings, we can conclude that the TINA incorporated into G-quadruplexes interacts better with [Ru(bpy)<sub>3</sub>]<sup>2+</sup> than in the structure of DNA duplexes. [Ru(bpy)<sub>3</sub>]<sup>2+</sup> significantly disrupts the excited dimer of the TINA when pyrene is placed outside of the G-tract. Even though **TG3XG3T** protects [Ru(bpy)<sub>3</sub>]<sup>2+</sup> more than **TG4TX** from quenching by [Fe(CN)<sub>6</sub>]<sup>4-</sup>, the excimer fluorescence is not quenched significantly, so **TG4TX** and **TG4XT** are more likely to function better in a photon upconversion system. [Ru(bpy)<sub>3</sub>]<sup>2+</sup> also exhibits similar excimer quenching characteristics with the duplex **D4**, with a thymidine in between TINAs, which also makes **D4** a good candidate for photon upconversion experiments.

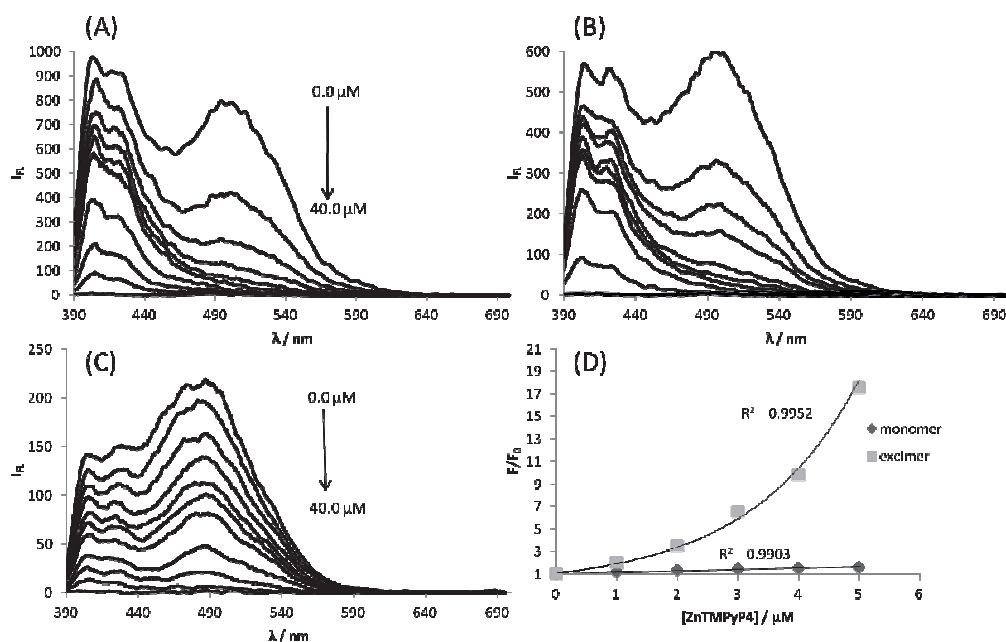
## 8.5 Fluorescence Spectroscopy of Porphyrin/ G-Quadruplex complexes

Addition of preformed **TG4T** led to enhanced ZnTMpyP4 fluorescence emission, whereas the TINA-containing G-quadruplexes quenched porphyrin fluorescence very effectively: a 3.5 times reduction in fluorescence intensity was observed in the presence of **TG3XG3T** (Figure 8.6). We assume that the **TG4T** protects the porphyrin from water quenching, whilst TINA quenching of the porphyrin counters the protection provided by the G-quadruplex.



**Figure 8.6** Fluorescence emission spectra of ZnTMPyP4 (4  $\mu\text{M}$ ) in the absence (solid line) of G-quadruplexes, and in the presence of **TG4T** (dashed line) and **TG3XG3T** (dotted line). G-quadruplex strand concentration = 10  $\mu\text{M}$ . Conditions are the same as in Figure 8.1.

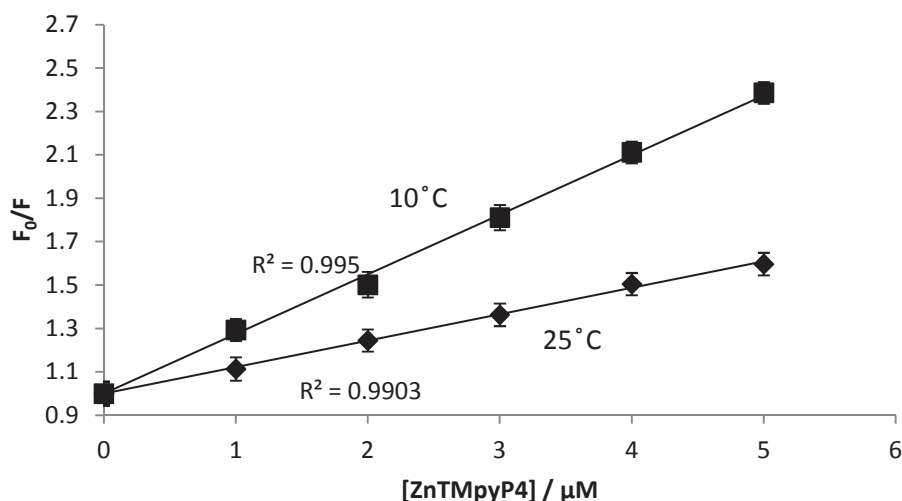
ZnTMPyP4 quenches both the TINA monomer and excimer fluorescence at 10  $\mu\text{M}$  strand concentration (Figure 8.7D). As previously observed for duplexes both the monomer and excimer are completely quenched at high porphyrin concentrations ( $\geq 30 \mu\text{M}$ ). In agreement with the case of  $[\text{Ru}(\text{bpy})_3]^{2+}$ , the porphyrin quenches the TINA excimer fluorescence in G-quadruplex structures more than the monomer fluorescence.



**Figure 8.7** Quenching of TINA fluorescence on titration with ZnTMPyP4 to (A) **TG4TX**, (B) **TG4XT** and (C) **TG3XG3T**. (D) Representative Stern-Volmer plots for steady state fluorescence quenching of **TG4TX** monomer and excimer by ZnTMPyP4. Strand concentration = 10  $\mu\text{M}$ . Conditions are the same as in Figure 8.1.

For all complexes, a straight line was observed for monomer quenching in Stern-Volmer plots as shown for **TG4TX** in Figure 8.7D. Temperature dependence measurements provided definitive evidence that monomer fluorescence is quenched by a static mechanism (Figure 8.8). Excimer quenching produced a curved line in Stern-Volmer plots, which means that both static and dynamic quenching mechanisms are present (Figure 8.7D). Quenching of the monomer band is approximately one order of magnitude higher for **TG4TX** and **TG4XT** compared to **TG3XG3T** (Table 8.4).



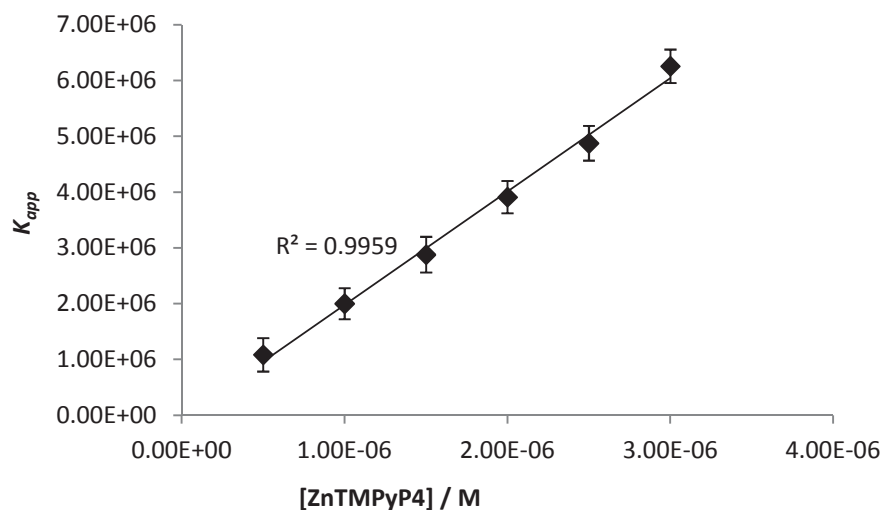


**Figure 8.8** Stern-Volmer plot for TINA monomer of **TG4TX** (10.0  $\mu\text{M}$  strand concentration) quenching by ZnTMpyP4 at 25 °C and 10 °C. Conditions are the same as in Figure 8.1.  $\lambda_{\text{ex}}$  = 375 nm.

**Table 8.4** Static and dynamic quenching constants for TINA monomer and excimer quenching by ZnTMpyP4. Conditions are the same as in Table 8.2.  $K_{SV}$ ,  $K_S$  and  $K_d$  values are reported within 3.5 % error.

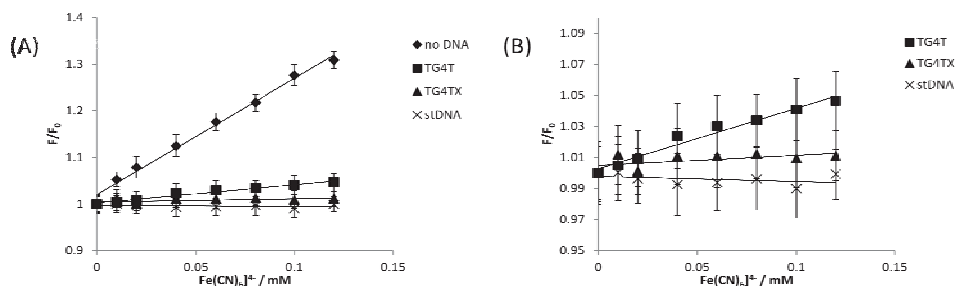
G-Quadruplex	Quenching mechanism		$K_{S(\text{mon})}, \text{M}^{-1}$	$K_{SV(\text{ex})}, \text{M}^{-1}$		$K_a, \text{M}^{-1}$
	Monomer	Excimer		$K_{d(\text{ex})}$	$K_{S(\text{ex})}$	
<b>TG4TX</b>	Static	Static + Dynamic	$1.2 \times 10^5$	$4.9 \times 10^4$	$5.5 \times 10^5$	$6.7 \times 10^5$
<b>TG4XT</b>	Static	Static + Dynamic	$2.4 \times 10^5$	$2.9 \times 10^4$	$1.7 \times 10^5$	$4.1 \times 10^5$
<b>TG3XG3T</b>	Static	Static + Dynamic	$2.1 \times 10^4$	$2.2 \times 10^4$	$7.7 \times 10^4$	$9.8 \times 10^5$

The static quenching constant ( $K_S$ ) and the dynamic components ( $K_D$ ) for the excimer were extracted from the modified Stern-Volmer equation (described in Chapter 6). Plots of the apparent quenching constant ( $K_{app}$ ) versus [ZnTMpyP4] yield straight lines, as shown in Figure 8.9 for the **TG4TX** TINA monomer quenching. The association constants were of the same order of magnitude and the [Ru(bpy)<sub>3</sub>]<sup>2+</sup> complex with **TG3XG3T** had the highest value (Table 8.4).



**Figure 8.9** A modified Stern-Volmer plot for the quenching of TINA monomer fluorescence of **TG4TX** (10.0  $\mu$ M strand concentration) with increasing concentration (0.0  $\mu$ M to 5.0  $\mu$ M) of ZnTMPyP4;  $\lambda_{ex}$  = 375 nm. Conditions are the same as for Figure 8.1.  $K_{app} = [(F_0/F) - 1]/(1/[Q]) = (K_D + K_S) + K_D K_S [Q]$ .

Quenching of the ZnTMPyP4 fluorescence by  $K_4Fe(CN)_6$  showed that even the unmodified G-quadruplex protects ZnTMPyP4 (Figure 8.10). Addition of the TINA further increases porphyrin protection from quenching by  $Fe(CN)_6^{4-}$  to the level obtained in the presence of stDNA (Table 8.5).



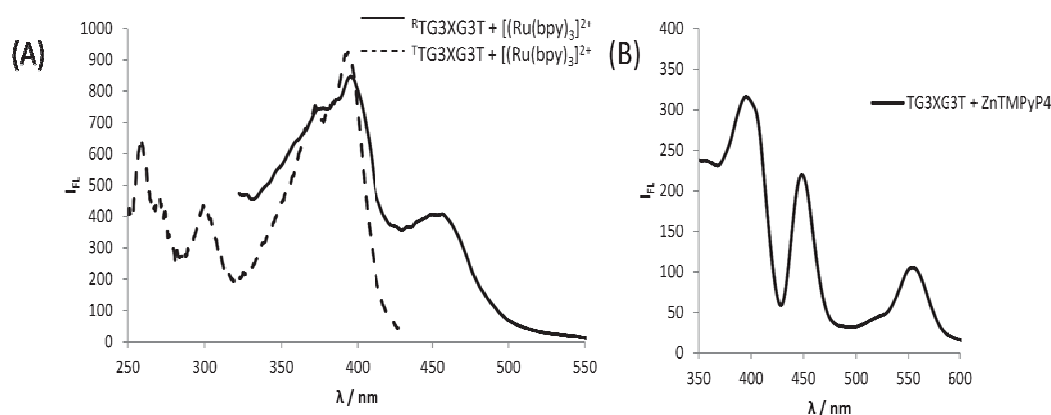
**Figure 8.10** Fluorescence quenching curves of ZnTMPyP4 with increasing concentration of quencher  $[Fe(CN)_6]^{4-}$  in the absence and presence of G-quadruplexes (A). The three bottom lines are expanded in B. [ZnTMPyP4] = 4  $\mu$ M, DNA:ZnTMPyP4 = 20:1. Conditions are the same as in Figure 8.1.

**Table 8.5** Slopes of Stern-Volmer plots of steady state fluorescence of ZnTMPyP4 quenched by  $[Fe(CN)_6]^{4-}$  after adding G-quadruplexes. Examples of Stern-Volmer plots in Figure 8.10 above. Conditions are the same as in Table 8.2.

Duplex	Slope	R <sup>2</sup> value
No DNA	2.50	0.991
TG4T	0.39	0.970
TG4TX	0.064	0.996
TG4XT	0.031	0.995
TG3XG3T	0.022	0.976
stDNA	-0.032	0.998

## 8.6 Energy Transfer

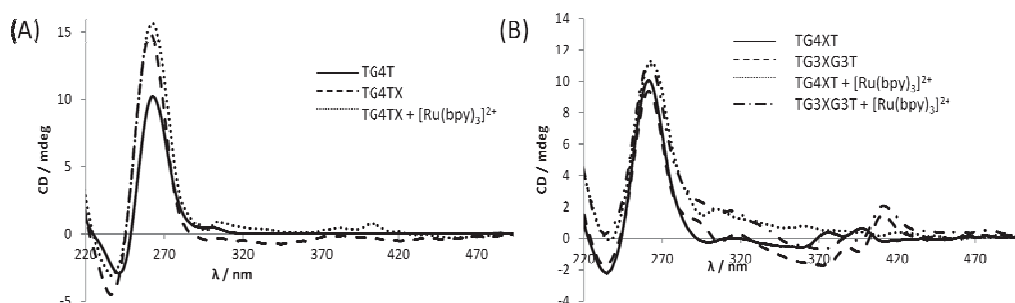
As discussed in Chapter 7, excitation spectra showed energy transfer from the TINA to  $[\text{Ru}(\text{bpy})_3]^{2+}$  and from the DNA bases to the TINA for all G-quadruplexes (Figure 8.1A for **TG3XG3T**). Likewise, energy transfer was also observed from the TINA to the ZnTMPyP4 porphyrin (Figure 8.11B).



**Figure 8.11** Fluorescence excitation scans for **TG3XG3T** (10  $\mu\text{M}$ ) in presence of  $[\text{Ru}(\text{bpy})_3]^{2+}$  (40  $\mu\text{M}$ ) monitoring  $[\text{Ru}(\text{bpy})_3]^{2+}$  emission at 600 nm<sup>R</sup>, and fluorescence of TINA at 405 nm<sup>T</sup> (A). Superscript R denotes  $[\text{Ru}(\text{bpy})_3]^{2+}$  emission and superscript T denotes TINA emission. Excitation scan for **TG3XG3T** (10  $\mu\text{M}$ ) in presence of ZnTMPyP4 (40  $\mu\text{M}$ ) monitoring emission at 630 nm (B). Conditions are the same as for Figure 8.1.

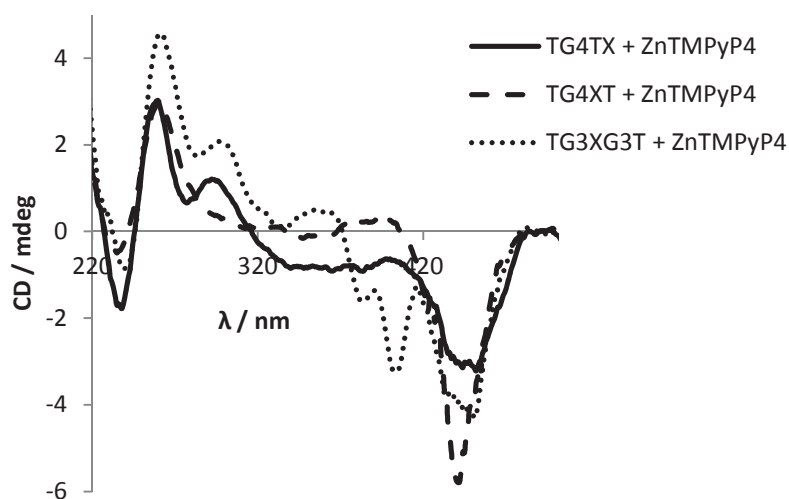
## 8.7 Circular Dichroism of $[\text{Ru}(\text{bpy})_3]^{2+}$ /G-Quadruplex and ZnTMPyP4/G-Quadruplex Complexes

CD spectra provided further information on the interactions of TINA-modified G-quadruplexes with  $[\text{Ru}(\text{bpy})_3]^{2+}$  and ZnTMPyP4. In the presence of  $[\text{Ru}(\text{bpy})_3]^{2+}$ , the **TG4T** CD profile stays unchanged with a positive ellipticity at 262 nm and a negative ellipticity at 239 nm in the nucleobase absorbance region.



**Figure 8.12** CD spectra of G-quadruplexes at 10  $\mu\text{M}$  strand concentration in the absence and presence of  $[\text{Ru}(\text{bpy})_3]^{2+}$  (40  $\mu\text{M}$ ). Conditions are the same as in Figure 8.1.

All TINA-containing G-quadruplexes exhibited the **TG4T** CD signals and additional peaks between 380 and 420 nm attributed to the TINA. The CD spectrum of **TG4TX** shows a positive peak at 384 nm and **TG4XT** has two positive peaks at 377 and 397 nm, **TG3XG3T** has two positive peaks at 388 and 411 nm. The TINA peaks intensities increase on adding  $[\text{Ru}(\text{bpy})_3]^{2+}$  to **TG4TX** (Figure 8.12A) and decrease with **TG4XT**. There was no change in TINA signal intensities for **TG3XG3T** in the presence of  $[\text{Ru}(\text{bpy})_3]^{2+}$ . No  $[\text{Ru}(\text{bpy})_3]^{2+}$  ICD signal in the  $[\text{Ru}(\text{bpy})_3]^{2+}$  absorbance region around 450 nm was observed for any G-quadruplexes. Annealing G-quadruplexes in the presence of  $[\text{Ru}(\text{bpy})_3]^{2+}$  did not produce any  $[\text{Ru}(\text{bpy})_3]^{2+}$  ICD signal either.



**Figure 8.13** CD spectra of G-quadruplexes at 10  $\mu\text{M}$  strand concentration in the absence and presence of  $\text{ZnTMPyP4}$  (40  $\mu\text{M}$ ). Conditions are the same as in Figure 8.1.

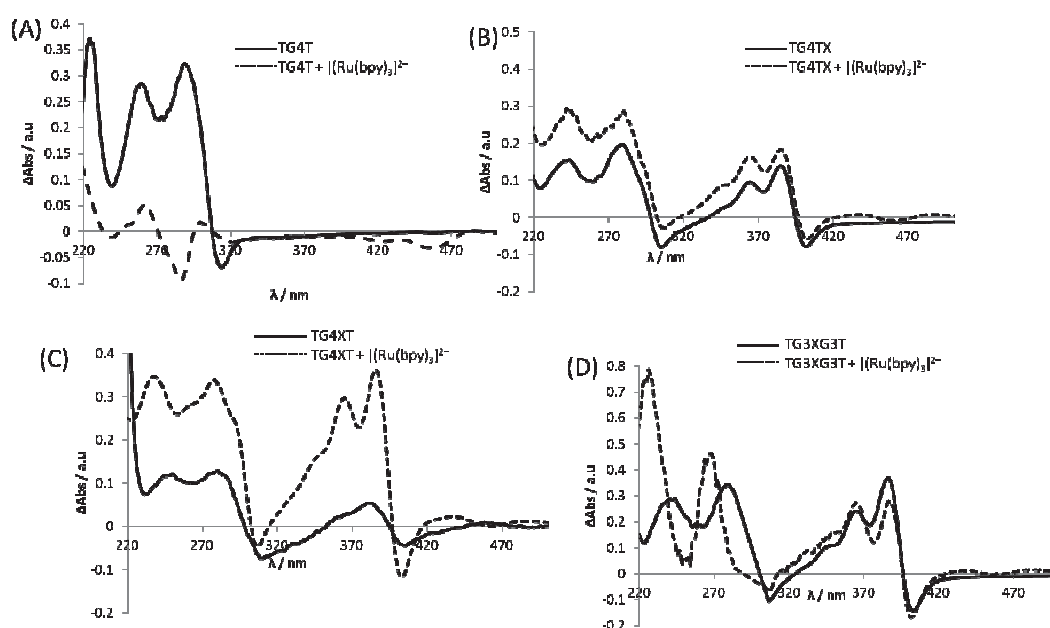
Unlike the  $[\text{Ru}(\text{bpy})_3]^{2+}$  cation, adding  $\text{ZnTMPyP4}$  to G-quadruplexes produced a negative ICD band around 440 nm in the Soret band region in addition to the **TG4T** nucleobase bands, which is indicative of an interaction with the G-quadruplexes. **TG3XG3T** caused the most intense Soret ICD band. The appearance of positive peaks for **TG3XG3T** at 296 and 292 nm for **TG4TX** suggests a topological rearrangement of the G-quadruplexes upon porphyrin addition. It should be noted that G-quadruplexes exhibiting a positive ellipticity at 295 nm and a negative ellipticity at 265 nm adopt an anti-parallel conformations. It is interesting that the appearance of a peak with positive ellipticity at 292 nm for **TG3XG3T** is accompanied by a positive band at 352 nm and a negative band at 400 nm, which arise from TINA.

This clearly suggests that ZnTMpyP4 perturbs G-quadruplex topology in the presence of TINA.

The intensity of the **TG4T** signal around 262 nm increased significantly in all G-quadruplexes in the presence of  $[\text{Ru}(\text{bpy})_3]^{2+}$ . This is a result of overlap with  $[\text{Ru}(\text{bpy})_3]^{2+}$   $\pi$ - $\pi^*$  intraligand absorption band.

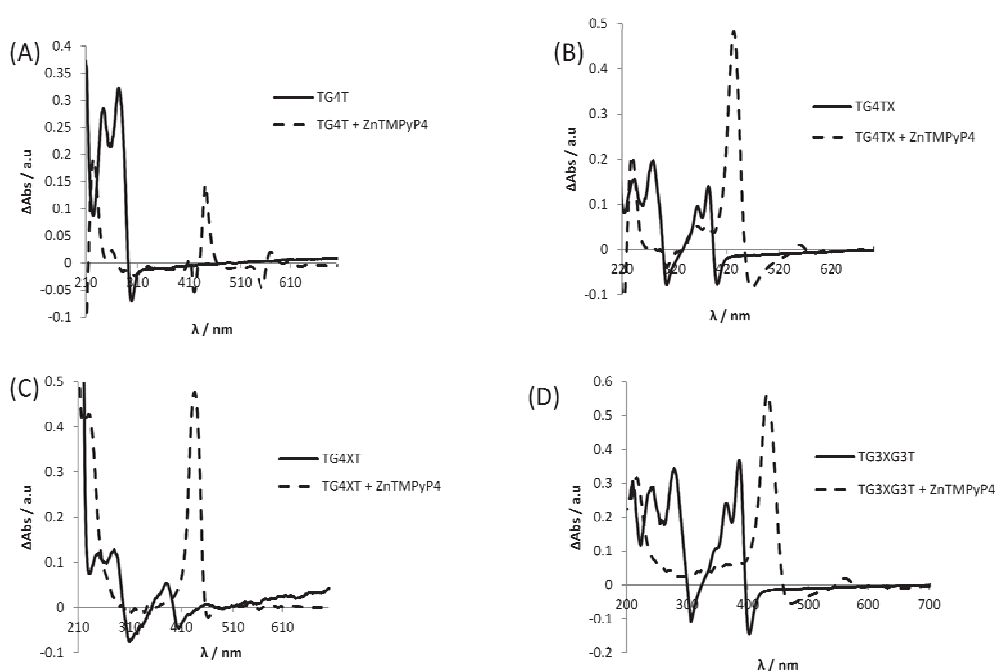
## 8.8 UV-Vis Thermal Difference Spectra (TDS) of $[\text{Ru}(\text{bpy})_3]^{2+}$ /G-Quadruplex and ZnTMpyP4/G-Quadruplex Complexes

The TDS profile of **TG4T** in a low salt buffer (NaCl) is characterized by two positive peaks at around 243 nm and 272 nm and a negative peak at 295 nm as described previously, Figure 8.14A.<sup>[8]</sup> Addition of  $[\text{Ru}(\text{bpy})_3]^{2+}$  resulted in a decrease of the TDS signatures of **TG4T**, followed by an appearance of a negative peak in the  $[\text{Ru}(\text{bpy})_3]^{2+}$  MLCT region at 458 nm. In the presence of TINA the TDS profiles were altered from that of **TG4T**. All TINA-containing G-quadruplexes have peaks in the range of 300–420 nm, in addition to the expected **TG4T** peaks which were retained, which indicates that TINA participates in the formation of folded structures, Figure 8.14.



**Figure 8.14** Thermal difference spectra of preformed G-quadruplexes at 10  $\mu\text{M}$  strand concentration in the absence (solid line) and presence (dashed line) of  $[\text{Ru}(\text{bpy})_3]^{2+}$  (40  $\mu\text{M}$ ). Conditions are the same as in Figure 8.1.

The TDS peak positions for preformed **TG4TX** and **TG4XT** did not change upon adding  $[\text{Ru}(\text{bpy})_3]^{2+}$  after annealing, but the overall peak intensities increased and a new smaller peak was detected around 450 nm. The magnitude of peak intensity increase is markedly higher in **TG4XT**, particularly in the 300 – 420 nm TINA region. This is an indication of  $[\text{Ru}(\text{bpy})_3]^{2+}$  being involved in folding and interacting more strongly with the TINA in the case of **TG4TX**. Interestingly, addition of the  $[\text{Ru}(\text{bpy})_3]^{2+}$  complex to **TG3XG3T** resulted in a hypsochromic shift of the 243 nm and 273 nm peaks accompanied by an increase in their intensity. The 243 nm peak shifted to 226 nm and 273 nm to 267 nm.



**Figure 8.15** Thermal difference spectra of preformed G-quadruplexes at 10  $\mu\text{M}$  strand concentration in the absence (solid line) and presence (dashed line) of  $\text{ZnTMPyP4}$  (40  $\mu\text{M}$ ). Conditions are the same as in Figure 8.1.

For all G-quadruplexes, in the presence of  $\text{ZnTMPyP4}$ , there was a blue-shift in the **TG4T** positive peaks at around 243 and 272 nm, and an appearance of porphyrin signals between 400 – 700 nm, Figure 8.15. The 272 nm positive peak was decreased significantly for **TG4T** and completely disappeared for all the TINA-modified G-quadruplexes. The 295 nm negative peak was retained for **TG4T** but disappeared for all TINA-modified G-quadruplexes.

In comparison to TDS of ZnTMPyP4 (Figure 6.5), a stray positive band at 420 nm is observed for all complexes with G-quadruplexes. The peak intensity was significantly higher for TINA modified G-quadruplexes ( $\Delta\text{Abs} = 0.4 - 0.6$  a.u) than for unmodified TG4T ( $\Delta\text{Abs} = 0.15$  a.u).

## 8.9 G-Quadruplex Melting Studies

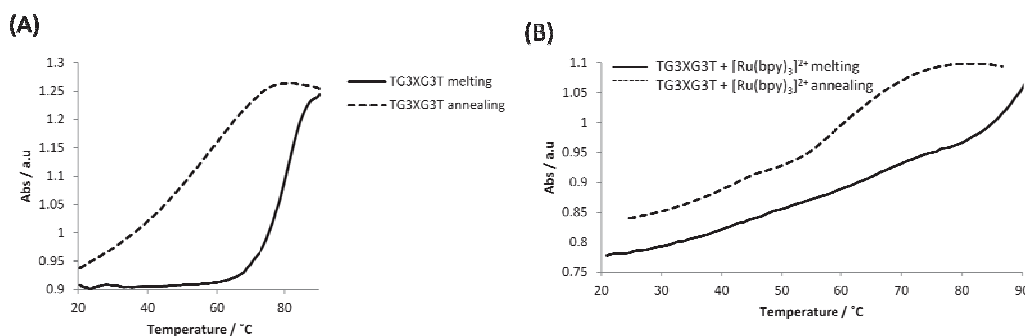
UV-Vis thermal stability studies were performed at various wavelengths guided by TDS data. The clearest meltings for TINA-modified G-quadruplexes were seen at 390 nm, as opposed to **TG4T** where it was 280 nm. The formation of G-quadruplexes was not interrupted by the presence of the TINA in all sequences studied. All sequences showed enhanced thermal stability with  $\Delta T_{1/2}$  values of 23, 23.5 and 20.5 °C for **TG4TX**, **TG4XT** and **TG3XG3T** respectively, Table 8.6.

**Table 8.6** UV-Vis melting and annealing temperatures ( $T_{1/2}$ ) of G-quadruplexes in the absence and presence of ligands were determined at 390 nm, except **TG4T** which was determined at 280 nm.  $T_{1/2}$  values were obtained from absorbance data with 0.25 °C/min temperature ramp.

G-Quadruplex	No Ligand (melting/ annealing)	[Ru(bpy) <sub>3</sub> ] <sup>2+</sup> present (melting/ annealing)	ZnTMPyP4 present (melting/ annealing)
<b>TG4T</b>	59.0 / < 20.0	50.5 / < 20.0	74.4 / < 20.0
<b>TG4TX</b>	82.0 / 45.0	82.5 / 43.0	78.5 / 25.0
<b>TG4XT</b>	82.5 / N.S	81.0 / 42.0	83.0 / 66.5
<b>TG3XG3T</b>	79.5 / 58.5	> 90.0 / 66.5	85.9 / 24.0

NS = No clear transition is seen in 20 – 90 °C region. Conditions are the same as in Table 8.2

We observed a decrease in the  $T_{1/2}$  values for **TG4T** in the presence of the [Ru(bpy)<sub>3</sub>]<sup>2+</sup> complex. For **TG4TX** and **TG4XT** we detected two transitions during melting, the first at low temperature attributed to dissociation of higher order aggregates, and the second at higher temperature due to denaturation of the tetramolecular G-quadruplex.<sup>[1]</sup> For **TG3XG3T**, in the presence of [Ru(bpy)<sub>3</sub>]<sup>2+</sup>, the melting occurred above 90 °C (Figure 8.16). The annealing profiles indicated faster association kinetics in the presence of [Ru(bpy)<sub>3</sub>]<sup>2+</sup> for **TG4TX** and **TG4XT**. G-quadruplex **TG3XG3T** did not show any significant changes during association kinetics in the presence of [Ru(bpy)<sub>3</sub>]<sup>2+</sup> (Figure 8.16 for **TG3XG3T**, other graphs are present in Appendix, Chapter 12, Figures 12.15 – 12.17).



**Figure 8.16** UV-Vis melting (solid lines) and annealing profiles (dashed lines) of **TG3XG3T** at 10  $\mu\text{M}$  strand concentration after annealing in the absence (A) and presence (B) of  $[\text{Ru}(\text{bpy})_3]^{2+}$  at 390 nm from absorbance data with 0.25  $^{\circ}\text{C}/\text{min}$  temperature ramp. Conditions are the same as in Figure 8.1

In the presence of ZnTMPyP4, all G-quadruplexes are more thermally stable, except **TG4TX** which is slightly destabilized (Table 8.6).

## 8.10 Conclusions

TINA-modified G-quadruplexes protect the chromophores ZnTMPyP4 and  $[\text{Ru}(\text{bpy})_3]^{2+}$  from quenching by  $[\text{Fe}(\text{CN})_6]^{4-}$  significantly better than TINA-modified duplexes as well as unmodified **TG4T**, to levels comparable with stDNA. We postulate that a hydrophobic TINA cluster is formed in G-quadruplexes, which is responsible for interaction between ZnTMPyP4 and  $[\text{Ru}(\text{bpy})_3]^{2+}$  with TINA. The association constants ( $K_a$ ) for TINA-modified G-quadruplexes and  $[\text{Ru}(\text{bpy})_3]^{2+}$  are one order of magnitude greater than that for duplexes. However, the association constants for ZnTMPyP4 and TINA-modified G-quadruplexes are similar to TINA-modified duplexes, but duplex **D3** exhibits a  $K_a$  value that is one order of magnitude greater than for G-quadruplex structures.

$[\text{Ru}(\text{bpy})_3]^{2+}$  quenches both TINA monomer and excimer fluorescence on G-quadruplexes by a purely static mechanism. The amount of TINA monomer fluorescence quenching by  $[\text{Ru}(\text{bpy})_3]^{2+}$  is comparable to duplexes, but excimer quenching by  $[\text{Ru}(\text{bpy})_3]^{2+}$  is far greater for G-quadruplexes than duplexes except for **TG3XG3T**. In addition TINA monomer is not completely quenched by  $[\text{Ru}(\text{bpy})_3]^{2+}$ . This makes a combination of TINA-modified G-quadruplexes and  $[\text{Ru}(\text{bpy})_3]^{2+}$  good candidates for EU, except for **TG3XG3T**. On the other hand, the TINA monomer is quenched by a static mechanism with ZnTMPyP4, but the



excimer is quenched by a combination of static and dynamic mechanisms. The extent of monomer and excimer quenching for G-quadruplexes is similar to duplexes, except for **TG3XG3T**. Furthermore, the TINA fluorescence is completely quenched by the porphyrin ZnTMpyP4 which poses a problem for EU.

## 8.11 References

- [1] O. Doluca, J. M. Withers, T. S. Loo, P. J. Edwards, C. González, V. V. Filichev, *Organic & biomolecular chemistry* **2015**, *13*, 3742.
- [2] J. Jaumot, R. Gargallo, *Current pharmaceutical design* **2012**, *18*, 1900.
- [3] G. Jia, Z. Feng, C. Wei, J. Zhou, X. Wang, C. Li, *The Journal of Physical Chemistry B* **2009**, *113*, 16237.
- [4] a)L. R. Keating, V. A. Szalai, *Biochemistry* **2004**, *43*, 15891; b)H. Han, L. H. Hurley, *Trends in pharmacological sciences* **2000**, *21*, 136; c)E. Izbicka, R. T. Wheelhouse, E. Raymond, K. K. Davidson, R. A. Lawrence, D. Sun, B. E. Windle, L. H. Hurley, D. D. Von Hoff, *Cancer research* **1999**, *59*, 639; d)S. Balasubramanian, S. Neidle, *Current opinion in chemical biology* **2009**, *13*, 345; e)T. Shalaby, G. Fiaschetti, K. Nagasawa, K. Shin-ya, M. Baumgartner, M. Grotzer, *Molecules* **2013**, *18*, 12500.
- [5] a)S. Cogoi, M. Paramasivam, V. Filichev, I. Géci, E. B. Pedersen, L. E. Xodo, *Journal of medicinal chemistry* **2008**, *52*, 564; b)S. Cogoi, M. Paramasivan, L. E. Xodo, V. V. Filichev, E. B. Pedersen, *Nucleosides, Nucleotides and Nucleic Acids* **2007**, *26*, 1641; c)E. B. Pedersen, J. T. Nielsen, C. Nielsen, V. V. Filichev, *Nucleic Acids Research* **2011**, *39*, 2470; d)M. Paramasivam, S. Cogoi, V. V. Filichev, N. Bomholt, E. B. Pedersen, L. E. Xodo, *Nucleic Acids Research* **2008**, *36*, 3494.
- [6] N. Sancho Oltra, W. R. Browne, G. Roelfes, *Chemistry-A European Journal* **2013**, *19*, 2457.
- [7] Q. Yu, Y. Liu, C. Wang, D. Sun, X. Yang, Y. Liu, J. Liu, *PloS one* **2012**, *7*, 5902.
- [8] J.-L. Mergny, J. Li, L. Lacroix, S. Amrane, J. B. Chaires, *Nucleic Acids Research* **2005**, *33*, e138.



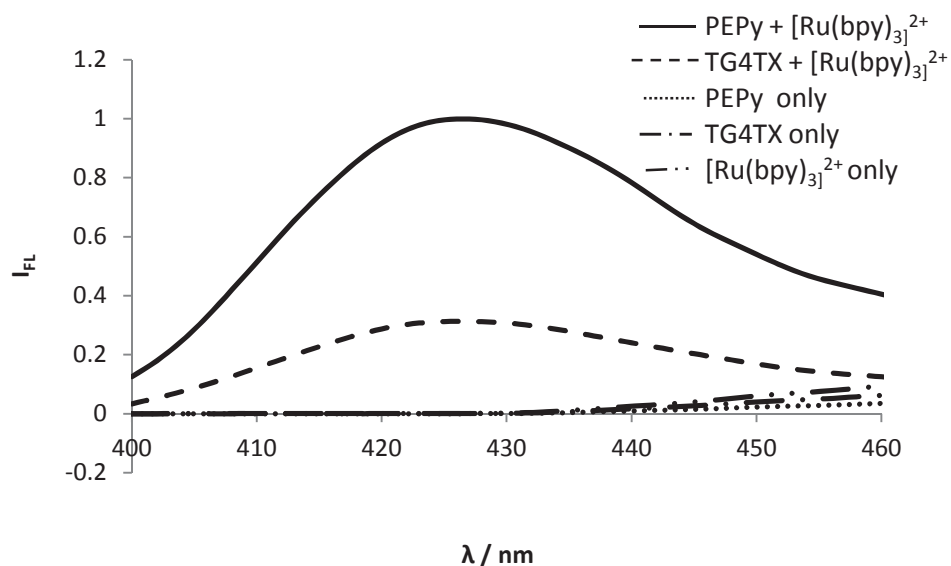
## 9 DNA-based Energy Upconversion (EU)

### 9.1 Introduction

The final aspect of this project, to develop a photon upconversion system using a supramolecular approach based on a DNA scaffold, was met with lot of challenges but shows promise. The photon upconverting potential of systems comprising of the TINA-modified DNA duplexes or G-quadruplexes, in combination with ZnTMPyP4/[Ru(bpy)<sub>3</sub>]<sup>2+</sup>, was investigated in this chapter. Several trials were performed in which the DNA/chromophore ratio was varied. As a result quantifiable upconverted fluorescence was observed with **TG4TX**, **D2 - D4** as acceptors, and [Ru(bpy)<sub>3</sub>]<sup>2+</sup> as a donor in aqueous solution. To the best of our knowledge, this is the first demonstration of EU achieved *via* arrangement of chromophores on a DNA scaffold.

### 9.2 TINA-modified G-quadruplex DNA in EU

Based on the fact that [Ru(bpy)<sub>3</sub>]<sup>2+</sup> and ZnTMPyP4 have higher affinity to TINA-modified G-quadruplexes than to TINA-modified duplexes, we decided to evaluate TINA-modified G-quadruplex DNAs in EU first. A solution containing the TINA-modified **TG4TX** (10 μM strand concentration) and [Ru(bpy)<sub>3</sub>]<sup>2+</sup> (30 μM) produced an upconverted fluorescence between 420–430 nm after [Ru(bpy)<sub>3</sub>]<sup>2+</sup> perturbation at 500 nm using a conventional fluorimeter fitted with a 400 nm long pass filter on the excitation beam (Figure 9.1).



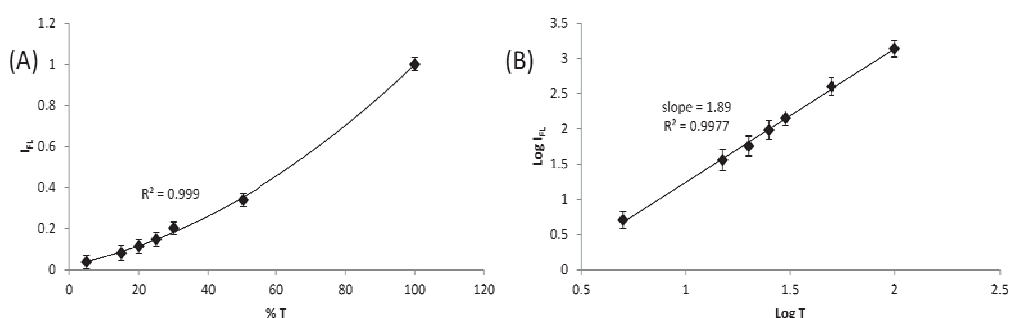
**Figure 9.1** Normalized upconverted fluorescence emission spectra of (i)  $[\text{Ru}(\text{bpy})_3]^{2+}$  (46  $\mu\text{M}$ ) and PEPy (4.6 mM) measured in a deaerated dichloromethane solution (solid line) and (ii)  $[\text{Ru}(\text{bpy})_3]^{2+}$  (30  $\mu\text{M}$ ) and **TG4TX** (10  $\mu\text{M}$  strand concentration) measured in a deaerated aqueous solution (dashed line).  $[\text{Ru}(\text{bpy})_3]^{2+}$  - **TG4TX** fluorescence was adjusted to match TINA concentration to PEPy concentration. Conditions for **TG4TX** system: pH = 7.0, 10 mM sodium phosphate buffer, 0.1 mM EDTA, 50 mM NaCl.  $\lambda_{\text{ex}}$  = 500 nm, 25 °C. The fluorescence spectra of the individual components under the same conditions are also illustrated; concentrations are  $[\text{Ru}(\text{bpy})_3]^{2+}$  (46  $\mu\text{M}$ , aq), PEPy (4.6 mM, DCM) and **TG4TX** (10  $\mu\text{M}$  strand concentration, aq).

The upconverted emission profile looks similar to the TINA monomeric emission upon 375 nm excitation of the individual chromophore and closely resembles free  $[\text{Ru}(\text{bpy})_3]^{2+}$ -PEPy upconverted emission in DCM (Figure 4.3). To observe photon upconversion it was necessary to degas all DNA solutions by argon purging for at least 24 hours without sonication. This is because sonication degraded DNA into a gel-like structure. DCM solutions were degassed by argon purging in a sonicator as described in Chapter 4. The individual chromophores, PEPy  $[\text{Ru}(\text{bpy})_3]^{2+}$  and **TG4TX** alone in solution did not produce upconversion upon 500 nm excitation (Figure 9.1).

We used the upconverted fluorescence intensities as a measure of comparison of efficiencies of upconversion between the free chromophores system and the DNA-based systems. It is important to mention that intensities only give a qualitative analysis of upconversion. The DNA-based aqueous system only produced about 20 % of the upconversion produced by the free chromophores system after adjusting the fluorescence intensities to match the TINA concentrations. This is further supported

by the fact that EU was not observed by the naked eye using a commercial green laser (5 mW, 532 nm) in the DNA-based system, as was seen with the free chromophores system in Chapter 4. However, this is more likely a result of using low chromophore concentrations in DNA-based systems.

The quadratic incident power dependence of this sensitized TTA mechanism based **TG4TX**-[Ru(bpy)<sub>3</sub>]<sup>2+</sup> EU system is illustrated below in Figure 9.2.

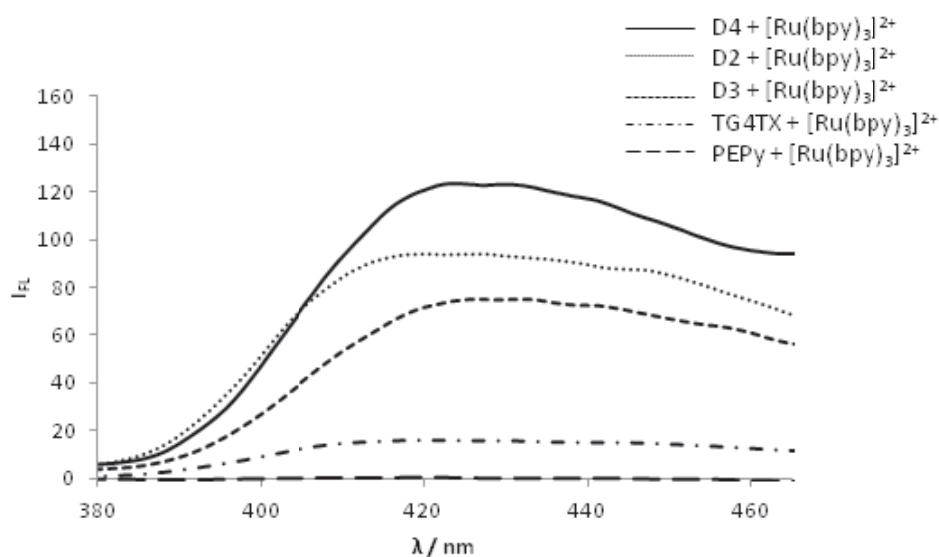


**Figure 9.2** A plot of the normalized upconverted integrated fluorescence emission profiles of [Ru(bpy)<sub>3</sub>]<sup>2+</sup> (30  $\mu$ M) and **TG4TX** (10  $\mu$ M strand concentration) as a function of neutral density filter percent transmission. (B) A double logarithm plot of the data in (A). Buffer conditions are the same as in Figure 9.1.

Of particular importance to our project is the observation of EU with a G-quadruplex **TG4TX** and [Ru(bpy)<sub>3</sub>]<sup>2+</sup> in an aqueous solution at low chromophore concentrations ([Ru(bpy)<sub>3</sub>]<sup>2+</sup> (30  $\mu$ M) and **TG4TX** (10  $\mu$ M)), Figure 9.1. Free chromophores in DCM produce upconverted fluorescence at higher concentrations ([Ru(bpy)<sub>3</sub>]<sup>2+</sup> (46  $\mu$ M) and PEPy (4.6 mM)), Figure 9.1. This demonstrates that DNA acts as a scaffold and brings chromophores in close proximity for upconversion to occur using G-quadruplex based assembly.

### 9.3 TINA-modified DNA, extended study

EU observation using **TG4TX** and [Ru(bpy)<sub>3</sub>]<sup>2+</sup> posed a question whether TINA-modified DNA duplexes would also be suitable for EU. Results of this study are summarized in Table 9.1 and Figure 9.3.



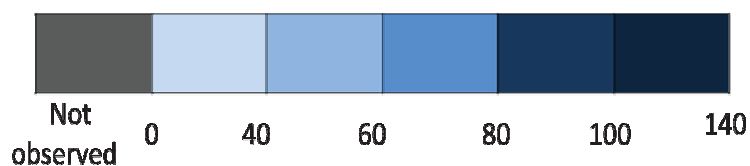
**Figure 9.3** Upconverted fluorescence emission spectra of **TG4TX**, **D2**, - **D4** (10  $\mu\text{M}$  strand concentration), in the presence of  $[\text{Ru}(\text{bpy})_3]^{2+}$  (10.0  $\mu\text{M}$ ) measured in deaerated aqueous solution. Experimental conditions for DNA-based systems are the same as in Figure 9.1.  $[\text{Ru}(\text{bpy})_3]^{2+}$  (10  $\mu\text{M}$ ) and PEPy (10  $\mu\text{M}$ ) in a deaerated DCM solution does not produce upconverted fluorescence.  $\lambda_{\text{ex}} = 500 \text{ nm}$ ,  $25^\circ\text{C}$ .

EU was observed when **D2-D4**, and **TG4TX** was added to  $[\text{Ru}(\text{bpy})_3]^{2+}$ , whereas **TG4XT**, **TG3XG3T** and free chromophores in DCM did not produce EU under the tested concentrations (2.5 – 40.0  $\mu\text{M}$   $[\text{Ru}(\text{bpy})_3]^{2+}$  and 1.0 – 80.0  $\mu\text{M}$  TINA-DNAs (Table 9.1). It is interesting that under the same DNA strand concentrations, TINA-modified DNA duplexes produce upconverted fluorescence of higher intensity in comparison with TINA-modified G-quadruplexes at 420 nm ( $\lambda_{\text{ex}} = 500 \text{ nm}$ , Figure 9.3). This is despite the fact that binding affinity of  $[\text{Ru}(\text{bpy})_3]^{2+}$  to TINA-modified duplexes is lower ( $K_a = 6.5 - 6.7 \times 10^4 \text{ M}^{-1}$ ) than G-quadruplexes ( $K_a = 4.6 - 6.3 \times 10^5 \text{ M}^{-1}$ ). The EU trend within duplexes is also interesting. No fluorescence intensity at 420 nm was detected for duplexes **D2-D4** in the mixture with 40  $\mu\text{M}$   $[\text{Ru}(\text{bpy})_3]^{2+}$  upon excitation at 500 nm. An increase in DNA duplex concentrations from 1.0 to 5.0 and then to 10.0  $\mu\text{M}$  and a subsequent decrease in  $[\text{Ru}(\text{bpy})_3]^{2+}$  concentrations from 40 to 2.5 – 10.0  $\mu\text{M}$  resulted in EU (Table 9.1, Figure 9.3).

**Table 9.1** Fluorescence intensity at 420 nm at different ratios of TINA-modified DNA duplexes/G-quadruplexes and  $[\text{Ru}(\text{bpy})_3]^{2+}$ ,  $\lambda_{\text{ex}} = 500 \text{ nm}^a$ 

DNA	DNA strand concentration ( $\mu\text{M}$ )	$[\text{Ru}(\text{bpy})_3]^{2+}$ concentration ( $\mu\text{M}$ )					
		2.5	5	10	20	30	40
D2	1	-	-	-	-	-	✓
	5	✓	✓	-	-	-	-
	10	-	✓	✓	-	-	-
D3	1	-	-	-	-	-	✓
	5	✓	✓	-	-	-	-
	10	-	✓	✓	-	-	-
D4	1	-	-	-	-	-	✓
	5	✓	✓	-	-	-	-
	10	-	✓	✓	-	-	-
TG4TX	10	✓	-	✓	-	-	-
	20	-	✓	✓	✓	✓	✓
	30	-	-	-	-	-	✓
	40	-	-	-	-	-	✓
	60	-	-	-	-	-	✓
	70	-	-	-	-	-	✓
	80	-	-	-	-	-	✓
	80	-	-	-	-	-	✓
TG4XT	10	✓	✓	✓	✓	✓	✓
	20	✓	✓	✓	✓	✓	✓
	30	✓	✓	✓	✓	✓	✓
	40	✓	✓	✓	✓	✓	✓
	100	✓	✓	✓	✓	✓	✓
TG3XG3T	10	✓	✓	✓	✓	✓	✓
	20	✓	✓	✓	✓	✓	✓
	30	✓	✓	✓	✓	✓	✓
	40	✓	✓	✓	✓	✓	✓
	100	✓	✓	✓	✓	✓	✓

(a) Tick stands for experiments performed; dash line stands for experiments not performed. Grey color represents that no fluorescence intensity was observed at 420 nm; Different shades of blue represent different magnitudes of fluorescence intensity at 420 nm in arbitrary units upon excitation at 500 nm (key below, a.u). Conditions: pH = 7.0, 10 mM sodium phosphate buffer, 0.1 mM EDTA, 50 mM NaCl, 25 °C. Excitation slit = 4 nm and emission slit = 8 nm. All solutions were carefully degassed with argon for at least 24 hours before measurements





The fact that EU is observed with duplex **D2** is intriguing. For EU through a TTA mechanism to occur two acceptor molecules (i.e. two TINAs) are required to be present within Dexter distances, which in case of **D2** is not realized: TINA monomers present at 5'-ends are separated by twelve base-pairs. A discrete intermolecular clustering of pyrene,<sup>[1]</sup> perylene<sup>[2]</sup> and porphyrin<sup>[3]</sup> containing DNAs have been suggested in the past based on observations using CD, UV-Vis and EPR spectroscopies. Recently, TINA-assisted formation of intermolecular G-quadruplexes was also reported.<sup>[4]</sup> We propose that in the case of **D2** the intermolecular interaction between duplexes is responsible for TINA's clustering which results in EU in the presence of  $[\text{Ru}(\text{bpy})_3]^{2+}$ . In contrast, the presence of two TINAs at the end of the duplex (**D3** and **D4**) led to the observation of EU even at 5.0  $\mu\text{M}$  duplex concentration, which suggests that placement of two acceptor molecules at the end of the duplex is beneficial for EU.

All TINA-modified G-quadruplexes have a prominent excimer emission centered at 480 – 500 nm, which may contribute to a loss of EU at 420 nm. This is supported by the fact that even though duplex **D2** that does not exhibit any TINA excimer emission, it produces five times higher upconverted fluorescence than that of **TG4TX** in the presence of  $[\text{Ru}(\text{bpy})_3]^{2+}$  under identical conditions. It should be mentioned that  $[\text{Ru}(\text{bpy})_3]^{2+}$  and TINA in the structure of **D2** interact with each other in a dynamic mode, similar to free chromophores in solution. However, the assembly of these chromophores on DNA makes it possible to realize EU at concentrations as low as 10  $\mu\text{M}$ , which cannot be done for free chromophores in solution (Figure 9.3).

Quite disappointing is the fact that several trials involving all TINA-modified DNA duplexes and G-quadruplexes with ZnTMPyP4 did not produce photon upconversion. We used DNA duplexes and G-quadruplexes in combination with ZnTMPyP4 at various ratios (Table 9.2) all to no avail.

**Table 9.2** A table of EU experiments attempted using DNAs and ZnTMPyP4. Fluorescence intensity was measured at 420 nm at different ratios of TINA-modified DNA duplexes/G-quadruplexes and ZnTMPyP4,  $\lambda_{\text{ex}} = 565 \text{ nm}$ .<sup>a</sup>

DNA	DNA strand concentration ( $\mu\text{M}$ )	ZnTMPyP4 concentration ( $\mu\text{M}$ )				
		2.5	5	10	20	40
D2	1	<input type="checkbox"/>	<input type="checkbox"/>	<input type="checkbox"/>	<input type="checkbox"/>	✓
	5	✓	✓	<input type="checkbox"/>	<input type="checkbox"/>	<input type="checkbox"/>
	10	<input type="checkbox"/>	✓	✓	✓	<input type="checkbox"/>
	20	✓	✓	✓	✓	<input type="checkbox"/>
	30	✓	✓	✓	✓	<input type="checkbox"/>
	40	<input type="checkbox"/>	✓	✓	✓	✓
D3	1	<input type="checkbox"/>	<input type="checkbox"/>	<input type="checkbox"/>	<input type="checkbox"/>	✓
	5	✓	✓	<input type="checkbox"/>	<input type="checkbox"/>	<input type="checkbox"/>
	10	<input type="checkbox"/>	✓	✓	✓	<input type="checkbox"/>
	20	✓	✓	✓	✓	<input type="checkbox"/>
	30	✓	✓	✓	✓	<input type="checkbox"/>
	40	<input type="checkbox"/>	✓	✓	✓	✓
D4	1	<input type="checkbox"/>	<input type="checkbox"/>	<input type="checkbox"/>	<input type="checkbox"/>	✓
	5	✓	✓	<input type="checkbox"/>	<input type="checkbox"/>	<input type="checkbox"/>
	10	<input type="checkbox"/>	✓	✓	✓	<input type="checkbox"/>
	20	✓	✓	✓	✓	<input type="checkbox"/>
	30	✓	✓	✓	✓	<input type="checkbox"/>
	40	<input type="checkbox"/>	✓	✓	✓	✓
TG4TX	10	✓	✓	✓	<input type="checkbox"/>	<input type="checkbox"/>
	20	<input type="checkbox"/>	<input type="checkbox"/>	✓	✓	✓
	30	<input type="checkbox"/>	<input type="checkbox"/>	✓	✓	✓
	40	<input type="checkbox"/>	<input type="checkbox"/>	✓	✓	✓
TG4XT	10	✓	✓	✓	<input type="checkbox"/>	<input type="checkbox"/>
	20	<input type="checkbox"/>	<input type="checkbox"/>	✓	✓	✓
	30	<input type="checkbox"/>	<input type="checkbox"/>	✓	✓	✓
	40	<input type="checkbox"/>	<input type="checkbox"/>	✓	✓	✓
TG3XG3T	10	✓	✓	✓	<input type="checkbox"/>	<input type="checkbox"/>
	20	<input type="checkbox"/>	<input type="checkbox"/>	✓	✓	✓
	30	<input type="checkbox"/>	<input type="checkbox"/>	✓	✓	✓
	40	<input type="checkbox"/>	<input type="checkbox"/>	✓	✓	✓

(a) A tick stands for experiments performed.

Since porphyrin quenches the TINA fluorescence completely at high concentrations, it is quite possible that if any EU occurred it was significantly suppressed. In addition, the porphyrin quenches the TINA by both a static and dynamic mechanism. This could mean that the porphyrin is still significantly drawn to the polyphosphate backbone of DNA, thereby minimizing its interaction with TINA. In the case of

**TG4XT** and **TG3XG3T**, the undesirable excimer band is more prominent than the monomer band which could hamper EU. In addition, **TG3XG3T** is the least promising of all the DNAs studied as ZnTMPyP4/[Ru(bpy)<sub>3</sub>]<sup>2+</sup> did not quench the excimer fluorescence more than the monomer fluorescence, meaning that the excimer emission is still quite prominent even in the presence of a donor. This means that very little contact between TINA and [Ru(bpy)<sub>3</sub>]<sup>2+</sup> is realized with **TG3XG3T**.

## 9.4 References

- [1] I. J. Lee, B. H. Kim, *Chemical Communications*. **2012**, 48, 2074.
- [2] a)C. Wagner, H. A. Wagenknecht, *Organic. Letters*. **2006**, 8, 4191-4194; b)D. Baumstark, H. A. Wagenknecht, *Angewandte. Chemie., International. Edition*. **2008**, 47, 2612.
- [3] a)T. Nguyen, P. Hakansson, R. Edge, D. Collison, B. A. Goodman, J. R. Burns, E. Stulz, *New Journal of Chemistry*. **2014**, 38, 5254; b)A. W. I. Stephenson, A. C. Partridge, V. V. Filichev, *Chemistry: A European Journal* **2011**, 17, 6227; c)G. Sargsyan, M. Balaz, *Organic and Biomolecular Chemistry* **2012**, 10, 5533.
- [4] a)E. B. Pedersen, J. T. Nielsen, C. Nielsen, V. V. Filichev, *Nucleic Acids Research* **2011**, 39, 2470; b)O. Doluca, J. Withers, T. S. Loo, P. Edwards, C. Gonzalez, V. Filichev, *Organic and Biomolecular Chemistry* **2015**, 13, 3742.
- [5] a)R. R. Islangulov, J. Lott, C. Weder, F. N. Castellano, *Journal of the American Chemical Society* **2007**, 129, 12652-12653; b)T. N. Singh-Rachford, J. Lott, C. Weder, F. N. Castellano, *Journal of the American Chemical Society* **2009**, 131, 12007-12014; c)K. Tanaka, K. Inafuku, Y. Chujo, *Chemical Communications* **2010**, 46, 4378-4380; d)P. Ceroni, *Chemistry – A European Journal* **2011**, 17, 9560-9564; e)T. N. Singh-Rachford, F. N. Castellano, *Coordination Chemistry Reviews* **2010**, 254, 2560-2573.



## 10 Final Conclusions and Future Directions

### 10.1 Final Conclusions

This thesis aimed to develop viable supramolecular assemblies based on a DNA scaffold favourable for photon upconversion based on TTA mechanism by bringing organic chromophores in close proximity. Of primary importance was the selection of organic chromophores with the requisite properties to ensure TTA-based energy upconversion is feasible. Green-to-blue energy upconversion was observed in a system consisting of a TINA monomer (PEPy) as an acceptor and  $[\text{Ru}(\text{bpy})_3]^{2+}$  as a donor in DCM. This work was the basis for developing supramolecular systems using TINA-modified DNAs in combination with  $[\text{Ru}(\text{bpy})_3]^{2+}$  and ZnTMpyP4 as ligands.

Free  $[\text{Ru}(\text{bpy})_3]^{2+}$  and ZnTMpyP4 quenched TINA monomer fluorescence emission by a dynamic mechanism. The attachment of TINA monomers to synthetic short stranded DNA duplexes and G-quadruplexes led to mostly static quenching as a result of ground state complex formation facilitated by the DNA template in each of the cases studied. The interaction of DNA, and particularly the TINA monomer with  $[\text{Ru}(\text{bpy})_3]^{2+}$  and ZnTMpyP4, was supported by CD, UV-Vis and fluorescence spectroscopy. We observed induced CD peaks from the ligands as well as perturbation of UV-Vis and fluorescence spectra. Most significantly, TINA-modified DNAs resulted in a stronger interaction with the ligands compared to unmodified DNAs, as shown by Stern-Volmer fluorescence analyses and association constant values.

Quite noteworthy is the fact that the degree of TINA fluorescence emission static quenching differs with each DNA and chromophore combination. ZnTMpyP4 quenched the fluorescence of the studied TINA-modified DNAs by a combination of dynamic and static quenching, whilst  $[\text{Ru}(\text{bpy})_3]^{2+}$  quenches by a static mechanism if more than one TINA is in the assembly. In addition, the degree of excited dimer

quenching (longer wavelength emission) by both  $[\text{Ru}(\text{bpy})_3]^{2+}$  and ZnTMPyP4 was higher than monomer quenching (short wavelength emission). This is desirable for EU applications. We have also observed that the porphyrin quenches TINA fluorescence completely at high concentrations, whereas  $[\text{Ru}(\text{bpy})_3]^{2+}$  does not. This had implications on our strategies of building a viable EU system as the TINA acceptor emission can be silenced by high porphyrin concentrations. In the case of  $[\text{Ru}(\text{bpy})_3]^{2+}$ , TINA monomer fluorescence was quenched to the same order of magnitude for duplexes and G-quadruplexes, whilst the excimer was quenched to a higher degree for G-quadruplexes than for duplexes. On the other hand, both monomer and excimer fluorescence were quenched to a similar extent by ZnTMPyP4. We showed, from Stern-Volmer analyses using  $[\text{Fe}(\text{CN})_6]^{4-}$  that our ligands engage more prominently with TINA-modified G-quadruplexes than with duplexes.

We observed EU with TINA-modified duplexes **D2 – D4** and one G-quadruplex **TG4TX** and  $[\text{Ru}(\text{bpy})_3]^{2+}$  in aqueous solution after bubbling the solution with argon for 24 hours. It shows that EU is possible with DNA when present at low chromophore concentrations and in aqueous solution. This work lays the foundation for controllable EU using a DNA scaffold.

## 10.2 Future Directions

This thesis has clearly shown improved communication between organic chromophores of particular importance to EU with a DNA scaffold. These results give a platform for developing conditions required to produce DNA-based EU systems.

In the light of our systems, incorporating a  $[\text{Ru}(\text{bpy})_3]^{2+}$  donor and TINA-modified DNAs as acceptors producing energy upconversion, we have established the proof of concept of a DNA-based supramolecular assembly. In terms of design, a broad range of improvements are possible. Based on our results in Chapter 9, the initial step should be to explore higher concentrations of the chromophores. The concentrations we used are quite low in comparison to what has been used in previous EU studies, and the ones we used for free chromophores for EU in DCM ( $46.0\ \mu\text{M}$   $[\text{Ru}(\text{bpy})_3]^{2+}$  and  $4.6\ \text{mM}$  PEPy in Chapter 4). The chromophore concentrations, in particular acceptor concentrations could be increased to millimolar values. In terms of DNA-based design, this may require a subsequent increase in the concentrations of TINA-modified DNAs.

Aqueous solutions contain more dissolved oxygen and hence are more difficult to degas. In this regard, TINA-modified DNA/chromophore EU systems can be made lipophilic by complexing DNA with amphiphilic agents such as cetyl trimethylammonium bromide (CTAB) and then re-dissolved in organic solvents like DCM which are relatively easy to degas. Furthermore, since TTA-based EU is dependent on diffusion controlled bimolecular processes we suggest future studies should also explore the temperature dependence of EU efficiency. Other strategies for future work should focus on exploring different chromophores, positioning chromophores on various positions on the DNA template (Figure 3.9), using different DNA sequences, and investigating alternative scaffolds.





## 11 Experimental Methods

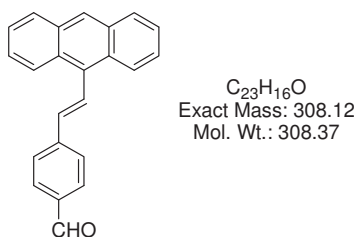
### 11.1 Experimental Procedures for Chapter 5

#### 11.1.1 General Experimental

Reagents and solvents used were supplied from different sources. AR grade reagents and solvents were generally used for the syntheses. Column chromatography solvents were distilled laboratory grade. THF was dried by passing degassed solvent through activated alumina columns. Dry DCM and DMF were prepared by distilling AR grade solvent over  $\text{CaH}_2$  under a  $\text{N}_2$  atmosphere. Most reactions were monitored by thin layer chromatography (TLC) using 60 F254 TLC plates from Merck and visualized under 254 nm UV light where necessary. Column chromatography was done using 0.040-0.063 mm silica gel. Mass spectra were obtained using a Waters Micromass MALDI in the positive ion mode. NMR spectra were obtained on a 500 MHz Brüker instrument using Topspin software. UV-Vis spectroscopy was carried out using a Shimadzu UV-3101PC UV-VIS-NIR-scanning spectrophotometer. IR spectra were recorded on a Nicolet 5700 FT-IR from Thermo Electron Corporation using an ATR attachment.

#### 11.1.2 Synthesis of Organic Chromophores

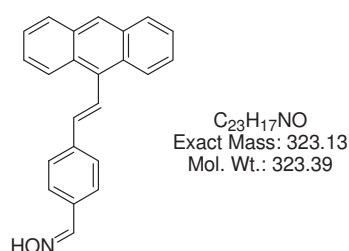
##### 11.1.2.1 9-[2-(4-Formylphenyl)vinyl]anthracene (1B)



9-(Triphenylphosphoniumbromide)methylanthracene (500.0 mg, 0.94 mmol) and potassium *tert*-butoxide (115.0 mg, 1.03 mmol) were dissolved in THF (50 mL) quickly forming a dark 'beetroot coloured' solution. Terephthalaldehyde (122 mg, 0.94 mmol) was added immediately and the reaction was refluxed for 3 h yielding a bright orange-yellow solution. The mixture was cooled to room temperature, washed with 10% aqueous HCl solution (50 mL), followed by water (50 mL), and then

sodium bicarbonate solution (50 mL) and water (50 mL). The resulting solution was treated with  $I_2$  (3.0 eq.) overnight, followed by the addition of saturated aqueous  $Na_2S_2O_3$  for 30 mins (100 mL), separation of the organic layer from the aqueous phase. The organic layer was dried over  $MgSO_4$ , filtered and the solvent was removed in *vacuo*. The product **1B** was obtained after silica gel column chromatography (75:25, hexane: DCM). Yield (160.0 mg, 55%). The  $^1H$  NMR and IR spectra match that described in the literature.<sup>[1]</sup>

#### 11.1.2.2 4-(2-Anthracen-9-yl-vinyl)benzaldehyde oxime (1C)



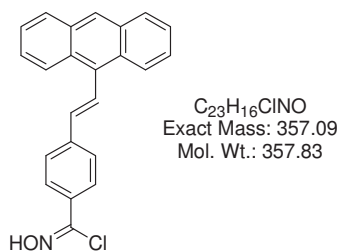
9-[2-(4-Formylphenyl)vinyl]anthracene (**1B**, 50.0 mg, 0.162 mmol) was added to sodium acetate (26.3 mg, 0.32 mmol) and hydroxylamine hydrochloride (22.4 mg, 0.32 mmol) in 1.5 mL EtOH/ $H_2O$  (9 : 1). The mixture was refluxed for 12 h and then cooled to room temperature. The product was extracted with dichloromethane (3 × 20 mL). The organic layer was dried over anhydrous magnesium sulphate, filtered and the solvent was removed *in vacuo*. The crude product was purified by silica gel column chromatography (80:20, hexane: DCM) to give compound **1C** (4-(2-anthracen-9-yl-vinyl)benzaldehyde oxime). Yield (27.1 mg, 52%).

$^1H$  NMR ( $CDCl_3$ ),  $\delta/ppm$ : 8.34 (1H, s, 10-Anth), 8.25 (2H, m, 4,5-Anth), 7.94 (2H, m, 1,8-Anth), 7.91 (1H, d,  $^3J = 16.45$  Hz,  $C=C(H)-Anth$ ), 7.59 (4H, m, 2,3,6,7-Anth), 7.40 (4H, m, Ph), 6.89 (1H, d,  $^3J = 16.62$  Hz,  $C=C(H)-Ph$ ).

$^{13}C$  NMR ( $CDCl_3$ ),  $\delta/ppm$ : 140.8, 136.9, 136.8, 135.8, 132.7, 131.5, 129.8, 128.2, 128.8, 127.5, 126.8, 126.5, 126.0, 125.6, 125.5, 125.2, 125.0, 68.0, 65.2.

ESI+: calcd for  $(M+H)^+$  324.13, found : 324.14.

IR (ATR attachment),  $cm^{-1}$ : 3273 (OH, b, w), 1601 ( $C=N$ , w).

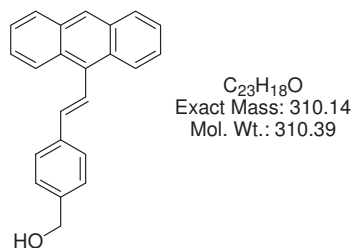
**11.1.2.3 4-(2-Anthracen-9-yl-vinyl)benzohydroximinoyl chloride (1D)**

To a stirred solution of 4-(2-anthracen-9-yl-vinyl)benzaldehyde oxime (**1C**, 52.4 mg, 0.162 mmol) in 20 mL of DMF was added solid NCS (70 mg, 0.162 mmol) gradually, with continuous stirring. The reaction mixture was heated at 60 °C in a water bath for 5 mins. The mixture was then stirred for a further 45 mins at room temperature, after which the reaction was deemed complete by TLC. The solution was poured into ice-water (80 mL). The mixture was extracted with ethyl acetate (3 × 50 mL). The combined extracts were washed with water (3 × 100 mL), dried over magnesium sulphate, filtered and concentrated under vacuum to give the title compound **1D**. Yield (45.2 mg, 78%).

$^1H$  NMR ( $CDCl_3$ ),  $\delta$ /ppm: 8.36 (1H, s, 10-Anth), 8.16 (4H, m, 3,4,5,6-Anth), 7.80 (2H, m, 1,8-Anth), 7.74 (1H d,  $^3J = 16.61$  Hz,  $C=C(H)-Anth$ ), 7.63 (2H, m, 3,7-Anth)], 7.54 (4H, m, Ph), 6.94 (1H, d,  $^3J = 16.70$  Hz,  $C=C(H)-Ph$ ).

$^{13}C$  NMR ( $CDCl_3$ ),  $\delta$ /ppm: 149.9, 138.9, 137.3, 136.6, 132.4, 131.7, 131.5, 128.8, 130.1, 126.8, 129.7, 128.8, 128.6, 127.5, 126.9, 126.7, 126.6, 12.3, 126.1, 125.9, 125.6.

IR (ATR attachment),  $cm^{-1}$ : 3283 (OH, b, w), 1705 (C=N, s).

**11.1.2.4 9-[2-(4-Hydroxymethylphenyl)vinyl]anthracene (1E)**

9-[2-(4-Formylphenyl)vinyl]anthracene (**1B**, 69.0 mg, 0.22 mmol) was dissolved in 20 mL THF/ $H_2O$  (9 : 1). Sodium borohydride (84.7 mg, 2.2 mmol) was then added with vigorous stirring. The reaction was complete by TLC after 30 mins. The reaction mixture was extracted with DCM (4 × 50 mL), dried over anhydrous

magnesium sulfate, filtered and the solvent was removed *in vacuo* to give the product **2B**. Yield (66.3 mg, 97%).

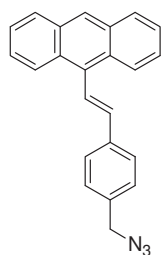
$^1\text{H}$  NMR ( $\text{CDCl}_3$ ),  $\delta$ /ppm: 8.33 (1H, s, 10-Anth), 8.27 (2H, m, 4,5-Anth), 7.95 (2H, m, 2,8-Anth), 7.84 (1H, d,  $^3J = 16.4$  Hz,  $\text{C}=\text{C}(\text{H})$ - Anth), 7.59 (2H, d,  $^3J = 8.1$  Hz, Ph), 7.38 (6H, m, Anth + Ph), 6.87 (1H, d,  $^3J = 16.5$  Hz,  $\text{C}=\text{C}(\text{H})$ -Ph), 4.68 (2H, s,  $\text{CH}_2\text{O}$ ), 1.53 (1H, s, OH).

$^{13}\text{C}$  NMR ( $\text{CDCl}_3$ ),  $\delta$  /ppm: 150.2, 139.0, 136.6, 132.4, 131.6, 131.5, 129.8, 128.8, 127.5, 127.0, 126.7, 126.2, 125.9, 125.7, 125.2, 27.3.

ESI+: calcd for  $(\text{M}+\text{H})^+$  311.14, found : 311.11.

IR (ATR attachment),  $\text{cm}^{-1}$ : 3308 (OH, b, w), 2955 ( $\text{sp}^3$  C-H, w).

#### 11.1.2.5 9-[2-(4-Azidomethylphenyl)vinyl]anthracene (1F)



$\text{C}_{23}\text{H}_{17}\text{N}_3$   
Exact Mass: 335.14  
Mol. Wt.: 335.40

To a stirred solution of compound **1E** (50.0 mg, 0.16 mmol) in dry  $\text{CH}_2\text{Cl}_2$  (20 mL) under argon at 0 °C were added dry triethylamine (24.3 mg, 0.24 mmol) and methanesulfonyl chloride (22.9 mg, 0.2 mmol). The mixture was stirred at room temperature for 6 h under argon before aq HCl (1 M, 2 mL) was added to the resulting solution. The organic layer was washed by water ( $2 \times 20$  mL) and saturated aq. NaCl (5 mL), dried over anhydrous  $\text{Na}_2\text{SO}_4$ , and then filtered. The solvent was removed on a rotary evaporator and the residue was dried *in vacuo* for 30 min. The resulting solid and sodium azide (52.4 mg, 0.81 mmol) were dissolved in DMF (50 mL). The solution was refluxed at 100 °C for 24 h. Water (50 mL) was added followed by extraction with EtOAc ( $2 \times 30$  mL). The combined organic layers were washed with water ( $2 \times 30$  mL), saturated aq. NaCl ( $2 \times 30$  mL), water (50 mL), dried with anhydrous magnesium sulfate and filtered. The solvent was removed *in vacuo* to afford the title compound **1F**. Yield (36.5 mg, 68 %).

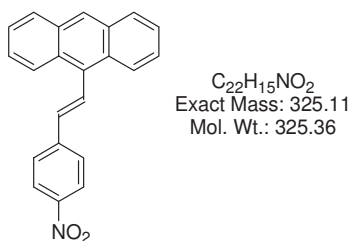
$^1\text{H}$  NMR ( $\text{CDCl}_3$ ),  $\delta/\text{ppm}$ : 8.31 (1H, s, 10-Anth), 8.24 (2H, m, 4,5-Anth), 7.92 (2H, m, 2,8-Anth), 7.82 (1H, d,  $^3J = 16.4$  Hz,  $\text{C}=\text{C}(\text{H})$ - Anth), 7.56 (2H, d,  $^3J = 8.1$  Hz, Ph), 7.37 (6H, m, Anth + Ph), 6.88 (1H, d,  $^3J = 16.5$  Hz,  $\text{C}=\text{C}(\text{H})$ -Ph), 3.23 (2H, s,  $\text{CH}_2\text{N}_3$ ).

$^{13}\text{C}$  NMR ( $\text{CDCl}_3$ ),  $\delta/\text{ppm}$ : 150.6, 139.8, 137.1, 133.5, 131.9, 131.5, 129.4, 128.8, 127.7, 127.0, 126.7, 126.0, 125.5, 125.0, 124.7, .56.7.

ESI+: calcd for  $(\text{M} - \text{N}_3)^+$  293.38, found : 293.46. Molecular ion not detected.

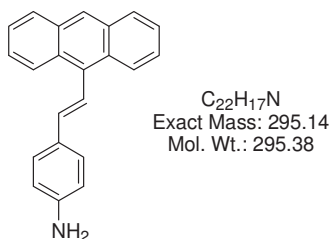
IR (ATR attachment),  $\text{cm}^{-1}$ : 2963 ( $\text{sp}^3$  C-H, w), 2144 ( $\text{N}_3$ , s).

#### 11.1.2.6 9-[2-(4-Nitrophenyl)vinyl]anthracene (2B)



9-[2-(4-Nitrophenyl)vinyl]anthracene (**2B**) was prepared as for **1B** using 4-nitrobenzaldehyde rather than terephthalaldehyde in a Wittig reaction. Yield (52.3 mg, 58%). The  $^1\text{H}$  NMR,  $^{13}\text{C}$  and IR spectra match that described in the literature.<sup>[2]</sup>

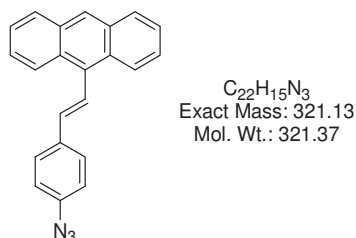
#### 11.1.2.7 9-[2-(4-Aminophenyl)vinyl]anthracene (2C)



To 9-[2-(4-nitrophenyl)vinyl]anthracene (100.0 mg, 0.31 mmol) was added  $\text{SnCl}_2$  (2 g) followed by concentrated HCl (10 mL), and then ethanol (50 mL). The resulting mixture was refluxed for 12 h at 90 °C after which the starting nitro reactant was gone by TLC. The amino product was washed with water ( $2 \times 100$  mL), followed by 2 M NaOH ( $3 \times 100$  mL), and then water (100 mL). The product was extracted with dichloromethane ( $3 \times 50$  mL), dried over magnesium sulfate and concentrated under vacuum to give the title compound **2C**. Yield (90.7 mg, 99%). The  $^1\text{H}$  NMR matches that described in the literature.<sup>[2b]</sup>

IR (ATR attachment),  $\text{cm}^{-1}$ : 3458 (N-H, w), 3354 (N-H, w), 1339 (C-N, s).

#### 11.1.2.8 9-[2-(4-Azidophenyl)vinyl]anthracene (2D)

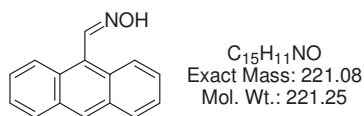


To a stirred solution of 9-[2-(4-aminophenyl)vinyl]anthracene (**2C**, 50 mg, 0.17 mmol) in 9 : 1 DMF/ $\text{H}_2\text{O}$  (6.0 mL) and concentrated HCl (3.0 mL),  $\text{NaNO}_2$  (12.9 mg, 0.19 mmol) in water (1.0 mL) was added dropwise at 0 °C. The mixture was stirred for 30 min, then  $\text{NaN}_3$  (12.4 mg, 0.19 mmol) in water (1.0 mL) was added slowly at 0 °C, and the mixture was stirred for an additional 1 h. The mixture was washed with water (20 mL), conc. HCl (5.0 mL), water ( $2 \times 20$  mL). The product was extracted with dichloromethane ( $3 \times 20$  mL), organic layer was dried over magnesium sulphate, filtered, evaporated and the residue was dried *in vacuo* overnight to give **2D**. Yield (33.9 mg, 62%).

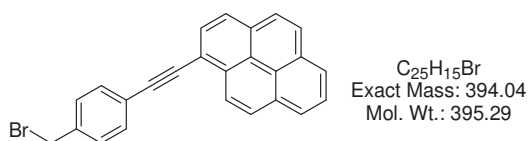
The  $^1\text{H}$  NMR matches that described in the literature.<sup>[2b]</sup>

IR (ATR attachment),  $\text{cm}^{-1}$ : 2141 (N=N=N, s), 1315 (C-N, s).

#### 11.1.2.9 9-Anthraldehyde oxime (3B)



9-Anthraldehyde oxime (**3B**) was prepared as for **1C** using 9-anthraldehyde rather than 9-[2-(4-formylphenyl)vinyl]anthracene. Yield (80.4 mg, 77%). The  $^1\text{H}$  NMR and IR spectra match that described in the literature.<sup>[3]</sup>

**11.1.2.10 1-(4-Bromomethylphenylethynyl)pyrene (4B)**

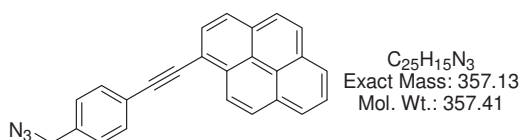
4-Iodobenzyl bromide (295.2 mg, 1.00 mmol) was dissolved in a mixture of DMF (10 mL) and Et<sub>3</sub>N (1.5 mL) and Ar was bubbled through the resulting solution for 30 min. To this solution was added 1-ethynylpyrene (250 mg, 1.11 mmol), CuI (14 mg, 0.075 mmol) and Pd(PPh<sub>3</sub>)<sub>4</sub> (0.3135 mg, 0.0275 mmol) under argon forming a dark 'coke coloured' solution. The reaction mixture was stirred at room temperature under Ar overnight, followed by the addition of an aq. solution of EDTA disodium salt (0.3 M, 2 × 50 mL) and extraction with ethyl acetate (2 × 40 mL) to give a pale orange solution with a blue-green fluorescence. The organic layer was washed with H<sub>2</sub>O (3 × 50 mL), dried over magnesium sulfate, filtered and concentrated under vacuum. The product was recrystallized from DCM/EtOH as an orange-brown solid. Yield (181.8 mg, 46%).

<sup>1</sup>H NMR (CDCl<sub>3</sub>), δ/ppm: 8.64 (1H, d, <sup>3</sup>J = 9.11 Hz), 8.43 (2H, d, <sup>3</sup>J = 9.22 Hz), 8.19 (4H, m), 7.90-8.10 (2H, m), 7.54-8.10 (2H, m), 4.84 (2H, s).

<sup>13</sup>C NMR (CDCl<sub>3</sub>), δ/ppm: 133.0, 130.2, 129.6, 129.1, 128.8, 127.0, 126.0, 125.7, 125.4, 122.3, 43.9.

MALDI-TOF MS calcd for (M-Br+H<sup>+</sup>) 315.14, found : 316.12. Molecular ion not detected.

IR (ATR attachment), cm<sup>-1</sup>: 2172 (C≡C, w).

**11.1.2.11 1-(4-Azidomethylphenylethynyl)pyrene (4C)**

1-(4-Bromomethylphenylethynyl)pyrene (96.7 mg, 0.25 mmol) and sodium azide (164 mg, 2.5 mmol) were dissolved in DMF (100 mL). The solution was refluxed at 100 °C for 24 h. Water (100 mL) was added followed by extraction with EtOAc (2 × 50 mL). The combined organic layers were washed with water (2 × 50 mL), brine (2



× 50 mL), water (50 mL), dried with anhydrous magnesium sulfate and filtered. The solvent was removed in *vacuo* to afford the title compound **4C**. Yield (56.3 mg, 63%).

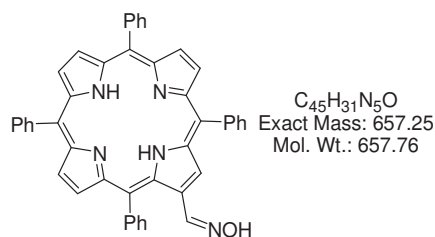
$^1\text{H}$  NMR ( $\text{CDCl}_3$ ),  $\delta/\text{ppm}$ : 8.57 (1H, d,  $^3J = 9.09$  Hz), 8.04 (4H, m), 8.00 (2H, m), 7.96 (2H, m), 7.65 (2H, d,  $^3J = 8.03$ , Ph), 7.30 (2H, d,  $^3J = 7.99$ , Ph), 4.33 (2H, s,  $\text{CH}_2$ ).

$^{13}\text{C}$  NMR ( $\text{CDCl}_3$ ),  $\delta/\text{ppm}$ : 135.6, 132.1, 132.0, 131.3, 131.1, 129.7, 128.4, 128.3, 127.3, 125.7, 124.5, 124.3, 123.6, 117.6, 94.5, 89.3, 54.6.

MALDI-TOF MS calcd for  $(\text{M}+\text{H})^+$  358.13, found, 358.13.

IR (ATR attachment),  $\text{cm}^{-1}$ : 2097 (N=N=N, s).

#### 11.1.2.12 2-(Hydroxyimino)methyl-5,10,15,20-tetraphenylporphyrin (5B)



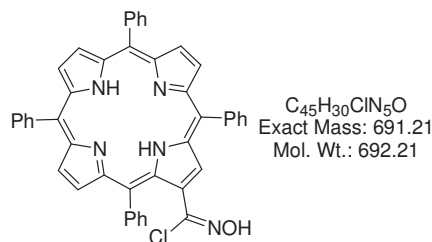
The title compound **5B** was prepared using the same procedure as for **1C** replacing 9-[2-(4-formylphenyl)vinyl]anthracene with the aldehyde **5A**. Yield (60.3 mg, 81%).

$^1\text{H}$  NMR ( $\text{CDCl}_3$ ),  $\delta/\text{ppm}$ : 9.15 (1H, s,  $\text{H}_3''$  ( $\beta$ -pyrrolic)), 8.03-8.89 (6H, m,  $\beta$ -pyrrolic), 8.16-8.25 (8H, m, *ortho*-Ph), 7.74-8.25 (12H, m, *meta*-Ph+*para*-Ph), 2.73 (2H, s,  $\text{CH}_2\text{O}$ ), -2.63 (2H, br s, NH).

MALDI-TOF MS calcd for  $\text{M}^+$  657.76, found : 658.13.

IR (ATR attachment),  $\text{cm}^{-1}$ : 1710 (C=N, s).

#### 11.1.2.13 2-(Chlorohydroxyimino)methyl-5,10,15,20-tetraphenylporphyrin (5C)



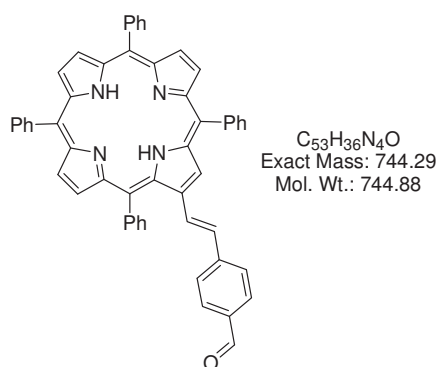
The compound **5C** was prepared by the same procedure as for **1C** replacing **1B** with the oxime **5B**. Yield (52.1 mg, 97 %).

$^1\text{H}$  NMR ( $\text{CDCl}_3$ ),  $\delta/\text{ppm}$ : 9.08 (1H, s,  $\text{H}_{3''}$  ( $\beta$ -pyrrolic)), 7.99-8.96 (6H, m,  $\beta$ -pyrrolic), 8.13-8.22 (8H, m, *ortho*-Ph), 7.71-8.26 (12H, m, *meta*-Ph+*para*-Ph), 2.76 (2H, s,  $\text{CH}_2\text{O}$ ),

MALDI-TOF MS calcd for  $\text{M}^+$  692.21, found : 692.85.

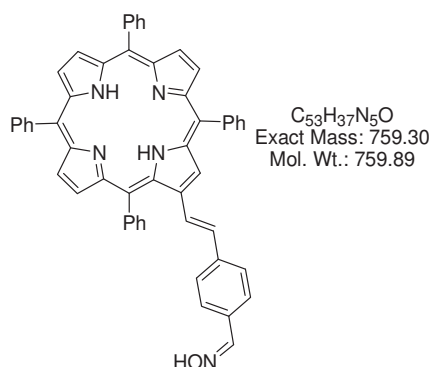
IR (ATR attachment),  $\text{cm}^{-1}$ : 1707 (C=N, s).

**11.1.2.14 4-(trans-2'-(5'',10'',15'',20''-Tetraphenylporphyrin-2''-yl)benzaldehyde (6B)**



The title compound **6B** was prepared using the same procedure as for **1B** using compound **6A** rather than 9-anthracene methylphosphonium salt (**1A**). Yield (56.3, 71%).  $^1\text{H}$  and  $^{13}\text{C}$  NMR data were in agreement with the literature data.<sup>[4]</sup>

**11.1.2.15 4-(trans-2'-(5'',10'',15'',20''-Tetraphenylporphyrin-2''-yl)benzaldehyde oxime (6C)**



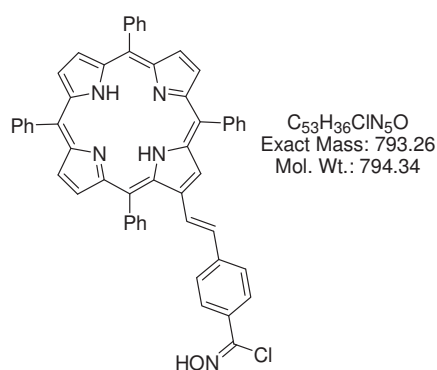
The title compound **6C** was prepared using the same method as for **1C** replacing 9-[2-(4-formylphenyl)vinyl]anthracene with compound **6B**. Yield (67.6 mg, 71%).

$^1\text{H}$  NMR ( $\text{CDCl}_3$ ),  $\delta/\text{ppm}$ : 9.00 (1H, s,  $\text{H}_3''$  ( $\beta$ -pyrrolic)), 8.70-8.83 (6H, m,  $\beta$ -pyrrolic), 8.15-8.32 (8H, m, *ortho*-Ph), 7.68-7.78 (16H, m, *meta*-Ph+*para*-Ph-styryl-Ph), 7.41 (1H, d,  $^3J = 16.29$  Hz,  $\text{C}=\text{C}(\text{H})$ -TPP), 6.80 (1H, d,  $^3J = 16.18$  Hz,  $\text{C}=\text{C}(\text{H})$ -Ph), -2.59 (2H, br s, NH).

MALDI-TOF MS calcd for  $\text{M}^+$  759.30, found : 759.49.

IR (ATR attachment),  $\text{cm}^{-1}$ : 1727 ( $\text{C}=\text{N}$ , s).

**11.1.2.16 4-(*trans*-2'-(5'',10'',15'',20''-Tetraphenylporphyrin-2''-yl)benzaldehyde hydroximinoyl chloride (6D)**



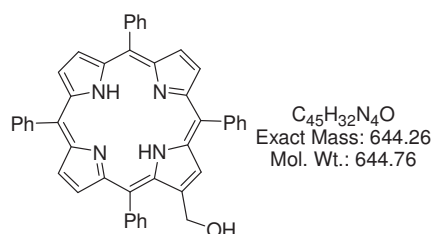
The title compound **6D** was prepared using the same procedure described for compound **1D** replacing 4-(2-anthracen-9-yl-vinyl)benzaldehyde oxime with compound **6C**. Yield (78.5 mg, 89%).

$^1\text{H}$  NMR ( $\text{CDCl}_3$ ),  $\delta/\text{ppm}$ : 8.55-8.70 (7H, m,  $\beta$ -pyrrolic), 8.00-8.12 (8H, m, *ortho*-Ph), 7.59-7.77 (16H, m, *meta*-Ph+*para*-Ph-styryl-Ph), 6.95 (1H, d,  $^3J = 16.47$  Hz,  $\text{C}=\text{C}(\text{H})$ -Ph), -2.68 (2H, br s, NH).

MALDI-TOF MS calcd for  $\text{M}^+$  759.30, found : 759.49.

IR (ATR attachment),  $\text{cm}^{-1}$ : 1597 ( $\text{C}=\text{N}$ , s).

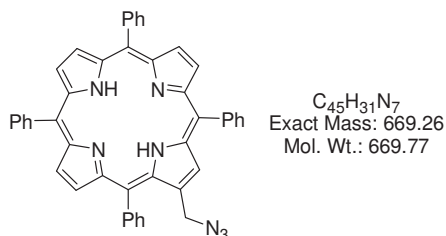
**11.1.2.17 2-Hydroxymethyl-5,10,15,20-tetraphenylporphyrin (7B)**



The title compound **7B** was prepared using the same procedure as for **1F** replacing 9-[2-(4-formylphenyl)vinyl]anthracene with compound **5A**. (Yield 60.1 mg, 81%).

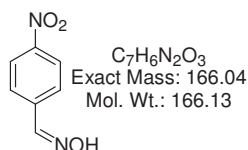
MALDI-MS: calcd for  $M^+$  644.26, found : 644.45. The  $^1\text{H}$  NMR spectrum matches that described in the literature.<sup>[5]</sup>

#### 11.1.2.18 2-Azidomethyl-5,10,15,20-tetraphenylporphyrin (7C)



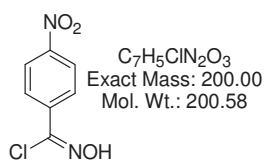
The similar procedure of preparation of compound **1F** was followed to prepare compound **7C**, replacing **1E** with **7B**.  $^1\text{H}$  NMR data were in agreement with the literature data.<sup>[6]</sup>

#### 11.1.2.19 4-Nitrobenzaldehyde oxime (8B)



The preparation of compound **8B** was accomplished using the procedure similar to that for **1C** using 4-nitrobenzaldehyde instead of 9-[2-(4-formylphenyl)vinyl]anthracene. Yield (95.4 mg, 77%).  $^1\text{H}$  NMR and  $^{13}\text{C}$  NMR data were in agreement with the literature data.<sup>[7]</sup>

#### 11.1.2.20 4-Nitrobenzaldehyde hydroximinoyl chloride (8C)



4-Nitrobenzaldehyde hydroximinoyl chloride (**8C**) was prepared using the same procedure as for **1D** replacing 4-(2-anthracen-9-yl-vinyl)benzaldehyde oxime with 4-nitrobenzaldehyde oxime. Yield (73.5 mg, 76%).  $^1\text{H}$  NMR and  $^{13}\text{C}$  NMR data were in agreement with the literature data.<sup>[7-8]</sup>

### 11.1.3 Synthesis of Oligonucleotides

Oligonucleotides were synthesized on a 1.0  $\mu\text{mol}$ , 1000 Å CPG supports with an Mer-Maid 4 automated DNA synthesizer from BioAutomation Corporation using 4,5-dicyanoimidazole in dry acetonitrile as activator. The synthesis was paused for 2'-*O*-Propargyl uridine phosphoramidite or (*R*)-1-*O*-(4-ethynylbenzyl)glycerol phosphoramidite coupling after the detritylation step. 2'-*O*-Propargyl uridine phosphoramidite/(*R*)-1-*O*-(4-ethynylbenzyl)glycerol phosphoramidite was hand coupled by adding the dry monomer (10 mg) on top of the column followed by 200  $\mu\text{L}$  of activator (0.25 M DCI in dry acetonitrile) that was directly injected into the column under argon after which the synthesis cycle was allowed to continue.

### 11.1.4 General Procedure for CuAAC Reaction on DNA

To a microwave reaction vessel containing 2'-*O*-propargyl uridine functionalized DMT-off oligonucleotides on CPG (0.076  $\mu\text{mol}$ ) was added azide functionalized organic chromophore (1.67  $\mu\text{mol}$ , 20 eq) followed by degassed DMSO (200  $\mu\text{L}$ ). Freshly prepared  $\text{CuSO}_4 \cdot 5\text{H}_2\text{O}$  solution (8  $\mu\text{L}$ , 40 mM) in degassed  $\text{H}_2\text{O}$  and sodium ascorbate solution (25  $\mu\text{L}$ , 50 mM) in degassed  $\text{H}_2\text{O}$  were added. The reaction mixture was then irradiated in a microwave synthesizer (Discover, CEM Corporation). The following settings were used: 70 °C, 100 watts, 20 min. The CPG supports were washed with DCM (3  $\times$  200  $\mu\text{L}$ ) to remove any unreacted azide followed by  $\text{H}_2\text{O}$  (200  $\mu\text{L}$ ) to remove any remaining  $\text{CuSO}_4$ .

### 11.1.5 Procedure for Nitrobenzaldehyde Oxime NO/AC Reaction on DNA

To a suspension of CPG supported **ON1** (5.0 mg, 152.0 nmol) in water (68.1  $\mu\text{L}$ ) was added  $\text{NaHCO}_3$  (15.2  $\mu\text{L}$ , 0.1 M, 1.5  $\mu\text{mol}$ ) and a freshly premixed solution containing nitrobenzaldehyde oxime **8B** (15.2  $\mu\text{L}$ , 0.1 M in DMF, 1.5  $\mu\text{mol}$ ) and *N*-chlorosuccinimide (15.2  $\mu\text{L}$ , 0.1 M in DMF, 1.5  $\mu\text{mol}$ ). The mixture was vortexed and shaken at RT overnight. The solid support material was thoroughly washed with DMF (200  $\mu\text{L}$ ) and  $\text{CH}_2\text{Cl}_2$  (2  $\times$  200  $\mu\text{L}$ ).

### 11.1.6 General procedure for nitrobenzaldehyde hydroximinoyl chloride NO/AC reaction on DNA

The hydroximinoyl chloride solution **8C** (30.4  $\mu$ L, 0.1 M in 1:1 ACN/H<sub>2</sub>O, 152 nmol) was added to CPG supported **ON1** (5.0 mg, 152.0 nmol). The mixture was vortexed and shaken at RT for 20 mins. The solid support material was thoroughly washed with ACN (2  $\times$  320  $\mu$ L).

In similar experiments ACN/H<sub>2</sub>O (1:1), was replaced by ACN/0.1 M NaHCO<sub>3</sub> (aq) (1:1), ACN/ 0.1 M NaHCO<sub>3</sub> (aq) (3:1), and ACN/ saturated NaHCO<sub>3</sub> (aq) (1:1), the solid support material was treated twice with the reagent mixture and different reaction times were explored (See table 4.2, Chapter 4).

### 11.1.7 General cleavage/deprotection and precipitation procedure

The obtained modified ONs were cleaved from solid support by treating with 32% aq NH<sub>4</sub>OH (250  $\mu$ L) at RT for 30 min and then at 55 °C overnight. The CPG supports were filtered off, aqueous sodium acetate (3M, 200  $\mu$ L) was added to the filtrate, followed by ONs precipitation from EtOH (1 mL) at -20 °C for 30 mins. The resulting mixture was centrifuged at 13000 rpm on a microcentrifuge and the supernatant was decanted. The ONs were then dissolved in milli-Q H<sub>2</sub>O (50  $\mu$ L).

**NB.** The volumes of NH<sub>4</sub>OH, sodium acetate and EtOH were appropriately adjusted in order to suit the different ONs amounts in the reaction mixture.

## 11.2 Experimental Procedures for Chapters 4, 5 - 8

### 11.2.1 Materials

All organic solvents were purchased from Sigma–Aldrich, Fluka and Fisher Scientific. Unmodified oligonucleotides were purchased from Integrated DNA Technologies. ZnTMPyP4 and [Ru(bpy)<sub>3</sub>]<sup>2+</sup> were synthesized previously in our laboratory according to published procedures.<sup>[9]</sup> The identities and purities of ZnTMPyP4 and [Ru(bpy)<sub>3</sub>]<sup>2+</sup> were verified using NMR and UV-Vis spectroscopies; the spectra are in the Appendix sections 12.1.1 and 12.1.2). All aqueous solutions were prepared in ultrapure MilliQ water (18.2 M $\Omega$ ·cm).

### 11.2.2 Synthesis and Purification of TINA Modified Oligonucleotides

Oligonucleotides were synthesized on a 1.0  $\mu\text{mol}$ , 1000 Å CPG supports using a Mer-Maid 4 automated DNA synthesizer from BioAutomation Corporation using 4,5-dicyanoimidazole in dry acetonitrile as an activator. The synthesis was paused for TINA coupling after the detritylation step. TINA was hand coupled by adding the dry phosphoramidite (10 mg) on top of the column followed by 200  $\mu\text{l}$  of activator (0.25 M DCI in dry acetonitrile) that was directly injected into the column under Ar after which the synthesis cycle was allowed to continue. The DNA synthesis was completed in DMT-off mode. The oligonucleotides were cleaved from the solid support, deprotected, and purified according to a previously published procedure.<sup>[10]</sup> Purity of TINA-modified oligonucleotides was monitored using denaturing 20% PAGE (7M urea) and was found to be over 90 %. Molecular weights of oligonucleotide sequences were confirmed using a Waters Micromass MALDI-TOF in the positive mode. Oligonucleotides were desalted using C18 zip-tips prior to loading on the MALDI plate, using anthranilic acid as a matrix and dibasic ammonium citrate as a co-matrix. The oligonucleotides are 5'-XCTCAAGCAAGCT (ON1), GAGTTCGTTTCGAX-5' (ON2), 5'-XXCTCAAGCAAGCT (ON3), GAGTTCGTTTCGAXX-5' (ON4), 5'-XTXCTCAAGCAAGCT (ON5), GAGTTCGTTTCGAXTX-5' (ON6), TG4TX, TG4XT and TG3XG3T, where X is TINA monomer.

**Table 11.1** Results of mass spectroscopy analysis of ONs synthesised.

Oligonucleotide	Calculated m/z, Da	Observed m/z, Da
ON1	4091.7	4086.6
ON2	4148.1	4153.7
ON3	4558.79	4555.4
ON4	4620.78	4620.4
ON5	4861.83	4860.8
ON6	4923.8	4922.6
TG4TX	2331.7	2330.6
TG4XT	2331.7	2330.6
TG3XG3T	2990.1	2989.6

### 11.2.3 Stock Solutions

ZnTMPyP4: A 2.0 mM stock solution was prepared by weighing the ZnTMPyP4Cl<sub>4</sub> salt (176.80201 mg) on an ultra-sensitive analytical balance and then dissolving the solute in MilliQ H<sub>2</sub>O (100 mL). The concentration was confirmed by UV-Vis spectroscopy, using an extinction coefficient at 437 nm of 230 000 L mol<sup>-1</sup> cm<sup>-1</sup>.<sup>[11]</sup>

[Ru(bpy)<sub>3</sub>]<sup>2+</sup>: A 0.5 mM stock solution was prepared by weighing the [Ru(bpy)<sub>3</sub>](BF<sub>4</sub>)<sub>2</sub> salt (23.84133 mg) on an ultra-sensitive analytical balance followed by dissolution of the solute in MilliQ H<sub>2</sub>O (100 mL). The concentration was confirmed by UV-Vis spectroscopy, using an extinction coefficient at 452 nm of 14 600 L mol<sup>-1</sup> cm<sup>-1</sup> corresponding to the MLCT transition.<sup>[12]</sup>

Oligonucleotides: Concentrations of stock solutions of single stranded oligonucleotides were determined by UV-Vis spectroscopy (see below for details).

### 11.2.4 DNA annealing procedures

DNA duplexes were prepared by first suspending both complementary single stranded oligonucleotides at the same molar concentration in MilliQ H<sub>2</sub>O. The equimolar complementary oligonucleotides were mixed in a 1.5 ml eppendorf tube, followed by the addition of the appropriate annealing buffer. The eppendorf tube was then placed in a heatblock at 90 °C for 10 minutes, removed from the heat block and allowed to cool to room temperature.

DNA G-quadruplexes were prepared by first suspending the single stranded oligonucleotide in appropriate annealing buffer in a 1.5 ml eppendorf tube. The eppendorf tube was placed in a heatblock at 95 °C for 10 minutes, and was allowed to cool to room temperature slowly on the heatblock for 12 hours.

### 11.2.5 Instrumentation

#### *11.2.5.1 UV-Vis Spectroscopy, DNA melting procedure and Thermal Difference Spectra (TDS)*

UV-Vis spectra for porphyrin and oligonucleotides were collected using a Shimadzu UV-3101PC UV-VIS-NIR-scanning spectrophotometer in 1 mL cuvettes at a



pathlength of 1 cm. UV-Vis spectra were taken at a concentration of 1.0  $\mu\text{M}$  of each oligonucleotide in 10 mM sodium phosphate buffer (pH 7), 0.1 mM EDTA at low salt concentration (50 mM NaCl) and high salt concentration (1 M NaCl) at room temperature. The concentration of ZnTMPyP4 was 10  $\mu\text{M}$ , both in the presence and absence of DNAs, whilst those for  $[\text{Ru}(\text{bpy})_3]^{2+}$  were 40 or 100  $\mu\text{M}$ . Melting temperature measurements of oligonucleotides were collected on a CARY 100 Bio UV-Vis spectrophotometer using a  $2 \times 6$  multicell block with a Peltier temperature controller from 20 to 80  $^\circ\text{C}$  at a rate of 1  $^\circ\text{C}/\text{min}$  for duplexes and 0.25  $^\circ\text{C}/\text{min}$  for G-quadruplexes. All melting temperatures are within the uncertainty of  $\pm 0.5$   $^\circ\text{C}$  as determined by repetitive experiments. Extinction coefficients for oligonucleotides were calculated using the extinction coefficients of each nucleotide and TINA at 260 nm. Extinction coefficients of nucleotides and TINA ( $\text{L mol}^{-1} \text{ cm}^{-1}$ ): dA (15400), dG (11700), dT (8800), dC (7300), TINA (22400). Thermal difference spectra for DNA complexes were determined by subtracting the UV-Vis spectra obtained at 20  $^\circ\text{C}$  from UV-Vis spectra obtained at 90  $^\circ\text{C}$  after 30 mins incubation in the appropriate buffer solutions.

#### 11.2.5.2 Circular Dichroism Experiments

CD spectra were recorded on an Applied Photophysics Chirascan CD spectrometer (150 W Xe arc) with a Quantum Northwest TC125 temperature controller using quartz cuvettes with an optical path length of 1 cm. All measurements were done at 25  $^\circ\text{C}$ . An average of three scans between 210 nm and 700 nm was recorded at 1 nm intervals, 240 nm/min scanning speed. A baseline correction was applied against the appropriate buffer followed by data smoothing using the Savitzky-Golay method. Data was recorded in mdeg and converted to delta epsilon from the formula  $\Delta\epsilon = \Theta(\text{mdeg}) / 32980 \times C \times l$  using software provided by Applied Photophysics. The porphyrin, DNA-porphyrin and DNA- $[\text{Ru}(\text{bpy})_3]^{2+}$  samples were prepared in the same manner and in the same buffer solutions as for UV-Vis measurements. The concentration of ZnTMPyP4 was 10  $\mu\text{M}$  except for  $K_a$  measurements, where the porphyrin was added stepwise (concentration 0.05, 0.1, 0.2, 0.3, 0.4, 0.6, 0.8, 1.0, 2.0, 4.0, 8.0, 16.0 and 20  $\mu\text{M}$ ). The concentration of  $[\text{Ru}(\text{bpy})_3]^{2+}$  was 40  $\mu\text{M}$  or 100  $\mu\text{M}$ . Concentrations of stock solutions were chosen such that the total dilution of the

analyte solution did not exceed 1% by each addition of ZnTMPyP4 or  $[\text{Ru}(\text{bpy})_3]^{2+}$ . CD spectra were recorded after each incremental addition of ZnTMPyP4 or  $[\text{Ru}(\text{bpy})_3]^{2+}$ , after which the solutions had reached equilibration ( $\geq 20$  min).

### 11.2.5.3 Fluorescence Spectroscopy

Fluorescence data were collected using a FluoroMax-4 spectrofluorimeter (Horiba Scientific Jobin Yvon) or a Perkin Elmer LS-50 Luminescence Spectrometer using 1 cm path length quartz cuvettes, volume 1 mL. The porphyrin and DNA-porphyrin samples were prepared in the same manner and in the same buffer solutions as for UV-Vis measurements. The concentrations of ZnTMPyP4 for  $K_a$  measurements were the same as for CD measurements. The fluorescence emission of ZnTMPyP4, the DNAs alone, and the DNA-ZnTMPyP4 complexes were measured at a wavelength range of 390-800 nm for TINA excitation ( $\lambda_{\text{ex}} = 375$  nm), and 460-800 nm for porphyrin excitation ( $\lambda_{\text{ex}} = 436$  nm). The excitation spectra were recorded at a wavelength range of 200-400 nm ( $\lambda_{\text{em}}$  TINA: 407 nm), and 200-600 nm ( $\lambda_{\text{em}}$  ZnTMPyP4: 630 nm). The fluorescence emission of  $[\text{Ru}(\text{bpy})_3]^{2+}$  were measured at wavelength range of 520-800 nm ( $\lambda_{\text{ex}} = 500$  nm) both in the absence and presence of DNAs.

## 11.3 Experimental Procedures for Chapters 4 and 9

### 11.3.1 Materials and instrumentation

Analytical reagent (AR) grade organic solvents and 9,10-diphenylanthracene (DPA) were purchased from Sigma-Aldrich and were used as received. (*R*)-1-*O*-[4-(1-pyrenylethynyl)phenylmethyl]glycerol (PEPy) and with tris(bipyridine)ruthenium(II) were synthesized previously in our lab. All aqueous solutions were prepared in ultrapure MilliQ water (18.2 M $\Omega$ ·cm). Stock solutions of DNAs, ZnTMPyP4 and  $[\text{Ru}(\text{bpy})_3]^{2+}$  were prepared as described for Chapters 4, 5 and 6. Anti-Stokes fluorescence emission spectra were collected using a Perkin Elmer LS-50 Luminescence Spectrometer using 1 cm path length quartz cuvettes, volume 1 mL.]

### 11.3.2 Upconverted fluorescence measurements

Energy upconversion solutions containing  $[\text{Ru}(\text{bpy})_3]^{2+}$  (46  $\mu\text{M}$ ) and PEPy (4.6 mM) in dichloromethane (DCM) were prepared from stock solutions of 0.5 mM  $[\text{Ru}(\text{bpy})_3]^{2+}$  and 5 mM PEPy. Solution of ZnTMpyP4 (5.0 – 200  $\mu\text{M}$ ), from a 0.5 mM stock and PEPy (0.01 – 5 mM) were prepared in a 9:1 (DMSO/ $\text{H}_2\text{O}$ ) solvent mixture. These solutions were deaerated by purging with argon gas in a sonicator for at least 30 min and were kept under argon in a silicon septum fitted quartz cuvette throughout the experiments. Aqueous solutions of TINA-modified DNAs with ZnTMpyP4 or  $[\text{Ru}(\text{bpy})_3]^{2+}$  were prepared in 10 mM sodium phosphate buffer (pH 7.0, 0.1 mM EDTA, 50 mM NaCl) and then degassed by argon purging for 24 hours.

Green-to-blue upconversion was demonstrated for  $[\text{Ru}(\text{bpy})_3]^{2+}$ /PEPy in DCM by illuminating a deaerated sample with a commercial green laser pointer ( $\lambda_{\text{ex}} = 532$  nm, 5 mW peak power). Anti-Stokes fluorescence spectra were measured on all deaerated samples with the excitation at 500 nm for  $[\text{Ru}(\text{bpy})_3]^{2+}$  and 565 nm for ZnTMpyP4 passing through a 400 nm long pass filter prior to incidence on the sample. The incident power dependence of EU was measured by systematically varying the excitation power through the use of neutral density filters.

## 11.4 References

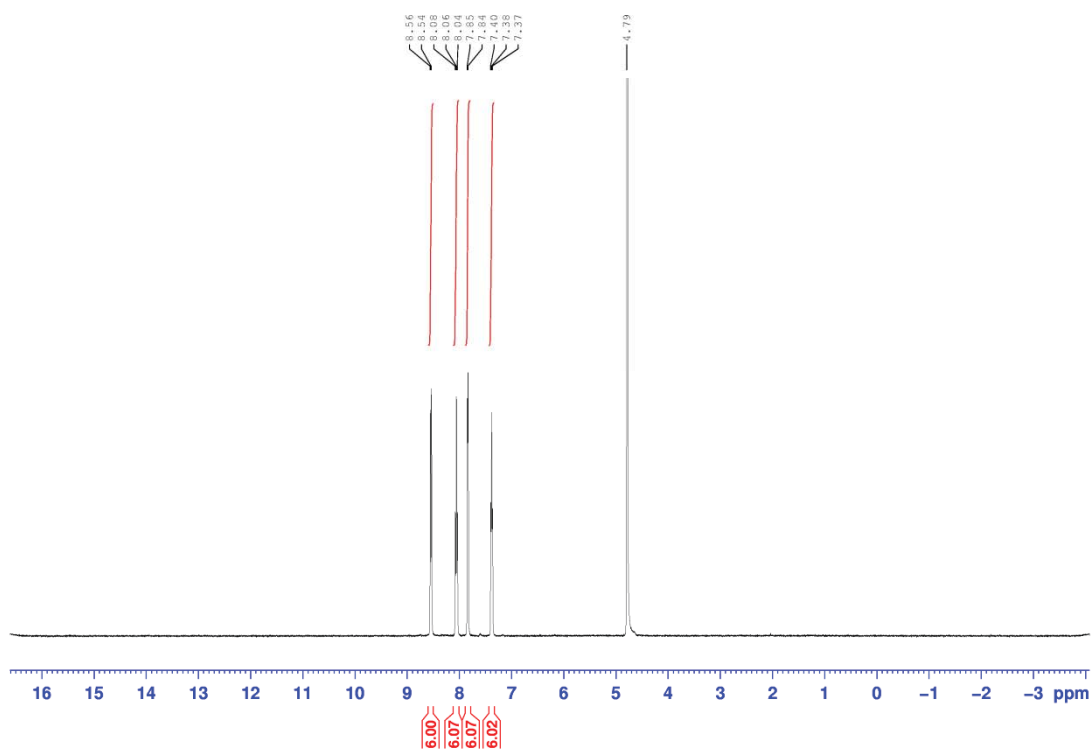
- [1] K. Sandros, H.-D. Becker, *Journal of Photochemistry and Photobiology A: Chemistry* **1988**, *43*, 291.
- [2] a)K. C. Kumara Swamy, V. Srinivas, K. V. P. Pavan Kumar, K. Praveen Kumar, *Synthesis* **2007**, *2007*, 893; b)G. G. Aloisi, F. Elisei, L. Latterini, M. Passerini, G. Galiazzo, *Journal of the Chemical Society, Faraday Transactions* **1996**, *92*, 3315.
- [3] a)M. Horiguchi, Y. Ito, *Tetrahedron* **2007**, *63*, 12286; b)J. S. Meek, J. R. Dann, *Journal of the American Chemical Society* **1955**, *77*, 6677.
- [4] a)E. Annoni, M. Pizzotti, R. Ugo, S. Quici, T. Morotti, M. Bruschi, P. Mussini, *European Journal of Inorganic Chemistry* **2005**, *2005*, 3857; b)W. M. Campbell, PhD thesis, Massey University (Palmerston North), **2001**.
- [5] E. E. Bonfantini, A. K. Burrell, W. M. Campbell, M. J. Crossley, J. J. Gosper, M. M. Harding, D. L. Officer, D. C. Reid, *Journal of Porphyrins and Phthalocyanines* **2002**, *6*, 708.
- [6] A. W. Stephenson, PhD thesis, Massey University (Palmerston North), **2010**.
- [7] B. C. Sanders, F. D. R. Friscourt, P. A. Ledin, N. E. Mbua, S. Arumugam, J. Guo, T. J. Boltje, V. V. Popik, G.-J. Boons, *Journal of the American Chemical Society* **2010**, *133*, 949.
- [8] R. Sun, Y. Li, M. Lü, L. Xiong, Q. Wang, *Bioorganic & Medicinal Chemistry Letters* **2010**, *20*, 4693.
- [9] a)F. Qu, N.-Q. Li, *Electroanalysis* **1997**, *9*, 1348; b)J. A. Broomhead, C. G. Young, P. Hood, *Inorganic Syntheses* **1982**, *21*, 127.
- [10] O. Doluca, A. S. Boutorine, V. V. Filichev, *ChemBioChem* **2011**, *12*, 2365.
- [11] J. M. Kelly, M. J. Murphy, D. J. McConnell, C. OhUigin, *Nucleic Acids Research* **1985**, *13*, 167.
- [12] K. Kalyanasundaram, *Coordination Chemistry Reviews* **1982**, *46*, 159.



## 12 Appendix

### 12.1 General

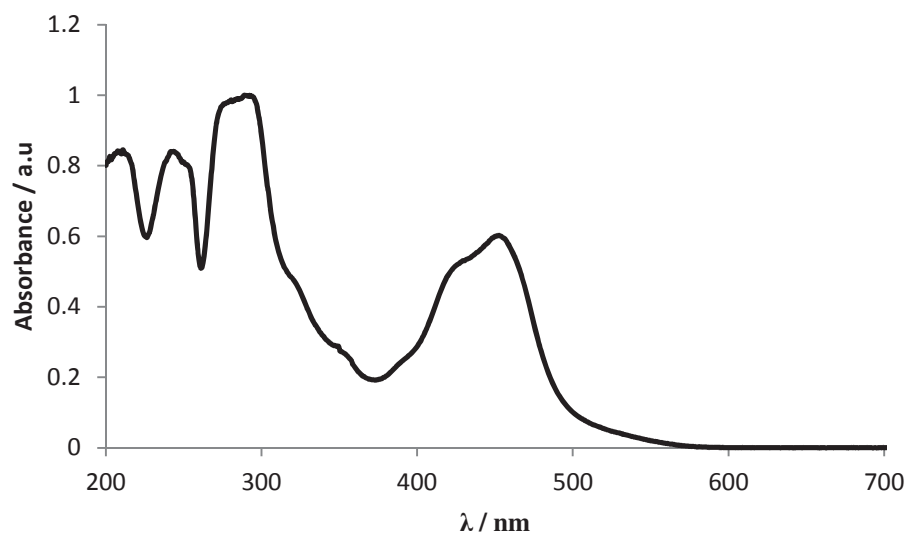
#### 12.1.1 NMR and UV-Vis Spectra of $[\text{Ru}(\text{bpy})_3]^{2+}$



**Figure 12.1**  $^1\text{H}$  NMR spectrum of  $[\text{Ru}(\text{bpy})_3]^{2+}$  in  $\text{D}_2\text{O}$  at  $25^\circ\text{C}$ .

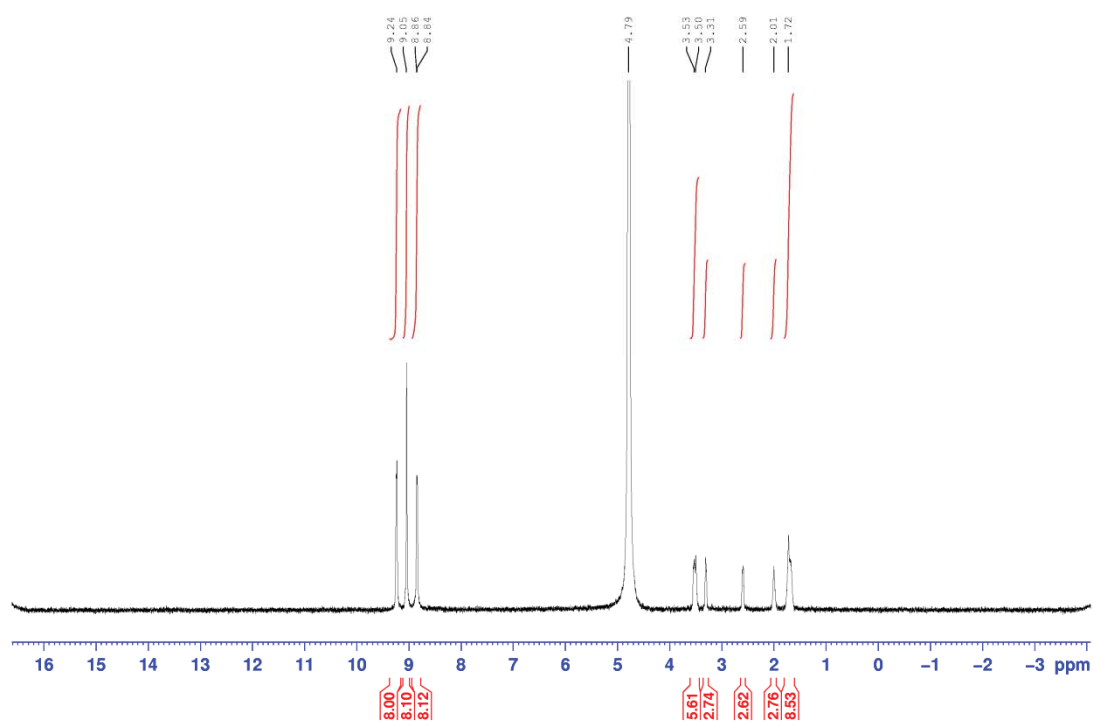
The  $^1\text{H}$  NMR spectrum of  $[\text{Ru}(\text{bpy})_3]^{2+}$  in  $\text{D}_2\text{O}$  shows 4 sets of the 2,2'-bipyridine (7.3 – 8.6 ppm) in addition to the DHO peak at 4.79 ppm with no signs of impurity (Figure 12.1).

The UV-vis spectrum of  $[\text{Ru}(\text{bpy})_3]^{2+}$  matches that from the literature (Figure 12.2).<sup>[1]</sup> The peaks in the UV range between 200 – 300 nm are assigned to ligand-ligand transitions (L-L) while the long wavelength absorption around 450 nm is assigned to a metal to ligand charge transfer ( $^1\text{MLCT}$ ).



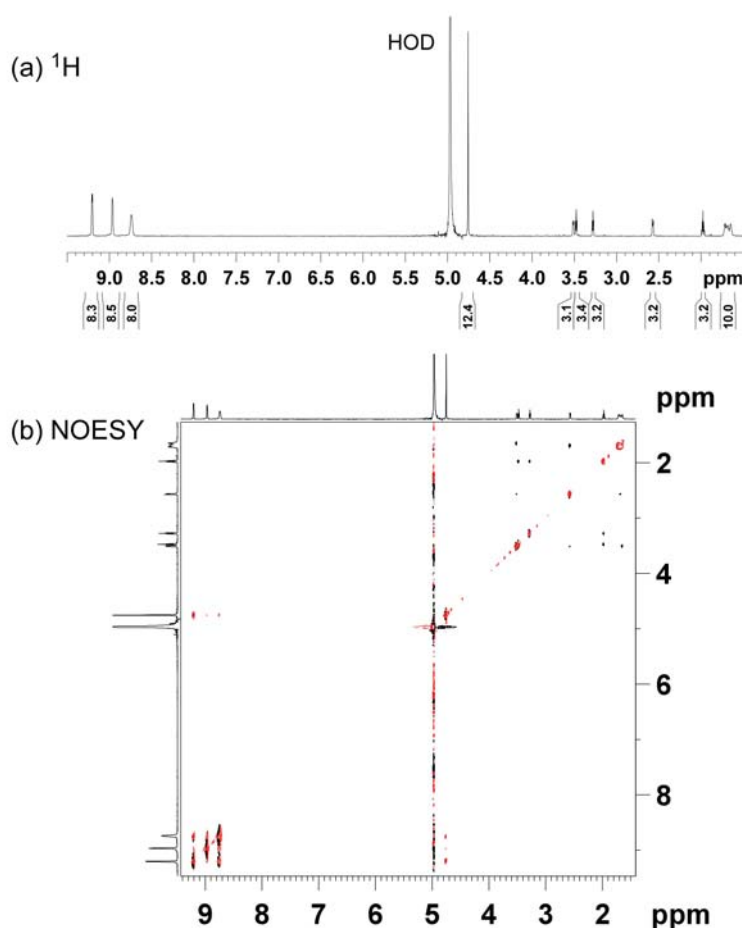
**Figure 12.2** Normalized UV-Vis absorption spectrum of 100  $\mu\text{M}$   $[\text{Ru}(\text{bpy})_3]^{2+}$  recorded in  $\text{H}_2\text{O}$  at 25  $^\circ\text{C}$ .

### 12.1.2 NMR and UV-Vis spectra of ZnTMPyP4



**Figure 12.3**  $^1\text{H}$  NMR spectrum of ZnTMPyP4 in  $\text{D}_2\text{O}$  at 25  $^\circ\text{C}$ .

A  $^1\text{H}$ -NMR spectrum was recorded on a 700 MHz NMR spectrometer at 281 K and is shown in Figure 12.4(a). At this temperature the residual HOD peak from the  $\text{D}_2\text{O}$  solvent did not obscure the signal from the porphyrin's methyl groups at 4.8 ppm. There are a number of unexplained signals between 1.5 and 3.6 ppm which belong to aliphatic protons of an impurity. The NOESY spectrum shown Figure 12.4(b) indicates that these signals are not related to the porphyrin molecule: there are no cross peaks visible between the signals attributable to the porphyrin and the additional signals. Furthermore the porphyrin cross peaks have the same sign as the diagonal whereas the cross peaks from the putative impurity do not. This is the expected behaviour of a mixture of a high ( $>\sim 1000$  Da) and low molecular weight solutes.

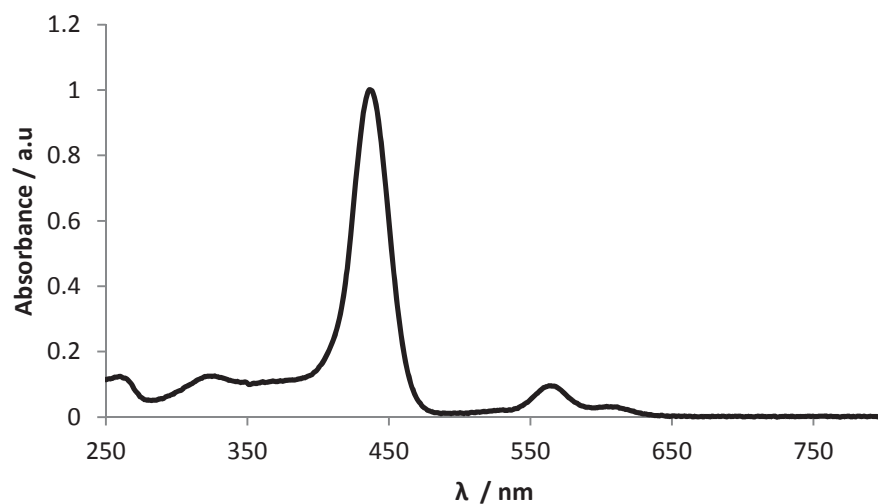


**Figure 12.4**  $^1\text{H}$ -NMR spectrum recorded for ZnTMPyP4 at 281 K (a) and NOESY spectrum (b).

The UV-Vis spectrum of a porphyrin (Fig. 12.5) shows no sign of demetallation: the Soret and Q bands of a free base porphyrin are blue-shifted by 20 and 50 nm in comparison with ZnTMPyP4, respectively.<sup>[2]</sup> The aliphatic impurity present in the sample does not absorb the light in the visible region and therefore does not



influence determination of the porphyrin concentration. Moreover, when the porphyrin was used in experiments with stDNA, the results obtained (UV-Vis, CD and fluorescence spectra as well as  $K_a$  values) were matching those reported in literature.<sup>[3]</sup> Therefore, the presence of the aliphatic impurity in the porphyrin has no influence on the results obtained in the thesis.



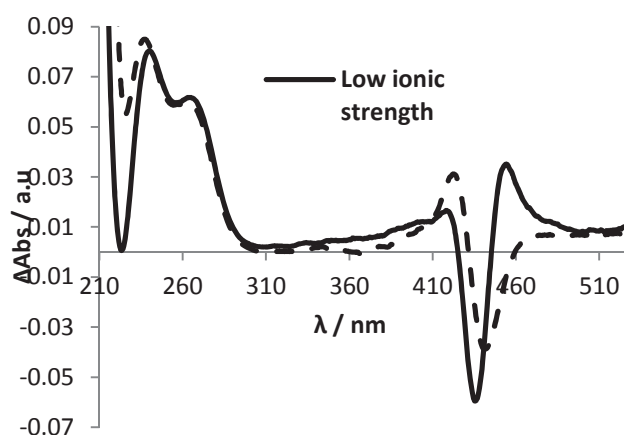
**Figure 12.5** Normalized UV-Vis absorption spectrum of 10.0 μM ZnTMPyP4 in MilliQ H<sub>2</sub>O at 25 °C.

## 12.2 Appendix for Chapter 6

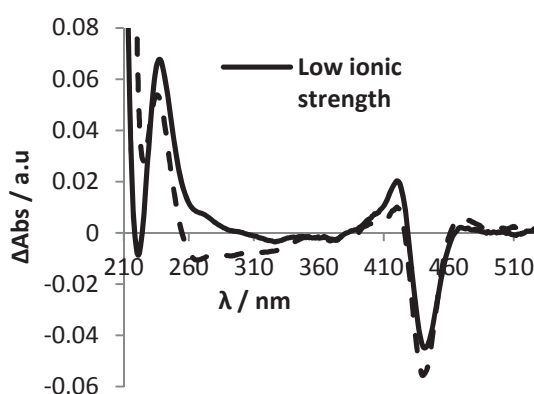
**Table 12.1** Melting temperatures of stDNA (stDNA) in the absence and presence of ZnTMPyP4 at 260 nm.

Duplex	$T_m$ , °C
stDNA <sup>L</sup>	31.0
stDNA <sup>H</sup>	54.5
stDNA + ZnTMPyP4 <sup>L</sup>	54.0
stDNA + ZnTMPyP4 <sup>H</sup>	56.0

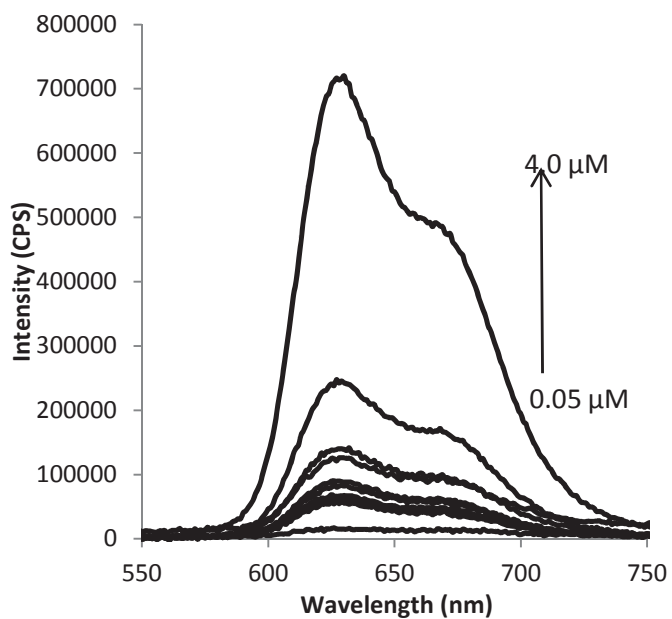
Conditions: ZnTMPyP4 = 10  $\mu$ M, Duplex = 0.04  $\mu$ M, 10 mM sodium phosphate buffer, 0.1 mM EDTA, in the presence of 50 mM (L) and 1M NaCl (H), pH = 7.0.



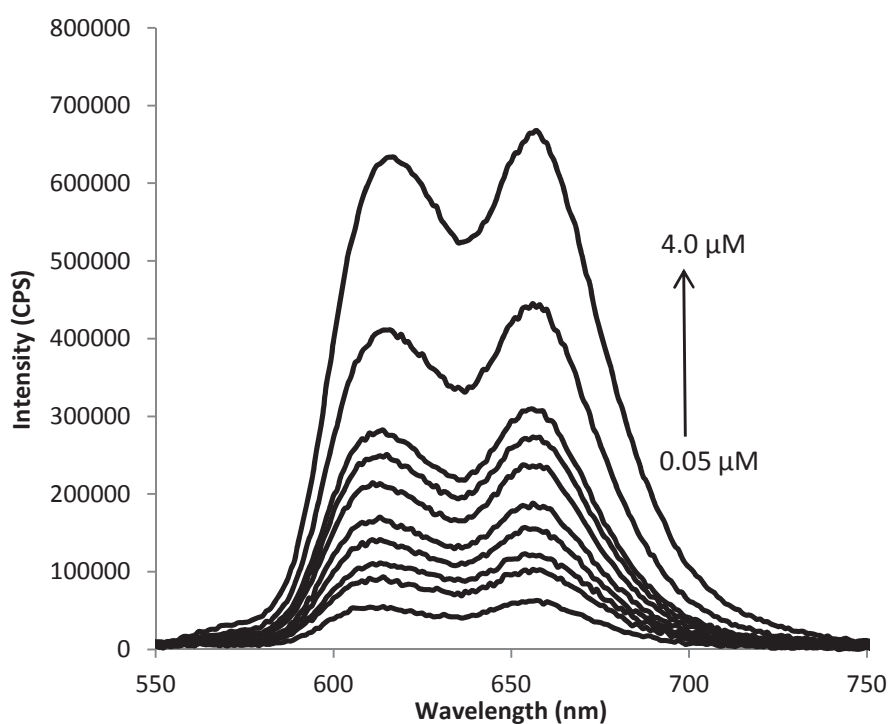
**Figure 12.6** Thermal difference spectra resulting from the subtraction of the 20 °C spectrum from the 80 °C spectrum of stDNA in the presence of ZnTMPyP4. Conditions: DNA = 0.02  $\mu$ M, pH = 7, 10 mM sodium phosphate, 0.1 mM EDTA, 50 mM NaCl (low ionic strength) or 1.0 M (high ionic strength).



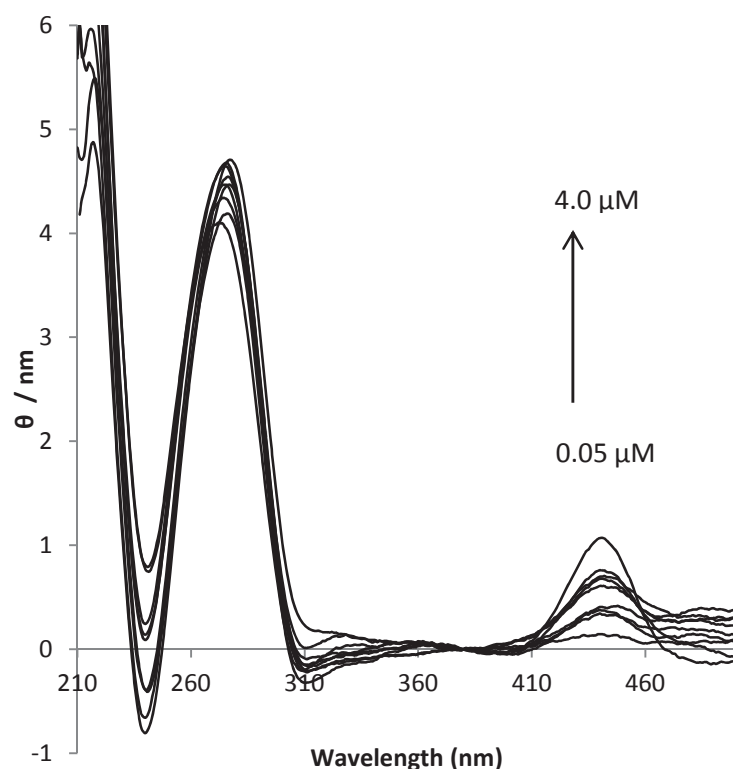
**Figure 12.7** Thermal difference spectra resulting from the subtraction of the 20 °C spectrum from the 80 °C spectrum of ZnTMPyP4. Conditions: DNA = 0.02  $\mu$ M, pH = 7, 10 mM sodium phosphate, 0.1 mM EDTA, 50 mM NaCl (low ionic strength) or 1 M NaCl (high ionic strength).



**Figure 12.8** Fluorescence emission spectra of ZnTMPyP4 with increasing concentration (0.05  $\mu\text{M}$  to 4  $\mu\text{M}$ ) in the absence of stDNA;  $\lambda_{\text{ex}} = 436 \text{ nm}$ . Conditions: 25  $^{\circ}\text{C}$ , pH = 7, 10 mM sodium phosphate, 0.1 mM EDTA, 50 mM NaCl.



**Figure 12.9** Fluorescence emission spectra of ZnTMPyP4 with increasing concentration (0.05  $\mu\text{M}$  to 4  $\mu\text{M}$ ) in the presence of stDNA;  $\lambda_{\text{ex}} = 436 \text{ nm}$ . Conditions: DNA = 0.04  $\mu\text{M}$ , 25  $^{\circ}\text{C}$ , pH = 7, 10 mM sodium phosphate, 0.1 mM EDTA, 50 mM NaCl.



**Figure 12.10** CD spectra of stDNA in the presence of ZnTMPyP4 with increasing concentration (0.05  $\mu\text{M}$  to 4  $\mu\text{M}$ ) accompanied by an increase of induced CD signal in the region of the porphyrin Soret band (420–450 nm) Conditions: DNA = 0.04  $\mu\text{M}$ , 20°C, pH = 7, 10 mM sodium phosphate, 0.1 mM EDTA, 50 mM NaCl.

### 12.2.1 Determination of Binding Constants of ZnTMPyP4 to Duplexes

$K_a$  values for duplexes with ZnTMPyP4 were determined by fluorescence spectroscopy according to a procedure described by Malinovskii *et al.*<sup>[4]</sup> Changes in fluorescence at 664 nm (as increasing signal upon binding) reflect the fraction of bound material upon increase of ZnTMPyP4 concentration (0.05, 0.1, 0.2, 0.3, 0.4, 0.6, 0.8, 1.0, 2.0 and 4.0  $\mu\text{M}$ ), Figure 11.3. The concentration of the duplex was kept constant at 1  $\mu\text{M}$ . Non-linear curve fitting was done using *OriginPro 8.1* and  $K_a$  was calculated using the formula  $K_a = 1/K_d$ .<sup>[4]</sup>

The binding isotherm, which represents the number of moles of ligand (porphyrin) bound per mole of macromolecule (DNA),  $r$ , was calculated as  $r = (F_{\text{obs}} - F_0)/(F_{\text{max}} - F_0)$ .  $F_{\text{obs}}$  is the observed fluorescence intensity of the DNA-porphyrin complex (Figure 12.9),  $F_0$  is the porphyrin fluorescence intensity in the absence of DNA (Figure 12.8) and  $F_{\text{max}}$  is the maximum porphyrin fluorescence intensity. The fluorescence intensities were measured at 664 nm (the increasing fluorescence

emission signal upon binding) upon 436 nm excitation. Porphyrin concentrations and  $r$  values were entered into the *OriginPro 8.1* program and a non-linear curve fit analysis was performed to generate the  $K_d$  value ( $6.4 \pm \times 10^{-7}$  M), listed as P2 on the *OriginPro 8.1* results sheet ( See section 12.2.2 below).

The reliability of the method was tested by comparing  $K_a$  data obtained from fluorescence spectroscopy with those from CD spectroscopy for a model system involving binding of ZnTMPyP4 to commercially obtained stDNA. Changes in the induced CD signal at 440 nm (as increasing signal upon binding) reflect the fraction of bound material upon increase of ZnTMPyP4 concentration. The raw CD data was processed in the same way as fluorescence data, replacing fluorescence intensity with  $\theta$ . Fluorescence spectroscopy was confirmed to be reliable as comparable  $K_a$  values of  $1.97 \pm 0.20 \times 10^6 \text{ M}^{-1}$  and  $1.56 \pm 0.10 \times 10^6 \text{ M}^{-1}$ , for CD and fluorescence spectroscopy were obtained, respectively. We decided to use fluorescence spectroscopy to determine binding constants for ZnTMPyP4 binding to our duplexes of interest, since the presence of TINA signals in the vicinity of the induced porphyrin signals complicated the analysis of CD data.

The  $K_a$  data for TINA-modified duplexes with  $[\text{Ru}(\text{bpy})_3]^{2+}$ , and G-quadruplexes with ZnTMPyP4 and  $[\text{Ru}(\text{bpy})_3]^{2+}$  were extracted from fluorescence Stern-Volmer quenching curves (as described in Chapters 7 - 8).

### 12.2.2 Example of binding constant calculation for the complex of salmon testes DNA-ZnTMPyP4 by fluorescence spectroscopy

Nonlinear Curve Fit (Hyperbl) (10/18/2012 16:48:42)

#### Parameters

		Value	Standard Error
B	P1	0.36207	0.03571
	P2	6.40325E-7	1.40344E-7

Reduced Chi-sqr = 2.82897622129E-4

COD(R^2) = 0.96260665478293

Iterations Performed = 12

Total Iterations in Session = 12

Fit converged - tolerance criterion satisfied.

#### Statistics

B	
Number of Points	9
Degrees of Freedom	7
Reduced Chi-Sqr	2.82898E-4
Residual Sum of Squares	0.00198
Adj. R-Square	0.95726
Fit Status	Succeeded(100)

Fit Status Code :

100 : Fit converged - tolerance criterion satisfied.

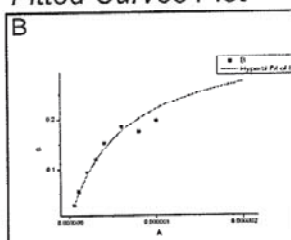
#### Summary

P1		P2		Statistics	
Value	Standard Error	Value	Standard Error	Reduced Chi-Sqr	Adj. R-Square
B 0.36207	0.03571	6.40325E-7	1.40344E-7	2.82898E-4	0.95726

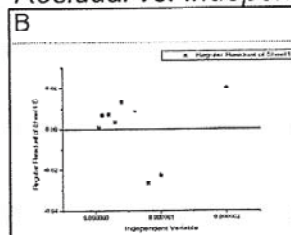
#### ANOVA

		DF	Sum of Squares	Mean Square	F Value	Prob>F
B	Regression	2	0.23829	0.11915	421.16586	1.63649E-7
	Residual	7	0.00198	2.82898E-4		
	Uncorrected Total	9	0.24027			
	Corrected Total	8	0.05296			

#### Fitted Curves Plot

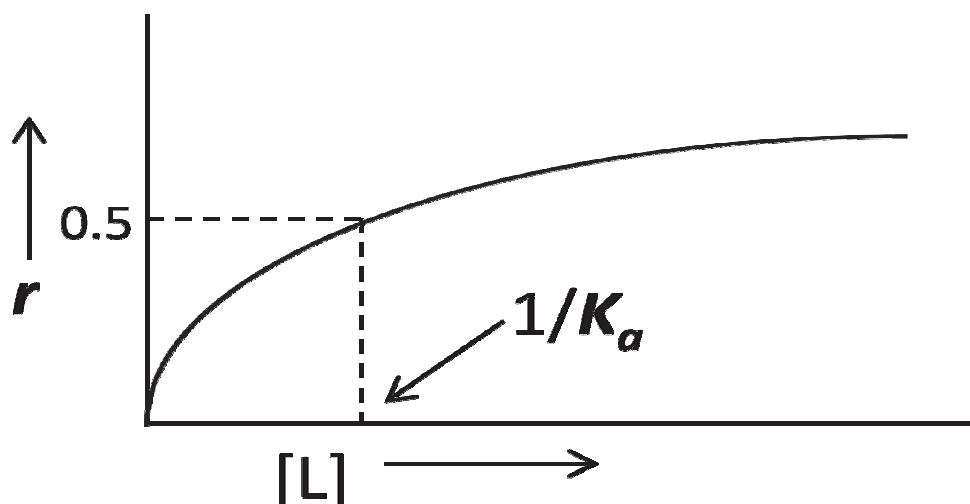


#### Residual vs. Independent Plot



### 12.2.3 Example of Stoichiometry calculation

The stoichiometry of binding, represented as the number of units involved in binding ZnTMPyP4, where each unit denotes a base pair or a TINA monomer attached to the 5' end of a duplex, was calculated based on the binding isotherm,<sup>[5]</sup> using the model described in detail by Malinovskii *et al.*<sup>[4]</sup> In this model, a Ligand (L) is bound to the Macromolecule (M), in our case the duplex, which contains  $n$  sites for the ligand. The binding equilibrium involving TINA-modified 12-mer duplexes is characterized by a binding isotherm, i.e. moles of ligand bound per mole of macromolecule (template),  $r$ .



**Figure 12.11** A binding isotherm of ligand (L) binding to a macromolecule (M).

$$K_a = [ML]/([M][L])$$

$$r = [ML]/([M] + [ML]) = K_a [L] / (1 + K_a [L])$$

$r$  versus  $[L]$  is a hyperbolic curve with a limiting value 1 at high ligand concentrations, and when  $r = 0.5$ ,  $[L] = 1/K_a$ , where  $K_a$  is the equilibrium association constant. If there are  $n$  identical binding sites on the macromolecule, the binding isotherm is the sum of those for each of the sites. Now the limiting value of  $r$  at high ligand concentration is  $n$ , the number of binding sites on the macromolecule template.

$$r = nK_a[L] / (1 + K_a[L])$$

$$\text{when } r = n/2, [L] = 1/K_a = K_d$$

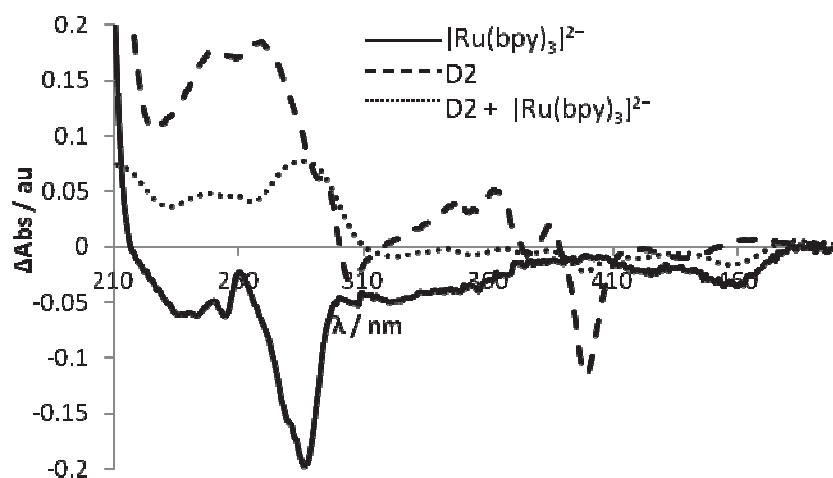
If  $K_d = 3.27 \times 10^{-6}$  M (for **D4**, 10 mM sodium phosphate buffer (pH 7.0, 0.1 mM EDTA, 50 mM NaCl ) from nonlinear least-squares curve fitting analysis, that gives  $n = 6.55 \times 10^{-6}$  M.

The concentration of **D4** was 1.0  $\mu$ M. Therefore, for **D4**, the ratio ZnTMPyP4 to the duplex at high ligand concentration (template saturation) is limited by a value of 6.55:

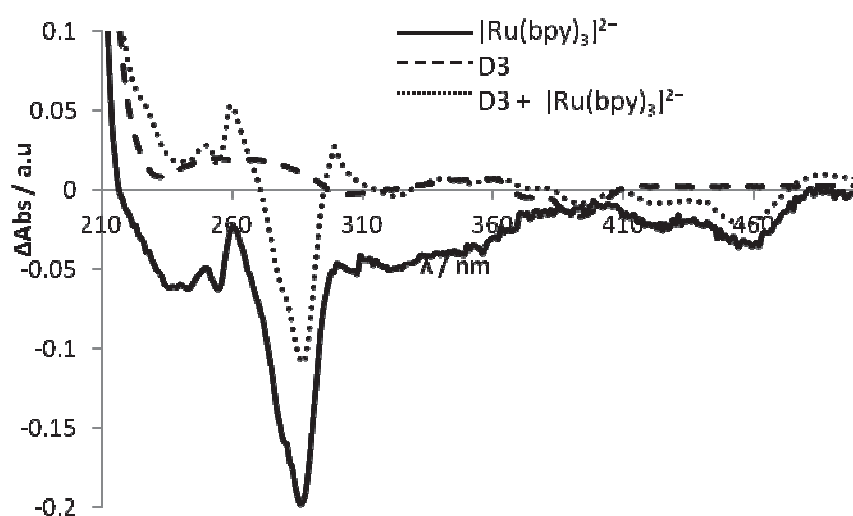
$$C_{(\text{ZnTMPyP4})} / C_{(\text{D4})} = 6.55 \times 10^{-6} / 10^{-6} = 6.55$$



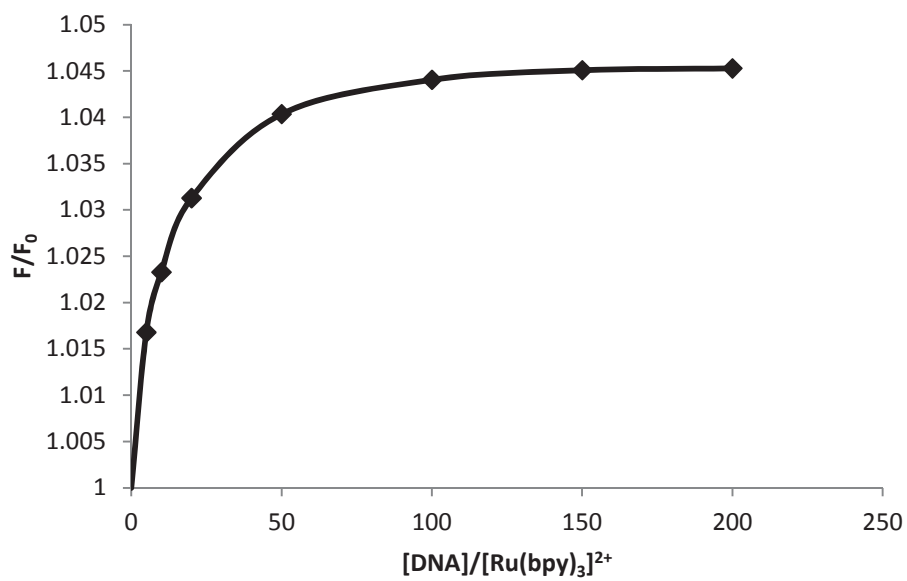
## 12.3 Appendix for Chapter 7



**Figure 12.12** Thermal difference spectra of free  $[\text{Ru}(\text{bpy})_3]^{2+}$  (40  $\mu\text{M}$ ), free D2 (1.0  $\mu\text{M}$ ), and D2 in the presence of  $[\text{Ru}(\text{bpy})_3]^{2+}$ . Conditions: Same as in Figure 12.6.



**Figure 12.13** Changes in thermal difference spectrum of D3 on adding  $[\text{Ru}(\text{bpy})_3]^{2+}$  (40  $\mu\text{M}$ ). Buffer conditions are the same as in Figure 12.6.



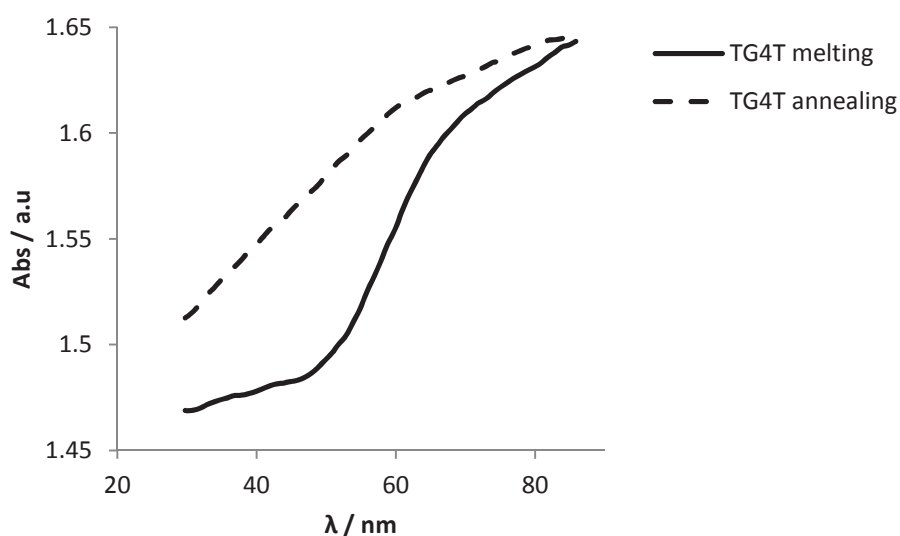
**Figure 12.14** Plot of relative fluorescence emission intensity *versus* **D1**:  $[Ru(bpy)_3]^{2+}$  ratio.  $[Ru(bpy)_3]^{2+} = 1.0 \mu M$ . Buffer conditions are the same as in Figure 12.6, low ionic strength.

## 12.4 Appendix for Chapter 8

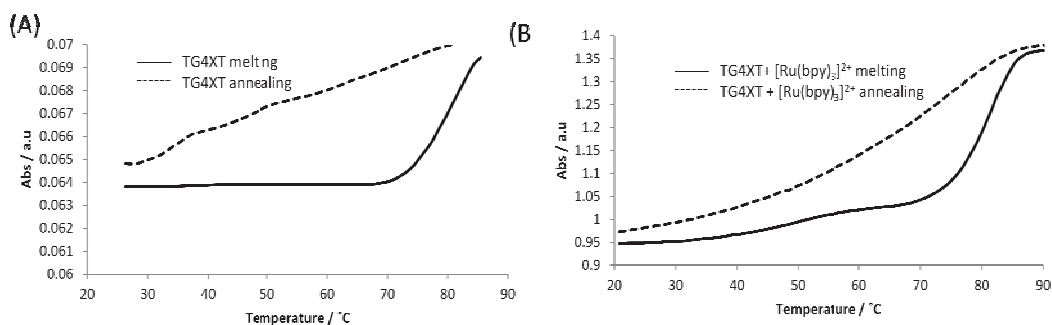
**Table 12.2** Changes in UV-Vis absorption in MLCT band for  $[\text{Ru}(\text{bpy})_3]^{2+}$  and Soret band for ZnTMPyP4 when bound to G-Quadruplexes.

Complex	<sup>a</sup> MLCT band/ <sup>b</sup> Soret band, % $\Delta A$
TG4T + $[\text{Ru}(\text{bpy})_3]^{2+}$	<sup>a</sup> -5.1
TG4TX + $[\text{Ru}(\text{bpy})_3]^{2+}$	<sup>a</sup> +10.7
TG4XT + $[\text{Ru}(\text{bpy})_3]^{2+}$	<sup>a</sup> +7.3
TG3XG3T+ $[\text{Ru}(\text{bpy})_3]^{2+}$	<sup>a</sup> +8.4
TG4T + ZnTMPyP4	<sup>b</sup> -3.9
TG4TX + ZnTMPyP4	<sup>b</sup> -15.2
TG4XT + ZnTMPyP4	<sup>b</sup> -13.5
TG3XG3T+ ZnTMPyP4 <sup>+</sup>	<sup>b</sup> -11.3

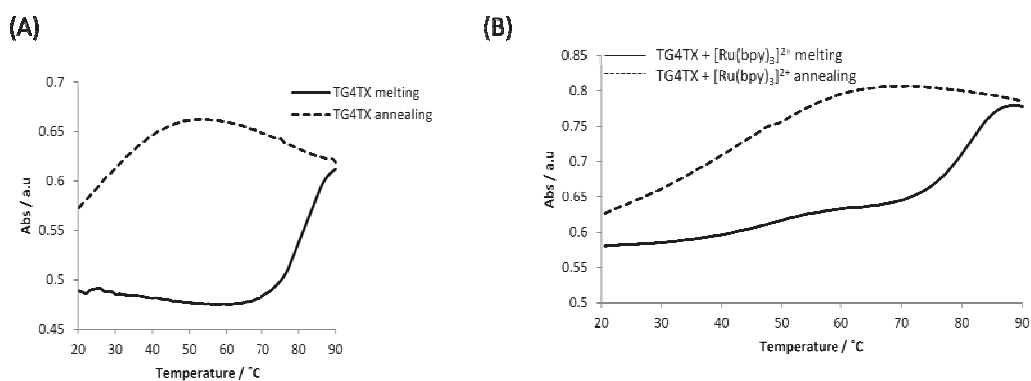
G-quadruplex strand concentration = 10  $\mu\text{M}$ ,  $[\text{Ru}(\text{bpy})_3]^{2+}$  = 40  $\mu\text{M}$ , 10 mM sodium phosphate buffer, 0.1 mM EDTA, pH = 7.0 in the presence of 50 mM NaCl, room temperature. Superscript a denotes changes in  $[\text{Ru}(\text{bpy})_3]^{2+}$  MLCT band (nm) and superscript b denotes changes in ZnTMPyP4 Soret band (nm).



**Figure 12.15** UV-Vis melting (solid line) and annealing profiles (dashed line) for **TG4T** (280 nm) at 10  $\mu\text{M}$  strand concentration in the absence (A) and after addition of  $[\text{Ru}(\text{bpy})_3]^{2+}$  to the pre-formed G-quadruplex (B). Conditions are the same as in Figure 12.6.



**Figure 12.16** UV-Vis melting (solid lines) and annealing profiles (dashed lines) for **TG4XT** (390 nm) at 10 μM strand concentration after annealing in the absence (A) and after addition of [Ru(bpy)<sub>3</sub>]<sup>2+</sup> to the pre-formed G-quadruplex (B). Conditions are the same as in Figure 12.6, low ionic strength.



**Figure 12.17** UV-Vis melting (solid lines) and annealing profiles (dashed lines) for **TG4TX** (390 nm) at 10 μM strand concentration in the absence (A) and after addition of [Ru(bpy)<sub>3</sub>]<sup>2+</sup> to the pre-formed G-quadruplex (B). Conditions are the same as in Figure 12.6, low ionic strength.

## 12.5 References

- [1] a)K. Lee, J. Slinker, A. Gorodetsky, S. Flores-Torres, H. Abruna, P. Houston, G. Malliaras, *Physical Chemistry Chemical Physics* **2003**, 5, 2706; b)A. Lewandowska-Andralojc, D. E. Polyansky, R. Zong, R. P. Thummel, E. Fujita, *Physical Chemistry Chemical Physics* **2013**, 15, 14058.
- [2] F. Qu, N. Q. Li, *Electroanalysis* **1997**, 9, 1348.
- [3] a)L. R. Keating, V. A. Szalai, *Biochemistry* **2004**, 43, 15891; b)N. Nagesh, V. K. Sharma, A. Ganesh Kumar, E. A. Lewis, *Journal of Nucleic Acids* **2010**, 2010.
- [4] V. L. Malinovskii, A. L. Nussbaumer, R. Häner, *Angewandte Chemie International Edition* **2012**, 51, 4905.
- [5] G. G. Hammes, *Physical chemistry for the biological sciences*, John Wiley & Sons, **2007**.